DOCTOR OF PHILOSOPHY

Phase change within flows from breaches of liquefied gas pipelines

Polanco Piñerez, Geanette Cleotilde

Award date:
2008

Awarding institution:
Coventry University

Phase change within flows from breaches of liquefied gas pipelines

G. C. Polanco Piñerez

A thesis submitted in partial fulfilment of the
Coventry University requirements
for the Degree of Doctor of Philosophy

2008

ABSTRACT

This thesis presents a compendium of work on superheated liquid releases. Superheated liquid releases are often subject to flashing. Nucleation has been identified as an important process in the early stage of flashing. The presence of strong nucleation and therefore flashing depends on the output of the balance of the promoting forces and dissipation forces inside the fluid released. A one dimensional model to classify the type of jet to be formed after the release has been developed based on the balance of these forces. The analysis is based on the assumption that the nucleation process can be modelled as a second order damped system. The model parameters are defined as a function of the pressure, temperature, fluid properties and geometric characteristic of the system. The results obtained have good agreement with the experimental results available for releases of different fluids, including both hydrocarbons and water.

The calculation of the velocity discharge, void fraction and mass flow of a flashing jet generated after the release is made based on the thermodynamics jump formulation approach. Due to the nature of the nucleation process, the assumptions of adiabatic flow with non reversible work for the surface tension forces are made. Those considerations are found to be more realistic that the isentropic condition used until now by different authors.

Numerical techniques are only applied after the flashing jet is formed, no droplets generation or vapour generation are included. Droplets are imposed as part of the boundary conditions of a gas jet. Droplets transport mechanics and momentum exchange with the gas current is made using Droplet Disperse Model (DDM) on the commercial code Fluent ®. DDM determines the distribution of the disperse phase over the continuous phase using a Lagrangian Eulerian approach. The influence of velocity, the dimension of the nozzle and mass flow used in the CFD modelling were analysed. Nozzle dimensions have a large impact on the core region length of the velocity profile. The $k-\varepsilon$ turbulent model was used. As expected, the numerical results do approach experimental values in the far region, suggesting that the momentum of the two phase jet is conserved. The one dimensional model thus provides the necessary boundary conditions for the application of numerical methods to superheated liquid releases including flashing.

CONTENTS

LIST OF FIGURES

LIST OF TABLES

NOMENCLATURE

A	Area, prefactor
a	Van der Waals's constant, Nukiyama and Tanasawa's constant, Upper limit dimensionless constant, diameter of the jet
$a1, a2, a3$	Drag coefficient constants
B, B'	Constant with order of magnitude about unit
b	Van der Waals's constant, Nukiyama and Tanasawa's constant
C	Bubble growth rate constant
$C_1,\ C_2$	Turbulent empirical constants
C_μ	Turbulent empirical constants
C_a	Cavitation number
C_D	Drag coefficient, discharge coefficient
C_p	Specific heat at constant pressure of the fluid.
c_α	Constant
c_{dp}	Discharge coefficient of the pipe
D	Nozzle diameter
D_{th}	Thermal diffusivity of the liquid
D_V	Diffusivity
$d_{0.5}$	Mass mean diameter
d_{10}	Arithmetic mean diameter
d_{32}	Sauter mean diameter
d_{50}	Diameter reading for cumulative function of 50% value
d_{90}	Diameter reading for cumulative function of 90% value
d_{32}	Sauter mean diameter
d	Droplet or particle diameter
d_{peak}	Peak diameter of the Rosin Rammler diameter distribution
$\overline{d}$	Droplet or particle mean diameter
$\overline{d}_{ng}$	Droplet or particle geometric mean diameter
$\overline{d}_{sg}$	Droplet or particle surface mean diameter
$\overline{d}_{vg}$	Droplet or particle volume mean diameter
E	Energy
Eo	Eötvös number
E_o	Constant

e Internal energy, roughness of the nozzle material

F External forces, constant

$F_{D/m}$ Drag force per particle mass

f Upper limit value's equation constant, Nukiyama and Tanasawa's equation, constant, number distribution function, frequency factor that in general is of the order of 10^{11} sec^{-1}

g Gravity acceleration, dimensionless derivative of the nucleation

g_c Conversion factor

$\vec{g}$ Gravity acceleration vector

$\dot{g}$ Mass flow per unit area

h Enthalpy, heat transfer coefficient

J Number of critical nuclei formed per unit time per unit volume

K Pressure cavitation number, dimensionless degree of superheat

K_c Diffusion rate

k Thermal conductivity

k_B The Boltzmann's constant

k_c Spring coefficient

L Characteristic length, core length

L_1, L_2 Characteristic domain lengths

l Eddy length, length of the nozzle

M Momentum, Morton number

M_{ki} Interface drag force

m Mass

m_{ent} Entrainment mass flux

$\dot{m}$ Mass flow

$\overrightarrow{m_i^{\sigma}}$ Traction associated with the surface tension and

N Number density of molecules in the superheated liquid, partial change of quality at the throat of the nozzle

Nu Nusselt number

$\vec{n}$ Normal vector

n Rosin Rammler function parameter, thermal equilibrium polytrophic exponent

P Total volume fraction of droplets with a diameter smaller than d

Pe Peclet number

Pr Prandtl number

p Pressure, volume distribution

Q Volumetric flow rate, heat

$\vec{q}$	Heat flux
q	Nukiyama and Tanasawa's equation exponent, specific heat
R	Gas universal constant
Re	Reynolds number
R_B	Constant
Ri	Richardson number
Rt	Droplets/gas mass ratio
r	Droplet radii, radial coordinate, nitrogen-to-liquid rate ratio, gas fraction
r_{nuc}	Volume fraction of the nucleation sites
Sc	Schmidt number
S_g	Geometric standard deviation
Sh	Sherwood number
S_{ki}	Interfacial source of turbulence
S_n	Square root of the variance
s	Entropy of the fluid
$\overline{\overline{T}}$	Stress tensor
T	Temperature
$T1, T2$	Evaluated temperatures at locations ‘1’ and ‘2’
t	Time
$\vec{u_i}$	Velocity vector of the interface
U	Internal energy of the fluid
u	Velocity
u_e	Velocity at which the liquid is entrained
u'_{RMS}	Root mean square velocity in the mixing layer
u_r	Relative liquid to gas velocity
$\bar{u}$	Mean velocity
u'	Turbulent velocity fluctuation
V	Volume
V_m	Molar volume
V_{rd}	Droplet velocity ratio
W	Work
We	Weber number
w	Relative velocity of the wave at the interface
X	Diameter such that 63.2% of the total volume is formed by droplet with diameters smaller than that value
x	Displacement parameter, coordinate axis
x_n	Actual displacement

x^*/d^*	Dimensionless displacement parameter
y	Coordinate axis, dimensionless deformation parameter
z	Axial coordinate

Greek symbol

α	Mass fraction
α_t	Thermal diffusivity
β	Half width spread angle of the jet
ς	Coefficient of nucleation
ΔG	Free energy barrier to nucleation
Δp	Pressure difference
$\Delta\rho$	Density difference
$\Delta\mu$	Chemical potential difference between the vapour and liquid phases
Δr	Droplet size ratio
ΔT	Temperature difference
ΔT_{sh}	Degree of superheat
ΔT *	Dimensionless degree of superheat
δ	Standard deviation related factor
ε	Kinetic energy dissipation
ε_i^σ	Surface energy associated with the interface
ϕ	Shape factor
k	Kinetic energy, ratio of specific heats
k_{BI}	Bubble induced turbulence
$\wp$	Dimensionless pressure
$\wp_{12}$	Pressure drop through the nozzle
μ	Dynamic viscosity
ν	Kinetic viscosity
ρ	Density
σ	Surface tension
η	Atomisation efficiency based on the performance of a particular injector
η_o	Initial amplitude of the wave
$\sigma_\varepsilon, \sigma_\kappa$	Turbulence model constants
τ_{ij}	Shear stress tensor
τ_b	Transit time of a bubble
Ω	Instability growth rate
Ψ	Flash evaporation
Γ'_g	Rate of vapour generation

ω	Break-up frequency
χ	Void fraction
x	Thermodynamics quality
∞	Infinity value

Subscripts

1	Position before the wave
2	Position after the wave
a	Air
c	Critical
ex it	Exit
exp	Expansion
fg	Flashing fluid gas
fl	Flashing fluid liquid
$flash$	Flashing
g	Gas
inj	Injection
jet	Location of the jet before break-up
l	Liquid
lam	Laminar
M	Mixture
m	Molar
max	Maximum
min	Minimum
n	Nozzle
$N2$	Nitrogen
o	Outward bubble pressure
p	Particle
$pipe$	Pipe
sat	Saturation
sh	Superheat
t	Turbulent
v	Vapour
w	Water gas
wl	Water liquid
0	Initial
∞	Ambient

Abbreviations

BSB	Bag and Stripping Breaking
CFD	Computational Fluid Dynamics
DDM	Discrete Droplet Model
GRT	Global Rainbow Thermometry
HEM	Homogeneous Equilibrium Model
ILIDS	Interferometric Laser Imaging for Droplet Sizing
IPI	Interferometer Particle Imaging
KH-RT	Kelvin-Helmholtz and Rayleigh-Taylor
LBM	Lattice Boltmann Method
LDA	Laser Doppler Anemometry
LES	Large-Eddy Simulations
LHF	Locally Homogeneous Flow
LID	Laser Induced Fluorescence
MD	Mean Diameter
MMD	Mass Median Diameter
MTD	Minimum Temperature Distance
PDA	Phase Doppler Anemometry
PDI	Phase Droplet Interferometry
PDPA	Phase Doppler Particle Analyser
PIV	Particle Image Velocimetry
PSIC	Particle Source in Cell
PTVS	Particle Tracking Velocimetry and Sizing
SF	Separated Flow
SMD	Sauter Mean Diameter
VMD	Volume Median Diameter

CHAPTER 1: GENERAL INTRODUCTION

1.1 INTRODUCTION

The accidental release of a flammable or toxic fluid represents a potential hazard to facilities, personnel and equipment, the environment, and the public. The knowledge of the behaviour of the fluid from the time of its release from containment until it has diluted below toxic or flammable limits is necessary. This has to be determined to some degree of accuracy to evaluate the potential risks involved in this situations, Allen (1996b). Many industries use materials that are stored above their atmospheric pressure boiling points (superheated liquids) which can form two-phase mixtures upon their accidental release to the environment at ambient conditions. The behaviour and the characteristics of these liquid-gas mixtures and the potential for the formation of vapour-liquid aerosols during a superheated liquid release due to the breaking of the metastable state can significantly affect the hazard zone and the mitigation steps that can be taken to minimize the release impact for the hydrocarbon industry, Deaves, Gilham et al. (2001), Michaella, Piccinini et al. (2004), or the quality of the combustion, or explosions inside the diesel engines, Diek and Roberts (1970), Lee and Park (2002a).

Flashing depends on the initial parameter values of the fluid as pressure and temperature as well as the type of fluid. A particular combination of those variables can create, for some cases, a complete breaking of the liquid core into droplets at the same time that it is going out of container like unstable two phase jet or liquid jet.

The physics of flashing is far too complex to be modelled even by numerical means. The major difficulty in the understanding of this flashing phenomenon and the parameters interactions within it belongs to the existence of a compromise between the physical and thermodynamics mechanism that acts on the released fluid.

After further analysis of the data available and the different analytical approaches used in the past, it is proposed here in this work that the nucleation process has a relevant role in the flashing phenomenon occurrence and in the generation of the two phase mixture jet after the leak. The nucleation mechanism is responsible for the breaking of the liquid continuum due to the appearance of number of vapour bubbles inside the liquid as result of the phase change which takes place inside the liquid. As the number of bubbles increases and the bubbles already created grow in volume the total presence of the vapour phase increases. However, after some distance downstream of the nozzle this process does not have the same relevance and the mechanics mechanism takes over the driving role of the flashing jet behaviour.

The new approach covers a one dimensional model based on a second order system which accounts for damping forces and stiffness forces during the nucleation process to estimated under certain conditions if flashing occurs or not. This is followed by a model based on jump condition definition to calculate liquid and vapour mass flow of fluid and other characteristics of the flow and finally, the performance of the simulations of releases with CFD using boundary conditions from the model described above.

1.2 AIMS

The main aim of this work is to contribute to the knowledge of the flashing process dynamics in normal industrial operating conditions. In order to achieve this, a complete chronological analysis is made. All the phases are considered, since the analysis of the initial conditions within the vessel where the superheated liquid is contained, passing through the generation of the two-phase jet, the calculation of the kinematics and mass flow parameters at the discharge position, then use that information to perform CFD modelling to finally compare with experimental work of Allen (1998a, b, c) ,Yildiz (2003) and Yildiz, Rambaud et al. (2004).

1.3 OBJECTIVES

The intention of this thesis is to contribute to the knowledge of the flashing process dynamics in normal industrial operating conditions. Based on the current understanding of this problem, it is clear that a more realistic approach is needed to model successfully this complex phenomenon.

As a result of the review done on previous works some weaknesses can be identified in the study of flashing. Unfortunately it is not possible to strengthen all of them. However it is intended here to propose a general approach of flashing study which starts with the actual knowledge of the flashing occurrence, follows by an analytical way of calculation of liquid and vapour mass flow as exit condition of the fluid and ends in the estimation of the whole setting needed for the CFD simulations.

This new approach is based on the identification of nucleation process as the more important process inside flashing phenomenon. From this statement three main objectives are designed to cover in this thesis:

- Develop a model to determine conditions when flashing occurs
- Develop a model to calculate liquid and vapour mass flow of fluid and other characteristics of the flow
- Perform simulations of releases with CFD using boundary conditions from the model described above

1.4 SUMMARY

This thesis consists of seven chapters. Following this introduction (Chapter 1), Chapter 2 is dedicated to reviewing background knowledge and literature resources. This includes definition of the problem, a discussion on the basic physical process, characterization of the phenomenon and summary of representative dimensionless group. Governing equations and mathematical models developed as well as the discussion of the assumptions taken are described in Chapter 3. Then the analysis of the influences of the information achieved on the result using CFD is outlined in Chapter 4. Chapter 5 gives a detailed discussion on the obtained results, creating the base for supporting the conclusions shown in Chapter 6.

CHAPTER 2: THEORETICAL BACKGROUND AND REVIEW

2.1 INTRODUCTION

This chapter is devoted to talk about the most important concepts and definitions related with flashing process as well as the review of previous works done in this subject.

The complexity of the physics involve in a flashing process requires to made links between mechanics and thermodynamics concepts in order to create a comprehensible background review to the reader.

The study of flashing problems have been developed in three main approaches such as the generation of criteria to know the type of jet that can be produced, procedures to do the calculation of mass going out through the jet and the modelling of flashing jet using CFD Technology. Most criteria to classify flashing jets found in the literature obey mainly to a visual characterization of pictures of graphs. However, some of them imply the existence of an explicit relationship between variables or even dimensionless number that can indicate the type of the resulting jet. The calculation of the quantity of mass transported by the jet remains as the most important aspect to be cover. The current models are based on the hypothesis of isentropic flow, which does not seem the more appropriate hypothesis for a flashing flow. In terms of CFD works, it can be identified simulations of the flashing jet (two-phase jet) using either experimental data or information obtained after using some of the mass calculation models available.

2.2 JET DYNAMICS

Most leakages from fluid filled vessels include fluid jets, originated by the pressure gradient between the internal pressure in the leaking vessel or container and the ambient pressure outside of the container or vessel. Since jets are an important part of the physics of a leak a brief review of jet behaviour is included in order to give an appropriate background of leakage physics.

The characterisation of jet properties and its dynamics behaviour has been carried using both experimental and numerical approaches. The numerical jet studies can be classified in three categories, which are two-dimensional approach (planar jet), axisymmetric approach (circular cross-section jet) and three-dimensional approach. The most common validation procedure of the numerical approaches is based on the comparison of these approaches with the experimental jet velocity profiles obtained from the experimental setup, Allen (1996a). The two-dimensional jet approach does not represent a real situation, but this simplification can reproduce higher aspect ratios (aspect ratios over 128:1) cross-section jets, for example jets formed from flange leaks, Simpson (1998). The centreline velocity presents a core region followed by a decay region, where velocity decreases proportionally to the downstream distance from the nozzle raised by 0.5, Wakes, Holdo et al. (2002). An axisymmetric jet velocity field has a potential core and a decay region, as shown in Figure 2-1. Potential core length is estimated as 6.9D from the jet exit, Wakes, Holdo et al. (2002). A conical shape in the velocity field identifies this core region, which is related to the vena contracta effect.

The centreline velocity decay is well established as proportional to 1/x and the angle of divergence is between 20 degrees and 25 degrees for a circular cross-section and about 5 degrees greater for a jet issuing from a rectangular slit, Massey (1989). The far field velocity decay of three-dimensional cases has similar trends to the axisymmetric jet cases for low speeds, i.e., a potential core region (constant velocity) near to the jet exit, followed by a characteristic decay region, where the centreline velocity decreases proportionally to the inverse of downstream distance from the nozzle.

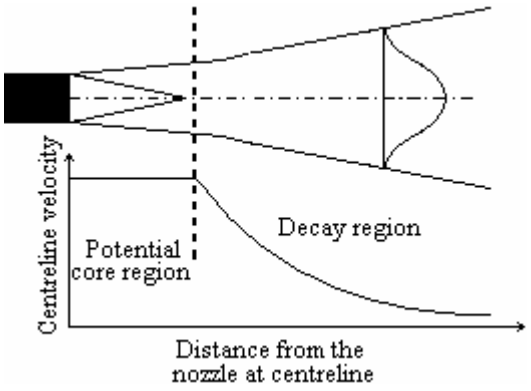

Figure 2-1 Spreading of an axisymmetric jet and its velocity profile along the centreline

The interaction between the jet and its surroundings is represented as the mass, momentum and energy exchange between both the jet and its surroundings. The entrainment mass flow from the reservoir into the jet, m_{ent}, affects the internal flow patterns and the general jet behaviour. The entrainment mass flow is proportional to the distance from the nozzle. It increases with the area around the shear layer of the jet, where the surrounding fluid is entrained into the jet. Equation (2.1) represents a simple expression for mass entrainment, Hill (1972).

$$m_{ent} = 2\pi \int_0^{\infty} \overline{\rho u} r dr \qquad \textbf{(2.1)}$$

The momentum of the entrainment mass compensates the losses generated by jet propagation, so, the momentum is kept constant at any cross section along the flow field. Liepman and Laufer (1947) developed an analytical expression for the jet momentum conservation:

$$M = \int_0^{\beta} \rho u^2 dr \qquad \textbf{(2.2)}$$

The knowledge about single phase gas jets is used as a starting point for a two-phase jets study. The gradual introduction of the effects of a second phase is the approach used for research purposes. Single-phase jets are used as a reference for further comparisons with two or multi phase jets.

2.3 FLASHING JETS

Flashing is the violent phase change of a super-heated liquid when it is exposed to a pressure gradient generated by the pressure difference between the vessel or pipe line and the atmospheric pressure, due to vessel or pipeline fracture. During the depressurisation of the liquid, it breaks into droplets at the same time as it exits the container in the form of an unstable jet. This is a consequence of the change in the metastable state of the superheated liquid stored, as shown in Figure 2-2.

Figure 2-2 Actual R134a two-phase jet. In this picture it is possible to see the distribution of the droplets transported by the flow. Source: Yildiz (2003)

Experimental research has found that for distances close to the nozzle liquid regions and large droplets are still superheated. These regions of liquid continuously break-up or evaporate further downstream from the nozzle, see Figure 2-3. This region is known as the expansion region. Downstream this section, the droplet velocity decreases due to effects of the entrainment of air into the jet, and this new region is known as the entrainment region, Yildiz (2003). Both the expansion and the entrainment regions are shown in Figure 2-3. The boundary between these two regions is characterized by the fact that internal pressure of the jet is equal to ambient pressure. The presence of the combination of hydrodynamic instabilities and thermal non-equilibrium conditions will then lead to break-up into small droplets, giving a violent and explosive characteristic to the flashing process, unless the heat inside of the liquid can be conducted at a sufficiently high rate to the surface of the liquid, in which case the surface evaporation takes place, Yildiz (2003).

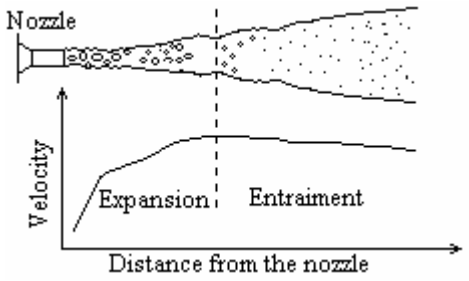

Figure 2-3 Expansion – Entrainment region into the jet. This figure shows the schematic velocity profile for the centreline of the flashing jet. Expansion region is characterized for big droplets and liquid ligaments and increasing velocity. The entrainment region has velocity decay due to air entering

The equilibrium conditions for the two-phase fluid inside the jet must likely correspond to a thermodynamics equilibrium condition for a phase change in a fluid due to boiling process, which takes when the vapour phase extract from the liquid phase enough energy, Brown and York (1962).

For a bubble to grow in a superheated liquid, the pressure acting outwards on the bubble must exceed those acting inward. This outward force will be as a result of the force balance generated by the pressure on the liquid, the vapour pressure and the pressure exerted by the interfacial tension, Brown and York (1962).

$$p_v > p_o + \frac{2\sigma}{r} \qquad \textbf{(2.3)}$$

The smaller bubble capable of growth is the one whose radius r just satisfies the equation

$$r = \frac{2\sigma}{p_v - p_o} \qquad \textbf{(2.4)}$$

2.3.1 Mechanical effects versus thermodynamic effects

Differentiating between roles of mechanical actions (momentum exchanges) and thermodynamic effects (phase change processes and heat transfer) is a complicated aspect of flashing. Aamir and Watkins (2000) investigated both thermodynamics and mechanical parts of the problem. The study first involved constructions of a thermodynamic model based on a quasi-state separated flow analysis, and then it involved the study of the spray behaviour. The result were validated at 95, 500 and 1028 mm from the nozzle against the experimental data from Hervieu and Veneau (1996) and Allen (1996a, b).

Mechanical effects of the two-phase jet produced

The effects of pressure on the final spray characteristics are not easy to recognize, due to its intimate relation with other factors such as the degree of superheat of the liquid and geometrical aspects. However, when the pressure is increased, the flow velocity increases as a function of the square root of the pressure difference between inside and outside the container. This increases the Reynolds number. Consequently, due to the flow rate increment the jet may have transitioned to turbulent somewhere in the supply

system or in the atomizer internal geometry. At higher Reynolds number, the disturbances in the liquid sheet are amplified. This tends to increase the magnitude of break-up forces. In addition to the increment of the inner forces respects to the surface tension forces, reflected in the increment of the Weber number. The Weber number is defined as ratio of the inertial force and the force due to surface tension of the fluid, as shown by Equation (2.5).

$$We_{\max} = \frac{u_r^2 \rho_g d_{\max}}{\sigma} \qquad \textbf{(2.5)}$$

The spray interaction with the ambient flow field is also known to affect droplet size distributions. At the exit of the nozzle, high liquid velocities will increase the entrainment air flow, which will assist in sheet break-up and, also it serves to redistribute the droplets by size class due to the direction of the entrainment flow toward the core of the spray cone.

The turbulence effect on the jet flow is definitively the most important mechanical factor in the determination of the behaviour of the two-phase jet flow. The influence of the turbulence fluctuating velocity components on the distributions of the droplets is crucial. Wu, Tseng et al. (1992) worked with water, glycerol and n-heptane, finding that drop formation on the surface of a liquid basically is due to turbulent eddies. Meanwhile, Lee and Park (2002b) determined that the break-up mechanism inside of a two-phase jet is related to Kelvin-Helmholtz and Rayleigh-Taylor (KH-RT) instabilities. Bricard and Friedel (1998) explored the mechanism named as aerodynamic atomisation, which is the result of turbulent instabilities at the liquid surface. For aerodynamics fragmentation the maximum stable drop size is usually given by a critical Weber number experimented by the gas phase.

The cavitation can be considered as another mechanical process which could influence the bubble formation in a flashing situation. The tendency for a flow to cavitate is characterised by the cavitation number, C_a. The tendency for a flow to cavitate increases as the cavitation number decreases.

$$C_a = \frac{p - p_v}{0.5 \rho u^2} \qquad \textbf{(2.6)}$$

where p is a reference pressure for the flow, p_v is the vapour pressure. The cavitation process is typically too rapid for the assumption of thermal equilibrium at the interface to be correct. In the simplest cavitation models, the mass transfer is driven by purely mechanical effects, namely liquid vapour pressure differences, rather than thermal effects. Gemci, Yakut et al. (2004b) showed that for a liquid with constant temperature but with decreasing pressure, which goes below its vapour pressure. Then, the mechanism responsible for the rupturing the liquid will be the cavitation as response to the presence of the critical pressure at that location.

Thermodynamic description

The current industrial activities imply the use and transport of substances at high pressure and high temperature levels, between different containers through a pipe network, and frequently these substances are found in superheated liquid state. The superheated condition implies that the liquid temperature is higher than its boiling temperature corresponding to its actual pressure. This condition is a metastable state, which means that irreversible changes in this characteristic can occur as a reaction to any significant perturbation, such as a large change in pressure.

Figure 2-4 shows a classical example of the equilibrium states. The black filled circles represent the state and the curve represents energy level. All systems tend to keep an equilibrium state if they kept under control any external contact or perturbation. Systems in stable equilibrium will keep their initial conditions after any perturbation, whilst the instable systems will achieve a new configuration after any perturbation. Metastable system behaviour will be similar to the stable system if the perturbation is not large enough, but if the perturbation is large enough then the system will achieve a new configuration after the perturbation. Normally, the pressure difference between the inside and the outside of an industrial vessel is considered as a large perturbation, so, depending as well on the characteristic of the liquid used, the system will tend to loss its initial superheated conditions and it will achieve a new state, Vandroux-Koenig and Berthoud (1997).

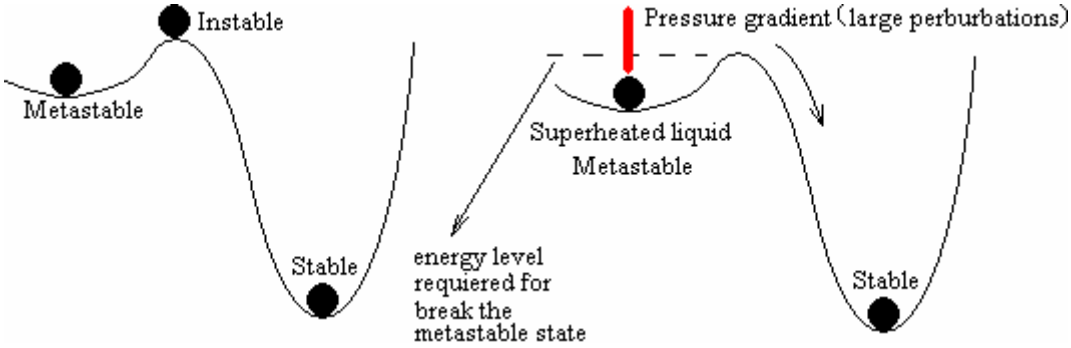

Figure 2-4 Schematic behaviour of superheated system in terms of types of equilibrium

Equation (2.7) shows the van der Waals equation of state which is used to define the stability limit inside of the fluid saturation range.

$$p = \frac{RT}{\left(v_m - b\right)} - \frac{a}{v_m^2} \qquad \textbf{(2.7)}$$

It is important to mention that there are some differences between van der Waals equation or any other equation of state and the real saturation line. The real isothermal line keeps a constant pressure inside the saturation dome. This behaviour within the saturation dome is probably familiar to most readers; it corresponds to a true fluid in saturation conditions. A true fluid would have constant pressure for values of molar volume between the molar volume of saturated vapour and the molar volume of saturated indicated by the horizontal line (bold line) in Figure 2-5.

Two van der Waals equation of state isothermals (full lines) have been drawn on the diagram for temperatures T_1 and T_2. Each isotherm may have any of three values of molar volume for a given value of pressure. The largest value corresponds to the molar volume of saturated vapour, the smallest represents the molar volume of saturated liquid and the middle value does not have any physical meaning. Additionally, each isotherm exhibits a minimum and a maximum point $\left(\partial p/\partial v_m = 0\right)$. The combination of all these points is known as a spinodal line (dashed line). The superposition, on the same diagram, of the saturation line (pointed line), which defines the equilibrium states for the hydrocarbon under consideration, intersects with the spinodal line to create three regions inside the saturation dome. These regions are superheated liquid; unstable fluid and sub cooled vapour. The location of such regions within a flashing jet is very important for its subsequent behaviour.

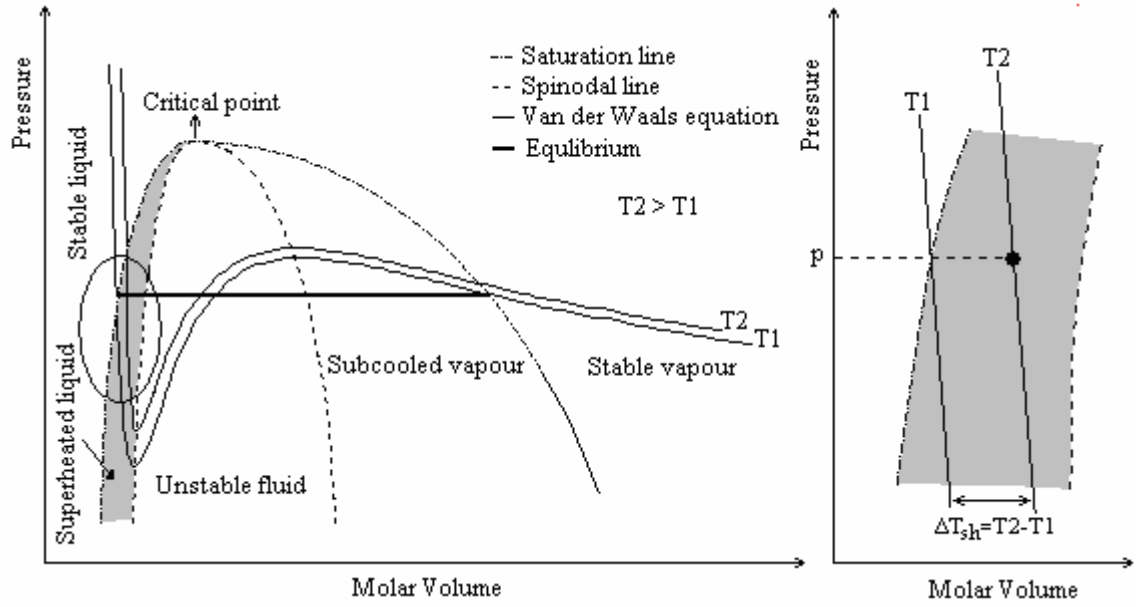

Figure 2-5 P-v diagrams showing the superheated state, initial condition for flashing process. It shows that for any pressure inside the superheated region the temperature of the fluid (T_2) is higher than the saturation temperature (T_1) at this pressure

A detailed view of the superheated liquid region is shown at the right hand side of Figure 2-5. The coordinates ($p, v_{m,1}$) represent saturated liquid condition, and the coordinates ($p, v_{m,2}$) represent a superheated liquid state. The difference between actual liquid temperature T_2 and the saturation temperature at its pressure T_1 is defined as the degree of superheat, ΔT_{sh}, as is shown in Equation (2.8). T_{sat} is the saturation temperature at the actual pressure of the fluid.

$$\Delta T_{sh} = T_2 - T_1 = T_2 - T_{sat} \qquad \textbf{(2.8)}$$

The evaporation and boiling mechanisms can help to explain part of the phase change from liquid to gas. While evaporation is a superficial phase change phenomenon, in which some molecules have enough kinetic energy to escape from the liquid to vapour state, without forming bubbles because the vapour pressure is lower than the atmospheric pressure. The boiling process is a volume phenomenon, where gas bubble formation is taking place due to the vapour pressure of a liquid being equal to the surrounding atmospheric pressure. Boiling temperature is the normal parameter used to characterise this phenomenon. Frequently, hydrocarbon fluids have a boiling point

under the standard ambient temperature. This suggests that combinations of evaporation and boiling processes can be present for this type of fluid at standard conditions.

2.3.2 Nucleation

For a superheated liquid jet to remain in equilibrium after any change in the pressure condition, due to the leak, it must lose internal energy, and this is preferentially achieved through latent heat transfer. The release of latent heat of vaporization is initiated through nucleation within the liquid, Whalley (1979). The critical nucleus radius at which nucleation begins is influenced by many factors and it can be estimated from a force balance on a spherical shape as shown by Equation (2.9).

$$r_c = \frac{2\sigma}{c_\alpha \Delta\mu} \tag{2.9}$$

If the gas phase can be considered as incompressible, the chemical potential can be replaced by the difference of the pressure of both phases, $p_\alpha - p_\beta$, and as result of that Equation (2.9) can rewritten as Equation (2.10), Schmelzer (2003):

$$r_c = \frac{2\sigma}{p_\alpha - p_\beta} \tag{2.10}$$

The classical nucleation theory is based on the thermodynamics of the phase change, on the bubbly dynamics and on the probability theory of the existence of molecular cluster within a liquid. Under this theory there are two types of nucleation processes, the homogeneous and the heterogeneous. The homogeneous nucleation process is considered as a fundamental mechanism of first-order phase transitions that will be presented in the absence of pre-existing interfaces, such as impurities inside the flow. For this type of nucleation the rate at which critical nuclei are formed is expressed by Schmelzer (2003):

$$J = A \exp\left(-\frac{\Delta G}{k_B T}\right) \tag{2.11}$$

The calculation of J, therefore, entails the kinetic problem of determining A and the thermodynamic one of determining ΔG. The pre-factor which can be written as:

$$A = Nf \tag{2.12}$$

And the free energy barrier, as predicted by the classical theory (see Das, Chatterjee et al. (2000) for details) is given by

$$\Delta G = \frac{16\pi\sigma^3 v^2}{3\Delta\mu^2} \tag{2.13}$$

However, for the case of nucleation in superheated liquids, the formation of cavities by density fluctuations and its relation with critically sized bubbles formed by a sequential single-molecule process is not obvious. Thus, the very notion of a spherical, macroscopic critical bubble formed by a succession of single-molecule events seems difficult to reconcile with actual processes occurring on a molecular scale. The heat involved in the process must be at least the heat necessary to induce the phase change from liquid to gas in the fluid, so, it is a limit for the energy contained in the fluid which will determine the type of jet after the leakage. The nucleation process is driven by near random fluctuations being determined by the critical free energy difference between two phases Frederic, Balibar et al. (2003). The nucleation rate J is characterized by a very strong dependence on the parameters of state of metastable liquid. For example, with the temperature rising by 1 K, the nucleation rate increases by two to five orders of magnitude, Reshetnikov, Skripov et al. (2002).

The value of the frequency of spontaneous nucleation of a particular process will indicate if it is possible to achieve some superheating before important quantity of bubble formation takes place. The dramatic increases in nucleation frequency also portray the catastrophic change of the metastable liquid to liquid-vapour mixture, Christensen and Tillack (2003).

Nevertheless, it is common to use the application of the phase transition models of first and second order to approach the actual phenomenon. For a first order phase transition the molar Gibbs energies or molar Helmholtz energies of the two phases are equal at the transition temperature, but their first derivatives with respect to temperature and pressure (for example, specific enthalpy of transition and specific volume) are discontinuous at the transition point. Then for two coexisting dissimilar phases can be transformed into one or another, a change in a field variable such as pressure,

temperature, magnetic or electric field is needed. Normally this type of transition entails dramatic and sudden changes in the characteristics of a system upon small infinitesimal changes to some control variable such temperature or pressure. Meanwhile; the second order transitions behave in a similar way except for the fact that they only present discontinuities in the second or higher derivatives.

2.4 REVIEW OF EXPERIMENTAL DATA

The complex nature of flashing phenomenon and the wide range of different parameters that intervene in it have driven authors to use distinct methodologies of study on this process. Both, experimental and analytical approaches have been used to identify the characteristics parameters within the two phase jet. However, no general agreement about the classification of flashing regimes under different flow condition exists. Therefore neither general calculation of mass distribution nor characteristic length of the jet or other jet parameters can be established.

2.4.1 Flashing flow regimes

The type of jet formed after the leakage on the experimental set up of the flashing process has been used as characterisation of the physical phenomena involved.

Brown and York (1962) made a distinction between the three regimes of flashing for low viscosity liquids, water and Freon. These three regimes are delimited by the gas Weber number (Equation (2.14)) $We < 0.2$, $0.2 \leq We \leq 8$ and $We > 8$. The first regime is characterized by the absence of any superficial disturbances and only the action of the interfacial tension applies. The second regime presents several sinuous distortions which whip the jet into segments and the third regime is characterized by the presence of more violent spreading with ligaments of fluid separating from the jet and the occurrence of the atomisation process. For larger Weber number the secondary atomization will occur, when the droplets formed originally from the main jet will be broken up still further.

$$We = \frac{u^2 \rho_g d}{2 g_c \sigma} \qquad \textbf{(2.14)}$$

Park and Lee (1994) found that the internal flow pattern inside the nozzle governs the behaviour outside the nozzle. For longer nozzle hole or larger degree of superheat the spray droplets are smaller and more uniform because of the active bubble formation inside the nozzle. The flow regime changes as a response to a continuous increasing of the superheat. The flow changes from the bubbly flow to slug flow, and then to annular flow and the spray droplets become smaller and more uniform, generating the classification of three different regime of flashing, named a, b and c respectively in Figure 2-6.

Figure 2-6 Relation between internal flow patterns and flashing liquid jet behaviour. Source: Park and Lee (1994)

The aspect ratio (L/D) used was about 7 and the fluid used was water. In the first place a large intact core region is observed, and the droplets are formed at the sides of it. For constant pressure, if the superheat is increasing, the nucleation and the growth of the bubbles become more active, then the bubbles collide with each other and coalesce inside the nozzle to form a large slug bubbles. When the slug flow is discharge from the

nozzle, the slug bubbles burst into ligaments and then disintegrate into small droplets, but the large liquid blobs originated from liquid slug are still observed. At the annular flow regime, a liquid film forms at the nozzle wall and the vapour flows at much higher velocity along the core region. When the annular flow is discharged from the nozzle, the liquid films disintegrate into fine droplets. The effect of the length of the nozzle on the droplet formation is quite similar to the superheat influence, which means both increase the smaller droplet formation outside the nozzle.

Johnson and Woodward (1999) reported some visual observations about the type of jet achieve as a function of the pressure and the temperature using water and CFC-11 (triclorofluoromethane) as work fluid. The mass recollection as a function of the temperature was reported. The experiments suggested that for a particular level of the degree of superheat the pressure influence on the final type of jet produced is reduced or neglected.

Lin and Reitz (1998) described the length of the coherent portion of the liquid jet or its unbroken portion for four different jet break-up regimes determined basically by the jet velocity, represented by the Weber gas number. At low jet velocities, the growth of the disturbances on the liquid surface promoted by the interaction between the liquid and ambient gas is believed to initiate the liquid break-up process. Here it is possible to locate the two first regimes known as: 1) The Rayleigh break-up, where break-up occurs many nozzle diameter downstream the nozzle and droplets have larger diameter than the jet diameter. 2) The first wind induced regime, similar to the previous one, but the droplets sizes are comparable to the diameter of the jet ($We_g < 13$). Whilst for high jet velocities, the break-up is due to the unstable growth of short wavelength waves at the liquid surface. Inside this classification it is found the last two regimes reported: 3) The second wind induced regime, break-up, where break-up occurs some nozzle diameter downstream the nozzle and the droplets have smaller diameter than the jet diameter ($13 < We_g < 40.3$) and 4) The atomisation regime, here the break-up occurs at the nozzle exit and the droplets have much smaller diameter than the jet diameter.

Lasheras and Hopfinger (2000) represented various regimens of liquid jet break-up in a coaxial stream tested in their experiments as Figure 2-7 shown. These regimens are represented on the map parameter space of the liquid Reynolds number, the

aerodynamic Weber number and the ratio of momentum fluxes between the gas and the liquid stream, shown in Figure 2-8.

Figure 2-7 Images of jet break-up by a coaxial gas flow. The nozzle contraction is 7:1 and the liquid and gas diameters are 7.6 mm and 11.3 mm respectively. A) We=38, b) We=58, c) We=118 and d) We=316. Source: Lasheras and Hopfinger (2000)

Figure 2-8 Break-up regimens in the map parameter space of the liquid Reynolds number, the aerodynamic Weber number and the ratio of momentum fluxes between the gas and the liquid stream. Source: Lasheras and Hopfinger (2000)

The gas-liquid interfacial instabilities allow analyzing the mechanism of periodic stripping of liquid sheets, or ligaments, which subsequently break-up into smaller lumps or droplets. Although there is not enough experimental data to precise the location of the different limit or boundaries, it is known that good atomization or jet with fine spray with uniform and small droplets is achieved beyond the upper boundary of the membrane break-up.

Reshetnikov, Mazheiko et al. (2001) report that the shape of the jet suffers a transformation from a nearly cylindrical shape to a hollow cone shape when the degree of superheat increases.

Reshetnikov, Skripov et al. (2002) and Skokov, Koverda et al. (2003a) made an experimental study over the flicker noise, $1/f$, in the fluctuation power spectrum in a jet of superheated liquid. The homogenous and heterogeneous nucleation mechanisms for Khladon-11 refrigerant (Freon) were identified. Figure 2-9 shows three different shape of the jet originally at the saturation conditions. The cylindrical jet shape is observed by $T/Tc \leq 0.63$ or $\Delta T = T - T_b \leq 60K$, then when ΔT is increased the jet becomes conical shape, and if the temperature is increased even more the jet that the lower limit of the heterogeneous mode, $T/Tc \geq 0.90$, then an homogeneous fluctuation production of vapour bubbles take place and the jet shape becomes parabolic. The intensity nucleation in this flow mode corresponds to an explosive boiling of liquid under quasi-static conditions. For the experiments were performed using a cylindrical nozzles of 0.5 mm of diameter and a length of 0.7 mm.

Figure 2-9 Photographs of different regimes of flashing jet using Freon as working fluid. Source Reshetnikov, Skripov et al. (2002)

Based on the idea that for liquid-liquid or liquid-gas system three principal break-up regimes can be present depending on the liquid flow rate, know as:

a) The dripping regime, in which the droplet are formed at the outlet of the capillarity, conserving the symmetry of the jet,

b) The laminar regime, in which the jet has a smooth and continuous aspect before a break-up zone where there is quasi-periodic emission of droplet identical in size generating asymmetry in the jet

c) The turbulent regime, in which the jet surface presents irregularities and the resulting droplets have different sizes and the jet becomes atomized.

Badens, Boutin et al. (2005) studied the jet atomization was studies on jet of water, methylene, chloride and ethyl alcohol into pressurized carbon dioxide at 308K, using typical operational ranges for industrial processes of anti solvent precipitation processes as experimental conditions. The patterns identified in this research are shown in Figure 2-10. The pressure was ranging from 6 to 9 MPa and the volumetric flow speed varied from 0.14 to 8.02 ms^{-1} respectively. As a result a new empirical correlation corresponding to the transition boundary between the zone of an asymmetrical jet and the zone of an atomized jet as a function of the jet Reynolds number, Re, and the Ohnesorge number, Oh, was presented as follows and shown in Figure 2-11:

$$\mathrm{Re}_l = 3.92 Oh_l^{-1.22} \text{ or } \ln(\mathrm{Re}_l) = -1.2208 \ln(Oh_l) + 1.3669 \quad \textbf{(2.15)}$$

$$\mathrm{Re}_l = 5.17 Oh_l{}^{*-0.98} \text{ or } \ln(\mathrm{Re}_l) = -0.9864 \ln(Oh_l{}^*) + 1.6431 \quad \textbf{(2.16)}$$

the Ohnesorge number Oh is defined as

$$Oh_l = \frac{\mu}{\sqrt{d \rho_l \sigma}} = \frac{\sqrt{We_l}}{\mathrm{Re}_l} \quad \textbf{(2.17)}$$

And the modified Ohnesorge number Oh is defined as

$$Oh_l{}^* = \frac{\mu_l}{\sqrt{d \rho_l \sigma}} \sqrt{\frac{\rho_g}{\rho_l}} \quad \textbf{(2.18)}$$

Figure 2-10 Image of a dispersion of methylene chloride into carbon dioxide at 308K at flow of 0.5mLmin^{-1} at 6MPa (a), 7MPa (b) and 8MPa. Source: Badens, Boutin et al. (2005)

Figure 2-11 The Reynolds number versus the Ohnesorge number and the modified Ohnesorge number calculated at the boundary between an asymmetrical jet and an atomized jet in a logarithmic scale. Source: Badens, Boutin et al. (2005)

2.5 DROPLET DISTRIBUTION

Spatial distribution of the droplets inside the jet has a relevant place in the study of the general behaviour of these two-phase jets. The representation of the actual droplet size distribution is usually referred to as the frequency distribution curve, instead of describing it using the location of each group of droplet with the same size or the location of each droplet and its position. There are some different distributions functions based on theoretical or experimental fundaments.

The Rosin-Rammler distribution, P, shown in Figure 2-12 is one of the functions most frequently used to represent a probability volumetric size distribution, and it is based on just two parameters, the characteristic diameter X and the exponent of the function, n. Other form to represent droplet distributions is to use the volume distribution gives by the same Rosin Rammler distribution, which is the derivative of the Equation (2.19), and it is expressed as equation (2.20). Both, Rosin-Rammler distribution and volume distribution are represented in Figure 2-12.

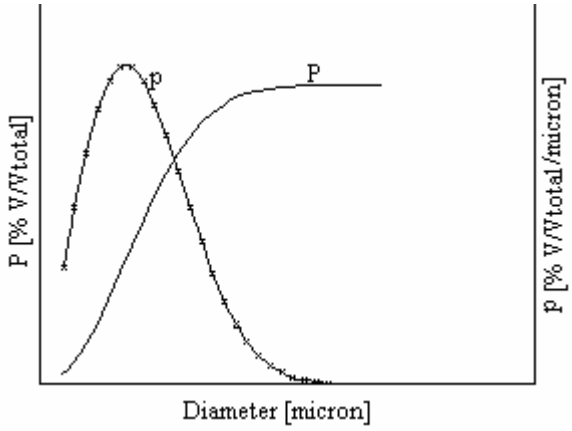

Figure 2-12 Schematic representation the fraction of the total volume occupied by droplets with a diameter smaller than d and the volume distribution as function of droplet diameter

$$P = 1 - e^{-\left(\frac{d}{X}\right)^n} \qquad \textbf{(2.19)}$$

$$\frac{dP}{dd} = p = \left(\frac{d}{X}\right)^n \frac{n}{d} e^{-\left(\frac{d}{X}\right)^n} \qquad \textbf{(2.20)}$$

There are different characteristic diameters used to describe the mean values of the droplet distribution in various scenarios, such as the Volume Median Diameter (VMD), the Mass Median Diameter (MMD), the Sauter Mean Diameter (SMD) and the Mean Diameter (MD), all defined in Table 2-1.

Table 2-1 Characteristic diameters meaning

Name	Symbol	Meaning
Volume Median Diameter (VMD)	d_{30}	diameter that represents 50% of the total volume of liquid sprayed at that location
Mass Median Diameter (MMD)	$d_{0.5}$	diameter that represents 50% of the total mass of liquid sprayed at that location
Sauter Mean Diameter (SMD)	d_{32}	Droplet diameter that has the same volume-to-surface area ratio as the total volume of all the droplets to the total surface area of all the droplets of liquid sprayed at that location.
Mean Diameter (MD)	d_{10}	Arithmetic mean diameter

For the Rosin Rammler distribution there is a correspondence between the representative diameters as the Sauter mean diameter (SMD), the mass mean diameter (MMD), and the peak diameter based on the parameter q and the gamma function, Γ, Lefebvre (1989)

$$\frac{d_{0.5}}{d_{32}} = (0.693)^{1/n}\Gamma\left(1-\frac{1}{n}\right) \quad \textbf{(2.21)}$$

$$\frac{d_{peak}}{X} = \left(1-\frac{1}{n}\right)^{-n} \quad \textbf{(2.22)}$$

$$\frac{d_{0.5}}{X} = (0.693)^{1/n} \quad \textbf{(2.23)}$$

$$d_{32} = \frac{X}{\Gamma(1-n^{-1})} \quad \textbf{(2.24)}$$

Above equations are represented schematically in Figure 2-13, together with the Rosin Rammler volume distribution. Here it can be seem that the MMD could be located at the left or right side to the peak diameter, for values of n larger and smaller than

3.2584, meanwhile the relative locations of the SMD and X keep constant, Chin and Lefebvre (1985). The limit value of n=3.2584 corresponds to the ratio $\frac{d_{peak}}{d_{0.5}} = 1$.

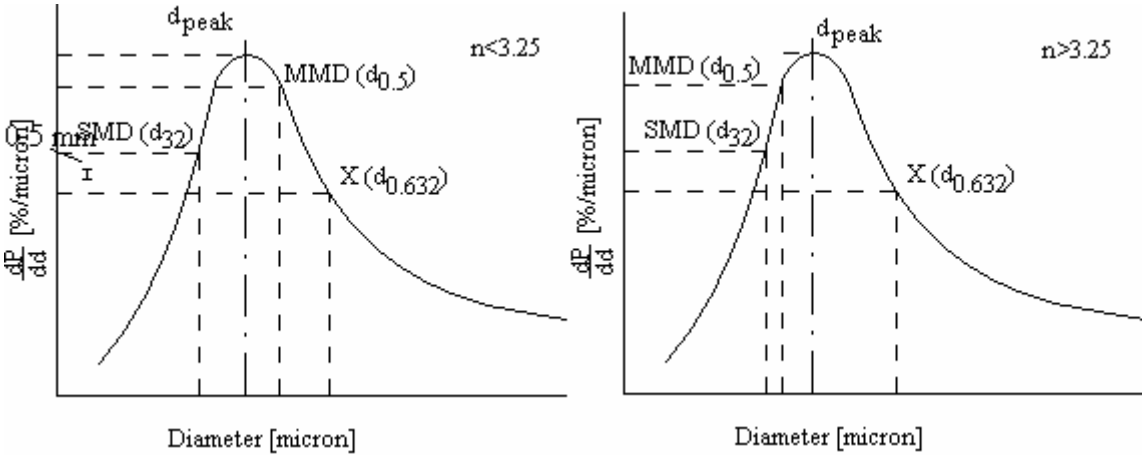

Figure 2-13 Graphic illustrations of various representative diameters

Nevertheless, it is important to keep in mind that in the experimental setup SMD is obtained using the sum form of the values taken directly from the instrument in the experimental setting. It is expressed as:

$$d_{32} = \frac{\sum_{1}^{np} V_p}{\sum_{1}^{np} A_p} \qquad \textbf{(2.25)}$$

where np is the total number of particles registered, V_p is the volume of each particle, and A_p is the surface are of each particle.

2.5.1 Droplet correlations review

Many experimental studies have been performed to obtain the actual value of the some characteristic diameters or the actual droplet size distribution inside of a two-phase jet. Some of them have achieved explicit relationships for the diameter estimation based on the initial conditions of the flow, as representation of the whole size distribution, Costa, Henrique et al. (2004). However, Bayvel (1982) and Fathikalajahi, Talaie et al. (1996) expressed the inconvenience of this use, after shown that the overall collection

efficiency could be very different, if the size distribution instead of a single mean diameter is used.

Brown and York (1962) observed that the jet stability may be an important effect on the type of jet formed after a release, and the size of the droplet generated. The growth rate constant, C, for the droplets was proposed as a function of the Weber number for each case, as it is shown in the Equation (2.26).

$$C = \left(\frac{C_p \Delta T}{L} \right) \left(\frac{\rho_2}{\rho_1} \right) (\pi D_{th})^2 \qquad \textbf{(2.26)}$$

The first parenthesis is the flashing weight fraction at the saturation temperature and the lower pressure, the second parenthesis encloses the specific volume ratio of the gas to the liquid and their product is then the volumetric increases upon flashing. The last term is a measure of the rate of heat conduction from the liquid to the vapour. Larger values of constant growth rate would indicate more rapid disintegration of the liquid mass.

The existence of a critical value of Weber number for water and Freon, both fluids considered as low viscosity liquids, equal to 12.5 was pointed. For Weber number larger than the critical value, the fluid will shatter at smaller superheat for the same velocity, giving smaller growth rate constant, meanwhile for lower Weber number that the critical value a significantly larger growth rate constant is determined, so, in summary, the mean drop size decreased with increasing Weber number for a given temperature.

$$C = \begin{matrix} 19.7 - 0.58We & We < 12.5 \\ 11.5 - 0.42We & We > 12.5 \end{matrix} \qquad \textbf{(2.27)}$$

The radius of the bubble formed follows the relation

$$r = r_1 + Ct^{0.5} \qquad \textbf{(2.28)}$$

Brown and York (1962) reported from their observation with water and Freon 11 for sharp-edged and rough surface orifices at 6 in (0.15 m) downstream from the nozzle, a linear correlation between the temperature and the MD.

$$d_{10}[\mu m] = \frac{1840 - 5.18T}{We} \text{ T in Fahrenheit degrees} \qquad \textbf{(2.29)}$$

Solomon, Ruupprecht et al. (1985) performed an experimental study on a flashing injector using two different fluids: the fuel named Jet-A containing dissolved air and pure Freon 11. A two stage expansion process was used, separated by an expansion chamber, which was found to be beneficial for good atomization of the jet. The mass flow, the mass velocity, the spray angle, as well as the SMD as a function of the pressure and the axial distance were reported. A comparison of the results of the SMD obtained by three different correlations as described below was made. Firstly, the correlation derivate by Mayer (1961) is followed by equations 2.30 and 2.31.

$$d_{32}[m] = 21.4B\left(\frac{\mu_l(\sigma_l/\rho_l)^{0.5}}{\rho_g u_l^{\,2}}\right)^{2/3} \qquad \textbf{(2.30)}$$

$$O[B] \approx 1 \qquad \textbf{(2.31)}$$

As second similar expression is recommended, in which the acceleration wave break-up region is given by Equation (2.32):

$$\left(\frac{\sigma_l}{\rho_g d u_l^{\,2}}\right)^{0.5} < E \qquad \textbf{(2.32)}$$

where the E value employed is approximately $8x10^{-3}$. Then

$$d_{32}[\mu m] = 1.2B' d^{0.5}\left(\frac{\mu_l(\sigma/\rho_l)^{0.5}}{\rho_g u_l^{\,2}}\right)^{1/3} \qquad \textbf{(2.33)}$$

A third expression was presented by Lefebvre (1980) as:

$$d_{32}[\mu m] = \left(1+\frac{\dot{m}_f}{\dot{m}_g}\right)\left[0.073\left(\frac{\sigma}{\rho_g u_g^{\,2}}\right)^{0.6}\left(\frac{\rho_l}{\rho_g}\right)^{0.1} d^{0.4} + 0.0006\left(\frac{\mu_l^{\,2} d}{\sigma\rho_g}\right)^{0.5}\right] \qquad \textbf{(2.34)}$$

Nagai, Sato et al. (1985) studied the atomisation of the superheated liquid jet using water as a working fluid, based on due to the bubble generation depends on the resident times inside the nozzle, so it depends on the length of the nozzle and the velocity of the fluid inside the nozzle and in the dimensionless degree of superheat of the fluid, defined as the ratio between the degree of superheat and the difference between the saturation

temperatures at the injection pressure and at the ambient pressure, taken as 100 Celsius degrees, as it is shown in the following expression:

$$\Delta T^* = \frac{T_{inj} - T_{sat}(p_\infty)}{T_{sat}(p_{inj}) - 100} \tag{2.35}$$

Then, the dimensionless expression of Reynolds time aspect ratio of the nozzle is used to determine the type of type of atomisation of the jet, as shown the following expression:

$$\mathrm{Re}\left(\frac{d}{l}\right) = \begin{cases} > 10^4 & liquid\ column\ break-up \\ \leq 10^4 & two\ phase\ flow \end{cases} \tag{2.36}$$

The next set of equations for the calculation of the SMD was developed:

$$\begin{aligned} &\mathrm{Re}\left(\frac{d}{l}\right) > 10^4,\ d = 0.5mm, \left(\frac{l}{d}\right) < 7,\ 0.55 \leq \Delta T^* < 1 \\ &d_{32}[\mu m] = 36.8\Delta T^{*-2.58} \end{aligned} \tag{2.37}$$

$$\begin{aligned} &\mathrm{Re}\left(\frac{d}{l}\right) \leq 10^4,\ d = 0.5 - 1.3mm, \left(\frac{l}{d}\right) > 7.8,\ 0 \leq \Delta T^* < 0.55 \\ &d_{32}[\mu m] = 70.4\left(0.14\left(\frac{l}{d}\right) - 1\right)^{-0.22} d^{0.72}(\Delta T^*)^{-0.38} \end{aligned} \tag{2.38}$$

$$\begin{aligned} &\mathrm{Re}\left(\frac{d}{l}\right) \leq 10^4,\ d = 0.5 - 1.3mm, \left(\frac{l}{d}\right) > 7.8,\ 0.55 \leq \Delta T^* < 1 \\ &d_{32}[\mu m] = 39.1\left(0.14\left(\frac{l}{d}\right) - 1\right)^{-0.22} d^{0.72}(\Delta T^*)^{-0.38} \end{aligned} \tag{2.39}$$

Wheatley (1987a) developed an expression for the maximum drop size, taken in account the implications for rain-out process, as a function of the Weber number, We_J, and Reynolds number, Re_J.

$$\mathrm{Re}_J = \frac{u_{jet} d_{jet} \rho_l}{\mu_l} \tag{2.40}$$

$$We_J = \frac{V_{jet}^2 d_{jet} \rho_l}{\sigma_l} \quad \textbf{(2.41)}$$

The maximum droplet size will correspond to the minimum value of Equation (2.42).

$$d_{\max}[\mu m] = \min\left(1.89 d_{jet}\left(1+3\frac{We_J^{1/2}}{\mathrm{Re}_J}\right)^{1/2}, \frac{20\sigma_l}{u_{jet}^2 \rho_{air}}\right) \quad \textbf{(2.42)}$$

Hervieu and Veneau (1996) made experimental determination of the droplet size and velocity distributions within a jet at the exit of a discharge pipe of a liquefied propane storage tank during a sudden blow down. A set of blow downs was performed varying the nozzle diameter (2, 5 and 8 mm), the initial pressure (5, 11 and 17 bar). The volume of the tank was 5 litres and it contained half level full of propane liquid. The diameter of the jet at 60 mm downstream from the nozzle for different nozzle size at 11 bars as initial pressure and for 2 mm nozzle for the three different pressures was determined. The mean droplet diameter always remained constant during the total liquid release, and for all the cases the flat shape of the diameter-velocity cross-correlation indicated that droplets of each size class flow with the same velocity. Meanwhile, the diameters and velocities decrease in the radial direction. This confirms the evaporation process in the flow direction. Measurements of the droplet size and velocity were reported at 95 mm from the nozzle.

Allen (1998a, b, c) reported the axial propane droplet velocity and relative volume, in size band, as a function of the radial distance from the centreline. He used 4 mm and 6 mm nozzle sizes. No observations about the jet shapes were reported. The first part of the centreline axial velocity is approximately constant, and then it starts decreasing in the axial direction as the distance from the nozzle increases. The exit velocity was estimated to be around 30 m/s (core section) and the average mass release rate for 4 mm nozzles was 0.11 kg/s with a standard deviation of 0.02 kg/s. The radial velocity profile at different positions has a Gaussian shape, as expected. The dimensionless plot of these suggests that the jet spreads at a constant rate. He also reported that for cases using R22 as fluid with 2.8 mm and 1 mm pinhole similar data were obtained. Allen (1996b) reported the fraction of the total droplet volume present along the measurement lines at axial position of 0.500, 0.688 and 1.088 m, as well as, along the centreline. The data

were reported in two ranges, 0 to 21.4 microns and 21.4 to 41.2 microns. The centreline measurements show an initial reduction in the relative fraction of both size bands up to between 0.5 and 1 m downstream of the nozzle, this was followed by an increase in the relative fraction of each size present, possibly, due to coalescence, or rates of evaporation varying with droplet size.

Dunbar, Watkins et al. (1997) reported a new empirical correlation for the MMD as follow:

$$d_{0.5}[\mu m] = \frac{8.02}{\chi^{0.56}\left(\frac{p_{inj} - p_{\infty}}{p_{\infty}}\right)^{0.46}} \qquad \textbf{(2.43)}$$

Gemci, Yakut et al. (2004b) made parametric studies of combined feed of binary mixture with the propellant gas (nitrogen) and found that the presence of the flashing fluid can markedly reduce the amount of propellant gas required for the same mean droplet diameter.

Deaves, Gilham et al. (2001) reported an empirical correlation based on data for sprays through orifices for the SMD calculation.

$$d_{32}[\mu m] = 3.09 \nu_l^{0.385} (\sigma \rho_l)^{0.737} \rho_g^{0.06} \left(p_{inj} - p_{\infty}\right)^{-0.54} \qquad \textbf{(2.44)}$$

Yildiz, Beek et al. (2002b, a) and Yildiz, Rambaud et al. (2004) carried out experimental research on R134a jet using Global Rainbow Thermometry (GRT), Phase Doppler Anemometry (PDA) and Particle Image Velocimetry (PIV) techniques. This investigation reported the SMD and the MD distribution on the centreline, the temperature profile and the velocity field distribution at the centreline and also at two different radial positions (x/d=187 y x/d=507). In addition, some displays of the jet behaviour were recorded. The droplet size evolution along the jet axis shows the presence of the expansion and entrainment regions. Meanwhile in the axial direction the larger droplets were located near the centreline of the jet, as was expected. A matrix of three distinct pressure values (8.2, 8.86 and 9.42 bar) in combination with three distinct degree of superheat values (43.4, 47.9 and 49.6 Celsius degrees) and two sizes of nozzles were set. The increase in the diameter of the nozzle resulted in a more violent break-up and a decrease of the disintegration distance from the nozzle. The degree of

superheat affects directly the number of bubbles generated, because this parameter reflects the level of energy available from the fluid (liquid). Thus, for larger superheat values more energy is released and more droplets are generated and a complete shattering of the jet takes place inside the flow.

Madsen, Harbo et al. (2003) reported the droplets size measurement, using Interferometry Particle Imaging (IPI) and PDA measurement, for a danfoss oil pressure-swirl atomiser operated with a flow rate approximately of 3.2 l/h of water, corresponding to an atomisation pressure of 850 kPa. The results obtained by these two methods were similar; however, the PDA results were consistently bigger than the IPI results. The value of the droplet diameter was located around 70 micron as maximum value and around of 20 micron as the minimum value.

Takeuchi, Kawaguchi et al. (2004) reported the measurement of the MD and the SMD of a water spray centrally injected into a swirling annular yet, with heated and non-heated airflow with an initial outer diameter 56.5 mm. The SMD and the MD decrease in the radial direction from the centreline towards the edge of the spray. As expected, the MD was smaller for the heated case due to the evaporation presented, even for the axial direction far from the nozzle.

Gemci, Yakut et al. (2004a) studied the flash atomisation of water/acetone solutions by varying the relative concentration of the propellant gas and the liquid, the injection temperature, and the pressure. The mean droplet diameters were measured as a function of the injection temperature, the pressure, and the nitrogen-to-liquid flow rate ratio, defined as r:

$$r = \frac{Q_{N2}}{Q_l} \qquad \textbf{(2.45)}$$

The presence of the liquid propellant improves the atomisation at all conditions. The presence of the gas propellant increases the injection velocity and promotes bubble formation. Both, temperature and pressure help to the atomisation process. The authors also found that the propellant gas has a stronger effect on neat water than on the acetone/water solutions. A linear relation for the SMD, based on data at 3 cm downstream from the nozzle, was proposed as follow:

$$d_{32}[\mu m] = 118.4 - 28.3(\Delta T^* - K) \quad \textbf{(2.46)}$$

$$K = \frac{p_\infty - p_v(T_{nozzle})}{\frac{1}{2}\rho_M (\bar{u})^2} \quad \textbf{(2.47)}$$

The cavitation number is ranging between -1.2 and 1.5, while dimensionless degree of superheat is ranging between -12 and 2.

Gemci, Yakut et al. (2004b) studied the flash atomisation of hydrocarbon solutions containing n-hexadecane and n-butane (2 and 5 weight % n-butane in hexane), with nitrogen as the propellant gas in different concentrations. The droplet diameters were presented as a function of operation conditions. A linear relationship was found between the SMD and dimensionless superheat number and the cavitation number. The presence of the liquid propellant promotes the atomisation process. The injection temperature improves atomisation for both single and binary liquid. The SMD was presented as a function of the injection temperature and the pressure.

Finally, Costa, Henrique et al. (2004) compared two correlations of SMD both developed for Venturi geometry in which gas was injected in some point upstream the liquid flow. However, it is believed that these correlations could be used in other situations. The gas velocity and the liquid gas ratio have a significant influence on the droplet size. The SMD decreases with the gas velocity increasing for the smaller value of liquid gas ratio, 0.07 l/m3, however, when the liquid gas ratio is increased this trend changes. In order to measure the size of the droplets, the attenuation of monochromatic light passing through a spray was used. This method does not give a size distribution, but rather only a mean diameter. The first correlation, the Nukiyama's correlation, tested is expressed as:

$$d_{32}[m] = \frac{0.585}{u_r}\sqrt{\frac{\sigma}{\rho_l}} + 1.683x10^{-3}\left(\frac{\mu_l}{\sqrt{\sigma\rho_l}}\right)^{0.45}\left(\frac{1000Q_l}{Q_g}\right)^{1.5} \quad \textbf{(2.48)}$$

for gas velocity values between 73 and 320 m/s and the liquid to gas ratio (L/G) values between 0.008 and 1.0 l/m^3, this correlation was published for first time in 1938. The second correlation of SMD used corresponded to the Boll's correlation published in 1974, which covers liquid to gas ratio range from 0.6 to 2.4 l/m^3.

$$d_{32}[m] = \frac{4.22x10^{-2} + 5.77x10^{-3}\left(\frac{1000Q_l}{Q_g}\right)^{1.932}}{u_r^{1.602}} \quad \textbf{(2.49)}$$

The Rosin Rammler distribution of droplet represents very well the actual droplet distribution for the three positions tested in the experiment.

2.6 JET CHARACTERISATION

2.6.1 Mass and velocity calculation at the exit of nozzle

The calculation of the mass and the velocity at the exit of the nozzle will strongly depend on the determination of the regime of the jet at the exit of the nozzle. The regime type will guide the applicability of the calculation procedure. For instance, if the fluid remains as a superheated liquid at the outlet, then a relative large discharge rate will be presented at the exit and it can be calculated with sufficient accuracy by the general equation used to determine the flow of cold fluid, named Bernoulli's equation. However, if flow type at the exit is described as a two-phase fluid then the flow can be estimated as a two-phase mixture in thermodynamic equilibrium or as a liquid-gas flow in no equilibrium according to the thermodynamics behaviour of the whole system, Khajehnajafi and Shinde (1994).

Solomon, Ruupprecht et al. (1985) described the Locally Homogeneous Flow (LHF) and the Separated Flow (SF) models, both developing to estimate the injector conditions based on the flow regime analysis. The LHF, also known as homogeneous equilibrium model (HEM), treats the fluid as a mixture of the different fluids, with mean properties based on the individual properties of the fluids. The SF treats the flow as a two-phase, liquid-gas flow, with individual properties. Both models have as common assumptions the steady state condition, the one-dimensional approach, the negligible inlet kinetic energy, the no wall friction and no wall heat transfer, and the convergent flow passage.

However, each model has other additional assumptions, as it is the case of SF model, which assumes the negligible exchange of heat, mass, and momentum between the phases, the incompressible treatment of the liquid phase with dissolved gas content frozen at the expansion chamber condition, and the adiabatic and frictionless expansion.

According to these assumptions a choked flow will be present if the pressure exit is bigger than ambient pressure. Where the exit pressure can be estimate by:

$$\frac{p_{critic}}{p_{inj}} = \left(\frac{2}{k+1}\right)^{k/k-1} \tag{2.50}$$

Then,

$$p_{exit} = \begin{matrix} p_{amb} & if & p_{critic} \leq p_{amb} \\ p_{critic} & if & p_{critic} > p_{amb} \end{matrix} \tag{2.51}$$

and

$$T_{exit} = T_{inj}\left(\frac{p_{exit}}{p_{inj}}\right)^{\frac{(k-1)}{k}} \tag{2.52}$$

$$u_l = \sqrt{\frac{2\left(p_{inj} - p_{exit}\right)}{\rho_l}} \tag{2.53}$$

$$u_g = \sqrt{2Cp_g\left(T_{inj} - T_{exit}\right)} \tag{2.54}$$

In contrast, the LHF assumes that the gas and liquid have the same velocity, temperature and pressure at each cross section. Then, from the energy balance the calculation of the velocity and the mass flow rate is:

$$u = \sqrt{2\left(h_{inj} - h_{exit}\right)} \tag{2.55}$$

$$\dot{m} = A_c C_{fc}\left(\rho u\right)_C \tag{2.56}$$

Wheatley (1987a) reported a model for the estimation of the velocity at the discharge location, based on the constant entropy formulation during the flow path. The model covers the cases of complete liquid discharge, critical and non-critical equilibrium gas-liquid discharges. For the pure liquid discharge, the velocity can be calculated from Equation (2.53) employed by Solomon, Ruupprecht et al. (1985). For the equilibrium flow case, the discharge velocity may be calculated by Equation (2.57) below. This result ignores the potential energy contribution and the loss coefficient of the nozzle.

$$u = \sqrt{2 * \left[\frac{\left(p_{inj} - p_{exit} \right)}{\rho_l} + Cp_l \left(T_{inj} - T_{exit} \right) - Cp_l T_{exit} \ln\left(\frac{T_{inj}}{T_{exit}} \right) \right]} \qquad \textbf{(2.57)}$$

This expression may be applied to both critical and non-critical discharges. However, the thermodynamic parameters corresponding to the exit location are different in each case.

For critical cases, also known as choked flow, the value of pressure at the exit will be the saturation pressure corresponding to the temperature calculated from the equilibrium expression for two phase flow Wheatley (1987a) as follows:

$$\begin{aligned} &\frac{1}{2}\left(v_L + \frac{C_L T_{exit}^2}{A^0 P_{exit}} \ln\left(\frac{T_{inj}}{T_{exit}} \right) \right)^2 = \frac{C_L T_{exit}^4}{A^0 P_{exit}^2} \left[1 + \left(\frac{A^0}{T_{exit}} - 2 \right) \ln\left(\frac{T_{inj}}{T_{exit}} \right) \right] \\ &\left[v_L \left(p_{inj} - p_{exit} \right) + C_L \left(T_{inj} - T_{exit} \right) - C_L T_{exit} \ln\left(\frac{T_{inj}}{T_{exit}} \right) \right] \end{aligned} \qquad \textbf{(2.58)}$$

Whilst, for non-critical cases, the pressure at the exit, p_{exit}, is the ambient pressure and the temperature is the saturation temperature at that pressure.

Additionally, Wheatley (1987a) based on the hypothesis of the flashing occurs just at the exit of the nozzle plus the assumption of no entrainment of air and no exchange of any momentum or heat between the jet and the air surrounding, and that the jet has half-angle after flashing, presented a calculation method for the velocity and quality after the flashing as:

$$u_{flash} = \frac{1}{\lambda}\left(\frac{A_{exit} p_{exit}}{G} - \frac{A_{flash} p_{amb}}{G} + u_{exit} \right) \qquad \textbf{(2.59)}$$

$$v_{flash} = \frac{T_{flash}}{p_a A^0} \left(\begin{aligned} &C_L T_{exit} + p_{exit} v_{exit} + X_{exit} p_{exit} \left(v_{gexit} - v_l \right) \left(\frac{A^0}{T_{exit}} - 1 \right) \\ &+ \frac{V_{exit}^2}{2} - C_L T_{flash} + p_a v_l \left(\frac{A^0}{T_{flash}} - 1 \right) - \frac{\lambda^2 u_{flash}^2}{2} \end{aligned} \right) \qquad \textbf{(2.60)}$$

$$\chi_{flash} = \frac{v - v_l}{v_g - v_l} \qquad \textbf{(2.61)}$$

In other hands, the report of Energy Analysis Inc (1990) shows that for liquid discharge the flow mass rate is:

$$\dot{m}_l = AC_d\sqrt{2\rho_l\left(p_{inj}-p_{amb}\right)} \tag{2.62}$$

Meanwhile for critical conditions for the gas at the exit but in equilibrium with the liquid phase, the calculation becomes slightly more complex.

$$\dot{m}_{eq} = \begin{matrix} AC_d\sqrt{2\rho_l\left(p_{inj}-p_{sat}\right)} & if \quad \eta \le \eta_{\lim} \\ AC_d\eta_c\sqrt{\dfrac{\rho_l p_{inj}}{\Omega\eta}} & if \quad \eta > \eta_{\lim} \end{matrix} \tag{2.63}$$

$$p_{eq} = \begin{matrix} p_{sat} & if \quad \eta \le \eta_{\lim} \\ \eta p_{inj} & if \quad \eta > \eta_{\lim} \end{matrix} \tag{2.64}$$

$$T_{eq} = \begin{matrix} T_{sat}\left(p_{eq}\right) & if \quad \eta \le \eta_{\lim} \\ T_{inj} & if \quad \eta > \eta_{\lim} \end{matrix} \tag{2.65}$$

The equilibrium condition must fulfil the thermodynamics restrictions represented by the physical limit of the liquid mass flow as the maximum rate possible, the absence of any choke wake in the flow or sub cooled condition of the fluid, all expressed in the following equation.

$$\begin{aligned} &\dot{m}_{eq} = \dot{m}_l \\ &p_{eq} = p_{amb} \quad if \quad p_{eq} \le p_{amb} \quad or \quad \dot{m}_{eq} \ge \dot{m}_l \quad or \quad T_{eq} \le T_b \\ &T_{eq} = T_{inj} \end{aligned} \tag{2.66}$$

For non equilibrium flow using equilibrium factor:

$$p_{nozzle} = p_{inj} - \xi\left(p_{inj}-p_{eq}\right) - \left(1-\xi\right)\left(p_{inj}-p_{amb}\right) \tag{2.67}$$

$$\dot{m}_{nozzle} = \sqrt{\xi\dot{m}_{eq}{}^2 + \left(1-\xi\right)\dot{m}_l{}^2} \tag{2.68}$$

$$T_{nozzle} = \xi T_{eq} + \left(1-\xi\right)T_{inj} \tag{2.69}$$

The liquid temperature is equal to the gas temperature and the quality.

$$\chi_{nozzle} = \frac{Cp_l \left(T_{inj} - T_{nozzle}\right)}{hfg} \tag{2.70}$$

$$\dot{m}_{l\,nozzle} = \left(1 - \chi_{nozzle}\right) \dot{m}_{nozzle} \tag{2.71}$$

$$\dot{m}_{g\,nozzle} = \chi_{nozzle} \dot{m}_{nozzle} \tag{2.72}$$

$$\alpha = \frac{1}{1 + \frac{1-\chi_{nozzle}}{\chi_{nozzle}} \frac{\rho_g}{\rho_l} slip} \tag{2.73}$$

$$\rho_{nozzle} = \left(1 - \alpha\right) \rho_l + \alpha \rho_g \tag{2.74}$$

And at last the velocity at the nozzle will be determined as:

$$u_{nozzle} = \frac{\dot{m}_{nozzle}}{A \rho_{nozzle}} \tag{2.75}$$

A report of the Fire science Centre (1994) presents a compilation of four different models of two phase flow through a nozzle, under different assumptions. The first, the homogenous frozen model (HFM), also assumes that the vapour and the liquid have the same velocity and that the quality of the fluid within the nozzle stays constant. The enthalpy, assuming a negligible liquid contribution, can be expressed as:

$$h_{inj} - h_{exit} = \frac{xk}{k-1} pv_g \left(1 - \eta^{\frac{k+1}{k}}\right) \tag{2.76}$$

The critical mass flux, G_c, is defined as:

$$G_c = \frac{1}{v_{exit}} \sqrt{\frac{2xk}{k-1} pv_g \left(1 - \eta^{\frac{k+1}{k}}\right)} \tag{2.77}$$

Under the assumption of the ratio of the specific volume of the liquid and gas is negligibly small as given by the expression, $\left(1-x\right)v_l / xv_g \ll 1$, Equation (2.77) simplifies to:

$$G_c = \frac{1}{v_{exit}} \sqrt{\frac{pk}{xv_g} \left(\frac{2}{1+k}^{\frac{k+1}{k}}\right)} \tag{2.78}$$

The second model, which applies to fluid conditions of low quality, consists of a modification of the HFM where the effects of the liquid are only taken in the final calculation of the mass flow

$$G_c = \frac{1}{v_{exit}} \sqrt{\frac{2xk}{k-1} p v_g \left(1-\eta^{\frac{k+1}{k}}\right) + 2p(1-x) v_f (1-\eta)} \qquad \textbf{(2.79)}$$

However, in the cases where the quality approaches zero the first term of the above equation can be neglected.

The Moody's model, which is the third model in this report, assumes that the two phases are in equilibrium but do not have the same velocity. This difference in velocity is represented by a slip ratio at the exit, $SLIP_{exit}$, which is equals to $SLIP_{exit} = \left(u_g / u_l\right)\Big|_{exit}$, Fire_Science_Centre (1994). The calculation proceeds assuming annular flow at the exit and then calculating the mass flow per unit area from Equation (2.79) before checking the assumption by the appropriate mass balance.

$$G_{exit} = \sqrt{\frac{2(h-h_{exit})}{\left(x_{exit}\left(v_{g\,exit}\frac{x_{exit}}{\alpha_{exit}}\right)^2 + (1-x_{exit})\left(\frac{1}{SLIP_{exit}} v_{g\,exit}\frac{x_{exit}}{\alpha_{exit}}\right)\right)}} \qquad \textbf{(2.80)}$$

The Henry and Fauske model is based on a presumption of non equilibrium flow but with liquid and vapour again possessing the same velocity. An isentropic expansion is assumed for each phase and the additional assumption is made of small heat and mass transfer between the phases. The critical mass flux is then given by:

$$G_c = \sqrt{\frac{x v_{g\,exit}}{n p_{exit}} + \left(v_{g\,exit} - v_f\right)\frac{(1-x_{exit})N}{s_{g\,exit} - s_{f\,exit}}\left(\frac{ds_{f\,exit}}{dp}\right) - \frac{x_{exit} Cp_{g\,exit}\left(1/n - 1/k\right)}{p_{exit}\left(s_{g\,exit} - s_{f\,exit}\right)}} \qquad \textbf{(2.81)}$$

N is a function of the flow regimes and the throat pressure gradient. If $N=1$, the mass flux is close to the HEM and if $N=0$, the mass flux is close to HFM.

In another study involving an investigation into shock regime in the flow of boiling liquids through a nozzle it has been shown that, as expected, the gas fraction and the velocity discharge depend on both the nucleation before the nozzle, $J(t=0)$, and the

pressure drop through the nozzle, $\wp_{12}$. The two equations for the two flow regimes are given below, Skripov, Sinitsyn et al. (1988).

$$u=\left[\frac{\rho_g g J(t=0) b(t=0) l^{\varsigma+1}}{(\varsigma+1)\wp_{12}}\right]^{\frac{1}{\varsigma-1}} \quad \text{for values of } \wp<<1 \qquad \textbf{(2.82)}$$

and

$$u=\left[\frac{(\varsigma+1)^{\varsigma+2}\rho_g g J(t=0) b(t=0) l^{\varsigma+1}}{\Gamma(\varsigma+1)\left[\Gamma\left(\frac{\varsigma+2}{\varsigma+1}\right)\right]^{\varsigma+1}}\right]^{\frac{1}{\varsigma-1}} \quad \text{for values of } \wp>>1 \qquad \textbf{(2.83)}$$

2.6.2 Spray angle

A technical report from Energy_Analysts_Inc (1990) describes a method for the definition of the jet angle based on the area and the length of the expansion region, as well as the area of the nozzle, as shown by Equation 2.84.

$$\beta=\sin^{-1}\left(\frac{A_{\exp}-A}{2l_{\exp}}\right) \qquad \textbf{(2.84)}$$

Park and Lee (1994) defined the spray angle as the included angle between the lines connecting the nozzle exit and the points at the spray edge at the 20 mm downstream location. The spray angle increases with the injection temperature increment up to certain value and then it decreases. The maximum angle value obtained was about 82 degrees, which corresponded to the maximum pressure of 400 kPa. The maximum spray angle was achieved at the dimensionless superheat, $\Delta T^*=T-T_b/T_{sat}-T_b$, of between 0.45 and 0.85. This dimensionless superheat was larger than the dimensionless superheat previously reported by Nagai, Sato et al. (1985) as 0.55.

An alternative approach to evaluation of the spray angle, based on swirling jet data, was used by Lasheras and Hopfinger (2000) involves the growth rate, γ, of the liquid-gas shear layer. This parameter is related to the ratio of liquid momentum to gas momentum, M.

$$M = \frac{\rho_g u_g^2}{\rho_l u_l^2} \tag{2.85}$$

$$\gamma \approx \arctan\left(\frac{\sqrt{M}}{6}\right) \tag{2.86}$$

This relation only applies for values of $M < 30$ and as long as the liquid core is conical in shape. The maximum value of gamma is then about 40 degrees. However, the spray angle is larger than the liquid-gas shear layer angle (growth rate) because the inertia of the droplets inside of the layer brings about further expansion of the fluid in the jet. The authors deduce from their studies that the spray angle, α, is 45 degrees when $\sqrt{M} >> 1$. Since it is known that the liquid cone angle increases with M and that the total angle, θ, of the spray decreases with M from 90 degrees to 60 degrees approximately, the following empirical expression has been suggested for the spray angle.

$$\theta = 2\left(\alpha - \frac{\gamma}{2}\right) \tag{2.87}$$

The spray angle, α, for a liquid cone surface determined by experiment is reported in Raynal, Villermaux et al. (1999) as being about 50 degrees.

2.6.3 Mass exchange between phases

Aamir and Watkins (2000) proposed a model for the evaporation mass rate developed based on a set of propane data as:

$$\dot{m}_{pv} = A_{pipe} c_{d,pipe} \left(2\rho\left(p_{v,pipe} - p_{pipe}\right)\right)^{0.5} \tag{2.88}$$

The flow evaporation is assumed to occur when the fluid enters the nozzle. An adiabatic heat balance to obtain the quantity of liquid that could flash within the pipe was proposed as follows:

$$\chi f_{lash} = \frac{h_f(T_p) - h_f(T_{wb})}{h_{fg}(T_{wb})} \tag{2.89}$$

The wet bulb temperature, T_{wb}, is taken as the temperature of saturated propane at atmospheric pressure and it is assumed constant throughout the calculations for the spray, as the temperature of the liquid phase.

The Rayleigh Plesset Model (RPM) provides the basis for the mass exchange rate, $\dot{m}_{fg}$, between the liquid and the gas phase equation controlling both, the vapour generation and the condensation processes.

$$\dot{m}_{fg} = F\frac{3r_{nuc}\left(1-r_g\right)\rho_g}{R_B}\sqrt{\frac{2}{3}\frac{\left|p_V-p\right|}{\rho_f}}\left(\frac{\left|p_V-p\right|}{p_V-p}\right) \qquad \textbf{(2.90)}$$

Equation (2.90) is maintained in the case of condensation. Note that there are two values of F for this equation F =50, for vaporising cases and F =0.01 for condensation.

Elias and Chambre (1993) presented a phenomenological model for the prediction of the thermodynamic conditions at the onset of flashing in liquid undergoing a static or flow depressurisation transient. It is obtained that for pulse expansion a liquid may reach the homogenous nucleation limit of superheat before appreciable phase transition occurs. The model considers the decompression of an initially sub-cooled fluid. The flashing inception point is identified as the point at which the rate of pressure recovery due to the phase change equals the initial imposed rate of depressurisation prior to flashing. For an adiabatic system the mass and energy conservation equations are formulated for an expanding volume of fluid expanding as:

Mixture mass

$$\frac{d}{dt}\left(\rho V\right)=0 \qquad \textbf{(2.91)}$$

Vapour mass

$$\frac{d}{dt}\left(\rho_g V_g\right)=\Gamma'_g \qquad \textbf{(2.92)}$$

Mixture energy

$$\frac{d}{dt}\left(\rho V u\right)=-\left(P_g\frac{dV_g}{dt}+P_l\frac{dV_l}{dt}\right) \qquad \textbf{(2.93)}$$

$$u \equiv \frac{\alpha\rho_g u_g + (1-\alpha)\rho_l u_l}{\overline{\rho}} \tag{2.94}$$

$$\overline{\rho} \equiv \alpha\rho_g + (1-\alpha)\rho_l \tag{2.95}$$

$$V \equiv V_g + V_l \tag{2.96}$$

in terms of enthalpy, h, the internal energy is expressed by:

$$U_l - U_g = h_l - h_g + \frac{p_l}{\rho_l} - \frac{p_g}{\rho_g} \tag{2.97}$$

After these definitions realising that prior to flashing point, and rewritten the expression above presented. An explicit expression for the normalised pressure rate as a function of the imposed expansion rate is shown as follow:

$$\frac{d\theta}{dt} = \frac{\gamma}{V}\frac{dV}{dt} - \beta\frac{\Gamma_g}{\rho_g} \tag{2.98}$$

$$\theta = \frac{p_s - p_l}{p_s} \tag{2.99}$$

$$\gamma = \frac{\rho_l^2}{p_s\left(a_h + \rho_l a_p\right)} \tag{2.100}$$

$$\beta = \frac{a_h\rho_g h_{\mathrm{lg}} + \rho_l\left(\rho_l - \rho_g\right)}{p_s\left(a_h + \rho_l a_p\right)} \tag{2.101}$$

At the onset of flashing time ($t = t_m$) the two term of Equation (2.98) balance each other, yielding.

$$\frac{\rho_g\gamma}{\beta V}\frac{dV}{dt} = \Gamma_g \text{ at } t = t_m \tag{2.102}$$

A vapour generation model applicable near the flashing inception point was developed as:

$$\Gamma_g = \int mI(\theta(t))\frac{dg(t,t')}{dt}dt' \tag{2.103}$$

where the bubble size is represented by the kernel function.

$$\frac{dg(t,t')}{dt} = \frac{4\pi r^2}{\sqrt{2\pi mkT}}\left(P_s - P_g\right) \quad \textbf{(2.104)}$$

2.6.4 Flashing location/ Penetration

In cases where the flashing does not occur before or inside the nozzle, the exact location of the flashing corresponds to the length of the liquid core break-up. The study of this length also called as the penetration length has been performed using an experimental technique in which using the discharging liquid in a coaxial gas flow. When a liquid jet emerges from a nozzle as a continuous cylindrical shape, the cohesive and disruptive forces acting on the surface of the liquid create oscillations and perturbations. Under certain conditions the oscillations are amplified and the liquid disintegrates into droplets. This phenomenon is known as primary atomization. If the diameters of droplets exceed some critical dimension they will then disintegrate even further into smaller droplets. This process is called secondary atomization. The phenomenon of disintegration has been studied from the theoretical and experimental point of view for a very long time. A diagrammatic representation of these perturbations of the liquid surface is depicted in Figure 2-14 together with the identities of some of the important parameters, such as velocity and diameters corresponding to each phase.

Figure 2-14 Schematic representation of the liquid break-up indicating the geometry and different lengths used in the analysis. Source: Lasheras and Hopfinger (2000)

Reitz (1990) found that the divergence of the spray cone is due to the expansion processes that occur in an under expanded compressible flow, since that theory implies that the liquid is already atomised upon leaving the nozzle. Instead, the photographs showed that droplets are expelled from the unbroken liquid jet starting at the nozzle exit (presumably by rapid vapour bubble growth within the jet). The core region remains intact for some distance downstream of the nozzle exit, and its break-up eventually producing relatively large droplets. As the liquid temperature approaches boiling, the intact length and the core drop decrease. Then, the operation close to boiling is desirable for effective atomisation. A liquid jet with low degree of superheat remains intact up to some distance from the nozzle, after which it is shattered due to the rapid bubble growth.

Lasheras and Hopfinger (2000) compiled information of coaxial jet identifying the break-up length corresponding to different dynamics mechanisms as a function of five parameters, known as the Reynolds number, Re, the aerodynamic Weber number, We_g, the ratio of the momentum fluxes between the gas and the liquid streams, M, the gas Reynolds number, Re_g, and the mass flux ratio, m. Specifically, this work includes a liquid jet injected into a high velocity annular coaxial gas stream. All the definitions of these parameters are shown below:

$$\mathrm{Re} = \frac{\rho_l u_l d}{\mu_l}, \qquad \mathrm{Re}_g = \frac{\rho_g u_g \left(d_g - d_l\right)}{\mu_g} \tag{2.105}$$

$$We_g = \frac{\rho_g u_g^2 d}{\sigma} \tag{2.106}$$

$$M = \frac{\rho_g u_g^2}{\rho_l u_l^2} \qquad m = \frac{A_g \rho_g u_g}{A_l \rho_l u_l} \tag{2.107}$$

When $M \ll 1$, the actual length of the liquid core is determined by the liquid jet, whilst if $M \geq 1$, the length is determined by the gas stream. The core length is inversely proportional to the M value. The core length, L, can be estimated from conservation mass fluxes using the capillarity wave theory by Mayer (1961) to estimate the mass flux, obtaining a direct expression for the length core calculation as:

$$\frac{L}{D} = \frac{1}{2C_1 M^{2/3}} \left(\frac{\sigma}{\mu_l u_l} \right)^{1/3} \tag{2.108}$$

where C_1 is an adjustable constant. Unfortunately, this expression does not give the correct limit when the surface tension goes to zero, as it is the case when the liquid operates under sub critical conditions. This lack of the prediction close to operating condition is also presented by other empirical correlations, as for instance:

$$\frac{L}{D} = C_2 We^{-a} \, \mathrm{Re}_l^b \tag{2.109}$$

with a between 0.3 and 0.7 and b equal to 0.5.

If the dynamic pressure continuity is establish at the interface between phases can be approximate as shown by Equation (2.110), Rehab, Villermaux et al. (1997).

$$\begin{aligned} &\rho_l u_e^2 = C_e \rho_g u_{RMS}^{'2} \\ &u_{RMS}^{'} \approx 0.17 \left(u_g - u_l \right) \\ &C_e \approx 0.25 \end{aligned} \tag{2.110}$$

Then the length core liquid can be estimated as:

$$\frac{L}{D} \approx \frac{6}{\sqrt{M}} \frac{1}{\left| 1 - u_l / u_g \right|} \tag{2.111}$$

For some cases the effects of the surface tension on the actual instability formation are considerable, so, it is necessary take in account this factor in the dynamic pressure balance at the interface. Then the balance equation becomes different to Equation (2.112), and consequently, the length of the liquid core too.

$$\rho_l u_e^2 + B\sigma/\delta = C_e \rho_g u_{RMS}^{'2} \tag{2.112}$$

$$\frac{L}{D} \approx \frac{6}{\sqrt{M}} \frac{1}{\sqrt{1 - B_1 \sigma / \mu_g u_g}} \tag{2.113}$$

The coefficient B_1 was estimated experimentally to be about 10^{-3}. This expression gives the correct limit when surface tension goes to zero.

Lee and Park (2002b) defined the liquid break-up length as a function only of the Weber number for the flashing fluid, We_l, as:

$$\frac{L}{D} = 8.51 We_l^{0.32} \quad \textbf{(2.114)}$$

In addition, the study of the instabilities of a jet emanating from a nozzle into quiescent surroundings has been performed by Lin and Reitz (1998). They considered using the length of the coherent portion of the liquid jet or its unbroken length, L, as a function of the jet exit velocity as convenient method for categorizing jet break-up regimes. Figure 2-15 shows that the unbroken length at first increases linearly with increasing jet velocity, reaches a maximum, and then decreases (regions A and B). Droplets are pinched off from the end of the jet, with diameters comparable to that of the jet. There then follows a region of discontinuous behaviour of the unbroken length curve. The unbroken length increases again with increasing jet velocity (region C) and then abruptly reduces to zero (region D).

Figure 2-15 Schematic diagram of the jet break-up length curve. Source: Lin and Reitz (1998)

For low velocities, small Weber numbers, it is reasonable to assume that disruption of the jet occurs when the dominant wave's amplitude is equal to the jet radius, and the break-up length is predicted by $\ln(a/\eta_o)$, which was determined to be equal to 12.

Where a is the diameter of jet, and η_o is the initial amplitude of the wave. Then the length of the liquid part of the jet is expressed as:

$$L = \frac{u_r}{\Omega \ln(a/\eta_o)} = \frac{u_r}{12\Omega} \quad \textbf{(2.115)}$$

When the jet velocity increases the definition of the break-up length becomes more difficult, because the break-up mechanism is no longer due to capillarity pinching, but is now due to the unstable growth of short-wavelength surface waves. Lin and Reitz (1998) reported that the break-up length for these cases can be expressed by Equations 2.116, 2.117 and 2.118. The typical value of constant B for diesel sprays nozzles and is 4.04.

$$\frac{L}{D} = 0.5 \frac{1}{f(T)} B \sqrt{\frac{\rho_g}{\rho_l}} \quad \textbf{(2.116)}$$

$$f(T) = \frac{\sqrt{3}}{6}\left(1 - e^{-10T}\right)$$
$$T = \frac{\rho_l}{\rho_g}\left(\frac{\mathrm{Re}_l}{We_l}\right)^2 \quad \textbf{(2.117)}$$

2.6.5 Temperature effects

Miyatake, Tomimura et al. (1981a) and Miyatake, Tomimura et al. (1981b) made an experimental study on spray flash evaporation on superheated water injected through a circular tube nozzle into low-pressure vapour zone. The inlet temperature was 40, 60 or 80 Celsius degrees. An empirical equation suitable for predicting variation of liquid temperature with residence time was presented. The nozzles used were made of glass tube, and had internal diameters of 0.346, 0.502 and 0.815 cm, with lengths of 12, 25 and 25 cm, respectively. The experiments were conduced based on the Reynolds and the Weber number, both based on the mean velocity of liquid in the nozzle, $\bar{u}$. The degree of superheat was defined as the difference between the temperature of liquid at the nozzle exit, T_o, and the temperature of the external vapour, which can be regarded as the saturation temperature corresponding to the vapour pressure in the flash chamber, $T_{sat}(p_v)$.

$$\Delta T_s = T_o - T_{sat}(p_v) \tag{2.118}$$

Whilst the dimensionless temperature of liquid in the centre of the jet, is defined as:

$$\theta = \frac{T_z - T_{sat}(p_v)}{T_o - T_{sat}(p_v)} \tag{2.119}$$

The range of variation of the superheat and dimensionless temperature of liquid in the centre of the jet was ±0.19 and ±0.08 respectively. The resident time is calculated, based on the assumption of the jet velocity is equal to $\bar{u}$ as:

$$t = \frac{z}{\bar{u}} \tag{2.120}$$

With the increment of ΔT_s the flashing becomes more violent, and the liquid column, which is seen near to the nozzle exit, becomes shorter, letting θ drop faster. For lower superheat although the droplets splash from the liquid surface, the liquid column remains in the core of jet and consequently, decreases slowly. When superheat increase the column is disintegrated in the early period of evaporation, after which slower evaporation of generated droplets is induces. As the spray flash evaporation undergoes two exponential decaying processes expressed as

$$\theta = e^{-s_1(t-t_o)} \qquad t_o \le t \le t_i \tag{2.121}$$

$$\theta = e^{-s_2(t-t_o)} \qquad t_i \le t \tag{2.122}$$

where t_o is the time lag of the initiation of flashing and t_i are the values of the interception of the two functions. The whole behaviour of the dimensionless temperature is shown in Figure 2-16.

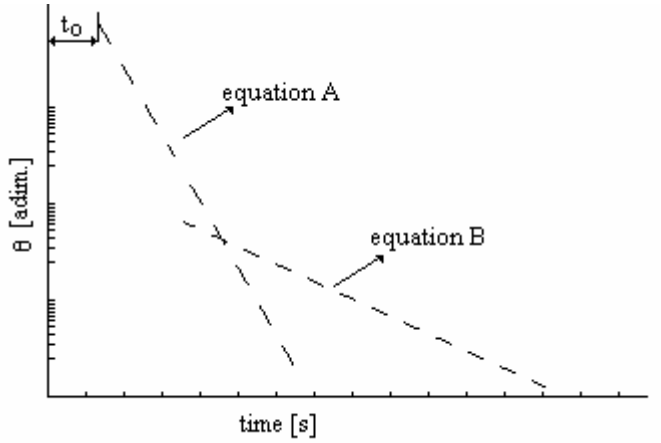

Figure 2-16 Typical relations between dimensionless temperature of liquid in the centre of the jet and time

For the first section denoted by the name of: equation A, the evaporation mass flux, m, can be estimated as:

$$\dot{m} = \frac{C_P \rho d}{4L} \frac{dT_z}{dt} \qquad \textbf{(2.123)}$$

As s_1 is also a function of the physical properties, the coefficient of the driving force for flash evaporation, Ψ, and the diameter.

$$s_1 = \frac{4L\Psi}{C_P \rho d} \qquad \textbf{(2.124)}$$

After comparison with experimental data, a expression for $s_1 d$ was reported as:

$$\left(s_1 d\right)_{max} = 52e^{0.053\Delta T_s} \qquad \textbf{(2.125)}$$

As well the value of s_2 was determined as:

$$s_2 = 0.22 s_1 \qquad \textbf{(2.126)}$$

The time lag of the initiation of flashing, t_o, correspond to the time required for the jet to flow through the liquid column region near to the nozzle, so the length of the dimensionless liquid column can be calculated from

$$\frac{z_o}{d} = \frac{\bar{u} t_o}{d} = \frac{21.9}{\left(\Delta T s\right)^{1/3}} \qquad \textbf{(2.127)}$$

The temperature profile along the centre line shown by Allen (1998a), suggests that the Minimum Temperature Distances (MTD) measured correspond to the limit of droplet existence, at 0.66 m. The measured temperature at this location was –70 Celsius degrees. After this point there is a rapid rise in temperature to 25 Celsius degrees in 0.1 m. Temperatures continues to rise downstream, though the rate of increase diminishes. It is believed that the MTD for any release will be between x/D=150 and x/D=170 Allen (1998a).

For the same diameter of discharge nozzle of 4 mm, experimental data from studies by MTD of R134a, Yildiz, Beek et al. (2002a), with similar values of MTD exhibit the same thermal profile behaviours as the data reported by Allen (1998a). Although the minimum temperature was about –60 Celsius degrees, different to that for propane, the gap between the minimum temperature and the boiling point of each fluid was about 30 degrees. Moreover, for different nozzle diameters the MTD increases but the temperature gap stays constant Yildiz, Rambaud et al. (2003).

2.6.6 Minimum Temperature Distance (MTD)

According to the work performed by Allen (1998a), it is believed that MTD for any release will be between x/D=150 and x/D=170, actually the MTD to his experiment done for a 4mm nozzle was located at x/D=165. Any difference from the full-scale release can be related to the influence of atmospheric conditions, e.g. wind. The data from Yildiz, Rambaud et al. (2004) for the same diameter as Allen's work maintain this trend, but data corresponding to smaller diameter (1 mm and 2 mm) nozzles showed MTD over this distance. So, it is not possible to make a conclusion about the location of MTD for general cases. Nevertheless, this situation suggests that propane and R134a exhibit similar thermal profile behaviours, in terms of minimum point location, for the same nozzle dimension, but the actual value of the minimum temperature was different, about –70 Celsius degrees for propane and about –60 Celsius degrees for R134a.

2.7 TURBULENCE

2.7.1 Effect of droplets on turbulence structures

The effects of the presence of droplets into a flow are not always clear to understand. Some simplifications are made to explain the basis of the physics behind of the droplets bodies. For example the study of cylinder submerged in a flow is used as a sort of 2D simplification of the whole process. So, Figure 2-17 shows the intrusion of a cylinder in a flow for low (140) and high (1000) Reynolds number. There it is possible to observe some turbulent structures behind those shapes, normally known as vortex shedding presented for a wide range of Reynolds number.

Figure 2-17 Vortex shedding at Reynolds number Re=10.000 (left part) and Re=140 (right part). Source: Potter, Wiggert et al. (1997)

However, due to the droplet presence in to a flow is taken as spheres shapes in to a flow, the three-dimensional characteristics of the turbulent structures formed behind those spheres are much more complicated that the one generated behind cylinders, and also due to the large number of droplets, which can interfere each other and with the structures already created by others droplets, as it is highlighted for the cases of two cylinder in Figure 2-18, the whole situation is even more complex. However, it is clear that from the conservation of energy law, the vortex created as result of a chain of events must contain less energy than the first one, so, for a flow through a large number of droplets the energy will be dissipated after a certain length.

Figure 2-18 Vortex Shedding. Flow around circular cylinders, Re=100. Source: Chalmers (2007)

For low Reynolds numbers and a pure undisturbed flow the effects of the presence of spheres particles into that flow consists basically in an induced deformation of the main flow stream lines around their bodies. This deformation will depend on the relative movement between the droplet and the mean flow. For a single droplet moving opposite to the main flow, with a relative low Reynolds number, the flow will follow its body and not vortex shedding are created after the particle, meanwhile, if the droplet has the same direction of the mean flow, the droplet surface attracts the streamlines of the flow close its body, as shown in Figure 2-19 and Figure 2-20, Happel and Brenner (1983).

Figure 2-19 Streamlines for streaming flow past a sphere. Source: Happel and Brenner (1983)

Figure 2-20 Streamlines for a moving sphere. Source: Happel and Brenner (1983)

Although the above explanation helps to draw a brief image about what happens when droplet are introduced into a flow, it does not cover the whole complex phenomenon presented. So, a more extend review will be displayed next.

If the particles are significantly smaller than the Kolmogorov length scale then the effects of the particles can be treated as point sources in the turbulent fluid. However, if the particles are comparable to, or larger than, the smallest scales of turbulence, the contribution of the boundary layers on these particles surfaces to the dynamics of the turbulent flow must be included, Crowe, Troutt et al. (1996).

The dispersion of the particles in the flow is controlled by the local velocity fluctuations. Also, the velocity fluctuations produced by the particles in the fluid affect the Reynolds stresses, as well as, the effective thermal conductivity of the carrier phase. The particles in turn, can affect the turbulence either by increasing the turbulence energy or increasing the dissipation rate (turbulence modulation). Other turbulence induced effects are the changes in the drag and the heat transfer rate between the fluid and the particle dispersion and turbulence modulation. The small particles will attenuate the turbulence while the large particles will generate turbulence, Crowe, Troutt et al. (1996).

Saffman (1973) showed that the perturbation in the fluid due to the presence of a particle decays as the sum of two contributions, one as $1/r$ (long range) and the other as $1/r^3$ (short range), with r as the radius of the droplet. For relatively small particles to the smallest length scale of the flow, and for particles separated by a distance L larger than their diameter d, the most important interactions are long-range, Koch (1990). Neglecting the short range interactions, e.g. particles wakes, is justifiable for particles

with diameters smaller than Kolmogorov's length scale of the flow field undisturbed by the presence of the particle, since in that case the short range perturbation are dissipated by the viscosity.

The force in the flow is opposite to the force applied to the particle 'n' by the fluid. The forces acting on a particle can be considered to come from three different sources or reasons. The first contribution is related with the virtual force that would apply on a fluid element that coincides with the particle position, i.e., the pressure forces and the viscous stresses. The second contribution is related with the perturbation of the fluid flow due to the presence of the particle, for a rigid sphere of diameter '*d*' in translation, this perturbation of the surrounding unsteady non-uniform flow results in the drag, added mass and the Basset history forces, and the third contribution is due to the gravitational settling, Saffman (1973).

Squires and Eaton (1990) and Wang and Maxey (1993) found that the overall reduction in turbulence kinetic energy for the increasing mass loading was insensitive to the particle relaxation time. A strong preferential concentration of particles into regions of low vorticity and regions with large strain rates were shown. For cases of turbulence modulation, Squires and Eaton (1994) attributed the non-uniform distortion of the turbulence energy spectrum by particles to preferential concentration.

Lance and Bataille (1991) identified three types of non-linear coupling: the first is the stretching of the shear-induced vortices in the potential flow around the bubbles. Second is the deformation of the bubbles by these vortices, which changes the virtual volume coefficient of the bubbles and also the drag force. Similarly, the liquid eddies may be deformed too, Kataoka and Serizawa (1989).

Elghobashi and Truesdell (1993) described the particle motion using the equations derived by Maxey and Riley (1983), which treats the forces from the undisturbed flow and the disturbance flow created by the presence of the particles, separately. For the larger density ratios considered in these simulations particle motion was influenced by the drag and the gravity. The coupling between the particles and the fluid resulted in an increment of the small-scale energy. The relative increasing in the energy of the high-wave number component of the velocity field resulted in a larger turbulence dissipation rate. The effect of gravity resulted in an anisotropic modulation of the turbulence and an

enhancement of turbulence energy level in the direction aligned with gravity. Furthermore, in the directions orthogonal to the gravity vector, the reverse cascade of energy from small to large scales was observed. Both Squires and Eaton (1990) and Elghobashi and Truesdell (1993) have shown that the distortion of the turbulence energy spectrum is sensitive to quantities such as the particle relaxation time. This implies that the energy transfer from the particles to the turbulence acts non-uniformly across of the spectrum.

Boivin, Simonin et al. (1998) highlighted the fact than in turbulent shear flows with particles, it is often difficult to separate the direct modulation of the turbulence due to the momentum exchange with particles from the indirect changes occurring through modification of turbulence production mechanisms via interactions with the mean gradients. This work was focused on the class of dilute flows in which the particle volume fractions and the inter-particle collisions are negligible as well as the gravitational setting. The particle motion was assumed to be governed by drag with particle relaxation times ranging from Kolmogorov's scale to the Eulerian time scale of the turbulence and for the particle mass loadings up to 1. The Direct Numerical Simulation (DNS) showed the particles increasingly dissipate the fluid kinetic energy with increased loading, with the reduction in kinetic energy being relatively independent of the particle relaxation time, meanwhile, the viscous dissipation in the fluid decreases with increased loading and it is larger for particles with smaller relaxation times. The energy spectra of the fluid showed that there is a non-uniform distortion of the turbulence with relative increasing in the small scale energy, and the non-uniform distortion mainly affects the transport of the dissipation rate.

2.7.2 Standard k-ε turbulent model

The standard κ-ε turbulent model is based on the proportionality of the turbulent kinetic energy, κ and the rate of viscous dissipation, ε, on the characteristic length scales (velocity and length). The κ-ε model was developed originally for a single phase fluid transport flow, and it comes from the application of the Reynolds hypothesis (see Appendix A) in the Navier Stokes equation. The κ-ε model is a mechanistic model, in which the transport equations for the turbulent kinetic energy and the dissipation rate are involved, Lee, Lahey et al. (1989). The main assumptions of this model are the

turbulence phenomenon as isotropic, homogenous, and it has a high Reynolds number. Under the isotropic turbulence assumption, the velocity turbulence fluctuation ($\overline{u_i^{'2}}$) is the same in all directions. Therefore the turbulence kinetic can be expressed as:

$$k = \frac{3}{2}\overline{u_i^{'2}} \tag{2.128}$$

The introduction of the only one turbulent velocity scale, in the order of magnitude analysis of the κ-ε model for single-phase flow turbulence, affirms the hypothesis of the turbulent flow is nearly isotropic, Tennekes and Lumley (1973).

Dissipation for an eddy of size l, is expressed by

$$\varepsilon = E_o \frac{k^{\frac{2}{3}}}{l} \tag{2.129}$$

The partial differential equations for the κ-ε are presented as following:

$$\frac{\partial}{\partial t}(k) + (\overline{u_i})\frac{\partial}{\partial x_j}(k) = \frac{\partial}{\partial x_j}\left(\left(\nu + \frac{\varepsilon_m}{\sigma_k}\right)\frac{\partial}{\partial x_j}(k)\right) + \frac{\varepsilon_m}{\sigma_k}\left(\frac{\partial}{\partial x_j}(\overline{u_i}) + \frac{\partial}{\partial x_i}(\overline{u_j})\right)\frac{\partial}{\partial x_j}(\overline{u_i}) - \varepsilon \tag{2.130}$$

$$\frac{\partial}{\partial t}(\varepsilon) + (\overline{u}_j)\frac{\partial}{\partial x_j}(\varepsilon) = \frac{\partial}{\partial x_j}\left(\left(\mu + \frac{\mu_T}{\sigma_\varepsilon}\right)\frac{\partial}{\partial x_j}(\varepsilon)\right) - \frac{\varepsilon}{k}\left(C_{\varepsilon 1}\overline{u_i u_j}\frac{\partial}{\partial x_j}(\overline{u_i}) + C_{\varepsilon 2}\varepsilon\right) \tag{2.131}$$

A general set of acceptable values are C_1=1.4, C_2=1.92, σ_ε=1.00, σ_k=1.30 and σ_μ=0.09. Additionally, Eddy viscosity is assumed as shown by Equation (2.132).

$$\nu_t = \frac{C_\mu k^2}{\varepsilon} \tag{2.132}$$

2.7.3 Two-phase flow k-ε applicability

Although the dynamics involved inside a two-phase jet seem to be very complex, the treatment of two-phase flow is based on the application of the continuity, the momentum and the energy equations for each phase. The application of the single phase developed κ-ε turbulence model for predicting the turbulent behaviour of the jet and the droplet inside rest on the assumption of the interactions between the phases can be introduced in the equations corresponding to using the one way or two ways coupling

methods. Different authors have studied the applicability of the κ-ε turbulent model to two-phase flow cases, as a natural extension of the single phase model, in which considerations about the generation or the dissipation of turbulence due to the presence of a second phase are incorporated, Lee, Lahey et al. (1989). For a one way coupling model, it is assumed the presence of the particle phases has a negligible effects on the properties of the carrier phase; this assumption is normally valid for small particle-fluid concentration ratios or high Stokes numbers (the particles motion is unaffected by the carrier flow field). The two ways coupled numerical method includes the effects of the particle in the carrier phase.

The experimental results from the study of turbulence on the bubbly flow confirm that the effect of the interfacial interactions on the turbulence of the liquid phase is important and it is assumed to have the same importance for any other disperse particle flow. However, the dynamics of the bubbles is far away from the dynamics of the particles or the droplets flow, because of the pliant surfaces, the significance of buoyancy forces presented, and the differences in the dominant physics on the particle motion based on the concentration of the disperse phase in the flow. Then, the determination of the type of flow as dilute or dense becomes also important. In the dilute flow the particle motion is controlled by the surface and the body forces on the particle, whilst in the dense particle flows, the trajectory is controlled by the particle-particle collision or interactions, Crowe, Troutt et al. (1996).

For droplets transported by the flow, the diameter size and the comparison with the size of turbulent structure, known as eddies, could be significant in the determination of the turbulence generation or dissipation. The effect generated by the mass exchange at the surface of the droplet with the main flow and in consequence the movement of the surface due to droplet diameter changes, can generate a considerable impact in the main properties of the fluid around the droplets.

2.8 SUMMARY

After the review done it comes out quite easy that there is not a unique criterion to identify the types of jets than can be founded after a leak under different circumstances. There are different categories which involve three or four kind of jet as output. These

categories in most cases correspond to researches descriptions rather than specific quantitative values. Therefore, it is difficult to compare the results of two or more distinct criteria. In term of the mass calculations, it is clear that the isentropic flow hypothesis does not represent the complex physics involves in a flashing yet. The obtained values of mass and velocity at the beginning of the jet can have a large variation according to the extra hypothesis used to treat the gaseous phase, such as critical condition. The use of CFD techniques to simulate flashing jet is limited by the understanding of the implications of the different effects that droplets and turbulence models can have of the general behaviour of the jet.

CHAPTER 3. ANALYTICAL DEVELOPMENTS

3.1 INTRODUCTION

The key of the original work developed and presented in this chapter is the understanding of the physics involved in a flashing process; therefore all the analysis and developing work shown here are the main contribution of this work.

There is an interaction between mechanical and thermodynamical mechanisms, as heat transfer, phase change, momentum transfer, etc. All these mechanisms are presented since the inside of the vessel which contains a superheated liquid up to the two-phase jet formed. This jet has the characteristic of been a vapour jet with liquid of superheated liquid inside the vapour stream. So, there is a transformation process inside the fluid governed by the nucleation process that goes from a 100% liquid condition, where the liquid is a continuous single phase, to different station of bubbles generation until the amount of bubbles breaks the liquid core and the vapour becomes the continuum phase and the liquid remains as droplets. After the analysis all the information available it is proposed that thermodynamical mechanisms has the most important role in the formation of the jet in the area around the nozzle, and the mechanics mechanisms are more relevant downstream of the jet after the expansion zone is over. However, both mechanisms are taken into account for developing of the qualitative model which determines whenever a jet after a leak is going to be a liquid jet of two-phase flashing jet.

3.2 FLASHING PROCESS

The flashing process is a non-isentropic process with highly complex physics. The process covers a large number of thermodynamic and mechanic interactions. Due to that, currently there is not a general model that can describe or reproduce the real characteristics of the process. Three dimensional modelling using computational means

is not possible at the moment. Consequently a one dimensional approach has been chosen.

The relationship between the nucleation process and the generation of a droplet in a discharge of superheated liquid relies on the nucleation mechanism, which is responsible for the breaking of the liquid continuum. Initially the phase change takes place inside the liquid. This process is manifest by the appearance of number of vapour bubbles inside the liquid. As the number of bubbles increases and the bubbles already created grow in volume, the total presence of the vapour phase increases. This can be expressed as an increase of the void fraction of the mixture.

The development of a macroscopic vapour bubble in a superheated liquid can be divided into two phases:

(i) In the first Rayleigh phase the bubble growth is limited by inertial forces

(ii) In the second (thermal) phase the growth is limited by the delivery heat

The drop in pressure causes the liquid to enter into the metastable region. In the first stage of the process the vapour content is considerably less than the content corresponding to equilibrium condition, the degree of disequilibrium being determined by the rate of vapour generation. The rate of vaporization varies the density of boiling centres, which depends strongly on the pressure and temperature. In turn, the nucleation kinetics is governed by the pressure in the system during the initial phase of explosive boiling. At moderate superheat the discharge rate through short nozzles is practically the same as of non-boiling liquids. However, at large superheat the intensity of the nucleation process is altered substantially. Because of the dependence of the rate of fluctuating nucleation on the location in the metastable region, the development of boiling is no longer limited by the rate of formation of vaporization centres. In fact, the quantities of vapour generated produce a blockage in the flow at the exit cross section. The vapour content causes the critical discharge conditions to be satisfied.

In superheated liquid the vapour first appears as individual bubbles by nucleation process. If a considerable number of nuclei are reached, the original liquid continuum will contain vapour bubbles covering the total volume. If the nucleation progresses further then the liquid breaks into droplets and the gas becomes a compressible continuous phase. The estimation of how many bubbles are created by nucleation inside

the liquid core, before it reaches the nozzle, is not well established in a quantitative manner.

The selected approach for this work is based on three separate, but connected parts based on the main role of the nucleation process. The first part is to determine if flashing is likely to take place or not under certain conditions. The second part is to carry out the actual calculation of the liquid mass flow, as well as, the vapour mass flow of the system and third the evaluation of flashing jet using those mass fluxes in junction with others considerations as boundary conditions of the CFD simulations.

3.3 AN ANALYTICAL MODEL OF FLASHING ACROSS AN APERTURE WITH PRESSURE CHANGE TO DETERMINE THE PRESENCE OF FLASHING

It is seen that nucleation has a significant effect on flashing as an initial process that produces the breaking of the liquid continuum, C Cartes (2004). Nuclei are the starting point of gas bubbles inside the liquid and they are in turn responsible for the liquid transformation into droplets after the release. The total nucleation is responsible for all the vapour in the jet, R Ramanathan (2005), Frost, Barbone et al. (1995).

Since the major changes in fluid are produced in the flow direction, the simplest model to represent the physics of flashing jet corresponds to a one dimensional model. The only dimension being in the direction of the flow. This model is based on a second order system which accounts for damping forces and stiffness forces over the nucleation process of a system driven by temperature differences and pressure differences at conditions where phase change occurs for liquids.

There are similarities between the parameters that influence the nuclei generation process and the physical parameters that take part in the motion generation within a damped second order system and the type of response that the system can have under certain circumstances. For instance, both system need to achieve a minimum level of energy to initiate the process, the type of response of the whole system to the velocity of the changes, the behaviour of the system will change drastically with the output of the system.

It is possible to think that, every case of leakage has the possibility to experience an explosive nucleation, a very weak nucleation or no nucleation at all. The possibilities of the actual system response will be determined by the interaction between the parameters involved in the stiffness coefficient and the dissipation coefficient. The variable to be consider as the modelled parameter for the model proposed is the number of bubble clusters generated, called N. The nucleation rate of bubble clusters, $\dot{N}$, is determined from the balance of those parameters by the second derivative of the numbers of nuclei, $\ddot{N}$, as expressed by Equations (3.1). This equation expresses the balance of forces acting on the vapour created by nucleation per unit volume. The terms K and C represent the stiffness coefficient per unit volume and the damping coefficient per unit volume of the equivalent system modelled.

$$\rho_g \ddot{N} = -C\dot{N} - \mathrm{K}N \qquad \textbf{(3.1)}$$

The normalized form of Equation (3.1) is presented by Equation (3.2). The normalization was made based on gas density value. The physical meaning of this normalization is that the coefficients of Equation (3.2) represent the stiffness and damping coefficient by unit mass instead of unit volume. No mass term is considered on its own. The solution of this equation will depend only on stiffness coefficient per unit mass, K^*, and damping coefficient per unit mass, C^*. The stiffness coefficient per unit mass and damping coefficient per unit mass will be named here after as the production coefficient and the dissipation coefficient of the nucleation system. So, the left hand side term represents the number of bubbles per second squared instead of defining the acceleration as distance per second squared.

$$\ddot{N} = -C^*\dot{N} - K^*N \qquad \textbf{(3.2)}$$

Where the production coefficient, K^*, at Equation (3.2) represents the interaction of all parameters that potentially promote of the nucleation process; meanwhile the dissipation coefficient, C^*, represents the influence of the parameters that tries to slow down the nucleation. The corresponding units of those coefficients are the inverse of second squared and the inverse of second, respectively. The natural frequency of this

type of system is defined by Equation (3.3) and $\varphi = \frac{C*}{2\sqrt{K*}}$ he damping ratio of the system is defined by Equation (3.4).

$$w_n = \sqrt{K*} \tag{3.3}$$

$$\varphi = \frac{C*}{2\sqrt{K*}} \tag{3.4}$$

Considering the homogeneous solution to Equation (3.2), it was find the following two roots based on the natural frequency and the damping ratio of the system, as Equation (3.5) shown. The output of the squared root will determine if the roots are real numbers or complex numbers.

$$N_{1,2} = -\varphi w_n \pm w_n \sqrt{\varphi^2 - 1} \tag{3.5}$$

The behaviour of the system will obey of the type of output obtained from Equation (3.5), especially from the term highlighted in Equation (3.6).

$$\sqrt{\varphi^2 - 1} = \sqrt{\frac{C*^{\,2}}{4K*} - 1} \tag{3.6}$$

When a system is suddenly exposed to a perturbation produced by the pressure gradient between the inside and outside of the vessel, the behaviour of the system could be identified as under damped, damped or over damped system.

- An over-damped system the liquid will stay liquid even after the nozzle
- A damped system will correspond to the case where the liquid has vapour bubbles inside of the core region is present after the nozzle
- An under damped system will correspond to the full atomized case, where the remaining liquid is present as droplets after the nozzle

All these conditions are connected with the solution of Equation (3.6), which can be expresses based on the balance of the characteristic coefficients involved in the system, as the following expression shown:

$$4K^* < C^{*2}\ over-damped \quad 4K^* = C^{*2} \quad damped \quad 4K^* > C^{*2} \quad sub-damped \qquad \textbf{(3.7)}$$

The first task is to identify the parameters that affect the damping and the stiffness coefficients of the equivalent system. These parameters must include the nature of the fluid represented by the pressure-temperature relationship, the fluid properties, as well as, the geometry characteristic of the system and the kinetic and thermodynamics characteristics of the flow.

3.3.1 Pressure-temperature relationship

The function of the saturation line, identified as sat in Figure 3-1, suggests that there is a stronger dependence on temperature over changes in pressure for small values of pressure ratio. When the pressure increases and becomes closer to the critical point the dependence of temperature on pressure is much smaller. However, for the case of the liquid spinodal line, defined by the van der Waals equation of state, also shown in Figure 3-1, this relationship is a linear function with positive gradient in the range evaluated. In the region limited by the spinodal line, the saturation line represents the theoretical range of superheat that the fluid can achieve. Figure 3-1 shows that when reduced pressure or reduced temperature increases, the range of possible degree of superheat is reduced. Based on this condition an increment of pressure will be related to an increment in temperature or the other way around. Larger values of temperature or pressure increase the thermal and pressure energy in the fluid, which in case of any release to ambient atmospheric conditions will need to be dissipated by the jet on its way out. The sudden dissipation of larger quantity of energy generates a more violent phase change inside the container and the jet, as the larger amount of energy have to be dissipated over a short distance.

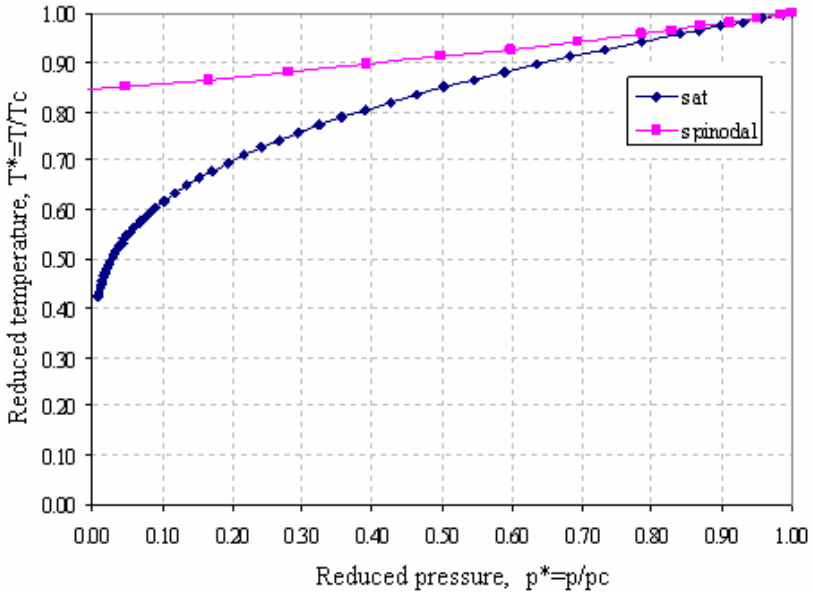

Figure 3-1 Schematic saturation and spinodal line for water. Saturation data taken from properties table, Spinodal data was calculated following the definition of Van der Waals equation of state

A convenient way to quantify the influence of the superheated condition on a flashing problem is to use a representation of the energy inside the superheated liquid state. E_S is proposed to be as the ratio of superheated temperature and saturation temperature at ambient condition times the injection pressure divided by the mixture density. This is shown in Equation (3.8). The first bracket of this equation represents the proportion of the injection temperature over the saturation temperature. The second bracket represents the kinetic energy of the fluid when it behaves as homogeneous mixture discharging to zero pressure ambient. This implies the maximum theoretical value of energy that the system can achieve, under Bernoulli's formulation for a homogeneous mixture.

$$E_S = \left(T_{inj} / T_{sat(Pamb)}\right)\left(p_{inj} / \rho_{mix}\right) \qquad \textbf{(3.8)}$$

The ratio of the kinetic energy of a mixture discharge calculated using Bernoulli equations and the energy of the superheated liquid state, Ge, is much more helpful. The denominator of this ratio contains the influence of the superheated temperature of the fluid, which involves two phase flow considerations. This ratio can be considered as a ratio of the kinetic energy and the thermodynamic energy available in the fluid. This ratio is expressed by Equation (3.9):

$$Ge = \frac{u_{discharge}^{2}/2}{\left(T_{inj}/T_{sat(Pamb)}\right)\left(p_{inj}/\rho_{mix}\right)} \quad \textbf{(3.9)}$$

The discharge velocity is proportional to the squared root of the pressure difference divided by the density of the mixture. In case of liquid discharge the mixture density becomes the liquid density, and if gas is present mixture density is calculated using the void fraction of the mixture. Either way mixture density in Equation (3.9) is cancelled out, then the ratio can also be rewritten as:

$$Ge = \frac{\left(p_{inj} - p_{amb}\right)T_{sat(Pamb)}}{T_{inj}\,p_{inj}} \quad \textbf{(3.10)}$$

Where T_{inj}, p_{inj} correspond to the temperature and the pressure at the injection point or vessel interior, p_{amb} is the ambient pressure and, T_b is the temperature at the boiling point. Frequently, the $T_{sat(Pinj)}$ is unknown, so, the real concept of degree of superheat is $\Delta T = T - T_{sat(Pinj)}$, which is substituted by the $\Delta T = T - T_{sat(Pamb)} = T - T_b$.

For a superheated liquid, the injection temperature will be larger than the saturation temperature at the corresponding pressure and also larger than the boiling temperature. Consequently, the ratio of T_b/T_{inj} will be smaller than unity. For smaller values of this ratio the perturbation of the single phase behaviour will be more important that for larger values of this ratio.

From Figure 3-2 it can be observed that the influence of a superheated condition on the flow is more noticeable at larger reduced temperature and larger reduced pressure. The area enclosed between the extremes of the lines of reduced pressure is reduced when the energy ratio increase, therefore, it is clear that any change produces by the rupture of the vessel that contains the superheated liquid will produce major effects of the fluid. So, the energy ratio can be used as indicative of trend of the fluid to be more affected by the two phase considerations.

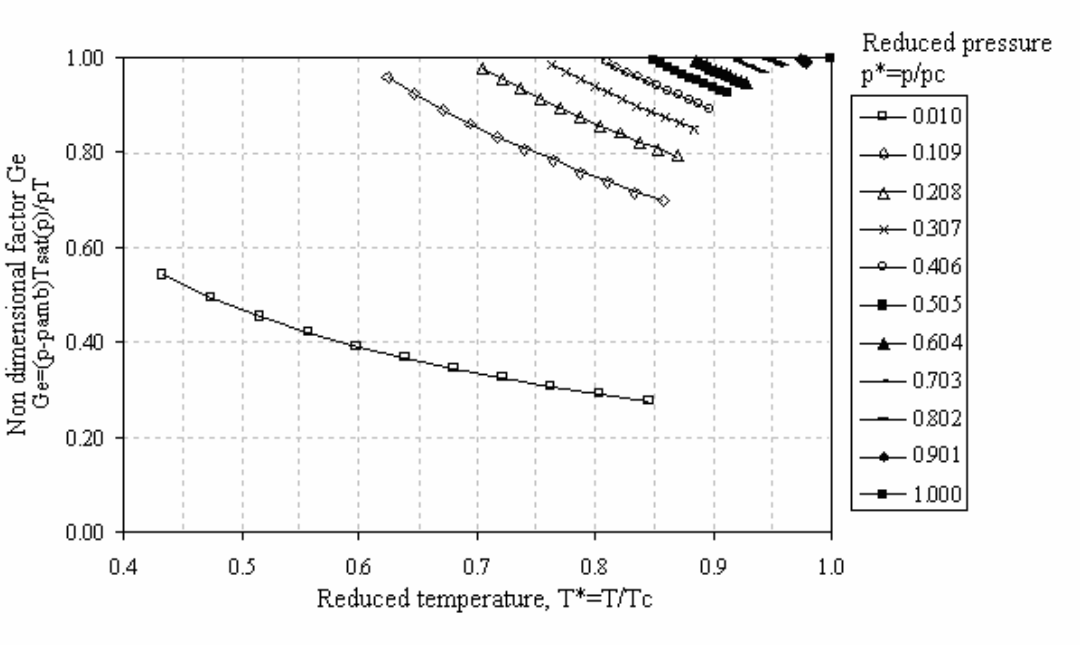

Figure 3-2 Schematic behaviour of the ratio of the kinetic energy and the thermodynamic energy available in the fluid as a function of reduced temperature and reduced pressure

The effect that the pressure-temperature relationship has on the stiffness and the damping of the overall system is significant. Even both parameter pressure and temperature are related it is proposed that the production coefficient of the system will be more influence by the pressure difference than the temperature difference as main source of energy in the fluid exit. The difference of pressure, $\left(p_{inj} - p_o\right)$, represents the total pressure range were the depressurization of the fluid is taking place. It is also related with the kinetic energy of the fluid at the exit. The effect of the temperature is proportional to the squared root of the normalized boiling temperature. The normalized boiling temperature is defined as the ratio of the difference of injection temperature and the boiling temperature and the injection temperature, $\sqrt{\Delta T_b / T_{inj}}$. The difference represents the range of the temperature variation of the fluid between the interior of the vessel and the nozzle, where the temperature has been reported to be the boiling temperature. This range is the maximum level of superheated that theoretically a fluid can achieve if the initial and final location are compared. The ratio represents the percentage of the temperature range of the total injection temperature. This ratio varies between 0 and 1. For higher values there is more heat which needs to be transported by

the fluid during the expansion process. The exponent 0.5 or squared root of this ratio introduces the non linear effect of the temperature on the production coefficient.

The effect on damping per unit mass or dissipation coefficient is based on the normalization of the pressure and temperature respect to the critical values. Both temperature and pressure by themselves do not mean how important is their influence, but their relative position to the critical values express the level of energy needed to produce a big change in the fluid condition. The relative position of those values with respect to the pressure and the temperature at the critical point, will give an indication of resistance of the fluid to nucleate. This resistance will vary from one fluid to another and from geometry to another. If those parameters are far to the critical values that mean that the terms, $\frac{(T_c - T)^2}{T}$ and $\frac{(p_c - p)^2}{p^{0.5}}$, will increase and therefore the dissipation coefficient will also increase. A large dissipation coefficient means the system is more likely to keep the liquid condition. The term $\frac{(T_c - T)}{T}$ is the normalized critical temperature. The normalized critical temperature is defined as the ratio of the difference of the critical temperature of the fluid and the injection temperature and the injection temperature. The difference represents the range of the temperatures variation of the fluid between the injection temperature and the maximum temperature that the fluid can achieve at the interior of the vessel. The critical conditions correspond to the most unstable state that the fluid can achieve. A smaller ratio implies more possibilities to the fluid to experience flashing. A similar situation is represented by the normalized critical pressure, $\frac{(p_c - p)}{p_o}$. If normalized critical temperature and critical pressure increase, the dissipation coefficient will also increase. A large dissipation coefficient means the system is more likely to keep the liquid condition. The contribution of both temperature and pressure to the dissipation coefficient is expressed as function of the normalized critical values as well as the difference of the critical value of the fluid and the value of the corresponding parameter.

Both terms, $\frac{(T_c - T)}{T}(T_c - T)$ and $\frac{(p_c - p)^{0.5}}{p_o^{0.5}}(p_c - p)^{1.5}$ can be interpreted as the weighting functions of the influence of injection temperature and kinetic energy inside the vessel, expressed by the pressure difference power 1.5. In particular the squared root in the normalized pressure implies the consideration of the order of magnitude of the pressure does not affect in major degree the dissipation process.

3.3.2 Fluid properties

To understand how the fluid properties dependence on pressure and temperature has a significant impact on the analysis of the characteristics of the resulting jet, as well as, on the dimensionless parameters that can be used to describe them.

Starting the study of the density behaviour, it is clear that when the pressure increases, a reduction of liquid density and the change in gas density can be observed on a T-v diagram of Figure 3-3.

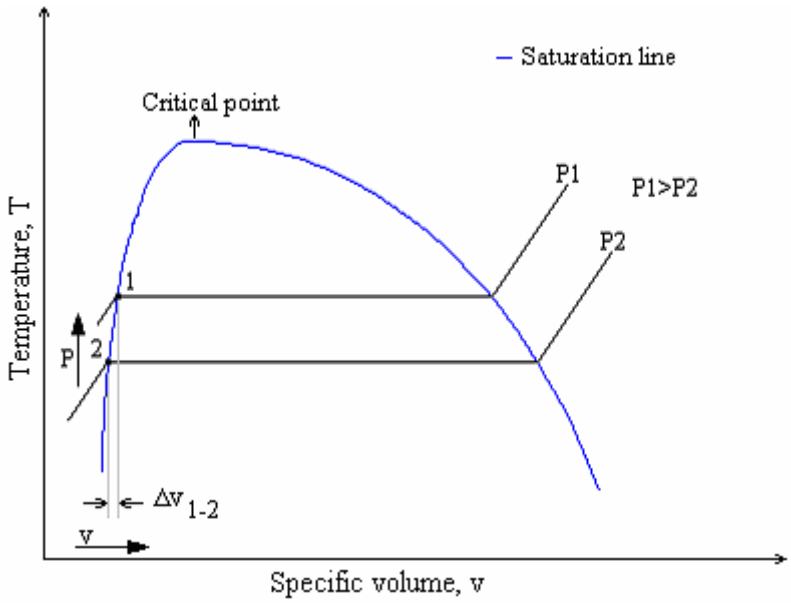

Figure 3-3 Schematic $T - v$ diagram for real fluids

The pressure increase also produces a rise of the discharge velocity at the exit of the system and a smaller liquid viscosity, but larger gas viscosity at the new condition, as is shown in Figure 3-4. In general the liquid phase density of the fluid is inversely proportional to the pressure, whilst the gas phase density is proportional to the pressure.

The thermo physical properties in the metastable region vary rather slowly along isotherms and isobars, Skripov, Sinitsyn et al. (1988).

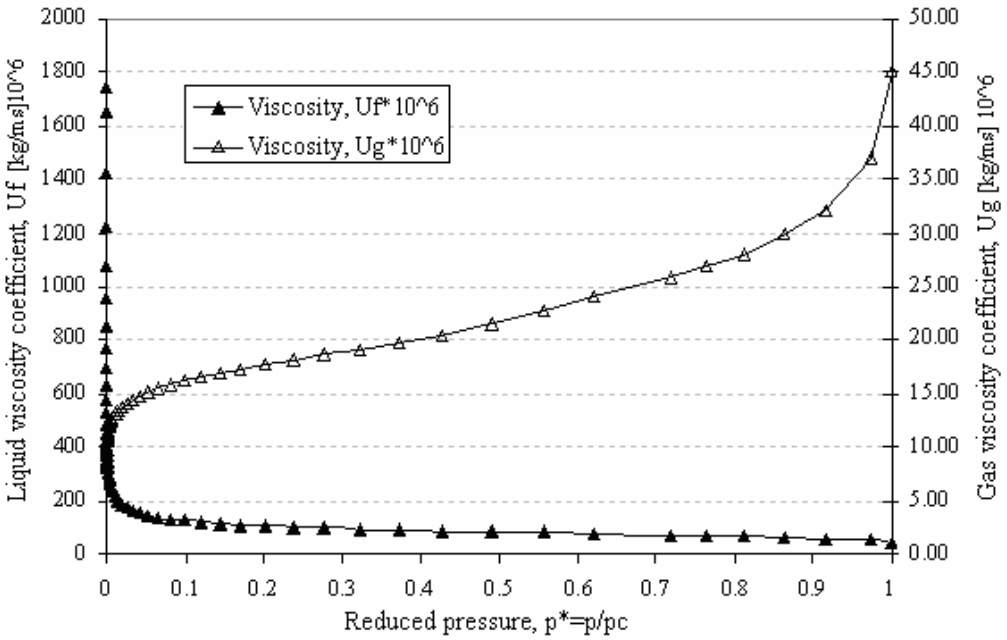

Figure 3-4 Fluid viscosity as a function of reduced pressure

Considering the variation in properties with pressure, the dependency of the Reynolds number on pressure rise will not only be a function of velocity increment. This dependency will be governed by the ratio of density and viscosity multiply the velocity. The size of the resulting inertial force will depend of the product of the new larger velocity multiply the new lower density. The viscous forces will reduce or increase the Reynolds number as shown in Equation (3.11).

$$Re = \frac{\rho u d}{\mu} \tag{3.11}$$

From a thermodynamics point of view, the enthalpy and the entropy of the liquid phase will also increase with a rise in pressure whilst the corresponding values for the gas phase are reduced. The liquid density to gas density ratio, ρ_{liq} / ρ_{gas}, is a measure of how much energy is necessary to overcome the phase change barrier through evaporation. For lower density ratios, less energy must be added to the system to achieve the evaporation than for higher density ratios. For every pressure and temperature condition the heat necessary to induce phase change from liquid to gas in

the fluid must be at least the corresponding enthalpy difference between the phases, h_{fg}, which decreases as the pressure increases. The boiling mechanisms inside of the fluid will depend on the introduction of sufficient kinetic energy for the molecules inside the fluid to change from liquid to vapour state. The variation of C_p with pressure suggests that for a certain mass of liquid, a fixed temperature difference would generate a larger change in energy of the fluid, augmenting the severity of the phase change in the flashing jet. The reduction of the thermal conductivity slows down the heat transfer by conduction. The Jacob number, Ja, is defined as the ratio of the energy supplied by the superheated liquid and the maximum energy necessary to make the transition between liquid and gas at atmospheric conditions, known as latent heat, is given by Equation (3.12). Clearly, The Jacob number increases as a result of rising pressure.

$$Ja = \frac{C_p \Delta T}{h_{fg}} \qquad \textbf{(3.12)}$$

Figure 3-5 shows the typical variation of some fluid properties. This is demonstrated as a function of the reduced pressure.

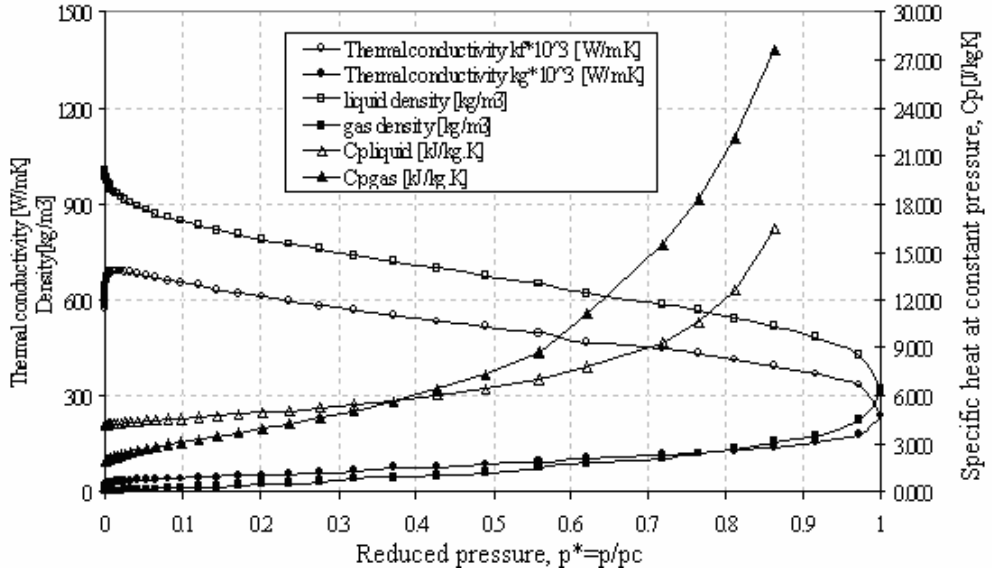

Figure 3-5 Density, specific heat and thermal conductivity as a function of reduced pressure

Another important property related to the phase change process is surface tension. Surface tension decreases as a function of an increase in pressure, as is shown in Figure 3-6. This reflects changes in the resistance of the liquid to keep itself together as liquid

jet. The time before the jet surface breaks-up reduces as the surface tension decreases. The resistance of the liquid to the generation and propagation of liquid surface instabilities waves is a proportional to the surface tension. These instabilities waves are produced by the interaction between the jet and its surroundings. Additionally, low surface tension will reduce the resistance of the liquid core to be ruptured by bubbles generated by nucleation. The ratio between inertial forces and surface tension, represented by the Weber number, will change as pressure increase. This change will be dictated by the ratio of the density and surface tension. However, it can be expected that the Weber number will also increase as result of the effect of the square exponent of the velocity, as is shown by Equation (3.13). It is suggested that there exists a critical Weber number that dominates the growth of the nucleated bubbles inside the fluid, Brown and York (1962).

$$We = \frac{\rho u^2 d}{\sigma} \qquad \textbf{(3.13)}$$

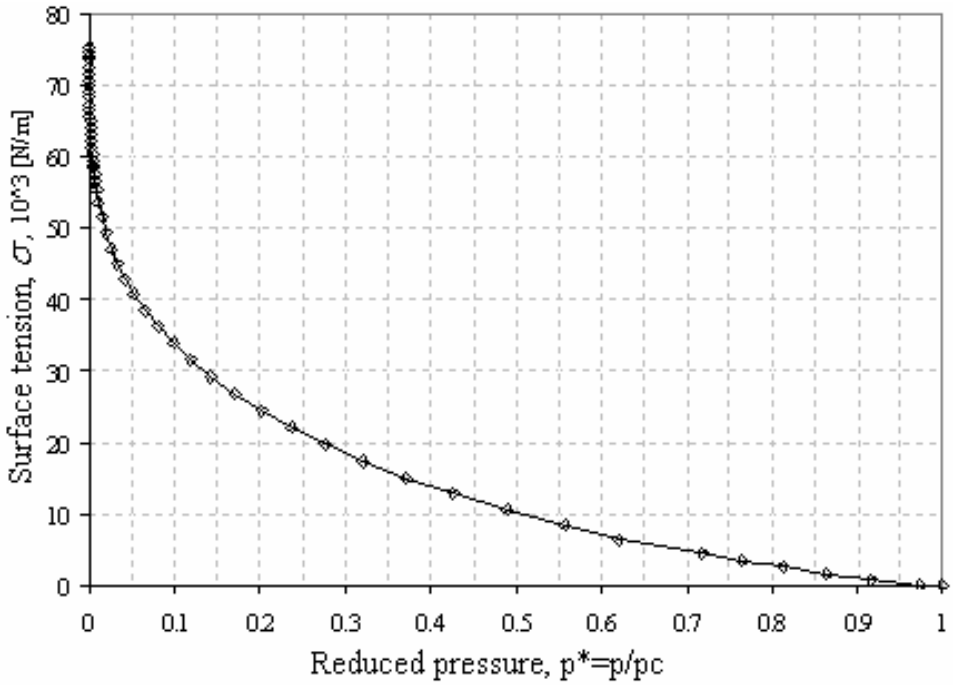

Figure 3-6 Surface tension as a function of reduced pressure

The information on properties is often available for liquid and gases at saturation conditions. The dependency of the properties on temperature inside the superheated region is not well known. Some studies on thermo-physical properties of superheated

liquid confirms that the surface tension, specific volume, specific heat, viscosity and thermal conductivity follow the same trend as the properties at saturation point as suggested by Skripov, Sinitsyn et al. (1988). Experimental data suggests that for superheated fluids the temperature at the injection is larger than the boiling point and the temperature will go below the boiling point only after some distance, named Minimum Temperature Distance (MTD), downstream of the nozzle. Consequently, the fluid properties at the injection conditions will be limited by the properties value at the boiling point, as Equation (3.14) shown.

The properties used to compute all non-dimensional numbers involved in a flashing problem will be assumed as the properties at the boiling point.

$$\left.\begin{aligned} \rho_l\left(T_{inj}\right) &< \rho_l\left(T_b\right) \\ \mu_l\left(T_{inj}\right) &< \mu_l\left(T_b\right) \\ \sigma_l\left(T_{inj}\right) &< \sigma_l\left(T_b\right) \\ C_p\left(T_{inj}\right) &> C_p\left(T_b\right) \end{aligned}\right\} for\ T_{inj} > T_b \qquad \textbf{(3.14)}$$

The effect that the fluid properties have on the stiffness and the damping of the overall system is significant. Although major influence of fluid properties is proposed to be in the dissipation term, they appear in the production coefficient by the presence of the inverse of the gas phase density value. This can be interpreted by the effect of the normalization over the stiffness coefficient per unit volume.

The effect that fluid properties have on the damping of the overall system is more significant that the effects of the stiffness. The effects on damping of the fluid properties are expressed using known dimensionless numbers as Reynolds, Weber and Jacob. The term $\frac{\sigma}{\mu u}$ represents the ratio of surface tension force and the viscous force in the nozzle. The viscous forced in the flow is generated by the shear stress induced by the internal geometry of the nozzle, as well as, the shear stress generated by the liquid-vapour inter-phases, Schmelzer (2003). The surface tension acts at the interface surface of every vapour bubble immerse in the continuum of the liquid. The viscous effects appear due to the motion of vapour bubbles within the continuum of the liquid, and the mean motion of the all mixture inside the vessel and the nozzle. The shear stress is

opposite to the motion direction and proportional to the viscosity coefficient. The order of magnitude of the coefficient of viscosity is always less than unity, so it will contribute to increase the overall value of C* and the order of magnitude of the surface tension coefficient is also Due to the direct proportionality of the liquid velocity and the square root of the pressure variation, the kinetic energy is proportional to the variation of the pressure, $\frac{u^2}{2} \sim \Delta p$. On the other hand the latent heat of vaporization is the energy absorbed during a change of state from liquid to a vapour. Its value is the same as the enthalpy difference between liquid and vapour phases of the fluid. The term $\frac{\Delta p_c}{L}$ [kg^3 m^{-2} s^{-2}] can be interpreted as the ratio of kinetic energy to thermal energy. This term reflects the experimental observations that there is a compromise between the pressure difference and the thermal contribution. This ratio indicates the importance of the pressure flow difference against the latent heat of the fluid. The term $\frac{C_p \Delta T_c}{L}$ [-] is the ratio of the energy supplied by superheated liquid and the maximum energy necessary to make the transition between liquid and vapour at atmospheric conditions, known as latent heat.

3.3.3 Geometrical considerations

The geometry of the nozzle, as well as, the piping system used in every experimental setting could affect the final output of the flashing jet. The diameter, the length and the shape of the nozzle have been taken as major characteristic parameters to be considered as suggested by Miyatake, Tomimura et al. (1981a), Reitz (1990), Park and Lee (1994) and Yildiz (2003). The energy conservation includes losses due to friction and the losses due to resistance of specific devices, such as valves and nozzles. The resistances of the devices are quantified by the local resistance coefficient, K_i. A small nozzle diameter corresponds to a high K_i and therefore it produces larger pressure drop at the discharge location than a large nozzle diameter. The influence of the shape of the nozzle on the flow is also included in the coefficient K_i, known as discharge coefficient, Potter, Wiggert et al. (1997). For instance, the discharge coefficient of a nozzle with sharper edges will be larger than for a nozzle with chamfered edges, and therefore, a

nozzle with sharper edges will produce a larger pressure drop in the flow, as well as, larger disturbances in the flow field. For circular cross section nozzles the loss is expressed by Equation (3.15) is proportional to the inverse function of diameter to the power of four, $\Delta H \propto 1/d^4 + f(d)/d^5$.

$$\Delta H = K_i \frac{Q^2}{2gA^2} + f\frac{L}{D}\frac{Q^2}{2gA^2} \qquad \textbf{(3.15)}$$

The total mass flow rate discharged is also affected by the diameter, as shown by Equation (3.16). For a circular nozzle the mass flow rate is proportional to the square value of the diameter, $\dot{m} \propto d^2$. Larger nozzle will increase the mass flow rate of the system.

$$\dot{m} = \rho u A \qquad \textbf{(3.16)}$$

The area available to conduct the heat transfer inside the fluid is also affected by the nozzle diameter. The cross sectional area of the fluid is drastically reduced from inside the tank to the exit passing through the nozzle. A smaller nozzle diameter will cause a reduction of the fluid heat transfer area, making it difficult for the fluid to keep the same conduction heat transfer rate on its way out, augmenting the possibilities of a violent and explosive flashing process, Yildiz (2003).

For a fixed velocity, the nozzle length determines the period of time required by the fluid to flow trough the nozzle. If the length is increased, the contact between the fluid and the internal surface irregularities of the nozzle will rise, promoting the formation of heterogeneous nuclei, Yan and Giot (1989). This will also intensify the generation of friction losses.

If, the fluid can still be liquid at the exit of the nozzle, then the length will affect the type and size of perturbation or instabilities in the jet surface, as product of the internal flow pattern. In cases of two-phase discharges the length is an important factor in the determination of the two phase flow pattern inside a pipe as suggested by Park and Lee (1994), Barnea, Shoham et al. (1980), Barnea, Shoham et al. (1982a) and Barnea, Shoham et al. (1982b).

The roughness height of the wall, e, of the vessel and the nozzle can also induce pressure drops. The relative roughness, e/d, reflects the influences of the roughness

again any hydrodynamics structure in the flow inside of a nozzle with diameter, d, especially at the boundary layer. For a large e/d the friction factor and the presence of turbulent structures close to the wall will increase resulting in fluctuating pressure due to the turbulence. Furthermore turbulence could promote the creation of nuclei. A typical value of roughness for cast iron is about 0.26 mm and for galvanized iron 0.15 mm. The relative roughness will depend on the pipe diameter.

Although the nozzle is considered the most influential part of the system, it is important to describe the effect of the pipe system used in typical experimental settings. The sizes, length and roughness of the pipe can induce major pressure losses in the fluid even before it reaches the nozzle. This changes the velocity and the mass flow rate of the system, either for liquid phase or for the gas phase discharges. Additionally the shape of this system can define a complete different flow patter before the nozzle. For instance, the presence of elbows or deviations too close to the nozzle induces a perturbed flow at the nozzle location and it also increase the general losses of the flow in the system.

The effect that the geometrical consideration has on the stiffness and the damping of the overall system is also significant. The effect on stiffness is represented by three terms. The first term is proportional to discharge coefficient, C_D , which represents the impact of the geometry of the nozzle on the pressure drop in the flow on its way out to the vessel, on the turbulence generated, and therefore, on the nucleation. This term has no dimension. The second term is proportional to the ratio of the length and diameter of the nozzle, $\frac{l}{d}$. This term represents the influence of the length of the nozzle over the time required by the fluid to flow through the nozzle, as well as, the increasing of the pressure drop. And the third term is proportional to $d^{1.25}$. If the two previous terms are combined then it is clear that a larger diameter will increase the production coefficient as well as the length of the nozzle. The influence of the diameter en average is driven by the exponent 0.25, which means that it influence is smaller that the length of the nozzle.

The effect of geometrical characteristic on dissipation coefficient are assumed to be part of the minimum level of energy that needs to be overcome to produce an explosive level of nucleation. This minimum level must be related with the ratio of diameter and length

of the nozzle, d/l. At least the energy available must be enough to pass trough the nozzle. Also the relative roughness of the nozzle material, e/d, could influence the dissipation forces. Although wall roughness can introduce more nuclei sites it also will produce more losses in the nozzle and it will reduce the total velocity of the system.

3.3.4 Water versus hydrocarbon behaviour

The applicability of any model to different types of fluids, such as hydrocarbons and water, is a considerable concern both for research and practical purposes. The extensive use of water instead of hydrocarbons in experimental tests is due to its versatility and non hazardous condition, Witlox and Harper (2005). However, the water behaviour differs from the behaviour of any hydrocarbon. The different behaviours of those types of fluids are reflected in the differences of their properties. Figure 3-7 shows the critical pressure and temperature for different fluids.

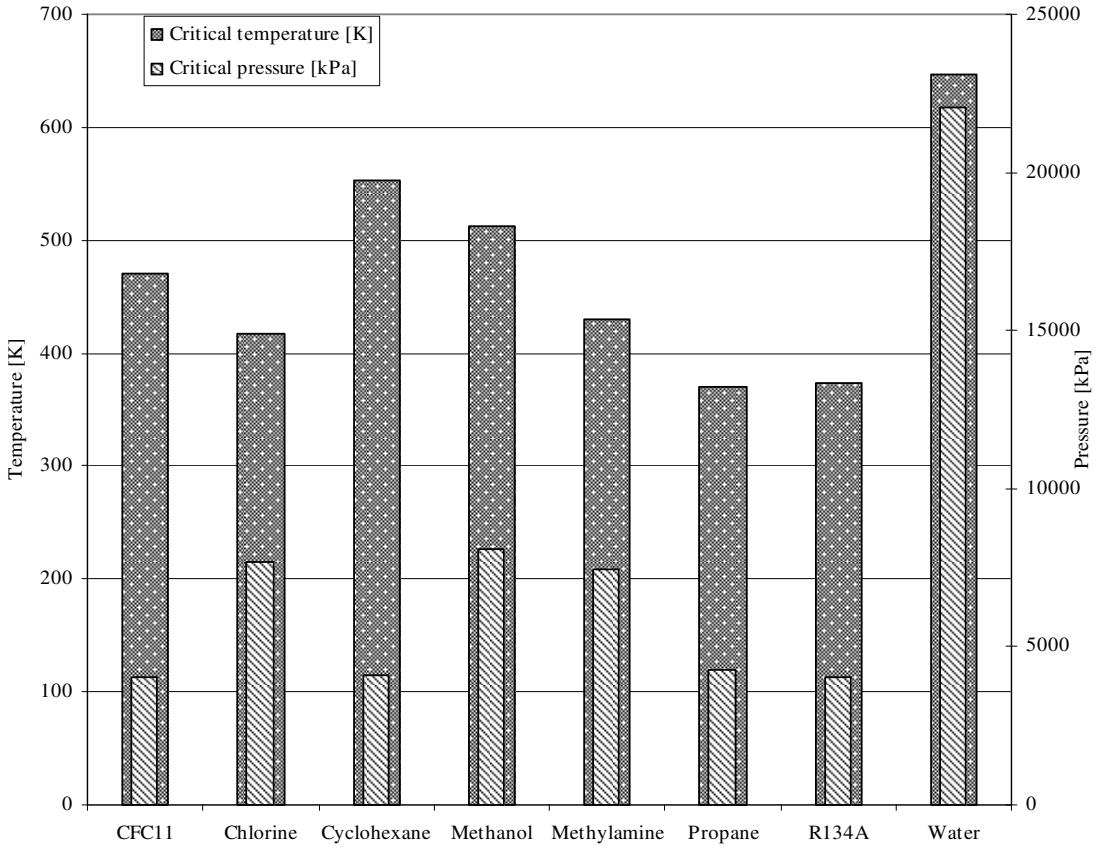

Figure 3-7 Critical temperature and critical pressure conditions for some hydrocarbons and water

It is clear that the critical pressure and temperature of the water is larger than any other critical pressure or temperature of the hydrocarbons fluids shown, such as chlorine, R134A, cyclohehane, methylamine, propane and CFC11. The ratio of critical pressures with respect to that the water also named dimensionless critical pressure, $p_c / p_{c\,water}$, for the fluids tested is smaller than 0.35, whilst corresponding ratio of critical temperatures or dimensionless critical temperature, $T_c / T_{c\,water}$, is smaller than 0.85, as shown in Figure 3-7. The relative position of dimensionless critical temperature and pressure respects to the unity is an indicative of the maximum range of operation condition the fluid could work. Consequently, for a fixed pressure level the model proposed predicts that the resistance of the water to flash is larger than any other fluids.

Figure 3-8 shows the liquid to gas density ratio, as well as, the liquid density and water liquid density ratio for different hydrocarbons fluids, such as chlorine, R134Aa, cyclohehane, methylamine, propane and CFC11.

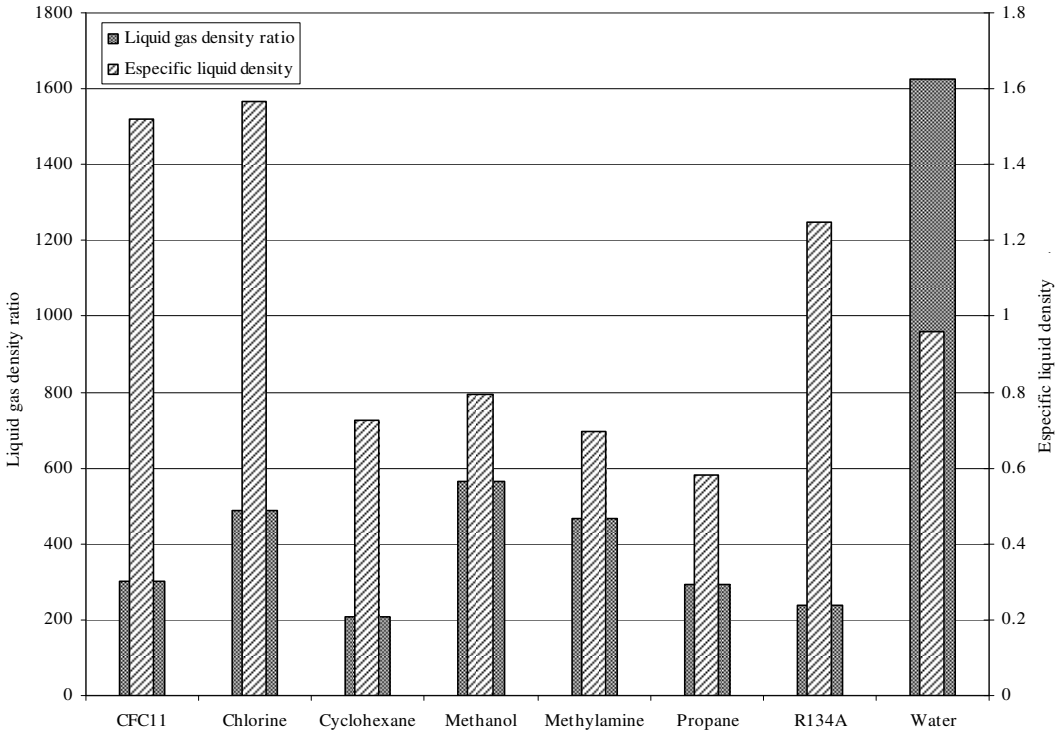

Figure 3-8 Liquid and gas density ratio and specific liquid density for different fluids

all cases the hydrocarbons ratios are at least one order of magnitude smaller that the corresponding ratio for water. The energy need to achieve even a pure evaporation process in water will be larger than the energy to achieve the same condition in any hydrocarbon. However, the density of hydrocarbon liquid and the liquid water density, taken as 1000 kg/m3, shows that the water does not have any distinctive larger value respect to the hydrocarbons. The consideration of this parameter helps to make an extrapolation of the model for the whole range of fluids tested including water.

Figure 3-9 shows the behaviour of the inverse of the liquid gas density ratio as a function of the reduced temperature, T/T_c, for R134a, R11 and water. Here it is observed that the dependency of the water ratio on reduced temperature is stronger that the corresponding to the hydrocarbons. Water density is typically a factor of 10^3 larger than the vapour density for temperature values less than the boiling point, $T/T_c \approx 0.57$, and for the hydrocarbons tested the maximum density is about 5.10^2.

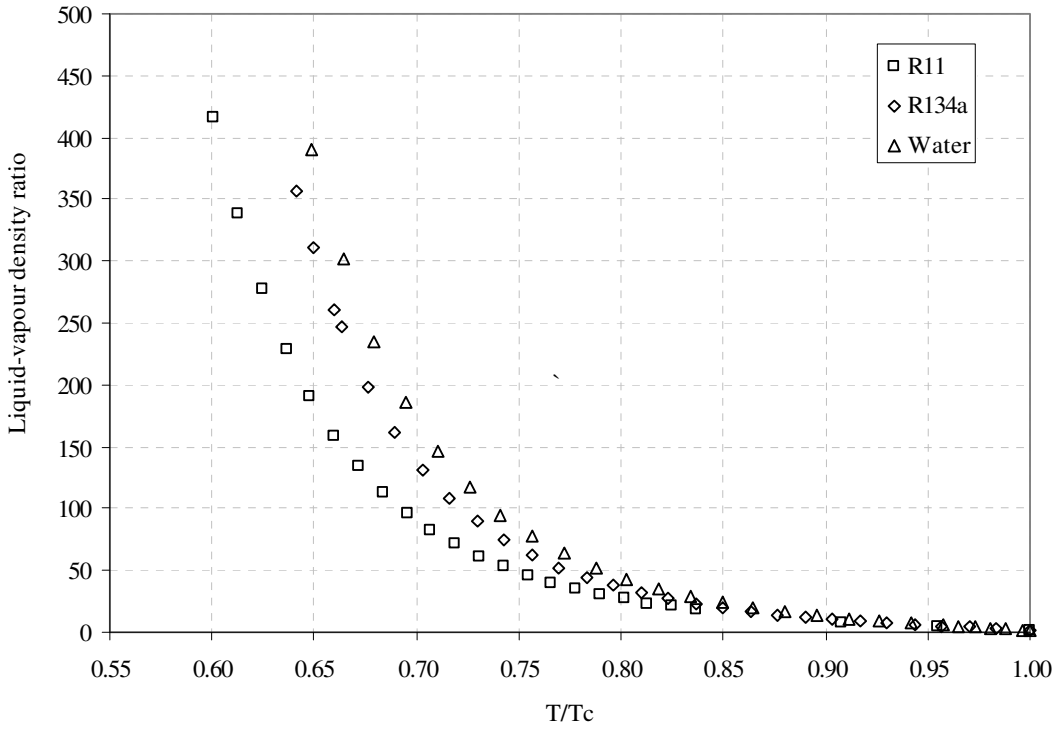

Figure 3-9 Ratio of liquid and gas density as a function of the dimensionless temperature

Figure 3-10 shows the fugacity for different fluids evaluated from the van der Waals equation of state. The calculation corresponds to the boiling temperature and the volume equals to the value of the B coefficient defines for the Van der Waals equation of state, Equation (3.17). This value is the minimum volume where the fugacity is defined. This property indicates the tendency of the vapour phase of a fluid to expand at certain pressure. The information reflected in Figure 3-10 corresponds to the fugacity at saturation at the standard ambient pressure. It is clear that the fugacity has the same general trend for all fluids; however, it is larger for hydrocarbons than for water when the volume tends to the saturation line. It means that superheated hydrocarbons will tend to escape faster than the water to the ambient from the liquid medium.

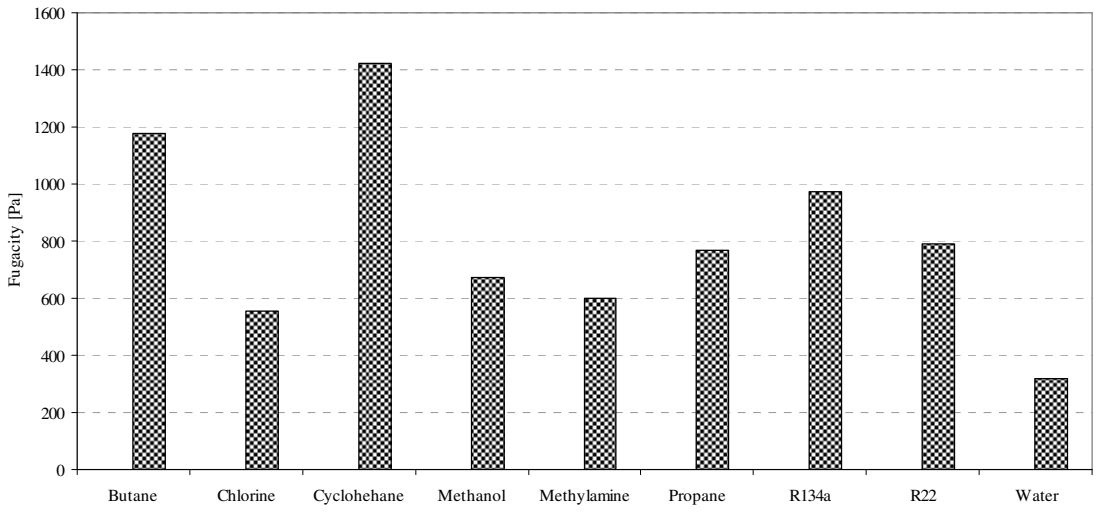

Figure 3-10 Compilation of fugacity of different fluids

Fugacity is a pseudo pressure. When pressure is substitute by fugacity the equation normally used for ideal gases can be applied to real gases.

$$\ln f = \ln\left(\frac{8.314T_b}{v-b}\right) + \frac{b}{v-b} - \frac{2a}{8.314T_b v} \qquad \textbf{(3.17)}$$

It is deduced from the previous discussion that to achieve a fixed amount of phase change in water at certain pressure and temperature conditions, the energy required is a lot larger than the equivalent energy to achieve the phase change in any hydrocarbon.

As a real example of the different behaviour between water and hydrocarbons, it is mentioned the experimental study presented by the Energy Analysts Inc (1990) in which experience the flashing jet going out of the nozzle was intercepted after certain downstream distance by an equipment to collect the liquid mass remaining at that point. The fluids tested were hydrocarbons as well as water. However, a visual description of the jet formed after the nozzle was only reported for Chlorine and water cases. Figure 3-11 shows the results of the mass collection quantities corresponding to four different types of hydrocarbons and water against the dimensionless boiling temperature. As a result of the information obtained from the visual description two horizontal lines, corresponding to the limit between totally spread jets, bubbly jet and completely liquid jet, were drawn over the data. According to the descriptions given in the same research about the type of jet obtained for each experimental run it was found that collected mass about 10% of the total mass delimit the totally spread jets and the bubbly jet. And the collected mass about 50% of the total mass described the limit zone between bubbly jet and completely liquid jet at the exit of the nozzle. As Chlorine is a hydrocarbon fluid, its behaviour was extended for the other hydrocarbons. If mass collected is plotted against dimensionless boiling temperature, T^*, it is clear that there is a linear relationship between the mass collected and dimensionless boiling temperature for all fluids. Changes in the flow patterns occur when the temperature changes. The analysis of data confirms that larger quantities of mass are collected from a liquid jet than from a complete sprayed jet, because part of the total mass released from the nozzle escape as vapour.

Figure 3-11 shows that the collected mass limit between two types of jet is related also with the boiling temperature of the fluid, as:

$$\Delta T_{50\%} = -0.0004T^* + 0.2473 \qquad \textbf{(3.18)}$$

$$\Delta T_{10\%} = -0.0005T^* + 0.2169 \qquad \textbf{(3.19)}$$

The expressions developed for hydrocarbons, particularly Chlorine, Equations (3.18) and (3.19) are only based on the mass capture for particular geometry conditions and do not fit for the case of water. The difference can be attributed mainly to the fact that water has a structure and properties different to any hydrocarbon.

If those equations are applied to R134 it is obtained that flashing limit corresponding to K%. When compared with data published by Yildiz, Rambaud et al. (2005), it can be observed that for 1 mm nozzle is below the limit temperature 293.15 K, as well as, for 2 mm nozzle. Unfortunately, this is not the case of the 4 mm nozzle where the flashing limits reduce to 286.15 K. The term flashing limit is understood as the limit between a totally spread jets and a liquid jet. Result of the application of this criterion is close to the expected temperature accordingly to the information of the test experience reported.

Figure 3-11 Percentage of mass collected from a flashing jet a fixed distance from the nozzle against dimensionless boiling temperature and respective linear approximations. Source: Johnson and Woodward (1999)

The effect of the type of fluid on the overall behaviour of the system is also accounted for within the model. For the production coefficient this effect is proportional to the density ratio of the fluid and water, in the general case. This is proposed that larger density ratio or specific density will increase the possibility of the fluid to flash. These coefficients will introduce a variable degree of sensitivity in the model according to the properties of the fluid tested.

The dissipation coefficient is also believed to be proportional to the density ratio, boiling temperature and the ratio of critical pressure and ambient pressure. The boiling temperature of the fluid has and important role in the representation of the minimum

energy that needs to be overcome for the fluid before nucleates. The ratio of ambient pressure and the critical pressure give in the dissipation coefficient shows a relative position of different fluid critical pressure again the ambient pressure. Water has the maximum critical pressure and ambient pressure ratio. So, for fluids which has smaller critical pressure will reduce the resistance of the fluid to nucleate.

3.3.5 A proposal for coefficients K^* and C^*

As a result of the analysis of the influences of the different parameters of the nucleation process under the similarities with a damped second order system, the stiffness coefficient per unit mass and damping coefficient per unit mass, also named the production coefficient and the dissipation coefficient of the nucleation system are expressed by Equations (3.20) and (3.21).

$$K^* = g_o C_D d^{1.25} \frac{l}{d}\left(p_{inj} - p_o\right)\sqrt{\frac{T_{inj} - T_b}{T_{inj}}}\frac{1}{\rho_g} \tag{3.20}$$

$$C^* = g_1 T_b \frac{d}{l} + g_2 \frac{\rho_{liq}}{\rho_{gas}}\frac{p_c}{p_o}\frac{e}{d}\frac{\left(T_c - T_{inj}\right)}{T_{inj}}\frac{Cp\left(T_c - T_{inj}\right)}{L}\left(\frac{\sigma}{\mu\sqrt{\frac{\rho_l}{2p_0}}}\right)\frac{\left(p_c - p_{inj}\right)}{\rho_g}\frac{\left(p_c - p_{inj}\right)}{L} \tag{3.21}$$

The production coefficient stands for the contributions of the injection conditions temperature and pressure related to the ambient conditions, ambient pressure and boiling temperature represented by the difference of pressure and the difference of temperature. Also the geometrical considerations are considered. The whole term is normalized by the gas density. The geometrical influence is mainly represented by the discharge coefficient, C_D, the aspect ratio of the nozzle, $\frac{l}{d}$, and the diameter, $d^{1.25}$. This term shows that the influence of the geometry is not linear. As it was discussed before the nozzle diameter influences the mass flow, the friction factor, the losses, etc.

The influence of the pressure and temperature at the injection point are measured against their relative position to the boiling temperature and the ambient pressure.

The production coefficient is consistent even for the cases characterised by extreme low pressure. For the first cases the mathematical limit of the pressure, $\lim \Delta P \to 0$, there is no depressurization process and no movement is generated, so no nucleation is promoted. However, the resistance coefficient will not be zero, which could be interpreted as the passive damping force inside the fluid.

The dissipation coefficient represents the resistance of the fluid to flash, which will be affected by nozzle geometry, fluid properties and initial conditions. This term can be zero, at any evaluated condition. The first term of the right hand side of Equation (3.21) represents the minimum resistance that a particular setting has to experience an explosive nucleation. The second term of the same equation combines the influence of the dimensionless critical normalized temperature, temperature ratio, Jacob number and Reynolds and Weber ratio. The Dissipation coefficient equation has been written in certain way where it can be easy to recognize the influence of the some well known dimensionless numbers. The influence of a particular variable is not exclusively in favour or against nucleation; there are some variables that have a relevant role in both aspects. As result of the analysis of experimental data it is clear that the influence of a particular variable depends on its proportion respect to a reference value, as for instance the critical conditions values of a substance or standard atmospheric conditions. In the same form the incorporation of the considerations about type of fluid, water or hydrocarbons, is presented in the model. So the added dissipation to the minimum value corresponds to the combination of temperature and pressure against the critical values of the fluid, as well as the own properties of the fluid.

To avoid the singularity in production and dissipation coefficients (Equations (3.20) and (3.21)) for the cases with zero nozzle length, it is assumed that the nozzle length will be at least of the typical roughness value of steel, which is about 0.0025 mm, in another words, $\lim l_{\to 0} \quad l = e$. This term is also related with the existence of a minimum resistance of any fluid to nucleate imposed by the fluid properties as well as the system characteristics, Frost, Barbone et al. (1995).

3.3.6 Constants of the model

To finish the model the incorporation of some constants was needed. The constant named g_0, g_1 and g_2 expressed in Equations (3.20) and (3.21). The values of these constants presented in Table 3-1 are the product of an empirical and numerical work of all the experimental set of data available for hydrocarbons, Brown and York (1962), Solomon, Ruupprecht et al. (1985), Hervieu and Veneau (1996), Reitz (1990), Park and Lee (1994), Bolle (1996), Yildiz (2003), Gemci, Yakut et al. (2004a), Gemci, Yakut et al. (2004b).

The unit of the constants g_0, g_1 and g_2 are reported in Table 3-1. Those units are consistent with the complete equation of balance of nucleation second derivative, nucleation first derivative and the nucleation itself. The nucleation is expressed by the number of nuclei created. The units of the whole equation will be number of nuclei per second squared. Then the unit of the production coefficient is the inverse second squared and the unit of the dissipation coefficient is the inverse of second.

The numerical values of the different coefficients allow the model to achieve the right level of sensibility according to the evaluated fluid, see Table 3-1**.** The values are quite close each other. Nevertheless, the values of the constants used do not modified the behaviour of the different fluid on the actual expression.

Table 3-1 Coefficients g_0, g_1 and g_2 for hydrocarbons type of fluids and water

	$g_0\left[m^{2.75}s^2\right]$	$g_1\left[K^{-1}s^{-1}\right]$	$g_2\left[Pa^{-1}s^{-1}\right]$
Hydrocarbons	106066	6E-02	6.5E-06
Water	106066	6E-02	5.5E-06

3.3.7 Application of the model K^* and C^*

The criterion to establish the characteristics of a damped second order system given by Equation (3.7), involves the difference of the magnitude of four times the production coefficient and the dissipation coefficient powered two.

For each set of geometrical conditions and a particular fluid the production and dissipation coefficients will only depend on the pressure and the temperature of the fluid at the injection point. If those parameter all used as generic values then a parametric function is achieve. An example of this situation is presented by Equations (3.22) and (3.23). The values expressed in those equations correspond to a discharge case of CFC11 reported by Johnson and Woodward (1999).

$$K^* = k_1 \left(p_{inj} - k_2 \right) \sqrt{\frac{T_{inj} - k_3}{T_{inj}}} \tag{3.22}$$

$$C^* = c_1 + c_2 \frac{\left(c_3 - T \right)^2}{T} \left(c_4 - p \right)^2 \tag{3.23}$$

Where the variables k_1, k_2, k_3, c_1, c_2, c_3 and c_4 are represented in Table 3-2.

Table 3-2. Numerical values of the variables of production and dissipation coefficient corresponding to an example of CFC11

k_1 [$Pa^{-1}s^{-2}$]	k_2 [Pa]	k_3 [K]	c_1 [s^{-1}]	c_2 [$Pa^{-2}K^{-1}s^{-2}$]	c_3 [K]	c_4 [Pa]
3.453	101325	295.6	450.494	2.102e-4	4378	101325

However, due to the criterion form of the model it is more convenient to the functions $4K*$ and $C*^2$ instead of the original production and dissipation coefficients. To assure the best understanding of these two functions it is convenient to use the dimensionless reduced temperature and reduced pressure parameters to be evaluated and also the parameters to be represented in the axes of a coordinate system, the resulting graph contains two different surfaces one for each function. The same example is shown as follow, but now the equations are represented based on reduced temperature and reduced pressure.

$$K^* = k_{1'} \left(p_r - k_{2'} \right) \sqrt{\frac{T_r - k_{3'}}{T_r}} \tag{3.24}$$

$$C^* = c_{1'} + c_{2'} \frac{(1-T_r)^2}{T_r}(1-p_r)^2 \qquad \textbf{(3.25)}$$

Table 3-3. Numerical values of the variables of production and dissipation coefficient corresponding to a example of CFC11, based on reduced pressure and temperature

$k_{1'}$ [s^{-2}]	$k_{2'}$ [-]	$k_{3'}$ [-]	$c_{1'}$ [s^{-1}]	$c_{2'}$ [s^{-1}]
15119267	0.0231	0.628	450494	41.177

Figure 3-12 shows the surface that involves production coefficient. This surface growth with the positive direction of dimensionless pressure axes and also with the positive direction of the temperature axes.

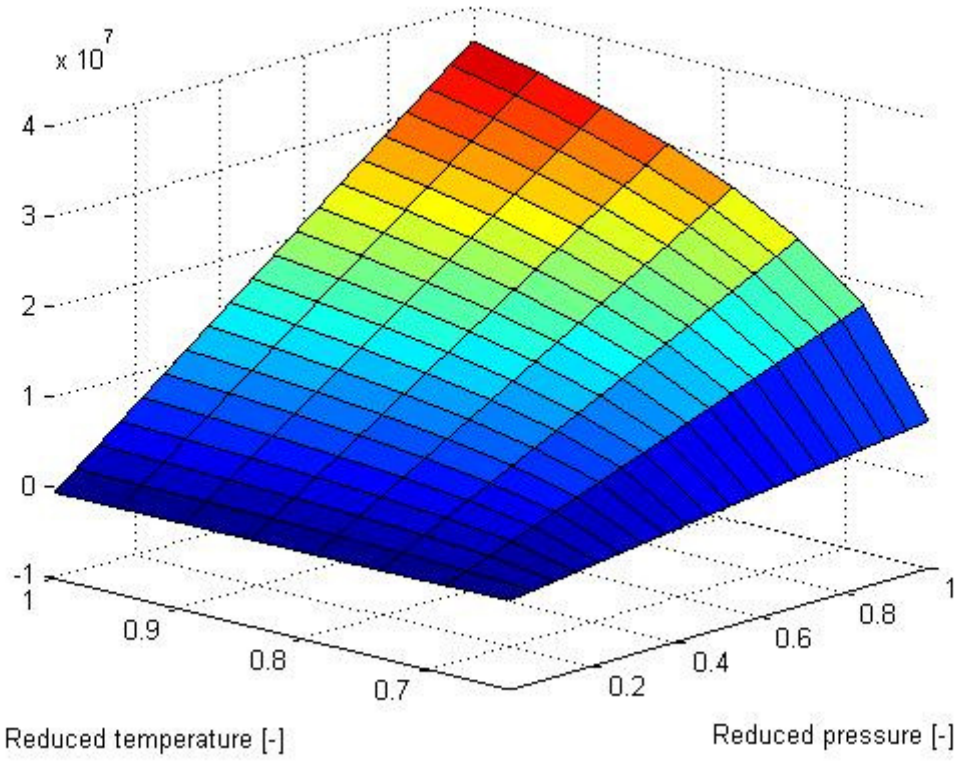

Figure 3-12. Schematic representation surfaces of 4K* of the model

Note that using reduced values it is clear that there are limits values of pressure and temperature for what a flashing discharge is not expected and therefore the functions of the production coefficient is not well defined. Those values correspond to a reduced

temperature of 62.8% of the critical temperature and the 2.31% of the critical pressure, for CFC11, but it will change for others fluid. So, flashing discharges are not expected for pressure values smaller than the ambient pressure, neither for temperatures smaller that the boiling point at ambient pressure.

Figure 3-13 shows the surface that involves dissipation coefficient. This surface decreases with the positive direction of dimensionless pressure axes and also with the positive direction of the temperature axes. It has a pick close to the corner defined by the smaller reduce pressure and the smaller reduce temperature.

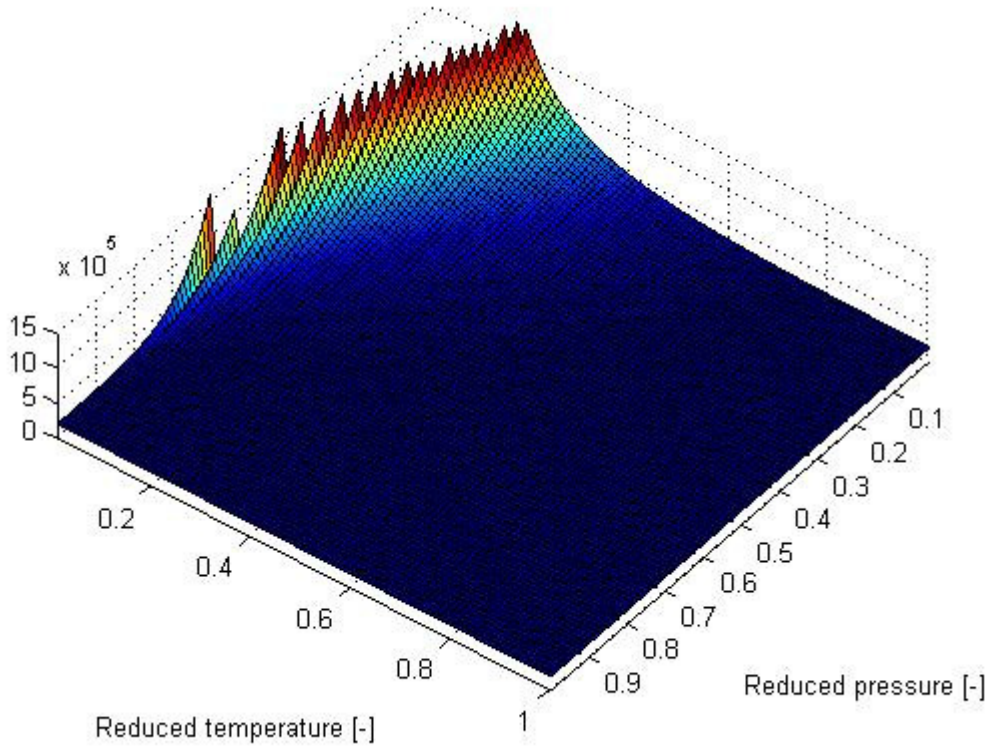

Figure 3-13. Schematic representation surfaces of C*^2 of the model

Due to the opposite behaviour of both surfaces respect to the axes when they are super imposed an interception line is produced. The interception line represents the limit between an over-damped system where the liquid will stay liquid even after the nozzle and an under damped system where the remaining liquid is present as droplets. For a low pressure, no interception between these two functions is presented in Figure 3-14, which means that the dissipation is larger that the production for the whole range, so the nucleation generated under these conditions will be insufficient to generate droplets at

the exit of the nozzle, and consequently a liquid jet will be formed. To know the type of discharge in a particular flashing case it is necessary to compute the exact location of this case in the corresponding 3D surface map. The possibility of been a liquid discharge or two-phase discharge will depend on the relative position of the case to the interception line of both functions $4K*$ and C^{*2} in Equation (3.7). If the point is located in a plane A depicts the fact that for the pressure level equal or smaller than one the limit values reported above the fluid will not achieve flashing behaviour for any condition. If the point is at the interception between the functions $4K*$ and C^{*2} then the case correspond to a critical condition. The interception constitutes the limiting condition when the nucleation process is sufficient to produce a two phases flashing jet. If the point is located in a plane where the production function is over the dissipation function, then that means than the jet will achieve the two phases condition.

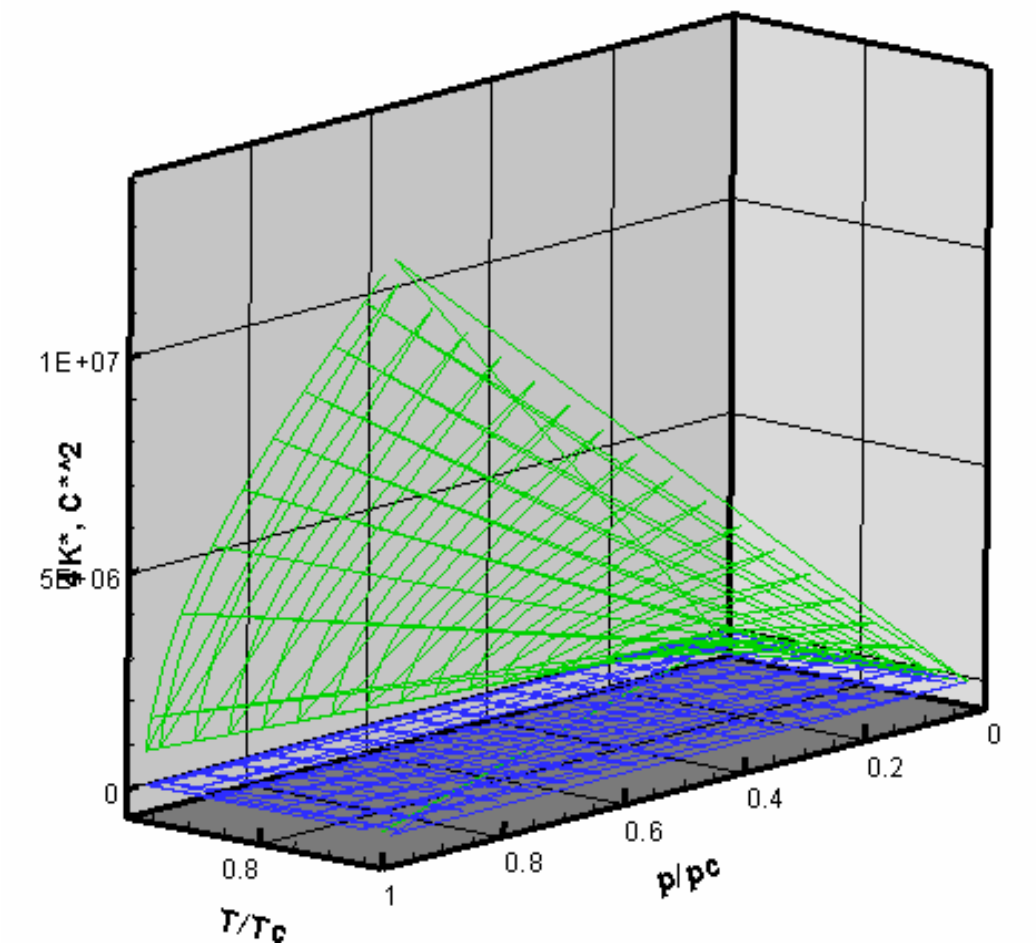

Figure 3-14 Schematic representation of both terms, 4K* and C*^2 of the model

3.3.8 Analytical solution for nucleation

The analytical solution of the differential Equation (3.2) shows above has a complex form. The solution of the nucleation of parcel of bubbles can be expressed as:

$$N = Ae^{\lambda t}\cos(w_d t + \phi) \tag{3.26}$$

With the exponent coefficient equal to:

$$\lambda = -\frac{C*}{2} \tag{3.27}$$

The cosine argument is given as

$$w_d = \frac{1}{2}\sqrt{4K* - C*^2} \tag{3.28}$$

The pre-factor A is considered to be a function of the parameter $K*$ and $C*$. In fact it defines the magnitude of the vector in the complex plane as:

$$A = \sqrt{\frac{C*^2}{4} + \frac{\left|C*^2 - 4K*\right|}{4}} \tag{3.29}$$

The integral of this function over time represents the total number of nuclei generated over the integration time by per unit volume.

$$N_{total} = \frac{1}{t*}\frac{A(e^{\lambda t*} - 1)}{\lambda} \tag{3.30}$$

$t*$ is the time in which the process takes place. Due to the order of magnitude of the time period within a flashing jet takes place, it is reasonable to assume that nucleation starts at the same moment the depressurization occurs. So there is not a phase time between these two points. The possibility to consider a phase time between the depressurisation and the nucleation beginning point in a generic case is take into account in Equation (3.26) by the parameter ϕ. According to the argument described before the parameter ϕ is assumed equals zero.

Frequently, authors report the rate of nucleation to be expressed as shown by Equation (3.26). The terms A' and λ' are quantities that obey different definitions according to the author, Brennen (1995), Shen and Debenedetti (1999) and Christensen and Tillack

(2003). However, in all the cases the nucleation rate involves the exponential function, which gives the nucleation strong dependence on the parameter considered.

$$J = A^{'} e^{\lambda^{'}} \tag{3.31}$$

The rate of nucleation that follows this work also contains the exponential function, however, it introduces an explicit dependence with the time.

A parameter called degree of flashing, ξ, which represents the ratio of the functions $4K*$ and $C*^2$ evaluated at the point tested, is also introduced to help defining the characteristics of the jet at the exit. As this parameter increases major and more violent phase change is produced.

$$\xi = 4K^* / C^{*2} \tag{3.32}$$

The ratio of the two terms inside the squared root of Equation (3.7), represent the ratio of the four times de production coefficient against the square value of dissipation. It can be related with the initial spray angle after the nozzle. It is expected that the flashing jet angle to be proportional to the ξ value. For larger degree of flashing the resulting jet will spread more widely. The growth of the jet sectional area after flashing can be expressed in term of the expansion angle. This argument was tested with for a propane case and a methane case, from data from Allen (1998a) and McDonell and Samuelsen (1995)

$$sign = \frac{4K^* - C^{*2}}{abs\left(4K^* - C^{*2}\right)} \tag{3.33}$$

The *sign* parameter only can be equals to positive unity or negative unity. A positive unity value of *sign* parameter means the system achieves flashing condition and a negative unity value means the system do not achieve flashing condition.

3.3.9 Results of the qualitative model

The results of the qualitative model are presented by reporting the values of the *sign*, which actually indicated what kind of the jet was resulted. Another way to publish the result is by the coordinate graph of the coefficient of the Equation (3.33) versus the

temperature. The relative position of those parameters compared each other will determine the type of yet.

Figure 3-15 shows the behaviour of the model for all the set of data tested for R134a. The model does not include the point were the initial temperature is below the boiling point. This is because the liquid should fulfil the condition of a superheated liquid at ambient conditions.

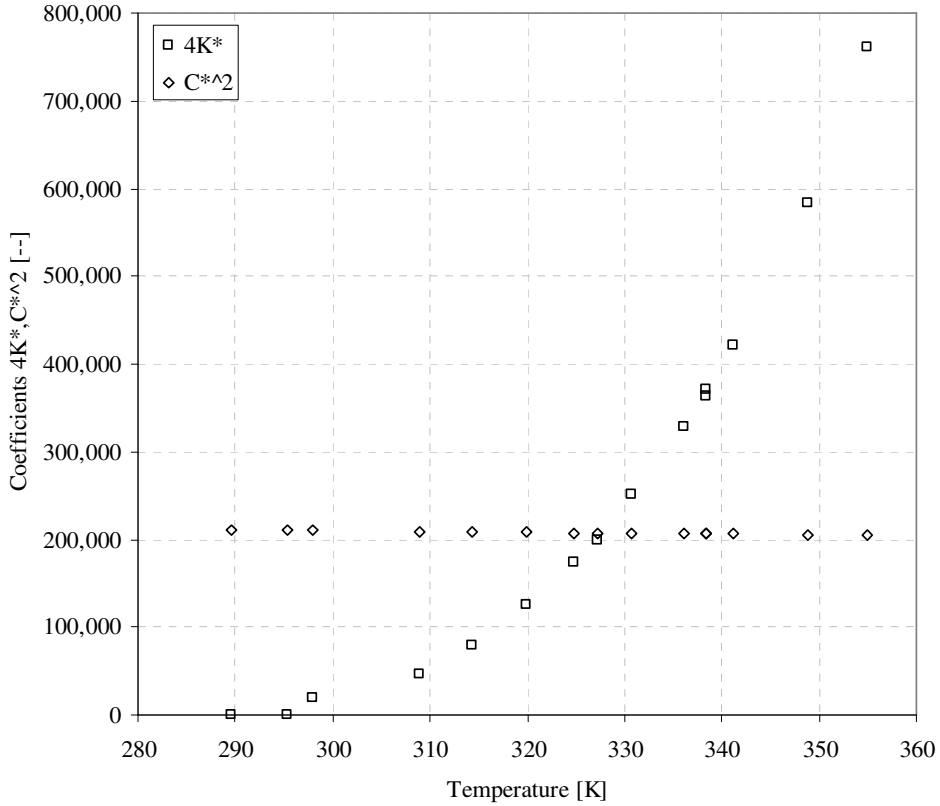

Figure 3-15 Model results on CFC11 data from Johnson and Woodward (1999)

The results of the model using chlorine and cyclohexane were satisfactory according to the limits calculated based on the mass recollection. However, the results of the model application to methylamine over-predict the behaviour of the fluid. The first three columns of the Table 3-4 contain the original data corresponding to CFC11 (trichlorofluoromethane) reported by Johnson and Woodward (1999) and the fourth column contain the results of the application of the definition of *sign* parameter, Equation (3.33), for all the chlorine cases tested. The degree of flashing and *sign*

parameter corresponding to the cases of temperature of 285.29 K and 289.63 K did not apply, due to the production and dissipation coefficient are not defined for temperature values smaller than the boiling temperature of the fluid. The pressure evaluated for the R134a cases is closer to the critical pressure of the fluid compared to any other fluid tested. As expected, this set of data allows testing the influence of the pressure, the pressure, and the effects of the nozzle characteristics on the release exit.

Table 3-4 Model results for CFC11. Information from Johnson and Woodward (1999)

Pressure [kPa]	Temperature [K]	Observations	*sign*
161,800	297.90	Liquid stream remained together until vertical movement of stream was dominant.	1.0
163,500	308.95	No break-up of liquid stream visible	1.0
166,800	295.29		-
168,100	289.63	Liquid stream breaks up during vertical portion of trajectory into large drops and globs of liquid. Considerable splashing of liquid when it contacts the capture surface.	-
190,400	314.40	Liquid stream begins to break up about 0.3 m from release point	1.0
224,100	319.94	Near the release point, the stream appears thicker and slightly more broken up.	1.0
254,900	324.77	Stream appears more broken up from 2 m on.	1.0
269,700	327.32	No vapour pockets were visible in stream. Break-up of liquid stream occurred, but more uniformly than 330 K liquid.	1.0
302,000	330.71	Definite liquid break-up about 0.2 m from release point.	-1.0
343,900	336.13		-1.0
362,500	338.37	Majority of liquid stream is being blown apart by vapour formation. The entire stream is broken apart about 20 percent of the time.	-1.0
366,700	338.42	Liquid stream begins to break-up near the release point. Complete shattering of the stream occurs occasionally.	-1.0
392,700	341.09	Stream break-up occurs about 2-3 cm from release point.	-1.0
470,600	348.81	Liquid stream has completely broken up. Visible drops appear infrequently.	-1.0
554,100	354.96	No large drops visible. Complete stream break-up within 1-2 cm (0.5-inch) of release point.	-1.0

Figure 3-16 shows the influence of the temperature of the type of jet generated after the nozzle, since a complete liquid jet to a fully sprayed type of jet. Figure 3-17 shows the pressure effect. Although both jets contain droplets after the nozzle, the spray angle is larger for the larger pressure.

Figure 3-16 Photograph of a flashing jet from a nozzle diameter of 1mm and fixed pressure of 85.000 KPa, showing five distinct temperatures, 13, 14, 18.5 and 20.2 °C respectively. Source: Yildiz, Rambaud et al. (2005)

Figure 3-17 Photograph of a flashing jet from the same temperature, 20 °C, and nozzle diameter, 1 mm, the effects of two pressure values, 850 kPa and 1250 Pa. Source: Yildiz, Rambaud et al. (2005)

Figure 3-18 shows the effects on the jet of the change in diameter of the nozzle. In this particular case it can be see that the jet flashing location becomes closer to the nozzle, changing the profile at the exit of the nozzle since a liquid jet discharge to a complete sprayed jet.

=-1

Figure 3-18 Photograph of a flashing jet from three nozzle diameters, 2 mm, 3mm and 4mm, respectively. All cases tested at 850 kPa and 13 °C. Source: Yildiz, Rambaud et al. (2005)

The effect of the length of the nozzle, is normally represented by the length diameter ratio, instead the actual value. Figure 3-19 shows three cases of 850 kPa and 20°C for L/D, 0, 2 and 7 respectively.

=-1

Figure 3-19 Photograph of a flashing jet from a nozzle of 2 mm, 850 kPa and 20°C for L/D, 0, 2 and 7 respectively. Source: Yildiz, Rambaud et al. (2005)

The type of regime achieve by the fluid after the release is an indication of how strong the nucleation rate was inside the fluid. The stronger the nucleation is, the breaking of the liquid core will be more extreme and the droplets generated tend to be smaller.

The model was also tested in water. The results for water are presented in Table 3-5 Description of the experimental test cases using water. Source: Brown and York (1974). The model seems to reproduce the system in good agreement with the observations reported, Johnson and Woodward (1999), as well as with the set of data reported by Reitz (1990). However, the same level of agreement is not achieve by other data set available, as for instance, Miyatake, Tomimura et al. (1981a), Miyatake, Tomimura et al. (1981b) or the

data from Park and Lee (1994). The discrepancies between the result and the observations reported can be due to use of quite large length diameter ratio, above $L/D = 30$ until a maximum of $L/D = 78.2$. When, the length of the nozzle becomes large in comparison with the diameter, then the temperature effect becomes stronger as the pressure energy is mainly used to overcome the losses through the nozzle. Consequently the expression of the production coefficient does not take into account the correct proportion of those mechanisms.

Table 3-5 Description of the experimental test cases using water. Source: Brown and York (1974)

Table 3-6 Description of the experimental test cases using water. Source: Reitz (1990)

Table 3-7 Description of the experimental test cases using water. Source: Energy Analysis INC (1990)

Table 3-8 Description of the experimental test cases using water. Source: Miyatake, Tomimura et al. (1981a)

3.3.10 Advantages of the model

A direct comparison between the present model and the models described in the review (Chapter 2) is not an easy task. The existing models are restricted to the use of one or two dimensionless groups to characterize the jet and normally those dimensionless groups differ from one model to other, Brown and York (1962), Park and Lee (1994), Peter, Takimoto et al. (1994), Johnson and Woodward (1999), Lasheras and Hopfinger (2000) and Skokov, Koverda et al. (2003b). In general the liquid velocity is used as the discharge velocity to compute liquid and vapour Weber and Reynolds numbers in the distinct models. Applying a criterion to distinct data to the one used to develop the proper criterion; it was found the application to another fluid under other conditions of

pressure and temperature in the vessel, as well as, different nozzles configurations do not generate a match in the results obtained by the authors. The values obtained for liquid Weber numbers show that this parameter was larger that the value of 8 reported by Brown and York (1962) as the limit between a jet with sinuous distortions and a spread jet. Although Peter, Takimoto et al. (1994) and Park and Lee (1994) did not establish any written expression to compare their results with any other equation to establish the limit between two different jet regimes. Their description is based on the behaviour of the jet in response to certain variation in the degree of superheat. The model follows the same trend to reproduce major nucleation for larger degree of superheat. Due to the availability of the experimental setting as well as the description of the type of resulting jet Johnson and Woodward (1999), it was possible to compare directly the results obtained by the model and the actual data. The comparison of the previous models with the results obtained by Lasheras and Hopfinger (2000) is not possible, due to the experimental setting used them introduces a coaxial stream around the jet exit. Therefore the physic modelled differs from one experiment to other.

The majority of the experiments are carry out at temperatures about sixty percent of the critical temperature of the fluid, which Reshetnikov, Skripov et al. (2002) and Skokov, Koverda et al. (2003a) suggest must correspond to jet with conical shape generated by homogeneous nucleation mode. However, some of the results correspond to a liquid jet, so again the use of this parameter only is insufficient to characterize the jet.

There are cases in which the criterion of flashing type of jet is based on two distinct parameters represented in a two-coordinate system graph. That is the cases of the work described by Lasheras and Hopfinger (2000). Although this map was developed for coaxial jets the comparison with other type of data was made. Figure 3-20 shows a compilation of the data tested for the production, dissipation model on a map space defined by Reynolds and gas Weber numbers.

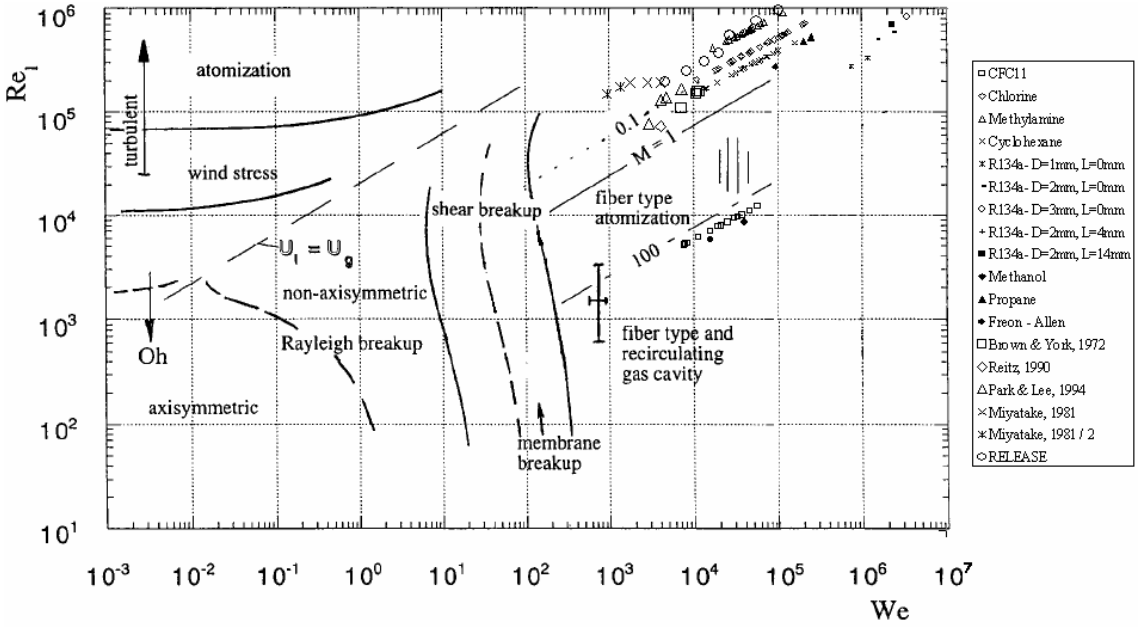

Figure 3-20 Liquid Reynolds number and aerodynamic Weber number map showing the different break-up regimes discussed by Lasheras and Hopfinger (2000). On the same map the location of different data listed in the legend is presented.

Water and hydrocarbons data are located in the left corner of the map, which means that all cases presented certain degree of atomization even in the cases where a complete liquid discharge is described. This inconsistency with the data is suggested to obey the no inclusion of the any thermal parameter is the model and also the influence of the coaxial jet flow. However, it is a consideration that when the velocity of the coaxial flow is far slow the physical situation correspond to a discharge to the ambient.

The application of the criterion proposed by Badens, Boutin et al. (2005) leads all the data points in the turbulent regime, in which the jet surface presents irregularities and the resulting droplets have different sizes and the jet becomes atomized. Figure 3-21 shows the Re, Oh map according to this criterion.

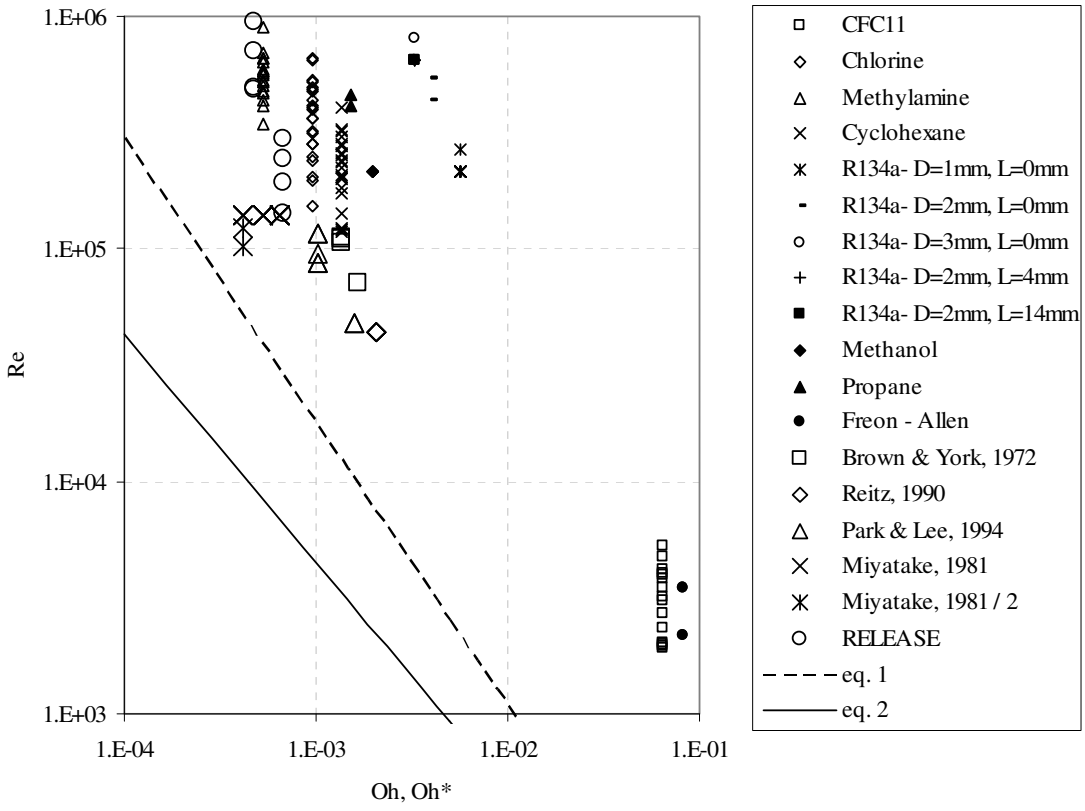

Figure 3-21 Map parameter space of the liquid Reynolds number and Ohnesorge number

In summary, it is clear that the influence of pressure, temperature and the condition of the nozzle are so close each other that it is not possible to express their effect on the jet using a criterion on a single parameter or even a combination of two of them. No model before has been applied to different settings with good agreement on the results, so here it is the main contribution of the new proposed model for flashing.

3.4 CALCULATION OF LIQUID AND VAPOUR MASS FLOW: "THE QUANTITATIVE MODEL"

3.4.1 Physical considerations – non isentropic process

To go into the actual calculation of the mass flow at the exit of the nozzle, the first task is to understand the implications of the simplification of the physics that can be done along the calculation procedure. Some authors have been using different hypothesis referred to the type of process based on energy arguments, such as, isothermal or isenthalpic process, isentropic process, etc. Those hypotheses allowed the authors to

obtain a complete set of equations to do the calculations of mass flow and other variables.

Along this section a discussion of these hypotheses will be presented as well as the discussion of the hypothesis used for this work.

Work performed by Wheatley (1987a), Solomon, Ruupprecht et al. (1985), and Fire_Science_Centre (1994) used an isenthalpic (isothermal) expansion of the flashing to estimate the conditions at the exit to ambient from the containment of a superheated liquid. The theoretical temperature limit for an isothermal is defined for pressure values larger than the liquid spinodal temperature at ambient pressure defined as $T_{vdW}\left(P_{amb}\right)$. If the initial temperature of the fluid is larger than this limit then the isothermal expansion is not possible. The green section in Figure 3-22 corresponds to the set of superheated condition that could theoretical fulfil an isothermal path between superheated pressure and ambient pressure. Note that the theoretical saturation line (sat) can be above the gas region of the fluid, due to the differences between the saturation line and the theoretical saturation line defined the Maxwell area construction on the van der Waals equation of state (sat_vdw). Although if the isothermal path is theoretically possible. It is known that this assumption is not true, due to observations in experimental setting that the temperature at locations close to the nozzle exit is close to the boiling temperate value.

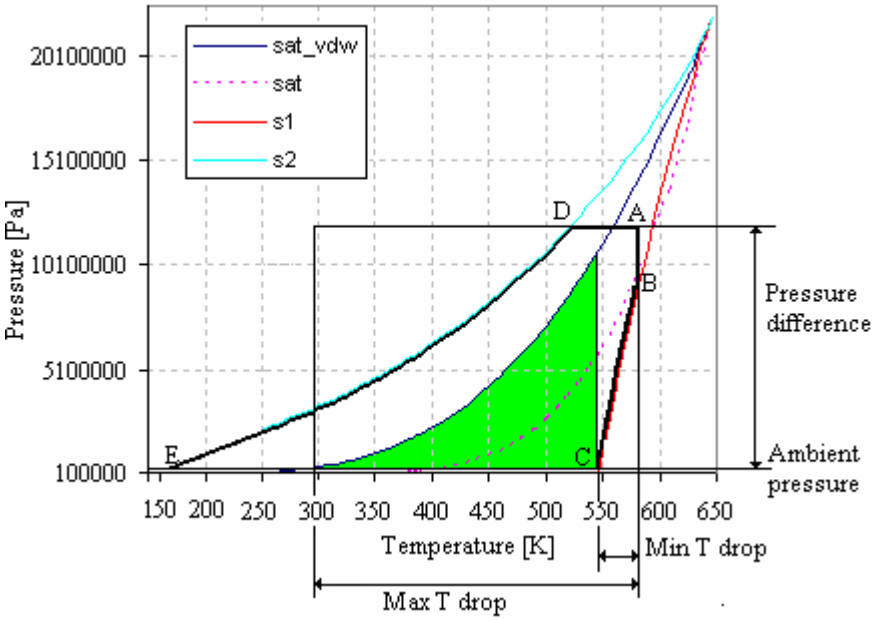

Figure 3-22 Schematic temperature-pressure path for the flashing expansion before the jet takes place

Table 3-9 Theoretical van der Waals spinodal temperature for standard ambient pressure (101325 Pa)

Van der Waals	TvdW(Pamb) [K]	Tb [K]
Butane	360	261.5
Chorine	353	236.6
Clorodifluoromethane- R22	313	232.65
Cyclohexane	469	350.3
Methanol	433	337.85
Methylamine	364	264.3
Propane	313	231.05
Tetrafuoroethane – R134A	316	246.6
Water	5460	371.9

Table 3-9 contains the temperature, $T_{vdW}\left(P_{amb}\right)$, that delimits the mentioned region for distinct fluids. Note that the gap between $T_{vdW}\left(P_{amb}\right)$ and the boiling point varies from case to case. This gap can be used as an indication of the possibility of a fluid to follow the theoretical path of isothermal process. However, the gap corresponding to water is larger than any gap of the hydrocarbons collected in the table, which suggests that the water could cover a larger range of initial condition (temperature and pressure) keeping the possibility of experience an isothermal expansion, but for hydrocarbons this possibility become smaller.

The HEM model and Moody's model cover the possibility of the initial stagnation point correspond to liquid condition, and the generation of vapour takes place under saturation or equilibrium conditions during the expansion process. This situation does not represent the bubble generation in a metastable liquid, once created the bubbles and the existing stream flow suffer an expansion process before across the nozzle. This

expansion is normally assumed to be isentropic, in HEM, or polytrophic in Henry and Fauske model, Fire Science Centre (1994).

An isentropic process assumption implies that the phase change occurs in adiabatic form as well as in absence of any non reversible work. The adiabatic consideration is based on the heat involved in the whole process came from the energy freed by the latent heat of the fluid, therefore non external sources of heat are not needed. This situation is supported by the temperature profile at the centreline of the flashing jet. It has an initial decrease due to the continuation of the expansion process and heat transfer between phases then a posterior increasing related to the entrainment gas from the surrounding is presented, which permits to establish ambient temperature as final state. It is clear that the initial behaviour close to the nozzle does not show too much interaction with the surroundings. An important interaction only appears after some distance downstream of the nozzle, named Minimum Temperature Distance (MTD), where temperature achieves its minimum value which is around 30 degrees smaller than of the corresponding boiling temperature. This situation is repetitive for different temperatures and pressure values inside the vessel before the leak takes place, fluids, as well as the geometrical configurations of the leak or nozzle, as it is shown in Table 3-10**.**

Table 3-10 Compilation of minimum temperature and other properties of flashing jet

	Propane Allen (1998a)	Butane McDonell and Samuelsen (1995)	R22 Chlorodifluoromethane Allen (1998a)	R134a Yildiz (2004)
Diameter [mm]	4	4	1 and 2.8	1,2 and 4
Boiling temperature [K]	231.05	261.5	232.35	246.6
Minimum temperature [K]	201	228	200	218.15
Tb-Tmin	**30**	**33**	**32**	**27.85**
Tinj [K]	288.95, 290.85 290.85	-		286.15, 295.15 295.15

The *MTD* can be described as the distance from the nozzle where the droplet transport phenomenon becomes more important than the thermodynamic effects, and it was discusses that the main thermodynamics process can be assumed adiabatic. Figure 3-23 shows the *MTD* corresponding to each case reported in Table 3-10. It is safe to assume that flashing takes place as an adiabatic process for the calculation of mass flow for different fluids with different diameters and conditions.

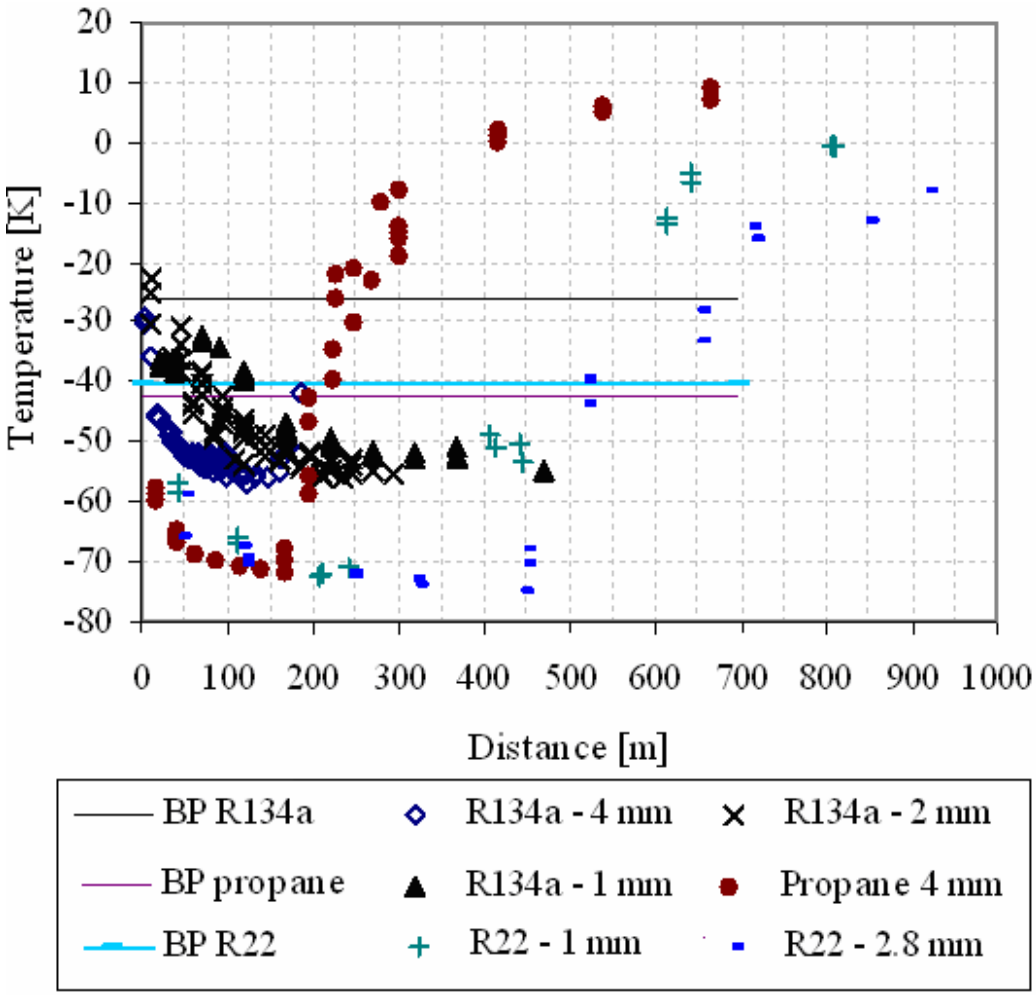

Figure 3-23 Compilation of temperature profiles for different fluids and nozzles. Sources: Allen (1998a, b, c), Yildiz, Beek et al. (2002a, b), Yildiz (2003);Yildiz, Rambaud et al. (2003) and Yildiz, Rambaud et al. (2004)

Table 3-11 Compilation of MTD for different experimental settings

Diameter [mm]	Fluid	MTD (x/d)
1	R134a	~600
2	R134a	300
4	R134a	150
4	Propane	150
1	R22	200
2.8	R22	450

The absence of work done by non-reversible field is an assumption a lot more difficult to justify due to the aggressive characteristic of the nucleation process. Especially, considering that the calculation of the mass flow will be carried out only for cases where flashing took place already. A closer look of the experimental data is made it is possible to deduce from the radial flashing jet velocity profiles that there is an initial rapid expansion process close to the nozzle characterized by a big spray angle when compared with the single phase jet angle.

A convenient way to see the mechanics nature of the expansion process experiences by a flashing jet is look into the spray angle of the jet. For this work the spray angle was determined based on the development of the radial jet velocity profile at four different measurement location from the nozzle corresponding to Allen (1998a) work and McDonell and Samuelsen (1995) for propane and methane respectively. The line called "Edge data 1%", in Figure 3-24, represents the connection of the points characterized by 1% of the maximum velocity value of the profile for four axial locations. The propane jet spreads more widely at the earliest part of the jet, for distance less than L/D about 3. The methanol also presents a larger angle in the earliest part, but as large as the propane angle. It can be related with the condition of the jet itself. After some distance far from the nozzle the angle tend to decrease approximately to the expected value of 15 degrees for single phase jet and it seem to be the same trend for both fluids, as is shown in Figure 3-23**.**

Both Figure 3-24 and Figure 3-25 show that there are two regions with two different spray angles along the downstream direction of the flow. The region closer to the nozzle has the larger angles and this region coincides with the adiabatic expansion discussed before. The second region far from the nozzle experiments a smaller spray angle. This new angle is related with the interaction between the jet and its surroundings. A large spray angle suggests an expansion process which is more likely to be violent and driven by non reversible field than a small spray angle. Therefore, in this work it is establish that an isentropic assumption is not the best hypothesis to follow.

Even so, in more recent works, some authors as Moreira (2000) and Moreira and Bullard (2003) applied the jump condition analysis to the shock waves in the discharge of a superheated liquid. Due to the metastable liquids supply the energy stored within them via the latent heat of vaporization, the evaporation wave was assumed as an adiabatic phase transition. Additionally, assuming the absence of work against the flow, the flow was defined as isentropic. The jump conditions leaded them in the Rayleigh equation and the evaporation adiabatic equation. The point where the Raleigh is tangent to the evaporation adiabatic curve, known as the lower Chapman-Jouguet point, is a unique solution to the jump condition for which the down stream condition is sonic or chocked in relation to the moving wave. However, depending on the initial thermodynamics conditions and the fluid boundary condition the subsonic flow can take place. The formulation involves a quasi one-dimensional steady evaporation wave inside the superheated liquid. The downstream condition has to be in thermal equilibrium, neglecting gravitational effects and the initial liquid condition as stagnation point. So, the results obtained will not suit the real physics of the problem.

It is still far too difficult to establish the path between the superheated liquid state involved in flashing and the final ambient conditions of the fluid, however, if the adiabatic assumption is taken together with an irreversible work assumption that will definitely suit better the real case of a flashing jet.

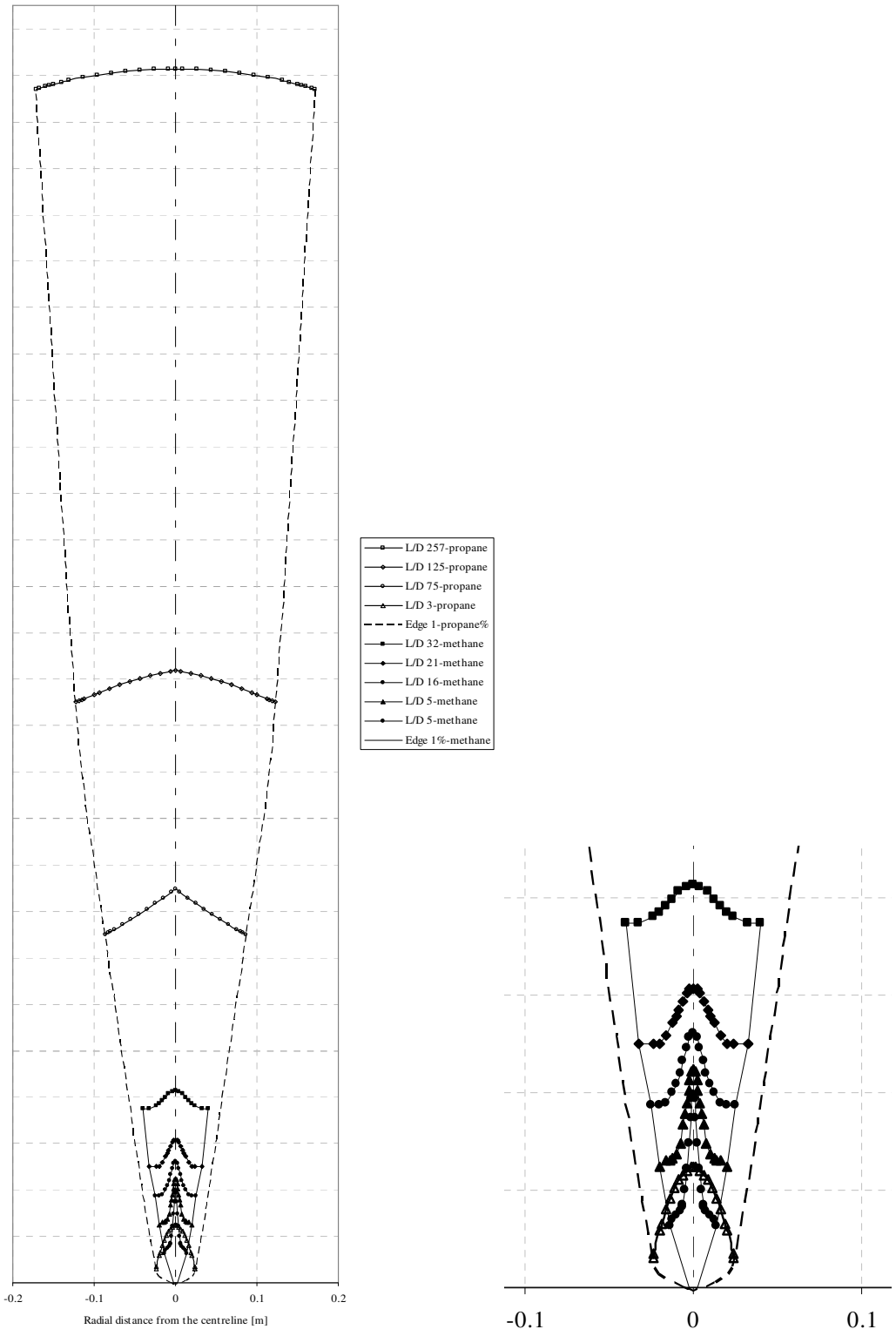

Figure 3-24 Jet velocity profiles at distinct downstream locations and jet borders for two different settings. The borders are determined joining extremes radial points of each velocity profile. Data from Allen (1998a) and McDonell and Samuelsen (1995)

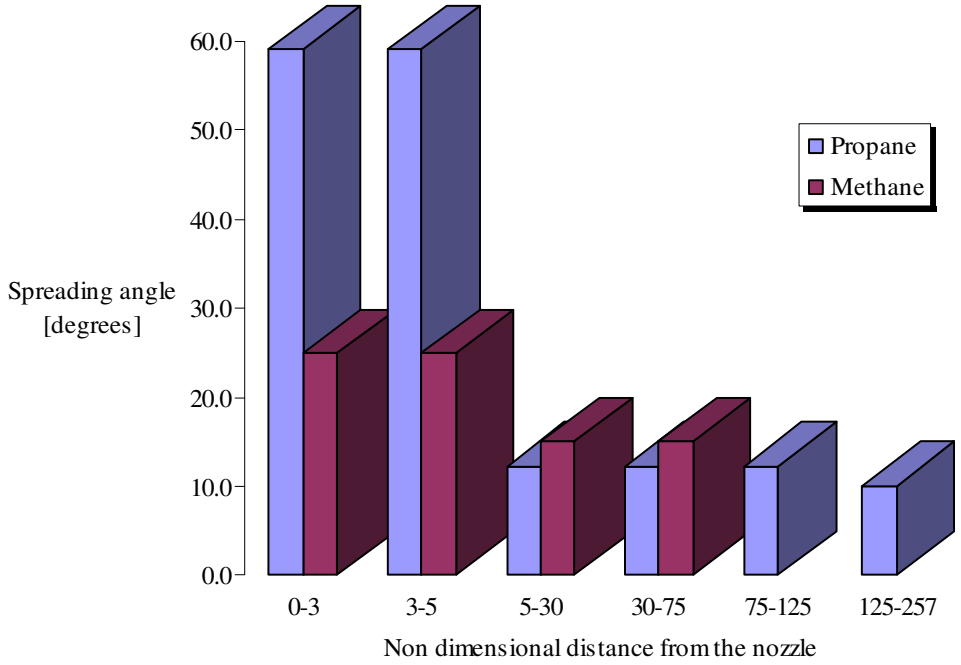

Figure 3-25 Compilation of spreading angle calculation based on data from Allen (1998a) and McDonell and Samuelsen (1995)

3.4.2 The critical condition for the gas phase and velocity model

It normally is considered to be in critical condition as extreme condition or at least subsonic. However, due to the coexistence of liquid and gas in a mixture the critical condition differs from the well know sonic condition of a single phase compressible gas. The speed of sound in gas-liquid mixtures is much lower than the speed of sound in each individual phase. The velocity of the sound in a vapour is often at least one order of magnitude larger that the velocity of the sound in the corresponding liquid. For instance, experiments and model calculations for air-water mixtures flowing in pipes at near-atmospheric pressures show that the speed of sound for void fraction in the range 0.2-0.8 was in the range 30-40 m/s for line with an absolute pressure in the range 1.4-1.6 bar, giving a good match with the experimental results, Gudmundsson and Celius (1999).

As the discharge flow of any flashing phenomenon can involve gas and liquid stream produced by a severe nucleation processes, this consideration must be included in the velocity calculation of the superheated velocity discharge of flashing cases. In a first approximation the kind of two-phase flow presented in a flashing process is a bubbly flow. The general expression for the velocity of the sound within a bubbly flow

considered it as a function of the void fraction of the flow, α, and independent of the size of the bubbles, Brenner (1995) and Young (1998).

$$c = \sqrt{\frac{v_l p}{\alpha(1-\alpha)}} \tag{3.34}$$

Table 3-12 contains the velocity of the sound according to Equation (3.34) for propane and for R134a as a function of the volume fraction. The classical critical single-flow approach often over predict the discharge velocity discharge of superheated fluid and therefore of the momentum distribution at the exit, even for low quality values.

Table 3-12 Velocity of sound as a function of the void fraction

Void fraction	u propane $[m/s]$	u R134a $[m/s]$
α	Propane	R134a
0.1	43.869	30.011
0.2	32.901	22.508
0.3	28.719	19.646
0.4	26.864	18.377
0.5	26.321	18.006
0.6	26.864	18.377
0.7	28.719	19.646
0.8	32.901	22.508
0.9	43.869	30.011

3.4.3 Jump conditions

As it is the case nucleation process involves an interface between phases. It can be modelled by introducing the thermodynamic definition of jump condition, which establishes that at the interface between phases properties are discontinuous. However

mass, momentum and energy must be conserved, Lahey (1992) and Drew and Passman (1999). The phase change process is confined to a discrete zone that moves inside the undisturbed metastable liquid and the two phase mixture downstream as a wave. The whole statement is made based on the differences of the mass, momentum and energy before and after the transition wave between the initial superheated liquid state ($_1$) and the final mixture state ($_2$). This difference is denoted by using squared brackets, [ ] around of the interested term. The term $[f]$ represents the difference of the variable f between the final and initial conditions, $f_2 - f_1$. The mixture at the final state must be in thermal equilibrium, Drew and Passman (1999), and it is assumed to be a homogenous mixture therefore it can be described by the void fraction of the mixture.

The general continuity, momentum and energy balances using the jump conditions are expressed by Equations (3.54), (3.55) and (3.56) Drew and Passman (1999).

$$\left[\rho\left(\vec{u}-\vec{u_i}\right)\right]\cdot\vec{n}=0 \qquad \textbf{(3.35)}$$

$$\left[\rho\vec{u}\left(\vec{u}-\vec{u_i}\right)+\overline{\overline{T}}\right]\cdot\vec{n}=\overrightarrow{m_i^{\sigma}} \qquad \textbf{(3.36)}$$

$$\left[\rho\left(U+\frac{u^2}{2}\right)\left(\vec{u}-\vec{u_i}\right)+\overline{\overline{T}}.\vec{u}-\vec{q}\right]\cdot\vec{n}=\varepsilon_i^{\sigma} \qquad \textbf{(3.37)}$$

The definition of the stress tensor can be observed in Equation (3.38).

$$\overline{\overline{T}}=-p\overline{\overline{I}}+\tau \qquad \textbf{(3.38)}$$

At the interface the viscous effects can be neglected in front of the effects of the surface tension on the interface and the creation of nuclei. It is know that for a bubble to growth a work must be done against the surface tension forces represented by Equation (3.39).

$$r=\frac{2\sigma}{p_v-p_o} \qquad \textbf{(3.39)}$$

No viscous influence has been reported on nucleation or boiling process. Under this approach, the second term of the Equation (3.38), the shear stress, τ, is neglected in this work.

$$\tau = \mu \left. \frac{du}{dy} \right|_{y=0} \approx 0 \qquad \textbf{(3.40)}$$

The absence of viscous effects of the fluid produces the absence of non-reversible work due to the stress tensor. Under these arguments the stress tensor is defined only by the pressure field of the flow. The term $\left[\overline{\overline{T}}.\vec{u}\right]$ in Equation (3.55) becomes $\left[\overline{\overline{p}}.\vec{u}\right]$. The assumption of the only heat source is the latent heat of the fluid becomes into the assumption of the process around the volume control is adiabatic and therefore the heat flux is null. After these assumptions the Equations (3.41) and (3.42) become:

$$\left[\rho\vec{u}\left(\vec{u}-\vec{u_i}\right)+\overline{\overline{p}}\right]\cdot\vec{n}=\overrightarrow{m_i^{\sigma}} \qquad \textbf{(3.41)}$$

$$\left[\rho\left(u+\frac{u^2\left(\vec{u}-\vec{u_i}\right)}{2}\right)+\overline{\overline{p}}.\vec{u}\right]\cdot\vec{n}=\varepsilon_i^{\sigma} \qquad \textbf{(3.42)}$$

The physical meaning of those equations can be described of the jump conditions to an inviscid fluid under an adiabatic condition. However, the surface tension effects are considered important to the development of interface and or course the flow. Surface tension influence is recorded in both the momentum and energy equation by the traction associated with the surface tension and the surface energy associated with the interface.

3.4.4 Velocity and void fraction calculation

Considering the study proposed for this work of the nucleation process is based on the assumption of adiabatic process in a presence of the non-reversible work due to the surface tension forces, the jump condition formulation describes above can be used to compute the velocity and the void fraction of the mixture.

The void fraction is the most common variable to define two phase fluid and their characteristics, Collado, Monné et al. (2006). The density of the mixture using the void fraction instead of the quality of the mixture is expressed as follow:

$$x = \frac{\rho_g}{\rho_M}\chi \qquad \textbf{(3.43)}$$

The density, internal energy and enthalpy of the mixture will be calculated using the following relations:

$$\rho_M = \rho_l (1-\chi) + \rho_g \chi \quad \textbf{(3.44)}$$

$$U_M = U_l (1-x) + U_g x \quad \textbf{(3.45)}$$

$$h_M = h_l (1-x) + h_g x \quad \textbf{(3.46)}$$

To simplify the equations to be used a change of variable is made. The relative velocity of the wave at the interface, w, the mass flow per unit area, $\dot{g}$, the force F and the term W are introduced as follow:

$$w = \left(\vec{u} - \overrightarrow{u_i}\right) \cdot \vec{n} \quad \textbf{(3.47)}$$

$$\dot{g} = \rho_1 \left(\overrightarrow{u_1} - \overrightarrow{u_i}\right) \cdot \vec{n} = \rho_2 \left(\overrightarrow{u_2} - \overrightarrow{u_i}\right) \cdot \vec{n} = \frac{w_1}{v_1} = \frac{w_2}{v_2} \quad \textbf{(3.48)}$$

$$\left|\overrightarrow{m_i^\sigma}\right| = F \quad \textbf{(3.49)}$$

$$\varepsilon_i^\sigma = W \quad \textbf{(3.50)}$$

Hereafter the equation used will be expressed as the product of the scalar product of the vector involved, which means that the velocity taken in to account is the parallel component to the normal of the interface surface. This fact assures that the velocities obtained from this approach are the velocity in the flow direction. In practice of flashing discharges, this model will be applied to the flow inside the nozzle, and then the direction of the flow is the axial direction of the nozzle.

Considering that the first point in the jump equations coincides with the superheated liquid without motion inside the containment, that means this can be modelled as the stagnation point, $u_1 = 0$, then the relative velocity of the fluid at that point corresponding a that point is only the negative of the interface velocity, $w_1 = -u_i$. However, the absolute velocity component after the wave is not null ($u_2 \neq 0$) and the relative velocity have both terms the absolute velocity and the interface velocity. The

work done against the system within the control volume is considered to be equal to the force per unit area multiply the absolute velocity after the wave.

$$W = Fu_2 \tag{3.51}$$

The absolute velocities of the flow before the wave, w_1, and after the wave, w_2, are both related to the velocity of the wave, u_i, as follows:

$$w_1 = u_1 - u_i \tag{3.52}$$

$$w_2 = u_2 - u_i \tag{3.53}$$

The continuity, momentum and energy balances using the relative velocity of the wave at the interface, w, and the mass flow per unit area, $\dot{g}$, are expressed by Equations (3.54), (3.55) and (3.56).

$$\left[\frac{w}{v}\right] = 0 \tag{3.54}$$

$$\left[p + \dot{g}u\right] = F \tag{3.55}$$

$$\left[\left(U + \frac{u^2}{2}\right)\dot{g} + pu\right] = W \tag{3.56}$$

For a position in the flow after the wave, the velocity must be different to above condition. In fact this velocity is proposed to be the velocity of the sound in that mixture. Based on the combination of the velocity can be expressed a relation between both velocities before and after the wave.

$$w_2 = u_2 + w_1 \tag{3.57}$$

Combining these equations with the mass conservation, the expression of velocity after the wave becomes a function of the void fraction after the wave and the wave velocity, as expressed by Equation (3.60).

$$w_1 \frac{v_2}{v_1} = u_2 + w_1 \tag{3.58}$$

$$u_2 = \left(\frac{v_2}{v_1} - 1 \right) w_1 = \left(\frac{\rho_1}{\rho_2} - 1 \right) w_1 \tag{3.59}$$

$$u_2 = \left(\frac{\rho_1 - \left(\rho_{2,l} + \alpha \rho_{2,fg} \right)}{\rho_{2,l} + \alpha \rho_{2,fg}} \right) w_1 \tag{3.60}$$

$$u_2 = \left(\frac{\rho_1 - \left(\rho_{2,l} + \alpha \rho_{2,fg} \right)}{\rho_1} \right) w_2$$

On the other hand, the velocity in the second point is expressed as the speed of sound in the flow.

$$u_2 = \sqrt{\frac{p_2}{\rho_{2,l} \alpha (1 - \alpha)}} \tag{3.61}$$

Using the relation between forces per unit area and the work done by the fluid, Equations (3.51), and the momentum and energy equations, the following equation can be written AS:

$$\left(p_2 - p_1 \right) + \dot{g} u_2 = F \tag{3.62}$$

$$\left(U_2 - U_1 \right) \dot{g} + \frac{u_2^2}{2} \dot{g} + p_2 u_2 = W \tag{3.63}$$

Further combination between the previous equations, it can be establish an implicit relationship of the void fraction which governs the characteristics of the flow after the wave. The solution of the system under the rule of Equation (3.51) will give then the void fraction of the mixture and therefore the all problem will be determined.

In cases where the internal energy information is not available, it can be calculated from:

$$\left[U \right] = \left[h - pv \right] \tag{3.64}$$

The behaviour of the term F showed by Equation (3.51) as a function of the void fraction is determined by the term mass flow per unit area multiply velocity after the wave, $\dot{g} u_2$. The rearranged form of the whole expression is reported as follow:

$$F = (p_2 - p_1) + \frac{w_2}{v_2} u_2 = (p_2 - p_1) + \left(\frac{\rho_1 (\rho_{2,l} + \alpha \rho_{2,fg})}{\rho_1 - (\rho_{2,l} + \alpha \rho_{2,fg})} \right) \frac{p_2}{\rho_{2,l} \alpha (1-\alpha)} \qquad \textbf{(3.65)}$$

The type of function expressed by Equation (3.65) has problem of been divided by zero when the void fraction is close to zero or one and also when the value of the density of the mixture after wave becomes closer to the liquid density before the wave.

Regarding to the behaviour of the energy equation, Equation (3.63), as function of the void fraction.

$$W = (U_2(\alpha) - U_1) \left(\frac{\rho_1 (\rho_{2,l} + \alpha \rho_{2,fg})}{\rho_1 - (\rho_{2,l} + \alpha \rho_{2,fg})} \right) \sqrt{\frac{p_2}{\rho_{2,l} \alpha (1-\alpha)}} + \frac{1}{2} \left(\frac{\rho_1 (\rho_{2,l} + \alpha \rho_{2,fg})}{\rho_1 - (\rho_{2,l} + \alpha \rho_{2,fg})} \right) \frac{p_2}{\rho_{2,l} \alpha (1-\alpha)} \sqrt{\frac{p_2}{\rho_{2,l} \alpha (1-\alpha)}} + p_2 \sqrt{\frac{p_2}{\rho_{2,l} \alpha (1-\alpha)}} \qquad \textbf{(3.66)}$$

The velocity of the wave is then computed from Equation (3.60). Finally the momentum and work done in the system by the transition between these two locations are computed from the momentum and energy conservation equations.

The total mass flow discharge by the system will be estimated by the velocity and the density establish by the jump condition at the nozzle.

$$\dot{m} = \rho_2 u_2 A \qquad \textbf{(3.67)}$$

The proportion of the gas mass flow and the liquid mass flow correspond to the void fraction of the mixture.

$$\dot{m}_l = (1-\alpha)\dot{m} = (1-\alpha)\rho_l u A \qquad \textbf{(3.68)}$$

$$\dot{m}_v = \alpha \dot{m} = \alpha \rho_g u A \qquad \textbf{(3.69)}$$

Due these calculations are made without any geometrical consideration rather that the wave area before and after is the same, the value of the area needed here should be the actual value of the area corresponding to the nozzle tested.

At this point the conditions for the simulations are established except for the droplet size and the droplet distribution characteristics.

3.4.5 Droplet distribution: Rosin Rammler distribution or uniform distribution

The size of the droplets generated depends on the potential energy of the fluid at the initial state, in other words, which level of the metastability the fluid has in the reservoirs. For high level of initial energy, the jet will disintegrate in small and uniform droplets; however, for lower energy level the droplets generated are not uniform in size.

The mass flow within a flashing jet contains a continuous vapour flow and droplets of liquid. These droplets can be dispersed in the cross section following a specific droplet distribution. The right estimation of this distribution is an important factor to perform further CFD modelling of flashing jet. Experimental settings have suggested that the Rosin Rammler distribution type of distribution has a good agreement with some of the results. However, due to the complexity of the process and the equipment needed, major of works done in this particular subject is related to the calculation of the droplets characteristic diameter, SMD or MD, not the distribution of different diameters of droplets. In some cases different correlations have been developed and reported.

To complete the necessary setting for the CFD simulation a group of correlations are used to establish the range of the droplet sizes to be tested. The actual proposal of a procedure to compute droplet characteristics inside a flashing jet is beyond this work. The range of diameter sizes obtained for the example used covers from 75 microns to 1500 microns. This range can be observed in Figure 3-26 contains not only the information of the droplet size but that information based on the two different velocity models, Separated flow (SF) and Homogeneous flow (HEM).

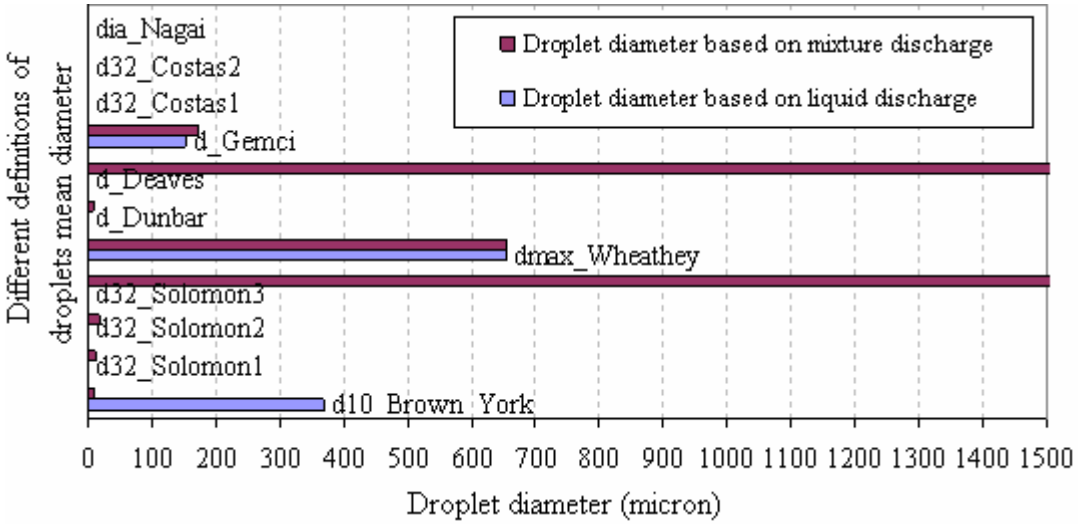

Figure 3-26 Compilation of droplet diameter calculation from distinct sources

3.4.6 Results

The results shown in this section corresponds to a hydrocarbon test case and a water case. When it was possible velocities calculated by others means are presented to facilitate the comparison of the results obtained.

The information of the experimental work performed by Allen (1998a), using propane was used as test case of the model developed and Table 3-13 summarizes the different values obtained by other methods on this case.

Table 3-13 Comparison of the result obtained by the experimental case of propane described by Kelsey (1999) and previously study by Allen (1998)

	Experiment	TRAUMA (liq)	TRAUMA (HEM)	Proposed model
Temperature [K]	~231	230.654	230.654	231
Pressure [Pa]	101325	101325	101325	101325
Jet diameter [m]	0.004	0.01525	0.0083	0.004 (actual nozzle) 0.031(CFD nozzle)
Vapour mass fraction [-]	-	0.22708	0.27806	0.001
Velocity [m/s]	~32	59.424	130.23	37.635
Mass flow rate [kg/s]	0.11	0.11	0.05854	0.236
SMD [m]	-	164.75e-6	116.4e-6	75e-6 - 1500e-6
Source	Allen (1998)	Kelsey (1999) Kelsey (2001)	Wheatley (1987a, 1987b)	

3.4.7 Water test cases

Table 3-14 Comparison of the result obtained by the experimental case of water by Reitz (1990).

	Experiment	Separated Model (SM)	Homogeneous Model (HEM)	Proposed model
Temperature [K]	-	373.15	373.15	373.15
Pressure [Pa]	-	101325	101325	101325
Jet diameter [m]	0.00034	0.00034	0.00034	0.00034 (actual nozzle) 0.010 (CFD nozzle)
Vapour mass fraction [-]		0	0.99	0.128
Velocity [m/s]	30	37.134	224.134	42.564
Mass flow rate [kg/s]	0.0020-0.0023	0.000329	0.000101	0.00366
Source	Reitz (1990)	Values obtained from procedure described in chapter 2	Values obtained from procedure described in chapter 2	

A comparison between three different approaches described by liquid discharge, HEM, and the proposed model, for water at the same initial conditions of temperature and pressure, is presented at Table 3-14**.** The exit velocity calculated using any of the two phase model seem to be larger than velocity obtained from the pure liquid condition. The introduction of any gas quantity to the original liquid will introduce larger velocities for the same mass flow, and then the pure liquid velocity can be used as inferior limit of the velocity.

The inclusion of the slip condition between phases makes a noticeable difference with respect to the other two phase case without the slip movement. The velocity value estimated for the mixture velocity (slip phases) is larger than the velocity for equilibrium case, due to the contribution of the gas phase velocity to the calculation of the total velocity directly as product of energy balance for the fluid as a whole.

Depicting the fact that the isentropic condition does not represent the actual physics involve. The results from the HEM usually have good agreement with experimental data in predicting the mass flow rate of refrigerant through a capillary tube, while it underestimates the mass flow rate for a short tube. For a short tube there is insufficient time for the liquid phase to form the bubble core and make bubbles grow. This results in large deviation from thermal equilibrium. The two-phase flow pattern inside a short tube may change from bubble flow to churn turbulent or annular flow with growing void fraction, but velocity slip the latter flow pattern will inevitably evoke big deviation from hydrodynamic equilibrium. From the above effects, the predicted flow rate will be underestimated in comparison with the measured. The effects of non-equilibrium characteristics on mass flow rate can also be verified by comparison of the results predicted by HFM and HEM models. For example, rapid acceleration or pressure changes cannot always be accurately modelled with the HEM model; i.e., discharge of flashing vapour-liquid mixtures, or shock wave propagation through a multiphase medium, Yang and Zhang (2005). This is especially true when the pressure change is large when compared to the ambient pressure, or any of the driving potentials are large relative to their reference values.

3.5 SUMMARY

The general idea of the proposed approach covers the qualitative and the quantitative aspect of flashing jet prediction, based on the statement that nucleation process has the more relevant role in the flashing occurrence. The qualitative part of the model can determine the type of jet at given conditions of pressure, temperature and nozzle geometry and the qualitative part is concerned about the calculation of the mass flow of each phase at the exit location of the jet.

Both qualitative and quantitative parts of the modelling correspond to a one dimensional approach of the behaviour of the whole system. The first part actually uses the similarities of the flashing problem and a second order system; therefore as a result of these similarities an analytical answer is obtained. The key task for this part of the work was the definitions of the stiffness and damping equivalent coefficients. They were established after a detailed study of the behaviour of each individual parameter on the phenomenon. The second part uses the jump condition approach of the conservation equation of mass, momentum and energy, to define the whole process in some way, as a one dimension problem. There are two main points before and after the transition wave, which it is assumed to be in the exit direction of the fluid. The results of the present model are superior to any other published models and in good agreement with most of the test cases. Table 3-15 shows the general trend of the influence of the parameters used to define the production and dissipation coefficients of the flashing system.

Table 3-15 Influence of initial parameters and fluid properties on the proposed model of nucleation process

Parameter	Change	Effect created on the nucleation
Pressure	Increase	Promote
Temperature	Increase	Promote
Diameter of the nozzle	Increase	Promote
Length of the nozzle	Increase	Promote
Liquid gas density ratio	Increase	Reduce
Specific liquid density	Increase	Reduce

CHAPTER 4: CFD MODEL OF FLASHING JET

4.1 INTRODUCTION

The one dimensional model described in Chapter 3 allows the calculation of the exit mass flow, the velocity and the void fraction at the nozzle needed to perform the simulations of the jet created.

Based on the premise of the mechanics mechanisms are more important for this part of the problem, the CFD simulations were established using gas as continuum phase with liquid droplets disposed at the inlet under the approach of the Droplet Discrete Model (DDM). DDM uses two frames, a Lagrangian frame for the droplets and an Eulerian frame for the gas in combination with the $\kappa-\varepsilon$ turbulent model.

The introduction of the concept of the computational model also obeys to the existence a region immediately after the nozzle where the thermodynamical mechanisms are too strong to be neglected. Therefore, it is proposed that there is a location inside the jet where these mechanisms become weak enough to be neglected. At this location the dimension of the jet, assumed circular, is defined by the computational nozzle. It is really important that the location where the simulations start is not the location of the experimental nozzle, in fact there is a distance between both, experimental nozzle and computational nozzle.

4.2 TEST CASE

The experimental data selected to perform the study of the influence of different parameters on the numerical simulation was from the work carried out by Allen (1998a). This data is the most complete set of data of its kind. The data covers the centreline velocity decay, the radial velocity profiles at four different locations far from the nozzle and the temperature profile at the centreline.

The first two phases of the flashing model calculation were applied to the experimental setting corresponding to the selected data. The information obtained and used as boundary conditions to be applied at the simulations as shown in Table 4-1.

Table 4-1 Results of the proposed model. The first column contains the experimental information at the nozzle location of a propane release, Allen (1998a). The second column contains the information from the application of the 1D model described in Chapter 3

	Experiment	Proposed model
Temperature [K]	~231	231
Jet diameter [m]	0.004	0.031 (CFD nozzle)
Vapour mass fraction [-]	-	0.001
Velocity [m/s]	~32	37.635
Mass flow rate [kg/s]	0.11	0.236
SMD [m]	-	75-1500

Experimental data from Allen (1998a) shows that the increase of the core region can be more than 120 times the nozzle diameter from the jet exit ($L/D > 120$). However, core region of single phase jets is estimated as 6.9 times the nozzle diameter from the jet exit, Wakes, Holdo et al. (2002). Longer core region of a flashing jet when compared with single phase core region for the same nozzle diameter suggest that the thermal processes compensate the possible velocity losses in the region close to the nozzle, allowing the fluid to keep the same velocity for longer period, although the transversal area of the jet is continuously growing as results of the expansion of the jet. This fact is an important point to take in consideration because the numerical modelling used did not include the thermodynamics process of nucleation, boiling or mass transfer.

Previous studies performed by Kelsey (1999) and Kelsey (2001) have demonstrated that the models that include droplets can match the experimental velocity profile only in the far region from the nozzle, even using over-predicted inlet velocities from the homogeneous equilibrium assumption. However, this fact suggests that the initial

momentum of the jet simulated is about correct since it matches the velocity downstream of the flow.

Therefore, it is clear that no matter if the inlet velocity and the mixture characteristics are correct, the process modelled on the computer will be different to the one that represent the complete physics.

The modelling made covers only the mechanical aspect of the droplets transport, such as drag, collisions and coalesce. A realistic result will be obtained if the thermal influence is taken into account before the simulation is started. Here it is proposed based on the conservation of momentum argument, that this can be made defining a computational model with represent a transversal section of the actual jet at some distance downstream the nozzle.

4.3 COMPUTATIONAL NOZZLE

The momentum of the whole jet along the jet axis must be conserved in the same way as it does in a single phase jet. The idea behind the 'Computational Nozzle' is to calculate the size of the cross section at which the jet has the same momentum at the actual jet calculated before.

As a result of the analysis of the experimental data available, it can be establish that the core region of flashing jets is longer than the core region of a single phase jet. This increment in length suggests that nucleation process plus the entrainment of air into the jet contribute to keep a constant velocity for longer.

It is proposed that for simulations using only the mechanical mechanisms, the initial location of the computational jet will be a cross section of the actual jet, instead of the nozzle exit, hereafter called Computational Nozzle or CFD nozzle. In this point density of the fluid will be taken as the corresponding vapour phase of the fluid and the density of the droplets will correspond to the liquid phase. Void fraction of the mixture changes along the axis of the jet. This variation in void fraction will produce a change in the density of the mixture, and of course it will change the liquid-vapour mass distribution along the axis.

For the location of this cross section which coincides with the computational nozzle, the momentum will be the same as the momentum at the nozzle, however, the contribution

to the total momentum of the vapour and liquid phases will be different. Due to the actual nature of the process and the presence of boiling as well as evaporation on the top of nucleation, the vapour phase portion will increase. Figure 4-1 shows the schematic location of the Computational nozzle. Computational Nozzle will be larger than the nozzle diameter. The proportion of liquid-mass phases at the Computational Nozzle is unknown, but it will be limited from the liquid-vapour proportion at the nozzle exit.

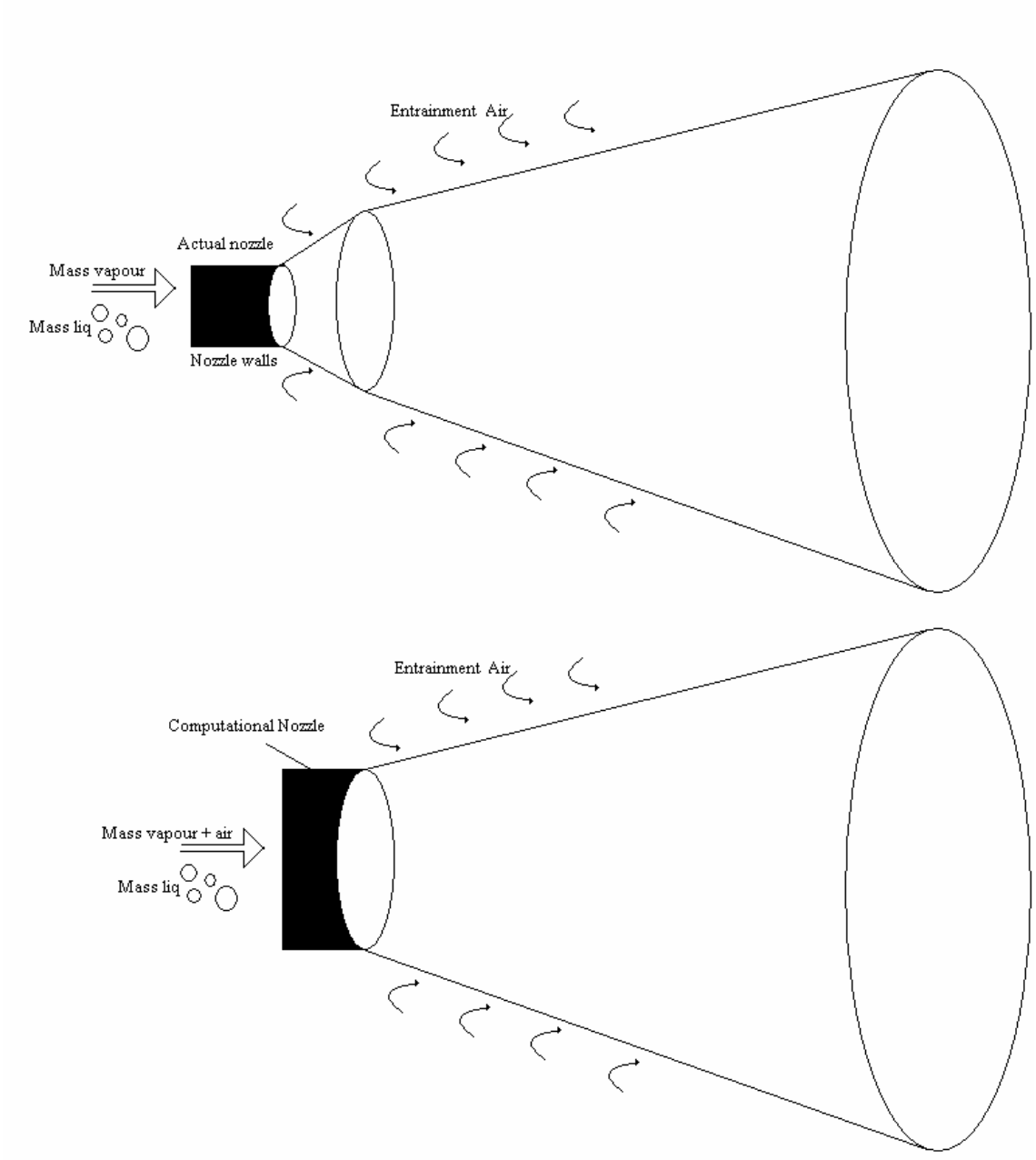

Figure 4-1 Schematic representation of Computational Nozzle and the actual nozzle of flashing jets. The computational nozzle represents a cross section of the actual jet. At this location the momentum of the jet must be conserved. Droplets also contribute to the momentum of the jet

The formula to calculate this CFD nozzle size is shown in Equation (4.1). This equation obeys to the momentum conservation in the jet, but due to the velocity is kept constant it becomes similar to the equation of mass flow conservation during the expansion zone. The quantity of mass that goes out at the nozzle is the same one that must be at the inlet condition. The transformation of the fluid between the real nozzle and the CFD nozzle is not well know yet. But in this portion of the jet must of the bubbles will growth and part of the remained liquid will evaporated. At the location of the computational nozzle the flow quality will be larger and there fore the momentum that need to introduce by the gas phase will be calculated from Equation (4.1).

$$D\big|_{CFD} = \sqrt{\frac{4\dot{m}}{\rho_v u_2 \pi}} \qquad \textbf{(4.1)}$$

where $\dot{m}$ is the vapour proportion of the total mass flow, ρ_v is the density of the vapour phase and u_2 is the velocity at the nozzle exit.

4.4 COMPUTATIONAL MODELLING

Based on the hypothesis that after the thermal expansion process takes place the mechanical mechanisms take over. The numerical approach of the modelling of flashing jets used in this work was restricted at the modelling of the droplet transport under mechanical actions, such as drag and momentum exchange with the flow. So, numerical modelling process of flashing jets consists in the modelling of droplet transport phenomenon along the jet axis. Often the criteria of comparison between experimental works and the simulation results are velocity and droplet distribution profiles along the flow direction.

Different processes related to droplets into gas surrounding have been developed, for single droplet and groups of them. All of these models assume that liquid phase can be considered as non-compressible fluid, while the gas phase is not. Some models can be applied to the situation with no relative motion between the droplet and the ambient gas in which a correlation based on Reynolds number can be applied to account for convective heat transfer from the gas to the liquid. Others models allow the relative movement between gas and droplets. Internal circulation is not considered for any of these; due to it has not impact on heating when the liquid temperature is uniform or constant, Sirignano (1999).

Unfortunately, the isolated droplet approach does not give a realistic representation of the actual situation. A grouping approach is necessary to achieve good modelling. Incorporation of processes like collision or break-up become important in this approach; because it represents another mechanism for exchange mass, momentum and energy between the liquid and gas phases and droplets themselves. However, the effects of the application of collision and coalesce models along the jet simulated here were not discussed further due to the focus of the CFD part of the problem was to establish where or not possible to use a two equation models in junction with the Droplet Discrete Model (DDM) reproduce the behaviour the flashing jet after the nucleation relevance cesses.

The Droplet Discrete Model (DDM) was selected to perform the simulation presented in this thesis. DDM solves equations for the continuous phase as an Eulerian flow field. The movement of the disperse phase through the calculated Eulerian flow field is performed separately using a Lagrangian frame of reference that permits the tracking of particles. The solutions of both phases are coupled by introducing appropriate source term in the continuous phase, allowing the inclusion of the effect of the discrete phase on the continuous phase and vice versa, and it permits alternate calculations of the continuous phase and discrete phase equations until a converged coupled solution is achieved.

Trajectory calculation of the particle is carried out by integrating a general force balance per unit particle mass that includes in addition to the drag and gravity effects, the force required to accelerate the fluid surrounding the particle, called virtual mass force, which becomes important if the density of the gas is larger than the density of the particle. Also are included, force due to the influence of pressure gradient, as well as the thermophoretic force due to the phenomenon known as thermophoresis, which generates of a force in the direction opposite to temperature gas gradient that affect small particles suspended in the gaseous fluid.

The general force balance equation can be written as follows:

$$\frac{du}{dt} = \underbrace{\frac{18\mu}{\rho_p d_p^2}\frac{C_D \,\mathrm{Re}}{24}\left(u - u_p\right)}_{Drag\ Force} + \underbrace{\frac{g\left(\rho_p - \rho\right)}{\rho_p}}_{Gravity\ Force} + \underbrace{\frac{1}{2}\frac{\rho}{\rho_p}\frac{d\left(u - u_p\right)}{dt}}_{Virtual\ mass\ force} + \qquad \textbf{(4.2)}$$

$$\underbrace{\frac{\rho}{\rho_p} u_p \frac{\partial u}{\partial x}}_{Force\ due\ to\ pressure\ gradient} \quad \underbrace{- D_{T,p} \frac{1}{m_p T} \frac{\partial T}{\partial x}}_{Thermophoretic\ force}$$

Where relative Reynolds number is defined as:

$$\mathrm{Re} = \frac{\rho d_p \left| u_p - u \right|}{\mu} \tag{4.3}$$

C_D is a function of Re and it normally can be written as:

$$C_D = a1 + \frac{a2}{\mathrm{Re}} + \frac{a3}{\mathrm{Re}^2} \tag{4.4}$$

where a1, a2 and a3 are constants that apply for smooth spherical particles over several ranges of Reynolds given by Morsi and Alexander (1972) as reported in FLUENT (2003), or

$$C_D = \frac{24}{\mathrm{Re}} \left(1 + b1 \mathrm{Re}^{b2} \right) + \frac{b3 \mathrm{Re}}{b4 + \mathrm{Re}} \tag{4.5}$$

where the variables $b1$, $b2$, $b3$ and $b4$ are function of the shape factor (ϕ), which is defined as surface area of a sphere having the same volume as the particle divided by the actual surface area of the particle, Haider and Levenspiel (1989) as it is also reported in FLUENT (2003).

4.5 EFFECTS OF BOUNDARY CONDITIONS ON CFD SIMULATIONS

There are three main parameters that can affect the momentum distribution inside the jet; they are the velocity, the area of the exit of the jet and the void fraction of the fluid. For two-phase jets the velocity of every phase also can induce the mentioned momentum variation. For this study the velocity of both phases is kept as the same. For this particular case of two phases problem, which deals with the presence of droplets of liquid within a gas stream, is important to highlight the behaviour of the droplets and their influence on the gas stream, if the momentum is conserved along the jet axis.

The angular momentum of the one individual circular turbulent structure, M_0, respect to the centre of the eddy can be expressed as:

$$M_0 = \int_0^{r_o} m\omega r dr \qquad \textbf{(4.6)}$$

where m is the mass of the fluid involved, ω the angular velocity of the eddy and r_0 is the radii of the eddy. Assuming that a droplet of mass m_d is captured inside of this structure then the angular momentum is conserved; then

$$M = \int_0^{r_o} (m + m_d)\omega r dr \qquad \textbf{(4.7)}$$

If these structure are located inside a jet, the angular momentum must be zero, and the lineal momentum across de flow for every distance, X_0, must be constant and equals to C.

$$\sum_0^n \int_0^{r_o} (m + m_d)\omega r dr \Big|_{X_0} = C \qquad \textbf{(4.8)}$$

If the total momentum is subscribed to a specific location downstream from the jet origin then this momentum must be equal to the momentum of the jet, and consequently it must be constant for any location in the axial direction of the jet. As first approximation no dependence with the time is considered.

$$C = \int m(r,x)\,du + \int u(r,x)\,dm \qquad \textbf{(4.9)}$$

Due that the density of the liquid phase is larger than the vapour phase, the mass brings for the droplet is larger than the vapour mass displaced by the droplet volume. So, the mass involved by the structure is larger. Then the product of angular velocity and the radii must decrease.

It is known that the mass of the droplets and vapour is not function only of radial distance to the centre; it is also function of the distance to the source and the time.

$$(m_d + m) = m(r,x,t) = f_1(r)\, f_2(x) \qquad \textbf{(4.10)}$$

Different authors have reported the droplet distribution as a Gaussian shape, with larger droplet located close to the centre, and this Gaussian shape becomes more flat as the

downstream distance from the nozzle increase. So, it can be proposed the following definition.

$$f_1(r) = \frac{1}{\sqrt{2\pi}\sigma_1} e^{-\frac{Ar^2}{2\sigma_1^2}} \tag{4.11}$$

$$f_2(x) = cont\ e^{-Bx} \tag{4.12}$$

While the velocity field corresponds to a typical jet profile:

$$u(r,x) = \frac{C_1}{\sqrt{2\pi}\sigma_1 x} e^{-\left(\frac{r^2}{2\sigma_1^2}\right)} \tag{4.13}$$

Come back to the integration for the axisymmetric domain, using the annular section

$$C = \int \sum_{o}^{n} \left(m + \frac{1}{\sqrt{2\pi}\sigma_1} e^{-\left(\frac{Ar^2}{2\sigma_1^2}+Bx\right)} \right) \frac{C_1}{\sqrt{2\pi}\sigma_1 x} e^{-\left(\frac{r^2}{2\sigma_1^2}\right)} 2\pi r dr \tag{4.14}$$

The total momentum of the jet also must include the effect of the entrainment, and the effect of the presence of the droplet and gas fluid. However, the mass function presented was set based on the droplet mass distribution measured in the experimental devices. It is clear also that the integration limits for this integral will change as function of the distance downstream of the nozzle, as result of the spreading angle of the jet. For rounded jet sources the spreading angle can be estimated as a function of the velocity at the inlet.

A series of simulations to establish the influence of the different boundary condition parameters as velocity magnitude, diameter of the injection and mass flows was performed. Droplet distribution was also tested as a parameter of variation of momentum inside a two phase jet. The results were analysed using the velocity profile at the centreline line. Comparisons with a single phase case with similar setting, as well as, with the experimental data available were performed. All the studies cases correspond to a circular jet, under 3D approach or axisymmetric approach, using the standard $k-\varepsilon$ turbulence model.

This section of the work described in first place the influence of each of the parameter that affects the momentum of the jet, using directly the experimental data of the velocity profile.

4.5.1 Nozzle diameter

The first variable to be discussed is the diameter of the CFD jet injection. In order to understand the influence of this parameter on the general behaviour of the jet, a matrix of four injection sizes, shown in Table 4-2, was selected two performance single phase simulations, with a constant velocity. Note that the column named Elements contains inside brackets the number of elements across the nozzle plus the elements across the rest of the domain in the same direction. The meshed presented in Table 4-2 are product of the results dependency on mesh study.

Table 4-2 Domains and meshes selected. First column contains the proposed diameter to be tested. Second, third and fourth columns have the number of elements specifying numbers of element by direction, the mesh size and the max aspect ratio present in the whole domain. Fifth columns contains the domain size in absolute and normalized by diameter values

Name	D [mm]	Elements X x Y	Mesh size	Max aspect ratio Xe/Ye (location)	Domain size (X x Y) (X/D, Y/D)
Case A	4 .(actual nozzle)	2200 x (10+240)	550000	13 (x=2m, y=0) 0.15 (x=0, y=0.15m)	2m x 0.15m 500 x 37.5
Case B	15.25	1300 x (10+150)	208000	12 (x=2m, y=0) 0.15 (x=0, y=0.15m)	2m x 0.5m 131 x 32.7
Case C	40	500 x (20+500)	260000	11 (x=2m, y=0) 0.15 (x=0, y=1.5m)	2m x 1.5m 50 x 37.5
Case D	48	500 x (24+500)	262000	(x=2m, y=0) 0.19 (x=0, y=1.5m)	2m x 1.8m 42 x 37.5

The inlet velocity was the same for all the cases shown in Figure 4-2, in principle the relative velocity between the jet and its surrounding is the same for all the cases. For circular nozzle the entrainment area is linearly proportional to the diameter of the jet and the transversal area of the jet is proportional to the square of its diameter, the ratio

of both, entrainment and transversal areas will be inversely proportional to the diameter, as expressed by Equation (4.15).

$$\frac{Perimeter.\Delta x}{Area} = \frac{2\pi D(x)\Delta x}{\pi D^2(x)/4} = \frac{8\Delta x}{D(x)} \qquad \textbf{(4.15)}$$

With Δx as a differential of length along the flow direction, and $D(x)$ as the diameter of the jet, which is a function of the distance downstream of the nozzle.

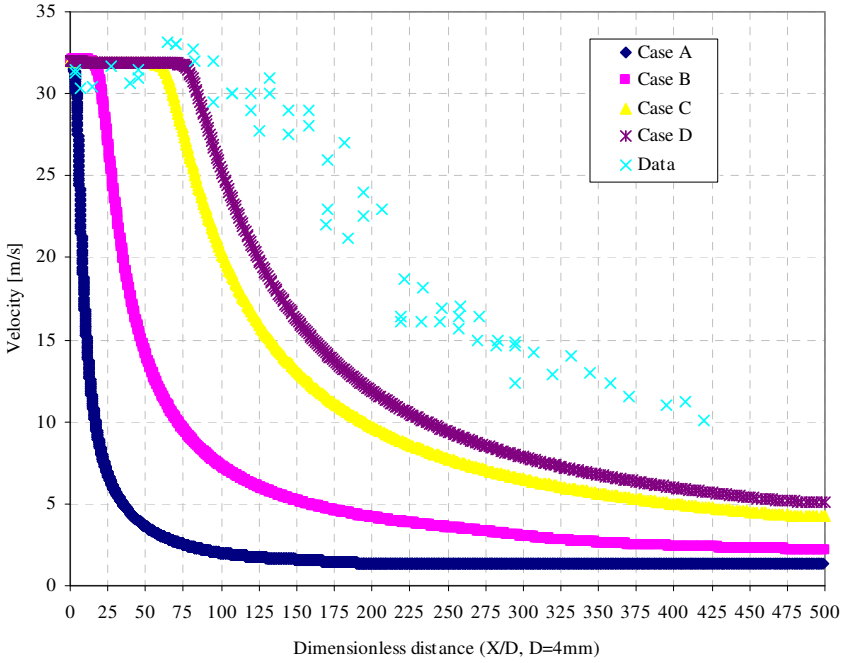

Figure 4-2 Influence of the CFD nozzle size on the velocity decay at centreline

This fact explains the inverse variation of core region length with the diameter. For larger diameter, the total air mass added from the surroundings respect to the jet mass will be reduced and the reduction in velocity due to the entrainment over the velocity profile will appear at longer distances. This effect can also be observed in the centre line temperature profile of the jet, where the temperature stays fairly constant inside the core region and after that region the temperature increases until achieve the ambient temperature.

4.5.2 Inlet velocity

Other mechanics to vary the momentum distribution are related to the change of the velocity at the inlet location. Table 4-1 contains experimental data on the test case selected, which correspond to the release of propane. The first and the second row of the table correspond to the original data from the centreline velocity and the radial velocity profile at 12 mm, Allen (1998a). The third value corresponds to the parabolic approximation of the velocity profile at that location. The fourth and fifth values of velocity shows in Table 4-3 correspond to the values reported by Kesley (2001), using the program named TRAUMA under the assumption of liquid discharge and the homogenous equilibrium model.

Table 4-3 Inlet velocities to be tested as boundary condition of CFD simulations. First and second columns have the diameter and velocity information from different sources. The third column information of the source or comments when appropriate

	D [mm]	U mean [m/s]	Observations
Experimental setting	4	≥ 32	Velocity must be larger or at least equal to the downstream measurement, Allen (1998a)
Velocity profile at 12 mm downstream from the nozzle (actual values)	40	~ 32	Maximum velocity = 37.72 m/s. The jet diameter corresponds to 35% of the maximum velocity, Allen (1998a)
Velocity profile at 12 mm downstream from the nozzle (approximation)	48	~ 32	The jet diameter corresponds to 1% of the maximum velocity
Liquid discharge condition	15.25	59.424	Kelsey (1999)
TRAUMA (HEM) discharge condition	8.3	130.23	Kelsey (1999)

As direct result of the inlet velocity the velocity profile at the centreline of the jet will match the experimental data or not. Often the available models over predict the velocity

at the discharge location therefore no match in the earlier zone of the profile is possible. However, for some cases large velocity at the inlet can be enough to mach the required momentum to simulate the actual jet. For those cases a later mach of the velocity profile in the direction of the flow is achieve. For instance, the case of the simulation by Kesley (2001) of the experimental case of propane reported by Allen (1998a), where the velocity used as inlet condition is about 130 m/s meanwhile the experimental data correspond to a velocity around 32 m/s, as can be observed in Figure 4-3.

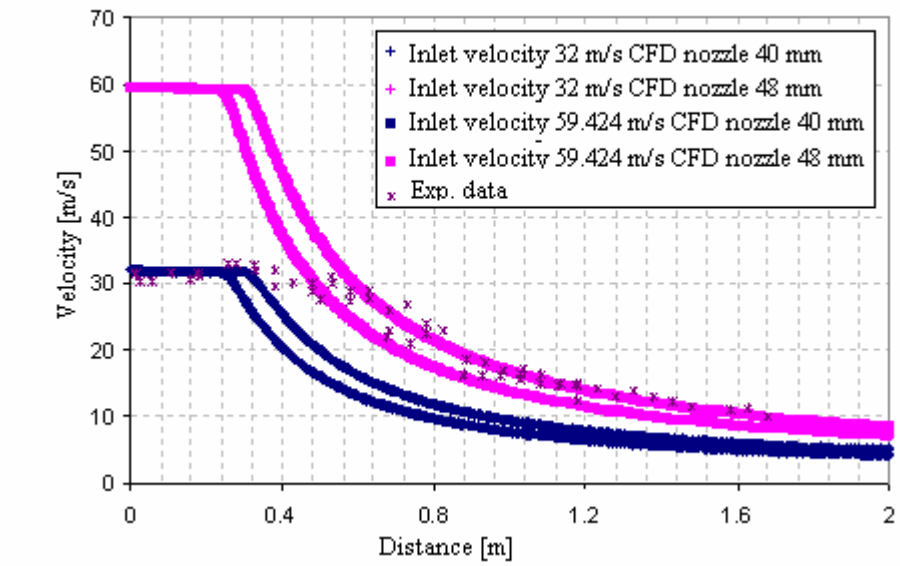

Figure 4-3 Influence of the inlet velocity on the velocity decay at centreline

Regarding the velocity distribution at inlet location, the influence of the velocity profile as boundary condition affects directly the shear layer close to the boundary at the interface between the jet and its surroundings. The application of a parabolic profile results in a little increase of the core region length. However, the application of a turbulent velocity profile at the inlet does not produce major differences with the constant velocity profile.

The application of the turbulent velocity profiles instead of a parabolic one seems to best represent the physics of the system. First at all, the mixture at the exit is affected by the nucleation process that introduce large number of discontinuity of the fluid and fluctuations in the main stream of the fluid, and secondly the characteristic Reynolds number of the liquid phase or for the mixture is often larger than the turbulent limit for

piping regimes. The possibility of the inclusion of different flow patterns as an annular, slug or bubbly flow is not considered.

The comparison between the experimental data obtained by Allen (1998a) and the result of the standard $k-\varepsilon$ turbulent model using the boundary condition corresponding to the TRAUMA liquid model is reported by Kelsey (1999) and Kelsey (2001). The last two points in Table 4-3, reveals that: the injection velocity of the jet is larger than the experimental velocity measured; the length of the core region seems three times shorter that the experimental results (L/4mm= 125); the slope of the computed velocity decay is quite strong at the beginning of the decay. The velocity slope looks similar to the experimental value only in the far field of the jet.

The velocity estimated for empirical model is larger in all cases than the experimental velocity and knowing for previous discussions about CFD injection diameter that the best approach to the experimental data is given by the larger diameters, 40 mm and 48 mm, a group of simulation using these two diameters and the velocity reported in Table 4-3 was tested.

The centreline velocity of simulations made is presented in Figure 4-3. The cases with inlet velocity of 32 m/s corresponding to 40 mm and 48 mm nozzle diameter do not have enough momentum to achieve the experimental behaviour over the complete near or even more in the far field. The cases with inlet velocity of 59.42 m/s, Kelsey (1999) and Kelsey (2001), do have enough momentum to reproduce the far field behaviour of the flow, although, the near filed in over predicted. This situation indicates that a best setting will correspond to a jet with velocity equals to 32 m/s but with an initial momentum equals to the larger inlet velocity case, 59.42 m/s. The results of the inlet velocity of 130.23 m/s, Wheatley (1987b), are not presented in Figure 4-3. However, as expected this condition also over predict both the near and the far regions of the jet.

The application of velocity as boundary condition is not only concerning to the speed of the fluid, it is also concerning about the velocity distribution. The influence of the velocity profile as boundary condition affect directly the shear layer close to the borders, in the interface between the jet and its surroundings. When a parabolic profile is applied, the shear layer between the jet and its surroundings decreases, due to the gradient of the velocity close to the border is smaller and therefore the drag of air inside

the jet decreases, decreasing the entrainment. As a result of the entrainment decreases the core region length increases. The differences between the application of a turbulent velocity profile and the constant velocity as inlet boundary condition are severe, due to the high gradient between the border the zone next to it.

The selection of one type or another of inlet boundary condition is a topic to be discussed due to the complex phenomenon that take place before the jet is formed. For instance is the discharge corresponds to a liquid discharge then the turbulent profile seems to be more appropriate due to the typical value of the Reynolds is normally large. However, if the discharge corresponds to a liquid–vapour mixture then the type of flow pattern developed before the exit, such as annular, slug or bubbly flow will determine a different profile at the exit. Unfortunately, it is part of the flashing process estimation that is not well established yet. However, for CFD purpose a constant profile seems to be well enough to do the simulations needed, except for the consideration of the core region length.

4.5.3 Void fraction: Single phase momentum vs. two phase momentum comparison

Table 4-4 summarize the computes of the mass flow and quality need in a two-phase jet to match the jet momentum at the inlet corresponding to the velocity of 59.42 m/s for nozzle diameter of 40 mm and 48 mm. It is assumed that liquid and gas have the same velocity at the inlet location and the gas mass flow is determined by the density at standard condition multiply the velocity multiply the area of the nozzle.

Table 4-4 Two-phase jet mass flow parameters.

Name	D [mm]	Gas mass flow [kg/s]	Liquid mass flow [kg/s]	Quality [-]
Case E	40	0.04926	0.1206	0.29
Case D	48	0.07930	0.1737	0.31

Due to the close value of the density of the propane gas to the density of the air, hereafter, the simulations of two phase jets involve propane droplets within an air gaseous jet. Initially, the droplet will be considered as constant diameter droplets.

Liquid droplets imposed at the inlet condition do not change the general trend of the velocity profile at the centreline. However there are some changes in the gradient of this profile. The core region keeps more or less the same length as the single phase cases. The velocity decay is smoother when droplets are added. This move forwards the decay of velocity reducing the gradient of the slope. The dimensions of the droplets added produce some differences in the magnitude of the velocity decay. Figure 4-4 shows the velocity profile for uniform droplets distribution of inert droplets with diameters from 75 microns to 1500 microns. Same quantity of momentum is added by the droplets to the flow, but its distribution varies.

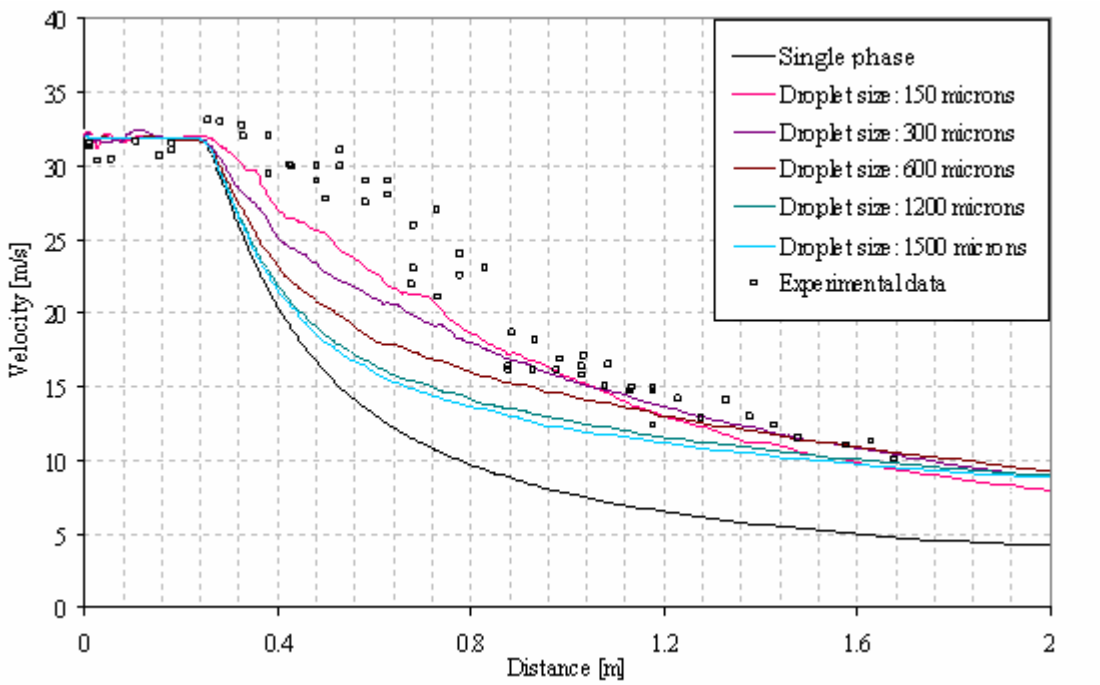

Figure 4-4 Influence of the droplet size on the velocity decay at centreline

The momentum incorporated by the droplets does not have major influence on the core region length. In fact the momentum added by the droplets, moves forward the decay of velocity reducing the gradient of the slope of the decay with respect to the single phase case. For distance up to 2 meters (X/D = 500) all the velocity lines are close to each another regardless the size of the droplet diameter tested. Larger numbers of smaller droplets actually help to reduce the slope of the velocity decay of the profile at the centreline compared to larger number of bigger droplets. In all cases, smaller droplets diameters, approach better the experimental values. The same trend was found for the

radial velocity profiles. The effects of the distribution of the momentum added by the nozzle are related to the balance of the drag forces on each droplet. Resulting drag forces on droplets are proportional function of the droplet diameter. Smaller droplet experience less drag and therefore they can carry for longer distance than the larger droplets before loss their initial momentum.

The comparison of the computed velocity for different droplets diameters with the experimental data, at 300, 500 and 1028 mm from the nozzle, is shown in Figure 4-5, Figure 4-6 and Figure 4-7. In all cases the smaller droplets diameters approach better the experimental values. However, both the axial and the radial velocity profiles have the same general trend as the experimental data.

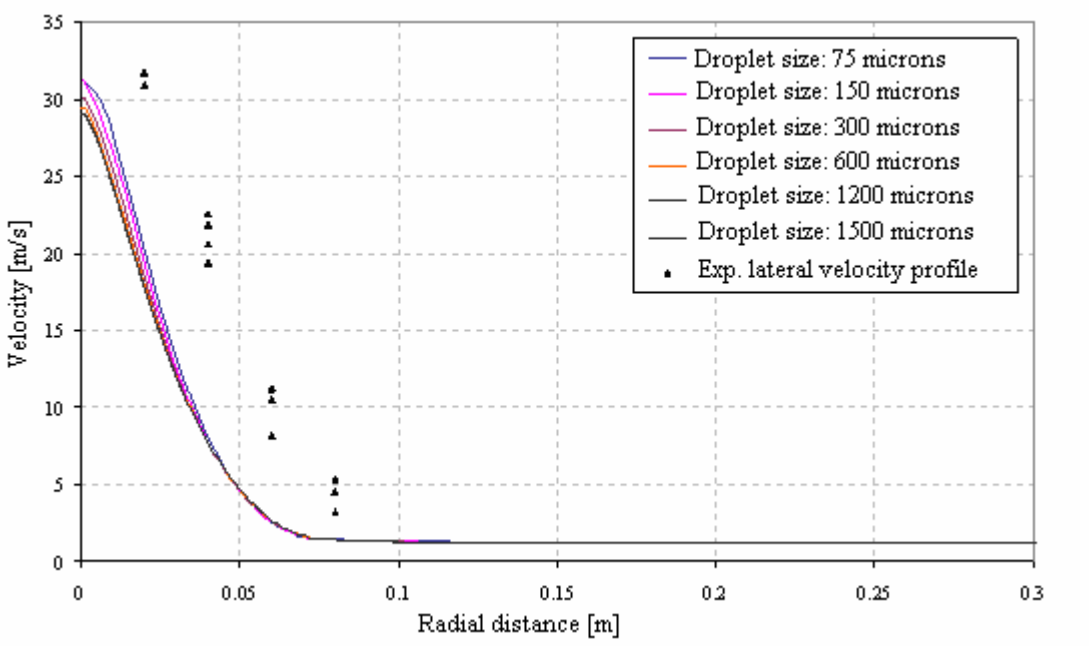

Figure 4-5 Radial velocity profile at 300 mm from the nozzle

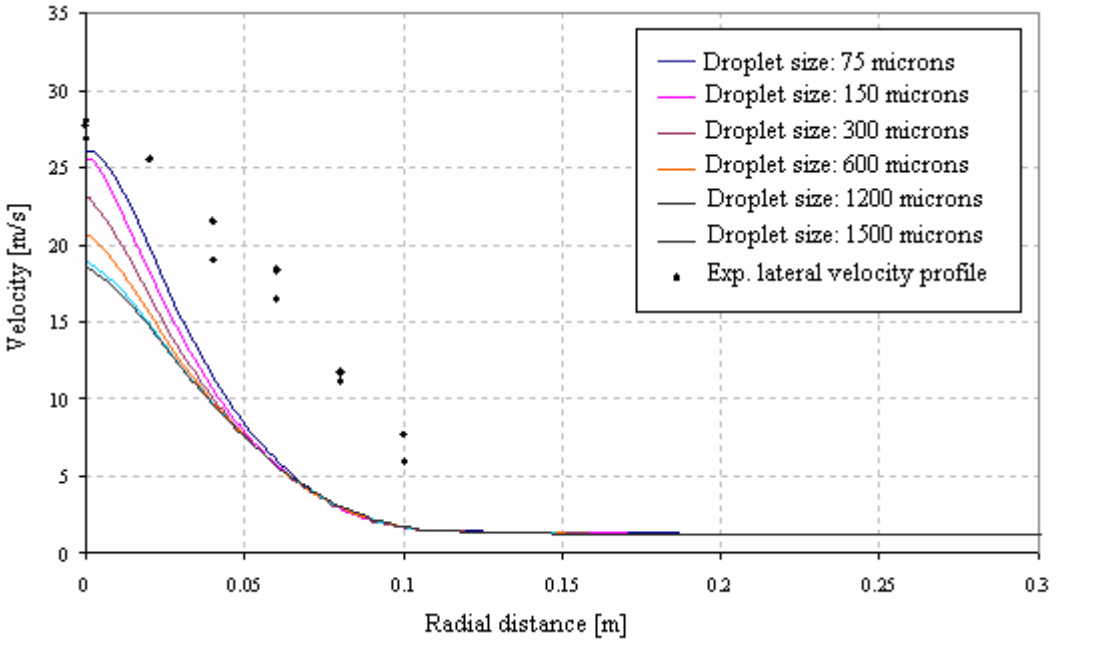

Figure 4-6 Radial velocity profile at 500 mm from the nozzle

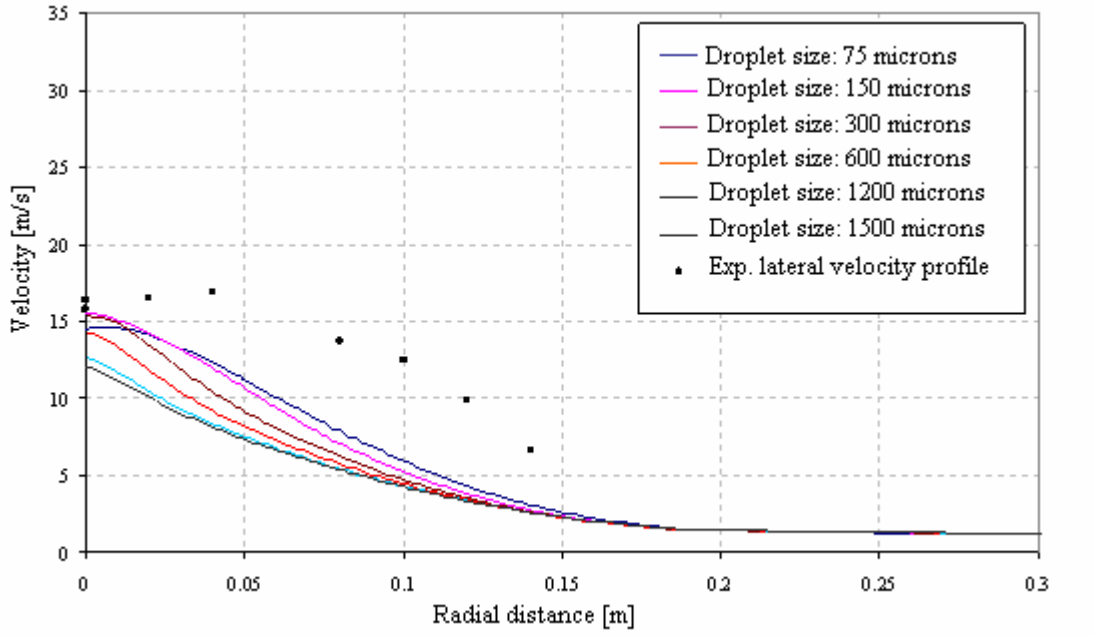

Figure 4-7 Radial velocity profile at 1028 mm from the nozzle

The size of the droplet imposed at the inlet affects the momentum that is added to the gas flow. The total droplet mass flow is a constant. The total momentum added by the droplets should be fixed. However, larger droplet will introduce more momentum per

droplet to the system than the small droplets. The drag forces generated bye the flow in each droplet is also larger. The results of the simulations show that the resulting forces from the balance between the momentum and the drag forces on each droplet size produces a larger decrease of the velocity in the centreline. This decrement in velocity is larger for larger droplets than for small droplets. Small droplets manage to kept larger velocity than larger droplets for longer, generating an extended velocity profile at the centre line when both sizes of droplets are compared. The drag force is expressed as:

$$Drag = C_D \frac{1}{2} \rho u^2 S \qquad \textbf{(4.16)}$$

Where the projected area of the droplet S is proportional to the droplet diameter

$$S \approx d^2 \qquad \textbf{(4.17)}$$

The drag increases as function of the droplet diameter.

4.5.4 Droplet distribution

Although a Rosin Rammler distribution at the inlet condition does not make any major difference in the axial or axial velocity profiles. It produces a more wide distribution of the droplets downstream the nozzle. The smaller diameters get dispersed in the radial direction as expected, conserving the larger diameter in the centre of the jet. The concentration variable of droplets in the radial direction for three different axial locations, 300 mm, 500 mm and 1024 mm downstream from the nozzle, are shown in Figure 4-8, Figure 4-9 and Figure 4-10.

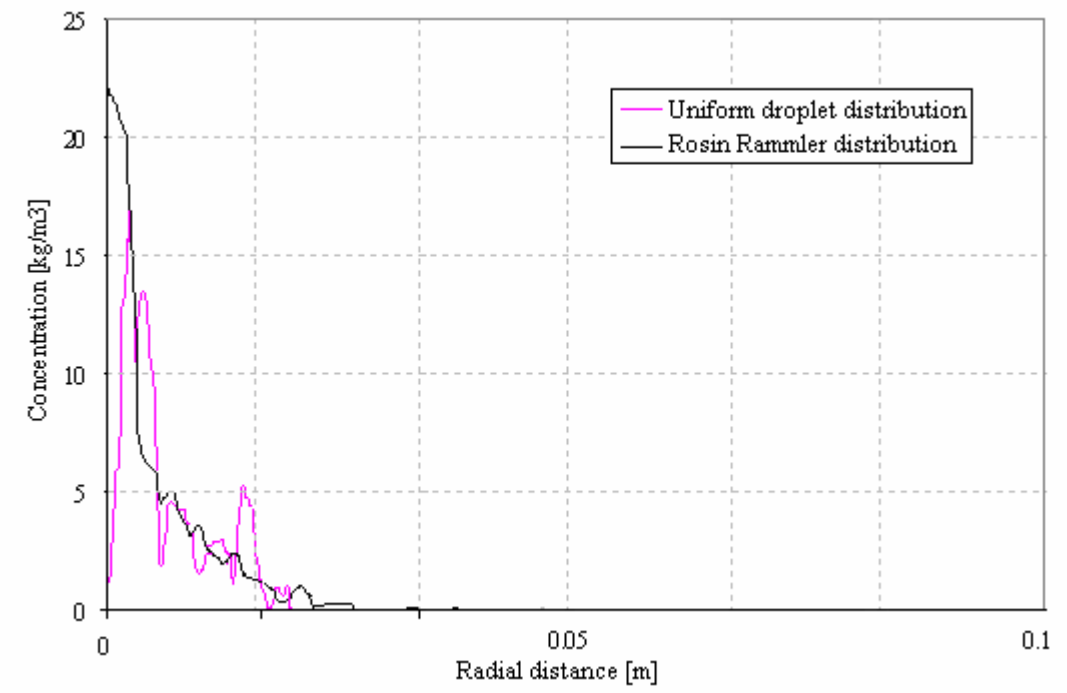

Figure 4-8 Radial droplets concentration profile at 300 mm from the nozzle

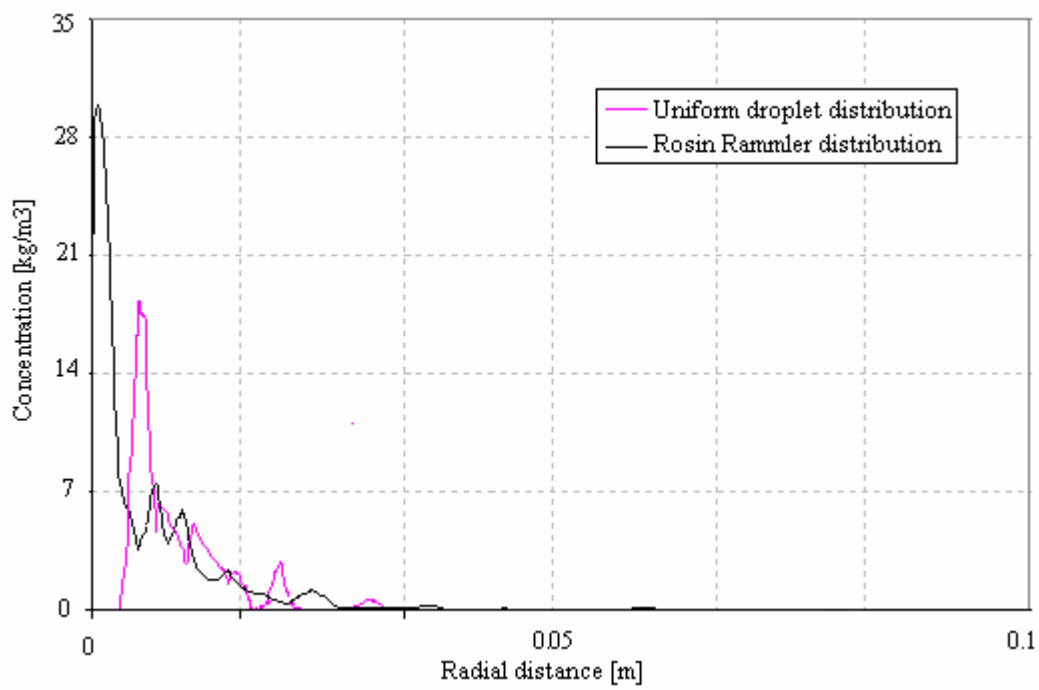

Figure 4-9 Radial droplets concentration profile at 500 mm from the nozzle

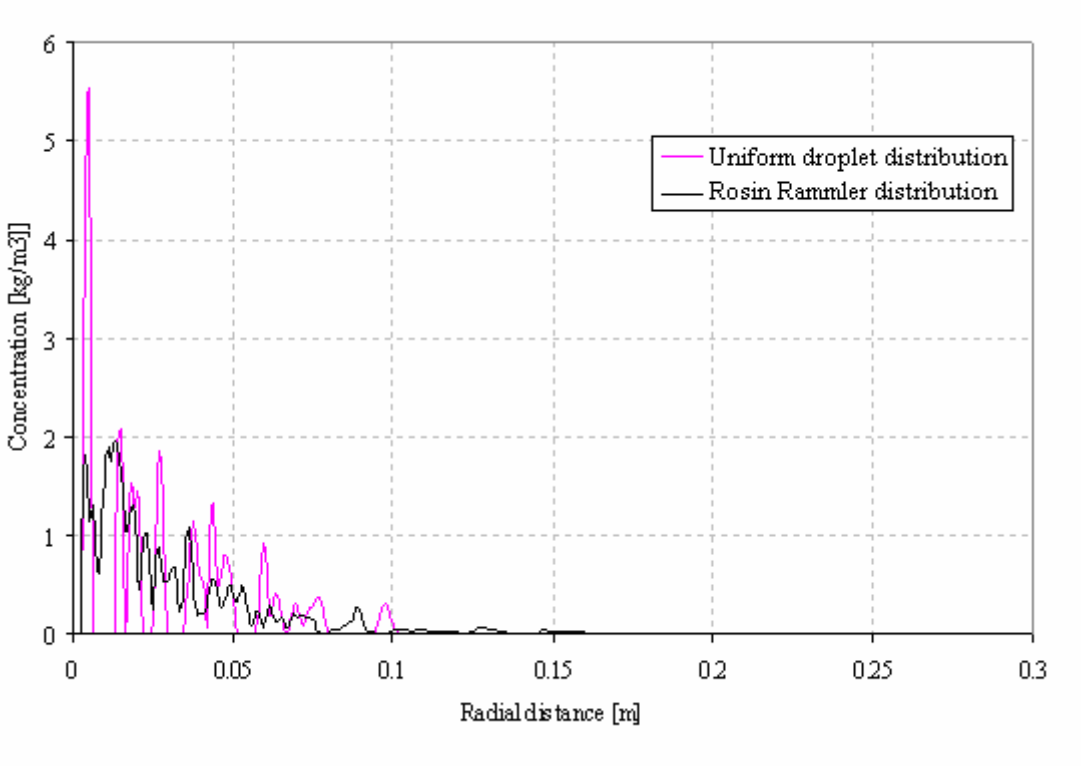

Figure 4-10 Radial droplets concentration profile at 1028 mm from the nozzle

The application of a Rosin Rammler distribution at the inlet produces a bit wider distribution of the droplets downstream the nozzle, but no significant differences are induced by this distribution of the axial or radial velocity profiles.

The dispersion of droplets in the flow depends on the particle size and the shear stress at what they are exposed. The dispersion function does not decrease monotonically as the particle size increase. The intermediate size particles are entrapped by the large eddies and then dispersed into the potential flow due to the centrifugal action, generating new larger level of turbulent kinetic energy.

The turbulent kinetic energy, the intensity and the dissipation of the kinetic energy decays corresponding to the smaller diameter of droplets represent the maximum situation. There is not any experimental data to compare with these simulations. The effects generated by the droplet presence can be explained as straighter the effect induced by larger droplet in the flow, reducing the total effect of it presence, when compared to the effect of the small droplet. In all cases the effects produced in these three variables for the droplet differ from the single phase profile of each parameter, as

expected. In the radial direction it is also shown that the parameters of turbulence are significantly larger for smaller droplets diameters.

The Kolmogorov's length scale and the Taylor length scale for the cases tested were about one hundred microns. So the ranges of droplets sizes include droplets sizes below and above these scales. The increment of the dissipation as well as the turbulent kinetic energy suggest that under the $k-\varepsilon$ model the droplet magnify the smallest turbulent structures in the regions where they are presented. The differences on the turbulent parameters obtained from a uniform droplet distribution and a Rosin Rammler distribution applied at the inlet are not significant, so the effect can be related to the mean diameter, d_{32}.

The effect of the droplets along the centreline shows two well defined sectors. The first effect decrease the carrier phase turbulent kinetic energy for a distance equivalent to the core region in the velocity profile at the centreline and it seems to be independent of the size of the droplet. The second effect is more complex and is related to the interaction between the turbulent structures of the jet and the entrainment of air from the surroundings which is more significant inversely proportional to the size of the droplets.

It is important to consider that the inlet location for the CFD study of flashing jet in reality represents a transversal section of the jet of the physical situation of post thermal expansion, where the phase change due to violent boiling is over, it is clear that the intensity of the turbulence at that location can vary in a wide range. To address this study the turbulence intensity and the length were fixed as 1% of turbulence intensity and a length of 0.0001 m. However, it is expected that for larger intensity the inlet velocity profile will smooth more rapidly, Byrne and Holdo (1994).

The turbulent kinetic energy, the intensity and the dissipation of the kinetic energy along the centreline are showed in the following Figure 4-11, Figure 4-12 and Figure 4-13, respectively. In all cases the effects produced in these three variables for the droplet differ from the single phase profile of each parameter, as expected. However, for the majority of the cases the differences in turbulent kinetic energy, turbulence intensity and dissipation is only noticeable after distance longer that the core region length, where the interaction between the flow and the fluid start to increase due to the velocity component of the flow as well as the droplets are not parallel any more, as they were in

the core region, where the leak of entrainment and the comparable small jet diameter does not produce major effect on the centreline line. Figure 4-14 and Figure 4-15 show the turbulent kinetic energy and the dissipation of the kinetic energy profiles in radial direction at 500 mm downstream the computational nozzle. It is clear that all the three parameters have a maximum for the case of the smaller diameter tested, especially in the regions close to the centreline where the droplets are concentrated. A large droplet introduces perturbations in the flow but it also goes through the flow imposing its direction of motion, which mainly will be straight. So, the large droplets act as flow straighter reducing the total effect of its presence when compared to the effect of the small droplet. Unfortunately, there is not any experimental information of these variables for the cases tested.

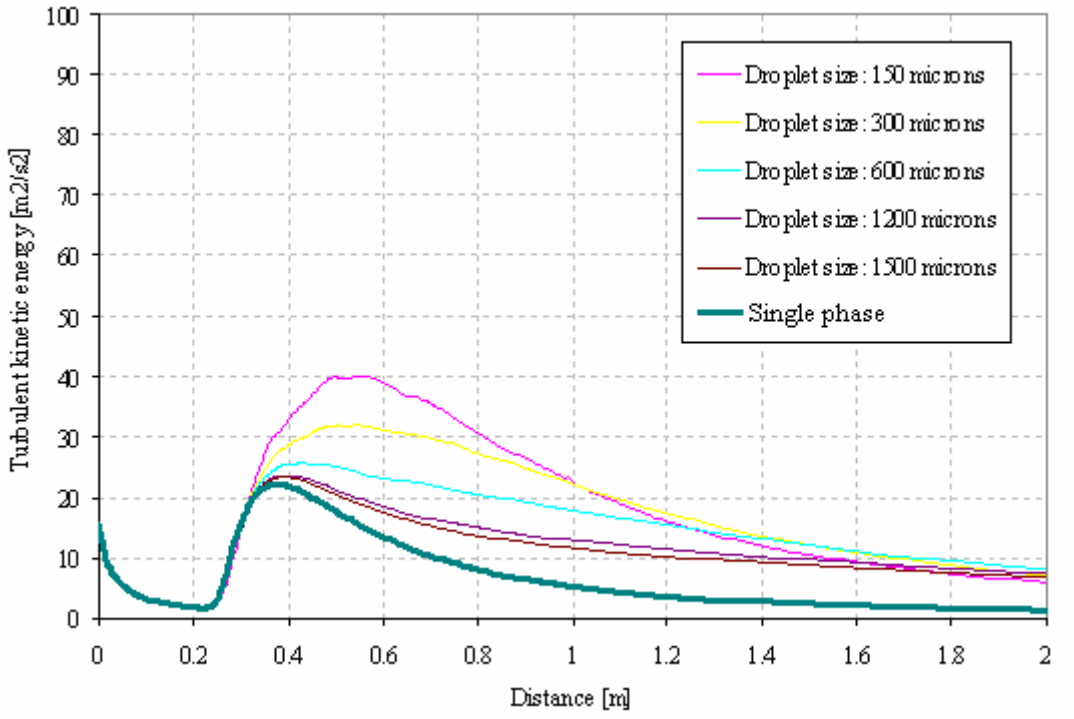

Figure 4-11 Centreline turbulent kinetic energy profile

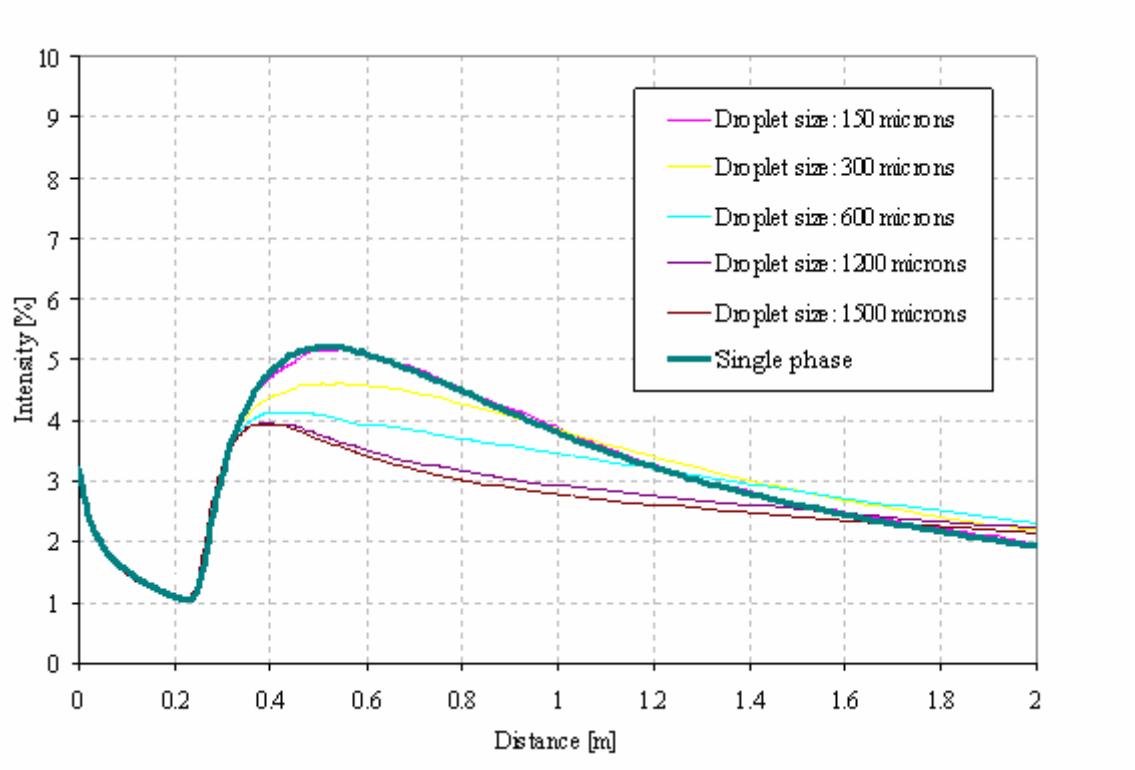

Figure 4-12 Centreline turbulent intensity profile

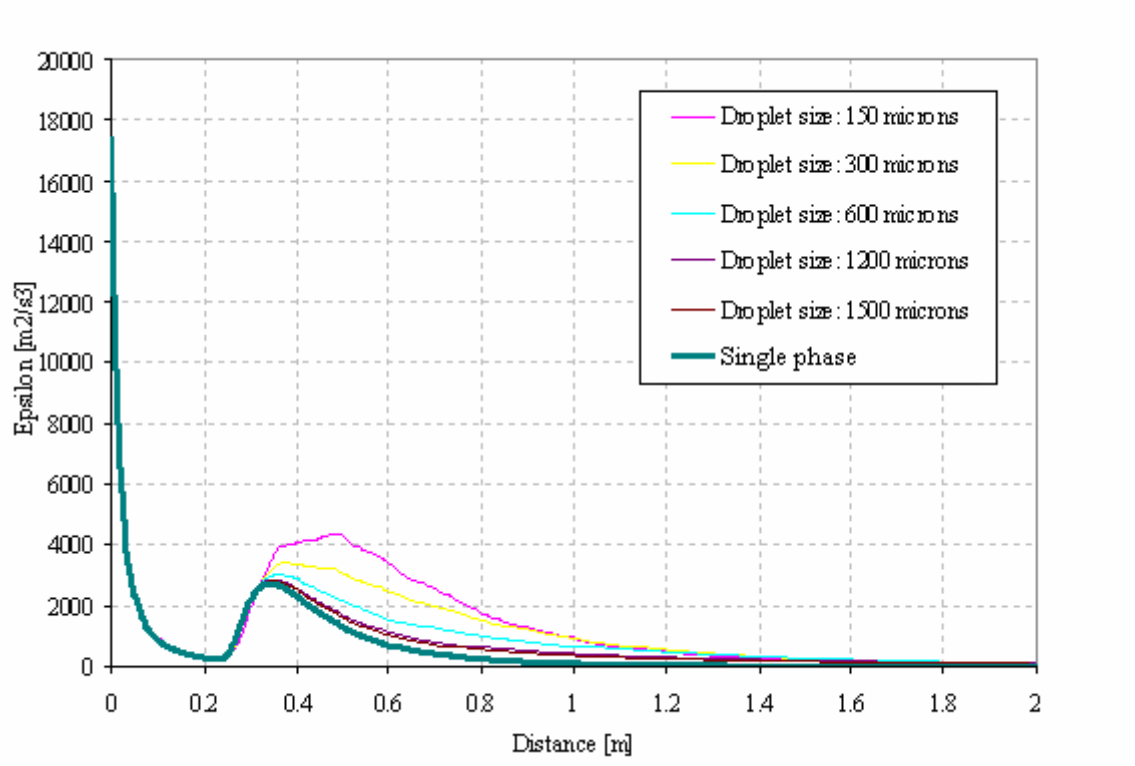

Figure 4-13 Centreline epsilon profile

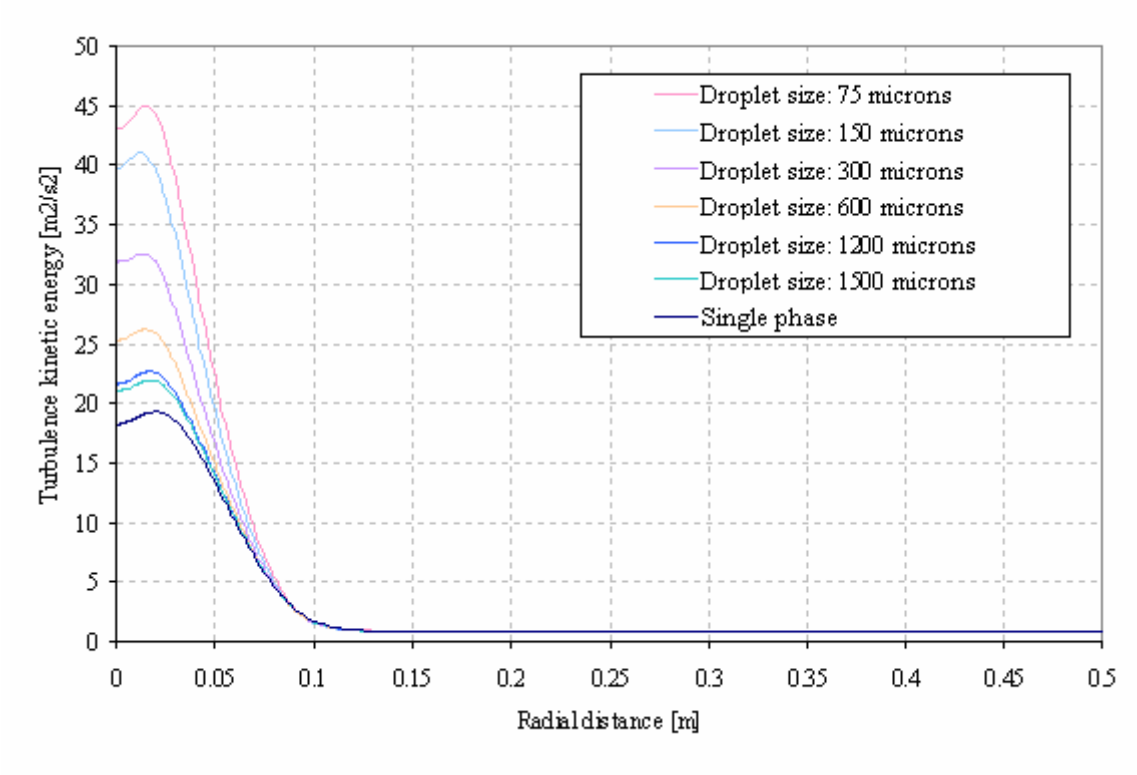

Figure 4-14 Turbulent kinetic energy profile at 500 mm from the nozzle

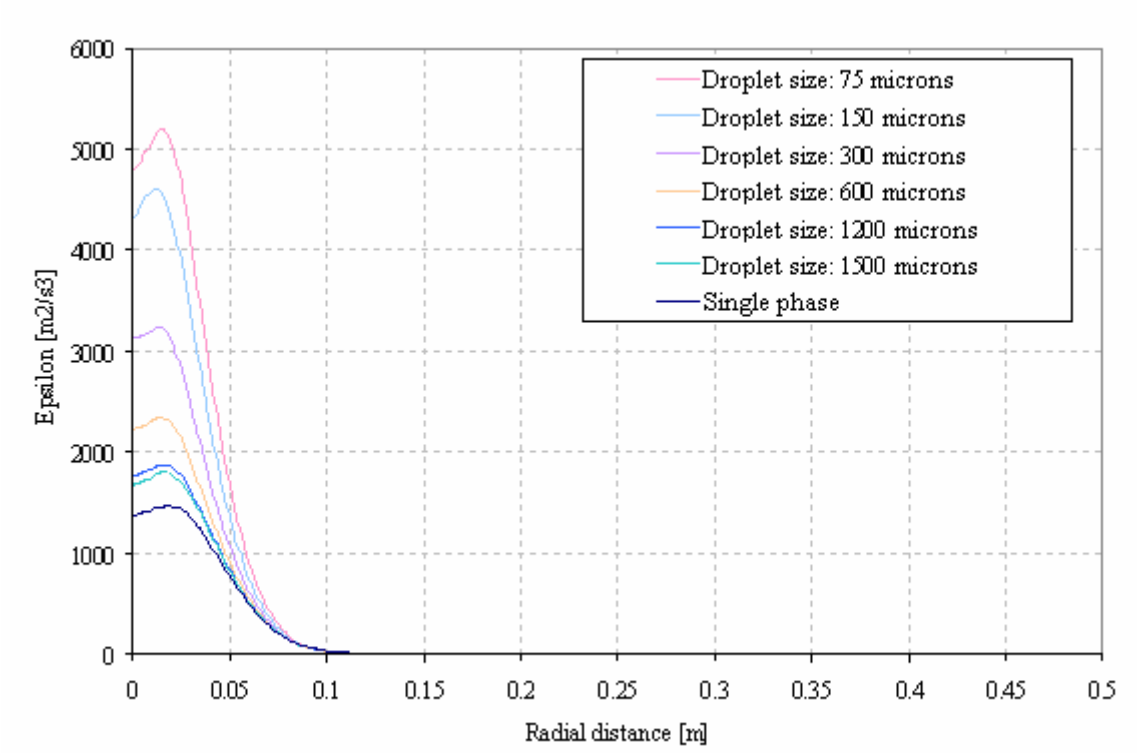

Figure 4-15 Dissipation of kinetic energy profile at 500 mm from the nozzle

In the radial direction it is also shown that the parameters of turbulence are significantly larger for smaller droplets diameters.

An estimation based on the Kolmogorov's length scale for the dissipation rate obtained in the simulation suggests this length is about one hundred microns as well as the Taylor length. This means the sizes tested cover the range over and under this important parameter. If the size is about Kolmogorov's scale then the particles tend to follow to the flow big turbulent structures, interacting closely with smallest turbulent structures. The increment of the dissipation as well as the turbulent kinetic energy suggests that under the $k-\varepsilon$ turbulent model the droplets magnify the smallest turbulent structures in the regions where they are presented. The differences on the turbulent parameters obtained from a uniform droplet distribution and a Rosin Rammler distribution applied at the inlet are not significant, so the effect can be related to the mean diameter, d_{32}.

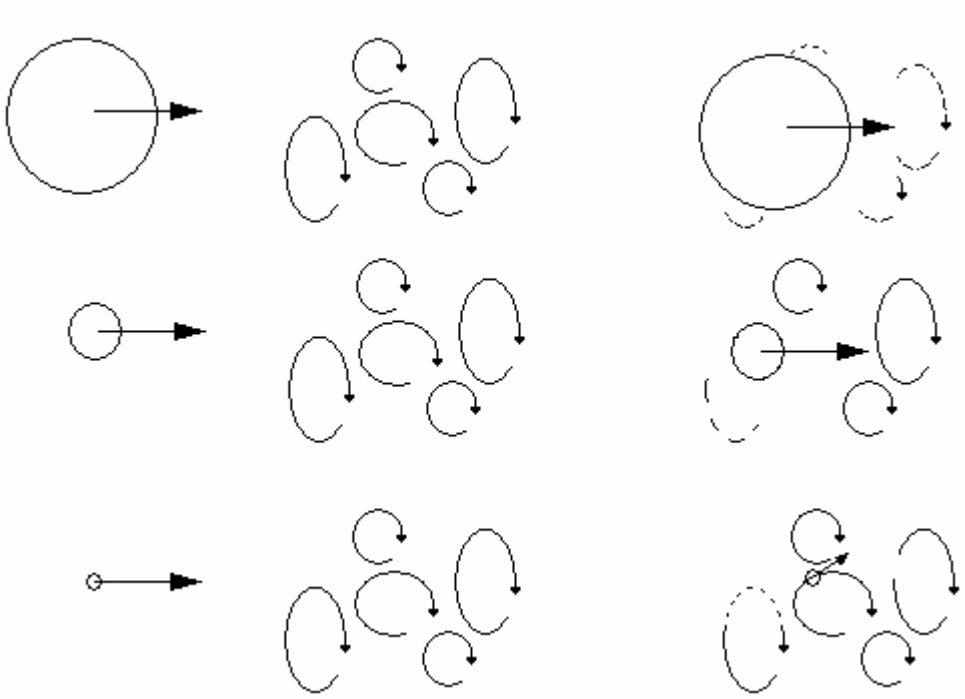

Figure 4-16 Effect of droplet diameter on the turbulent structures

Under the test presented above, the incorporation of the effects of droplets as generators of the turbulent structures has been made by the upgrading of the velocity profile. So, even using the standard $k-\varepsilon$ turbulent model without any special source term, the droplet presence constantly modifies the velocity field. However, the results involving

the interaction between the flow and the droplets affect the turbulent characteristic of the flow. Figure 4-16 shows a schematic representation of the effect of the droplet on the turbulent structure presented in the flow in front of the droplet. The larger droplet will go through the pre-existent structures and will break them. Medium droplets can destroy some of those structures but not all of them. The smaller droplet will be change partially the structures and it will be influenced by the structure, potentially changing it original direction through the structures.

Coming back to the concept of drag forces and assuming that the processes follow the isotropic condition in the turbulence. Due to small-scale motions can be assumed to be isotropic, this is known as local isotropy, even when the mean flow and motions of the large scale are not isentropic. Then the velocity affecting the droplet surface can be approximated as the turbulence velocity and therefore a relation between drag and the parameters of turbulence can be written as:

$$u \approx \sqrt{\overline{u'^2}} \tag{4.18}$$

$$k = \frac{3}{2}\overline{u'^2} \tag{4.19}$$

$$Drag = C_D \frac{1}{2}\rho\left(\frac{k}{3}\right)d^2 = C_D \frac{1}{6}\rho k d^2 \tag{4.20}$$

$$k = \frac{Drag}{C_D \frac{1}{6}\rho d^2} \tag{4.21}$$

The work done over the droplets, W, is established as drag force multiply the velocity

$$W = C_D \frac{1}{6}\rho k d^2 u = C_D \sqrt{\frac{2}{3}}\frac{1}{6}\rho d^2 k^{3/2} \tag{4.22}$$

and finally

$$k = \sqrt[2/3]{\frac{W}{C_D \sqrt{\frac{2}{3}}\frac{1}{6}\rho d^2}} \tag{4.23}$$

Basically the kinetic energy is inversely proportional to the diameter of the droplet.

4.5.5 Collisions and break-up model influence

The mechanics effect of the collision and the break-up model on the droplet distribution can be observed in the histograms at certain position. As it was described in previous section the radial droplet distribution follows an exponential shape. Additionally, it is reasonable to assume that the droplet already have a level of deformation at the inlet location. The deformation state of the droplet could have an important role in the simulations. An initial deformation of 5% is fixed.

From mechanical considerations the influence of the collision on the break-up and the distribution of the droplets, and consequently un the local generation of turbulence around the new droplets after the collision or even around the original droplets when them are close each other, depend on the velocity difference between the droplet involved in the collision, as well as, the relation of the droplets sizes. Then, it is possible to think in a relationship between the droplets collided and the turbulence generated as:

$$k = f_1 \frac{\left(\overline{u_{1,2}} - u_{vapour}\right)}{\left|u_d - u_{vapour}\right|} \tag{4.24}$$

$$u_{1,2} = \frac{u_{d,1} + u_{d,2}}{2} \tag{4.25}$$

The subscript 1 and 2 in the velocity, u, represent the velocities before and after the collision and f_1 represent the probability of the collision to happen.

4.6 TEMPERATURE PROFILE

Depicting the fact that the simulation here presented were made under the understanding that the gas jet with liquid droplets have no exchange of thermal energy between the phases, a variation in temperature is obtained along the centreline of the jet. This variation mainly obeys to the interaction of the jet and its surroundings. It is important that the simulations were started imposing an initial temperature of the fluid equals to the boiling temperature. Due to the absence of any model which implies any boiling, evaporation or even nucleation process in the jet there is not point in doing a comparison of the profiles obtained and the experimental data available. Due to as discussed before it is believe that the model using for the CFD simulation only can

apply with certain degree of accuracy after the nucleation process is cessed, therefore only a comparison of the change in temperature are comparable only after the MTD point is reached

From the experimental data, Allen (2002) and Yildiz, Rambaud et al. (2003), it is known that the temperature of the jet close to the nozzle correspond to the boiling temperature and the temperature far enough of the nozzle is the ambient conditions. The temperature profile at the centreline of the jet obtained using non evaporating droplets, showed in Figure 4-17 consists in an initial constant temperature until a distance consistent with the core region of the velocity profile, followed by a progressive increment until achieve the ambient temperature. Due to the absence of the evaporation and boiling characteristics in the droplet this behaviour does not mach the experimental data. However, it is clear that the gradient of the increment of temperature has quite different gradient respect to the experimental data, suggesting that the evaporation contribution is not only important in the region close to the nozzle, it is important along the whole jet. The standard $\kappa-\varepsilon$ does not reproduce the temperature decay in the system.

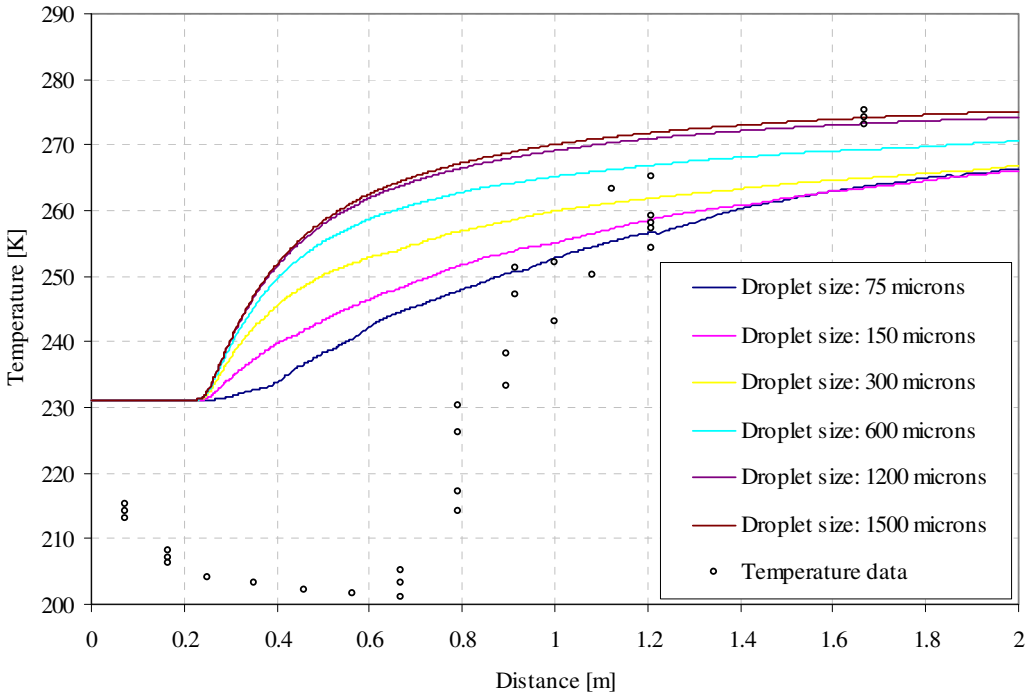

Figure 4-17 Centreline temperature profile for different droplets diameter

4.7 SUMMARY

The currents CFD models are not able to solve the nucleation process. However, with the computational nozzle the CFD simulations can be improved, due to the region where the nucleation has the most relevant influence is avoided. So, the actual jet is modelled after some distance where the droplets are already formed. Then the boundary conditions that impose droplets over a gas stream at the computational nozzle seem to represent quite well the reality. The results of the CFD simulations of the two-phase jet under the approach of the Droplet Discrete Model (DDM) in combination with the $\kappa-\varepsilon$ turbulent model can reproduce the behaviour of the jet downstream of the actual nozzle.

CHAPTER 5: DISCUSSIONS

5.1 INTRODUCTION

Flashing processes are both three dimensional and complex. They are at present far too complex to solve even by numerical means. Mechanics and thermodynamics interact to generate a specific type of two phase jet for given conditions. The identification of the predominance of a particular mechanism over the other in different situations helps to establish condition in a two phase jet. The nucleation process has been identified as an important part of the formation of flashing jets.

5.2 PRODUCTION – DISSIPATION MODEL

The general trend of the experimental information is reproduced by the present model. The information shown in Table 3-4 contains the original Freon11 data reported by Johnson and Woodward (1999) and the results of the application of the production dissipation model to establish if flashing jet takes place or not by the *sign* parameter. Results are satisfactory. Another way to reproduce the results of the model is represented the actual values of the functions that contain both production and dissipation coefficients in a two axis graph where the relative position of both function tells the type of jet generated under the circumstances evaluated.

The present model predicts that all the cases of R134a will produce a flashing jet. However, the experimental evidence is in some cases ambiguous. The criterion will depend on the accuracy in identifying a liquid with visible bubbles inside the jet or a complete liquid jet. It is important to mention that the order of magnitude of the reduced pressure range evaluated for the R134a cases is about 0.20, Yildiz, Rambaud et al. (2005). This value of reduced pressure is larger than any other experimental setting, where the common range for the evaluated reduced pressure is about 0.04. Therefore the dissipation coefficient has a smaller value which is overcome for the production coefficient. The model is capable of reproducing the experimental observations related

to basic influences of diameter increases, pressure increase, length increase, and temperature increase.

A good agreement was also obtained for experiments using water. Data reported by Brown and Roshko (1974), Reitz (1990) and Johnson and Woodward (1999) respectively all corresponding to water experiments were used to test the model. Table 3-8 contains the data reported. This table shows the results corresponding to the case reported by Miyatake, Tomimura et al. (1981a). In this case, the model fails to predict the liquid discharges. The discrepancies between the result and the observations reported can be related to presence of a large length diameter ratio, up to a maximum of $L/D = 78.2$. When, the length of the nozzle becomes large in comparison with the diameter, then the temperature effect becomes stronger since the pressure energy is mainly used to overcome the viscous losses through the nozzle and the viscous forces in the nozzle walls affects the force balance in the fluid. This alters the physics of the system modelled. In this case the surface tension will not be the major force acting on nucleation. Therefore the assumptions used to develop the expression of the production and dissipation coefficients do not apply in a correct way for this experimental data.

Application of the model is based on the fact that there is no need to calculate the velocity at the exit and the density at that location to compute the criteria proposed for the different authors. The proposed model only uses the pressure and temperature condition of the inside the vessel, the properties of the fluid evaluated at saturations condition and the nozzle dimensions.

5.3 MASS FLOW AND VOID FRACTION CALCULATION

Once it has been established that a flashing jet takes place. It is necessary to know more about the discharge conditions when the fluid leaves the nozzle.

The void fraction computed from the one dimensional model gives an indication of the expansion process that the fluid is experience through an aperture. Even when void fraction and quality of the mixture are related, in this work is believed that void fraction represent best the physics involved. After the comparison of the results obtained by the application of the proposed model to calculate the discharge velocity and other

characteristics of the flashing jet to hydrocarbon test cases and water cases showed in Table 3-13 and Table 3-14**,** respectively.

It was found the calculated velocity in all cases is smaller than the velocity estimated by the liquid discharge, HEM and two phase model in equilibrium condition and in not equilibrium condition models described by Solomon, Ruupprecht et al. (1985), Fire_Science_Centre (1994), Wheatley (1987a) and Kesley (1999), Kesley (2001). The addition of any vapour to the original liquid under any of the mentioned models will introduce larger velocities for the same mass flow. The velocity value estimated for the mixture velocity (slip phases) is larger than the velocity for equilibrium case, due to the contribution of the gas phase velocity to the calculation of the total velocity directly as product of energy balance for the fluid as a whole. The present model predicts discharge velocity from the data of Allen (1998a) better than other models, Solomon, Ruupprecht et al. (1985) and Wheatley (1987a). In the present model even when vapour and liquid are considered to be together, the assumption of that the flow must fulfil the critical condition together with the equilibrium condition, produces that the velocity discharge will be always delimited by the speed of the sound in the fluid.

5.4 SUMMARY

The CFD approach selected in this work concerns only the modelling of the droplet transport phenomenon once they are created. The reason for this selection is related to the initial hypothesis of the transition from liquid to a mixture flow will be cover by the proposed one dimensional model and the study of the droplets inside the jet will made based on mechanics aspects. The main objective of the simulations made in this work is to verify if the simulation of droplets transport mechanism using DDM is capable to reproduce the behaviour of the flashing jet after the expansion region. The numerical modelling will deal then with the mechanism aspect of the droplets transport, which are recorded on the Droplet Discrete Model. The present work uses the additional assumption of an adequate computational nozzle that will substitute the nucleation effects on the jet cross section diameter along the axis, but keeping the same fluid velocity at the nozzle location.

The results of the different simulations performed along this work show the relevance of the velocity magnitude used as inlet condition profiles. The core region length is

proportional to the size of the nozzle regardless to the inlet velocity. It is clear that the usage of the real nozzle as input information of the injection in the numerical simulation will never reproduce the physics of the system. The entrainment air interacts with the jet to keep constant mixture jet momentum. As a result of the approach chosen here the temperature profile along the centerline of the jet stays fairly constant inside the core region and after that region the temperature experience a progressive increment until achieve the ambient temperature due mainly to the entrainment. This profile does not match the experimental data in the early zone. The main difference between the experimental data and the results of the simulations can be located in the length of the core region even when a different computational nozzle is used. The cases with velocity of 32 m/s corresponding to 40 mm and 48 mm nozzle diameter for instance do not have sufficient momentum to achieve the experimental behaviour over the complete near or even more in the far field. The cases with velocity of 59.42 m/s, Kelsey (1999) and Kelsey (2001), corresponding to 40 mm and 48 mm nozzle diameter do have sufficient momentum to reproduce the far field behaviour of the flow, although, the near field is over predicted. This situation indicates that a best setting will correspond to a jet with velocity equals to 32 m/s, but with initial momentum equal to the larger velocity case, 59.42 m/s. However, if the computational nozzle is considered to be an cross section of the actual jet at certain distance downstream from the nozzle, then it is clear that the comparison can not be make base on the same axis reference. The location of the zero position for the CFD simulation will not be the same zero position of the real jet.

When liquid droplets are imposed at the inlet condition the general trend of the velocity profiles at the centreline do not change. The core region keeps the same length as the single phase cases. However, the velocity decay moves forward and slope of the decay of velocity reduces and it approaches the experimental slope, as it can be seem in Figure 4-4. Smaller droplet diameters approach best the experimental distribution of velocity.

A Rosin Rammler distribution produces a wider radial droplet distribution downstream the nozzle, however, no remarkable differences from a uniform droplet distribution are noticed.

The kinetic energy and dissipation of the kinetic energy decays corresponding to the smaller diameter of droplets show major interaction that than for larger droplets. The

smaller droplets are able to interact more closely to the flow structures. In the radial direction it is also shown that the parameters of turbulence are significantly larger for smaller droplets diameters.

It was tested that collision and the break-up mechanics introduced in the simulation by TAB and wave models, with an initial deformation of 5%, FLUENT (2003), have some effects on the droplet distribution only at far distance from the nozzle, even at further distances from the core region (x/d>150) along the axis. Collision model influence over the jet behaviour seems to be less important that the break-up influence along the jet axes, which means that the production of new droplet by break-up mechanism is more important than the number of new larger droplets product of the coalescence of two smaller droplet. However, no differences in terms of velocity profile at the centre line are noticed.

CHAPTER 6: CONCLUSIONS

A one dimensional model of flashing from an aperture has been developed. This model uses the nucleation process as the major process within flashing jet. This model covers the study the possibility of flashing occurrence under specific values of pressure and temperature, followed by an analytical calculation procedure to estimate the velocity, void fraction and droplets distribution of the liquid to be used as boundary condition of CFD simulations.

The CFD simulation will deal with only the transport droplets mechanisms without any further thermal influence. The accuracy of the result obtained by CFD means depend on the correct physics reproduced by the boundary conditions.

The following conclusion can be made:

- The occurrence of a flashing jet can be determined by the model based on the force balance between the promoting forces and dissipation forces of nucleation, in a similar way to a second order damped system. This balance take into account individual effect of the problem parameters, such as initial pressure and temperature as well as geometry dimensions represented by dimensionless parameters as Reynolds number, Jacob number, Weber number, ratio of density, friction factors or discharge coefficient. This model can be used for both water and hydrocarbons fluids. The solution of the model will determine the behaviour of the system as sub-damped (flashing jet), damped or over damped system (liquid jet).
- The model allows the inclusion of the friction factor or dimensionless roughness, as important parameter in the nucleation process sue to its important as a potential nuclei sources, which are not normally included in any other work presented in the literature.
- If was found that the different behaviour of water and hydrocarbon is based on the appreciable difference of their properties. In particular the liquid density and

gas density ratio, ρ_{liq}/ρ_{gas}, of hydrocarbons and water, which represents the quantity of energy needed to overcome the phase change barrier by evaporation and differences in surface tension.

- The study demonstrates that the ratio of kinetic energy and the thermal energy can be interpreted as the ratio of pure liquid velocity discharge and the velocity affected by the superheated temperature. This helps to characterize the potential energy contained in the flow under its initial pressure and temperature respect to the pressure and temperature at ambient conditions. Larger ratio means the fluids have high level of energy accumulate. The energy in the fluid is a balance between the mechanical energy represented by the pressure and thermal energy represented by the temperature.
- The production dissipation model of nucleation is capable of reproducing the effects on the jet of the change of diameter and length of the nozzle, as well as, the variation in temperature and pressure and their relative position to the critical temperature or pressure of the fluid.
- The results of the production dissipation model for CFC11, chlorine and cyclohexane were compared well with the experimental data reported by Energy_Analysts_Inc (1990).
- An effective new procedure, which introduces the jump formulation analysis to the shock waves in the discharge of superheated liquid. Considering the expansion of the system being affected by forces generated by surface tension, expansion of each phase, geometry complexity and other parameters are taken. The procedure consists in the resolution of an expression of void fraction of the mixture.
- The analysis of the temperature within the spray jet supports the assumption of an adiabatic process and non reversible force presence acting the flashing jet.
- The usage of a computational nozzle to do CFD simulations is a way to consider the effects of the expansion zone where the thermodynamics relations are predominant. The momentum of a two phase jet is kept constant along the jet axis.

- The velocity profile as boundary condition affects directly the shear layer close to the borders, in the interface between the jet and its surroundings. The application of a parabolic profile results in an increase of the core region length. However, the application of a turbulent velocity profile at the inlet does not produce major differences respect to the constant velocity profile. The application of the turbulence profiles instead as parabolic ones seems to represent best the physics of the system.

- Droplets at the inlet condition do not change the general trend of the velocity profile at the centreline. However there are some changes in the gradient of this profile. The core region keeps more less the same length as the single phase cases. The velocity decay is smoother when droplets are added; it moves forward the decay of velocity reducing the gradient of the slope. The dimensions of the droplets added produce some differences in the magnitude of the velocity decay, but all produce a similar effect.

- The effects of the distribution of the momentum added by the nozzle are related with the balance of the drag forces on each droplet. Resulting drag forces on droplets are proportional function of the droplet diameter. Smaller droplet experience less drag and therefore they can carry for longer distance than the larger droplets before loss their initial momentum. For the same quantity of momentum added by the droplets affected the flow when it is distributed varying the diameters of the droplets and therefore varying the number of droplets involved. More number of smaller droplets actually helps to reduce the slope of the velocity decay of the profile at the centreline respect to larger number of bigger droplets. In all cases the smaller droplets diameters approach better the experimental values. The same trend was found for the radial velocity profiles. The dispersion of droplet in the flow depends on the particle size and the shear stress at what they are exposed.

- The increase of the jet temperature, from the boiling temperature at the computational nozzle to the ambient temperature downstream, is well reproduced by entrainment phenomenon generated within the CFD model using the standard k-ε turbulent model.

CHAPTER 7: RECOMMENDATIONS FOR FUTURE WORK

The majority of the data available correspond to small scale. The scale will change the values of the ratio of the cross section area of the nozzle and the surface area. It will also change the scenario of balancing between surface tension force at the nucleation surfaces and the viscous forces at the nozzle. It is assumed that surface tension has a major impact on the system and the viscous force can be ignored, however, at larger scales this approach does not apply any longer. Thus large scale data is required. If the study is extended to long cracks the scale impact on the ratio of transversal area and surface area can be even more severe than for circular nozzles. The influence of the fluid properties in larger scales is an interesting point to develop.

The study of the real location of the computational nozzle to improve the comparison of the CFD simulations results with the experimental data available. It is known that flashing jet have longer core region than the core region obtained from numerical simulations for single phase jets and two phase jets when the phases are already in place. Compared with the arguments and results showed here, it is clear that the use of the appropriate computational nozzle helps to reproduce the right slope of the velocity profile; however, it does not achieve the required long region visualized in the experimental settings. Experimental work to identify the exact location of this cross section is necessary.

The development of a procedure to calculate the droplets size and droplet distribution after the nucleation is necessary. It has been found that the size of the droplet can make a large difference on jet behaviour.

In summary, good quality large scale results are needed to improve both 1D models such as that presented in the present work and for future model development.

CHAPTER 8: REFERENCES

Aamir, M. A. and A. P. Watkins (2000). "Numerical analysis of depressurisation of highly pressurised liquid propane." International Journal of Heat and Fluid Flow **21**: 420-431.

Allen, J. T. (1996a). Laser-based droplet size measurements in two-phase, flashing propane jets, Health and Safety Laboratory.

Allen, J. T. (1996b). Laser-based velocity measurement in two-phase flashing propane jet releases, Health and Safety Laboratory.

Allen, J. T. (1998a). Laser-based measurements in two-phase flashing propane jets, University of Sheffield.

Allen, J. T. (1998b). "Laser-based measurements in two-phase flashing propane jets. Part one: velocity profile." Journal of Loss Prevention in the Process Industries **11**: 291-297.

Allen, J. T. (1998c). "Laser-based measurements in two-phase flashing propane jets. Part two: droplet size distribution." Journal of Loss Prevention in the Process Industries **11**: 299-306.

Allen, J. T. (2002). Characteristics of impinging jets. FS/00/02. Buxton, Health and Explosion Laboratory.

Badens, E., O. Boutin, et al. (2005). "Laminar jet dispersion and jet atomization in pressurized carbon dioxide." The Journal of Supercritical Fluids **36**: 81-90.

Barnea, D., O. Shoham, et al. (1982a). "Flow pattern transition for downward inclined two phase flow; horizontal to vertical." Chemical Engineering Science **37**(5): 735-740.

Barnea, D., O. Shoham, et al. (1982b). "Flow pattern transition for vertical downward two phase flow." Chemical Engineering Science **37**(5): 741-744.

Barnea, D., O. Shoham, et al. (1980). "Flow pattern transition for gas-liquid flow in horizontal and inclined pipes. Comparison of experimental data with theory." International Journal of Multiphase Flow **6**(3): 217-225.

Bayvel, L. P. (1982). "The effect of polydispersity of drops and the efficiency of a Venturi Scrubber." Transaction of the Institution of Chemical Engineering **60**: 31-34.

Boivin, M., O. Simonin, et al. (1998). "Direct numerical simulation by particles in isotropic turbulence." J. Fluid Mechanics **375**: 235-263.

Bolle, L. a. D.-Z., P. (1996). "Experimental and theoretical analysis of flashing water flow through a safety valve." Journal of Hazardous Materials **Vol. 46.**: pp. 105-116.

Brennen, C. E. (1995). Cavitation and Bubble Dynamics, Oxford University Press.

Brenner, C. E. (1995). Cavitation and fluid dynamic. New York, Oxford University Press INC.

Bricard, P. and L. Friedel (1998). "Two-phase jet dispersion." Journal of Hazardous Materials **59**: 287-310.

Brown, G. L. and A. Roshko (1974). "On density effects and large structure in turbulence mixing layers." Journal of Fluid Mechanics **64**(4): 775-816.

Brown, R. and L. York (1962). "Sprays formed by flashing jets." American Institute of Chemical Engineers **8**(2): 149-153.

Byrne, C. E. I. and A. E. Holdo (1994). "The effect of choice of inlet boundary conditions for *k*-ε turbulence model." Computational Fluid Dynamics **3**: 321-327.

C Cartes, M. G. C. a. R. S. (2004). "Van der Waals normal form for a one-dimensional hydrodynamic model." Physics Review **70**(031302-1/8).

Chalmers. (2007). Retrieved 19 Oct. 2007, 2007.

Chin, J. S. and A. H. Lefebvre (1985). Some comments on the characterization of drop size distribution in sprays. ICLASS 85 International Conference on Liquid Atomisation and Spray Systems, Imperial College, London, Institute of energy.

Christensen, B. and M. S. Tillack (2003). Survey of mechanisms for liquid droplets ejection from surfaces exposed to rapid pulsed heating. UCSD-ENG-100. La Jolla, CA, Fusion division, Center for Energy Research, University of California.

Collado, F. J., C. Monné, et al. (2006). "Thermodynamics of void fraction in saturated flow boiling." Journal of Heat Transfer **128**: 611-615.

Costa, M. A. M., P. R. Henrique, et al. (2004). "Droplet size in a rectangular Venturi scrubber." Brazilian Journal Chemical Engineering **21**(2).

Crowe, Troutt, et al. (1996). "Numerical models for two-phase turbulent flows." Annual Reviews **28**: 11-43.

Das, M., B. K. Chatterjee, et al. (2000). "How high can the temperature of a liquid be raised without boiling?" PHYSICAL REVIEW E **62**(4).

Deaves, D. M., S. Gilham, et al. (2001). "Modelling of catastrophic flashing releases." Journal of Hazardous Materials(A88): 1-32.

Diek, H. and R. L. Roberts (1970). "The determination of the sauter mean droplet diameter in fuel nozzle sprays." Applied optics **9**(9): 2007-2014.

Drew, D. A. and S. L. Passman (1999). Theory of multicomponent fluids. New York, Springer-Verlag.

Dunbar, C. A., A. P. Watkins, et al. (1997). "Theoretical investigation of the spray from a pressurized metered-dose inhaler." Atomization and Sprays **Vol. 7**: pp. 417-436, 1997.

Elghobashi, S. E. and G. C. Truesdell (1993). "On the two-way interaction between homogeneous turbulence and dispersed solid particles. I: Turbulence modification." Physics Fluids A **5**: 1790.

Elias, E. and P. L. Chambre (1993). "Flashing inception in water during rapid decompression." Journal of Heat Transfer **115**: 231-238.

Energy_Analysts_Inc (1990). Release characteristics of superheated water and CFC-11 liquids an experimental program.

Fathikalajahi, J., M. R. Talaie, et al. (1996). "Theoretical study of nonuniform droplets concentration distribution on Venturi crubber performance." Particulate Science and Technology **14**: 153-164.

Fire_Science_Centre (1994). The blowdown of pressurized containers, Fire Science Centre. University of New Bruswick.

FLUENT (2003). FLUENT 6.3. User's guide. Lebanon. U.S.A.

Frederic, C., S. Balibar, et al. (2003). "Limit of metastability of liquid helium." Physica B **329-333**(1): 356-359.

Frost, D. L., R. Barbone, et al. (1995). TP 12123E. Small-Scale BLEVE Tests with Refrigerant-22. Quebec, Transportation Development Centre**:** 48.

Gemci, T., K. Yakut, et al. (2004a). "Experimental study of flash atomization of binary hydrocarbon liquid." International Journal of Multiphase Flow **30**: 395-417.

Gemci, T., K. Yakut, et al. (2004b). "Flash atomization of water / acetone solutions." Atomization and Sprays **14**: 459-475.

Gudmundsson, J. S. and H. K. Celius (1999). Gas-liquid metering using pressure-pulse technology. SPE Annual Technical Conference and Exhibition, Houston, Texas.

Haider and O. Levenspiel (1989). "Drag coefficient and terminal velocity of spherical and nonspherical particles." Power Technology **58**: pp. 63-70.

Happel, J. and H. Brenner (1983). Low Reynolds number hydrodynamics. The Hague, Martinus Nijhoff Publishers.

Hervieu, H. and T. Veneau (1996). "Experimental determination of the droplet size and velocity distributions at the exit of the bottom discharge pipe of a liquefied propane storage tank during a sudden." Journal of Loss Prevention in the Process Industries **9**(6): 413-425.

Hill, B. J. (1972). "Measurement of local entrainment rate in the initial region of axisymmetric turbulent air jet." Journal of fluid Mechanics **51**(4): 773-779.

Johnson, D. W. and J. L. Woodward (1999). RELEASE A Model with data to predict aerosol rainout in accidental releases. New York, American Institute of Chemical Engineers.

Kataoka, I. and A. Serizawa (1989). "Basic equations of turbulence in gas-liquid two-phase flow." International Journal of Multiphase Flow **15**(5): 843-855.

Kelsey, A. (1999). CFD modelling of two phase flashing jets: Simulation of evaporating sprays to inform modelling of flashing jet, Health and safety laboratory**:** 56.

Kelsey, A. (2001). CFD modelling of two phase flashing jets: Simulation of flashing Propane jets, Health & Safety Laboratory Report**:** 61.

Kesley, A. (1999). CFD modelling of two phase flashing jets: Simulation of evaporation sprays to inform modelling of flashing jets, Health & Safety Laboratory Report**:** 56.

Kesley, A. (2001). CFD modelling of two phase flashing jets: Simulation of flashing Propane jets, Health & Safety Laboratory Report**:** 61.

Khajehnajafi, S. and A. Shinde (1994). "Prediction of discharge rate from pressurized vessel blowdown through sheared pipe." Process Safety Progress **13**(2): 75-82.

Koch, D. (1990). "Kinetic theory for a monodisperse gas-solid suspension." Physics Fluids A **2**: 1711-1723.

Lahey, R. T. (1992). Boiling heat transfer. Modern developments and advances. Amsterdam, Elsevier Science Publishers.

Lance, M. and J. Bataille (1991). "Turbulence in the liquid phase of a uniform bubbly air-water flow." Fluid Mechanics **22**: 95-118.

Lasheras, J. C. and E. J. Hopfinger (2000). "Liquid jet instability and atomisation in coaxial gas stream." Annual Review Fluid mechanics **32**: 275-308.

Lee, C. S. and S. W. Park (2002a). "An experimental and numerical study on fuel atomization characteristics on high-pressure diesel injection sprays." Fuel **81**: 2417-2423.

Lee, C. S. and S. W. Park (2002b). "A numerical study on fuel atomization characteristics of high-pressure diesel injection sprays." Fuel **81**: 2417-2423.

Lee, S. L., R. T. Lahey, et al. (1989). "The prediction of two-phase turbulence and phase distribution phenomena using a k-e model." J. Multiphase Flow **3**: 335-368.

Lefebvre, A. H. (1980). "Airblast atomization." Progress in energy and combustion science **6**: 233-261.

Lefebvre, A. H. (1989). Atomization and Sprays. USA, Hemisphere Publishing Corporation.

Liepman, H. W. and J. Laufer (1947). Investigations of free turbulent mixing. NACA TN 1257. Washington, National Advisory Committee for Aeronautics.

Lin, S. P. and R. D. Reitz (1998). "Drop and spray formation from liquid jet." Annual Review Fluid Mechanics **30**: 85-105.

Madsen, f., J. Harbo, et al. (2003). Measurement of droplet size and velocity distributions sprays using interferometric particle imaging (IPI) and particle tracking velocimetry (PTV). ICLASS 2003, Sorrento, Italy.

Massey, B. S. (1989). Mechanics of fluids. London, Chapman & Hall.

Maxey, M. R. and J. J. Riley (1983). "Equation of motion for a small rigid sphere in a nonuniform flow." Physics Fluids **26**(4): 883-889.

Mayer, E. (1961). "Theory of liquid atomization in high velocity gas streams." ARS **31**(12): 1783-85.

McDonell, V. G. and G. S. Samuelsen (1995). "An experimental data base for the computational fluid dynamics of reacting and nonreacting methanol sprays." Journal of Fluids Engineering **117**: 145-153.

Michaella, M., N. Piccinini, et al. (2004). "Analysis of an LPG accidental release." Process Safety and Environmental Protection **82**: 128-131.

Miyatake, O., T. Tomimura, et al. (1981a). "An experimental study of spray flash evaporation." Desalination **36**(2): 113-128.

Miyatake, O., T. Tomimura, et al. (1981b). "Effect of liquid temperature on spray flash evaporation." Desalination **37**(3): 351-366.

Moreira, J. R. S. (2000). "Oblique evaporation waves." Shock Waves **10**: 229-234.

Moreira, J. R. S. and C. W. Bullard (2003). "Pressure drop and flashing mechanisms in refrigerant expansion devices." International Journal of Refrigeration **26**: 840-848.

Morsi, S. A. and A. J. Alexander (1972). "An investigation of particle trajectories in two-phase flow systems." The Journal of Fluid Mechanics **Vol. 55**(2): pp. 193-208.

Nagai, N., K. Sato, et al. (1985). Atomisation characteristics of superheated liquid jets. ICLASS-85, International Conference on Liquid Atomisation and Spray System, Imperial College, London.

Park, B. S. and S. Y. Lee (1994). "An experimental investigation of the flash atomization mechanism." Atomatization and Sprays **4**: 159-179.

Peter, E. M., A. Takimoto, et al. (1994). "Flashing and shattering phenomena of superheated liquid jets." JSME International Journal **37**(2): 313-321.

Potter, M., D. Wiggert, et al. (1997). Mechanics of fluids., Prentice Hall Inc.

R Ramanathan, Y. K. M., K. K. Gupta, Agam K Jha and S. S. Singh (2005). "A comparative study of two models of QCP-Fireball formation." eprint arXiv:hep-ph/0502046.

Raynal, L., E. Villermaux, et al. (1999). "Primary instability of a plane liquid-gas shear layer." J. Fluid Mechanics.

Rehab, H., E. Villermaux, et al. (1997). "Flow regimes of large velocity ratio coaxial jets." Journal of Fluid Mechanics **345**: 357-81.

Reitz, R. D. (1990). "A photographic study of flashing-boiling atomization." Aerosol, Science and Technology **12**: 561-569.

Reshetnikov, A. V., N. A. Mazheiko, et al. (2001). "Flicker-Noise in a Jet of Superheated Liquid." Physics **46**(9): 612-614.

Reshetnikov, A. V., V. P. Skripov, et al. (2002). "1/f Fluctuations in Critical Modes of Flow of Superheated Liquid." Heat and mass transfer and physical Gas dynamics **40**(3): 443-446.

Saffman, P. G. (1973). "On the settling speed of free and fixed suspension." Stud. Appl. Maths. **52**: 115-127.

Schmelzer, J. M. P. (2003). "Kinetic and thermodynamic theories of nucleation." Mater Phys Mechanics **6**: 21-33.

Shen, V. K. and P. G. Debenedetti (1999). "A computational study of homogeneous liquid-vapor nucleation in the Lennard-Jone fluid." Journal of Chemical Physisc **111**(8): 3581-3589.

Simpson, B. A. F. (1998). A computational study of gas leak jets relevant to offshore structures. Aeronautical, Civil and Mechanical Engineering. Hatfield, University of Hertfordshire.

Sirignano, W. (1999). Fluid dynamics and transport of droplets and Sprays. Cambridge, Cambridge University Press.

Skokov, V. N., V. P. Koverda, et al. (2003a). "1/f noise and self-organized criticality in crisis regimes of heat and mass transfer." International Journal of Heat and Mass Transfer **46**: 1879-1883.

Skokov, V. N., V. P. Koverda, et al. (2003b). "1/f noise and self-organized criticality in crisis regimes of heat and mass transfer." International Journal of Heat and Mass Transfer **46**(10): 1879-1883.

Skripov, V. P., E. N. Sinitsyn, et al. (1988). Thermophysical properties of liquids in metaestable (superheated) state. Amsterdam, Gordon and Breach Science Publisher.

Solomon, Ruupprecht, et al. (1985). "Flow and atomization in flashing injectors." Atomization Spray Technology **1**: 53-76.

Squires, K. D. and J. K. Eaton (1990). "Particle response and turbulence modification in isotropic turbulence." Physical Fluids A **2**: 1191.

Squires, K. D. and J. K. Eaton (1994). "Effect of selective modification of turbulence on two-equation models for particle-laden turbulent flows." Transaction of the ASME I: Journal of Fluids Engineering **116**: 778.

Takeuchi, G., T. Kawaguchi, et al. (2004). Spatial distributions of droplet size and velocity in air heated spray measured by interferometric laser imaging technique. 12th International Symposium Applications of Laser Techniques to Fluid Mechanics, Lisbon, Portugal.

Tennekes, H. and J. L. Lumley (1973). A First course of turbulence. Cambridge, Massachusetts, and London, England, The MIT Press.

Vandroux-Koenig, S. and G. Berthoud (1997). "Modelling of a two phase momentum jet close to the breach, in the containment of liquefied gas." J. Loss Prev. Process Ind **Vol. 10**: pp. 17-29.

Wakes, S. J., A. E. Holdo, et al. (2002). "Experimental investigation of the effect orifice shape and fluid pressure has on high aspect ratio." Journal of Hazardous Materials **A89**: 1-27.

Wang, L. P. and M. R. Maxey (1993). "Settling velocity and concentration distribution of heavy particles in homogeneous isotropic turbulence." Journal of Fluid Mechanics **256**: 27.

Whalley, P. (1979). Boiling, condensation and two-phase flow. London, Oxford University Press.

Wheatley, C. J. (1987a). A theoretical study of NH3 concentration in moist air arising from accidental releases of liquefied NH3, using the computer code TRAUMA, Health and Safety Executive.

Wheatley, C. J. (1987b). A user guide to TRAUMA - a computer code for assessing the consequences of accidental two-phase releases of NH3 into moist air, Health and Safety Executive.

Witlox, H. and M. Harper (2005). FLASHING LIQUID JETS AND TWO-PHASE DROPLET DISPERSION. American Society of Safety Engineers Middle East Chapter. 7th Professional Development Conference & Exhibition, Kingdom of Bahrain.

Wu, P. K., L. K. Tseng, et al. (1992). "Primary breakup in gas/liquid mixing layers for turbulent liquids." Atomatization and Sprays **2**: 295-317.

Yan, F. and M. Giot (1989). "A nucleation model for superheated liquids in adiabatic vessel and pipes." **323-331**.

Yang, L. and C.-L. Zhang (2005). "Two-fluid model of refrigerant two-phase flow through short tube orifice." International Journal of Refrigeration **28**: 419-427.

Yildiz, D. (2003). Dynamics of two-phase flashing jets. Belgium, von Karman Institute for Fluid Dynamic.

Yildiz, D., J. P. A. J. v. Beek, et al. (2002a). Global rainbow thermometry applied to a flashing two-phase R134-A Jet. 11th International Symposium on Application of Laser Techniques to Fluid Mechanics, Lisbon, Portugal.

Yildiz, D., J. P. A. J. v. Beek, et al. (2002b). Understanding of dynamics of a two-phase flashing jet using multi-intensity-layer PIV and PDA. 11th International Symposium on Application of Laser Techniques to Fluid Mechanics, Lisbon, Portugal, July 8-11.

Yildiz, D., P. Rambaud, et al. (2003). Thermal characterization of a R134A two-phase flashing jet. ICLASS 2003 – 9th International Conference on Liquid Atomization and Spray Systems, Sorrento, Italy.

Yildiz, D., P. Rambaud, et al. (2004). Break-up, droplet size and velocity characterisation of a two-phase flashing R134A jet. 5th International Conference on Multiphase Flow, Yokohama, Japan.

Yildiz, D., P. Rambaud, et al. (2005). Experimental Investigation of superheated liquid jet: Atomization due to flashing phenomena. Small scale tests and theoretical models. FLIE Seminar. Milan. Italy, Von Karman Institute.

Young, F. R. (1998). Cavitation. London, Imperial College Press.

APPENDICES

Appendix A. Properties of different fluids

Table A1. Properties of different fluids

Property	R134A	Water	CFC-11	Chlorine	Methylamine	Cyclohexane	Methanol	Propane
Cd	0.9	0.9	0.9	0.9	0.9	0.9	0.9	0.9
Viscosity [kg/ms]	0.0002	0.000284	0.045	0.0005	0.00018	0.0004	0.000584	0.000209
Liquid density [kg/m^3]	1250	958.4	1520	1564.5	697.5	724.1	791.8	582
Gas density [kg/m^3]	5.28	0.59	5.04	3.208	1.49	3.48	1.4	2
Latent heat [J/kg]	233800	2260000	182125.8	289720	847408.32	357971.4	1109000	233500
Surface tension [N/m]	0.001	0.059105	0.02-0.05	0.0272	0.0259	0.0185	0.0226	16.02
Specific heat capacity, Cp [J/kg K]	1100	4186	879.3	921.09	3265.704	2093.4	2550	1400
Thermal conductivity [W/m K]	0.014	0.02596	0.0356	0.165	0.21166	0.11048	0.25	0.090
Boiling temperature [K]	246.6	371.9	295.6	236.6	264.3	350.3	337.85	232.65
Density liquid/gas ratio [-]	237	1624	302	488	468	208	566	291
Specific liquid density [-]	1.25	0.9584	1.52	1.5645	0.6975	0.7241	0.7918	0.5820
Critical pressure [Pa]	4060000	22064000	4378171	7700000	7460000	4072300	8100000	4250000
Critical Temperature [K]	374.05	647.29	471	417	430.05	553.15	512.6	369.75

Appendix B. Program developed as an Excel Macro for velocity calculations

```
'función donde se determina la dirección los insumos de la tablas termodinámicas, las opciones son agua, R134A y ammonia
Public Function Inter(ByVal indT As Integer, ByVal T As Double, ByVal indP As Integer, ByVal Pressure As Double, ByVal indicador As Integer, ByVal numerodedatos As Long, ByRef variable As Double, ByVal m As Integer)

 If m = 0 Then
  Call InterR134a(indT, T, indP, Pressure, indicador, numerodedatos, variable)
 End If
 If m = 1 Then
  Call InterAgua(indT, T, indP, Pressure, indicador, numerodedatos, variable)
 End If
 If m = 2 Then
  Call InterAmmonia(indT, T, indP, Pressure, indicador, numerodedatos, variable)
 End If

End Function

Public Function InterR134a(ByVal indT As Integer, ByVal T As Double, ByVal indP As Integer, ByVal Pressure As Double, ByVal indicador As Integer, ByVal numerodedatos As Long, ByRef variable As Double)
'Comienzo de la interpolación la variable indicada, T o P'
 If indT <> Empty And indP <> Empty Then
  MsgBox "invalid data, no se puede interpolar con T y P paralelalmente"
 End If
 i = 1
 If indT = 1 And indP = 0 Then
  valormin = Worksheets("PropiedadesR134a").Cells(3, 1).Value
  valormax = Worksheets("PropiedadesR134a").Cells(numerodedatos + 2, 1).Value
  valoraevaluar = T
  ind = 1
 End If
 If indP = 1 And indT = 0 Then
  valormin = Worksheets("PropiedadesR134a").Cells(3, 2).Value
  valormax = Worksheets("PropiedadesR134a").Cells(numerodedatos + 2, 2).Value
  valoraevaluar = Pressure
  ind = 2
 End If
 If valoraevaluar < valormin Then
  MsgBox "temperatura suministrada es menor que la reportada en tablas"
  numero = 0.1
  variable = Worksheets("PropiedadesR134a").Cells(3, 1).Value
```

```
 End If
 If (valoraevaluar > valormax) Then
  MsgBox "temperatura suministrada es mayor que la reportada en tablas"
  numero = 0.2
  If indicador <> 1 Then
   variable = Worksheets("PropiedadesR134a").Cells(numerodedatos + 2, 1).Value
  End If
  If indicador = 1 Then
   variable = Exp(-Ao * T + Bo)
  End If
  variable = Worksheets("PropiedadesR134a").Cells(numerodedatos + 2,
indicador).Value
 End If
 If valoraevaluar <= valormax And valoraevaluar >= valormin Then
 'ubicar la linea donde se encuentra el valor a evaluar'
  i = 1
  Do While i < (numerodedatos + 1)
   If valoraevaluar >= Worksheets("PropiedadesR134a").Cells(Int(i) + 2, ind).Value
Then
    numero = Int(i) + 2
   End If
   i = i + 1
  Loop
  variable = ((valoraevaluar - Worksheets("PropiedadesR134a").Cells(numero,
ind).Value) * (Worksheets("PropiedadesR134a").Cells(numero, indicador).Value -
Worksheets("PropiedadesR134a").Cells(numero + 1, indicador).Value) /
(Worksheets("PropiedadesR134a").Cells(numero, ind).Value -
Worksheets("PropiedadesR134a").Cells(numero + 1, ind).Value)) +
Worksheets("PropiedadesR134a").Cells(numero, indicador).Value
 End If
 ReturnValue = variable
End Function

Public Function InterAgua(ByVal indT As Integer, ByVal T As Double, ByVal indP As
Integer, ByVal Pressure As Double, ByVal indicador As Integer, ByVal numerodedatos
As Long, ByRef variable As Double)
'Comienzo de la interpolación la variable indicada, T o P'
 If indT <> Empty And indP <> Empty Then
  MsgBox "invalid data, no se puede interpolar con T y P paralelalmente"
 End If
 i = 1
 If indT = 1 And indP = 0 Then
  valormin = Worksheets("PropiedadesAgua").Cells(3, 1).Value
  valormax = Worksheets("PropiedadesAgua").Cells(numerodedatos + 2, 1).Value
  valoraevaluar = T
  ind = 1
 End If
 If indP = 1 And indT = 0 Then
```

```
  valormin = Worksheets("PropiedadesAgua").Cells(3, 2).Value
  valormax = Worksheets("PropiedadesAgua").Cells(numerodedatos + 2, 2).Value
  valoraevaluar = Pressure
  ind = 2
 End If
 If valoraevaluar < valormin Then
  MsgBox "temperatura suministrada es menor que la reportada en tablas"
  numero = 0.1
  variable = Worksheets("PropiedadesAgua").Cells(3, 1).Value
 End If
 If (valoraevaluar > valormax) Then
  MsgBox "temperatura suministrada es mayor que la reportada en tablas"
  numero = 0.2
  If indicador <> 1 Then
   variable = Worksheets("PropiedadesAgua").Cells(numerodedatos + 2, 1).Value
  End If
  If indicador = 1 Then
   variable = Exp(-Ao * T + Bo)
  End If
  variable = Worksheets("PropiedadesAgua").Cells(numerodedatos + 2,
indicador).Value
 End If
 If valoraevaluar <= valormax And valoraevaluar >= valormin Then
 'ubicar la linea donde se encuentra el valor a evaluar'
  i = 1
  Do While i < (numerodedatos + 1)
   If valoraevaluar >= Worksheets("PropiedadesAgua").Cells(Int(i) + 2, ind).Value Then
    numero = Int(i) + 2
   End If
   i = i + 1
  Loop
  variable = ((valoraevaluar - Worksheets("PropiedadesAgua").Cells(numero,
ind).Value) * (Worksheets("PropiedadesAgua").Cells(numero, indicador).Value -
Worksheets("PropiedadesAgua").Cells(numero + 1, indicador).Value) /
(Worksheets("PropiedadesAgua").Cells(numero, ind).Value -
Worksheets("PropiedadesAgua").Cells(numero + 1, ind).Value)) +
Worksheets("PropiedadesAgua").Cells(numero, indicador).Value
  variable = ((valoraevaluar - Worksheets("PropiedadesAgua").Cells(numero,
ind).Value) * (Worksheets("PropiedadesAgua").Cells(numero, indicador).Value -
Worksheets("PropiedadesAgua").Cells(numero + 1, indicador).Value) /
(Worksheets("PropiedadesAgua").Cells(numero, ind).Value -
Worksheets("PropiedadesAgua").Cells(numero + 1, ind).Value)) +
Worksheets("PropiedadesAgua").Cells(numero, indicador).Value
  variable = ((valoraevaluar - Worksheets("PropiedadesAgua").Cells(numero,
ind).Value) * (Worksheets("PropiedadesAgua").Cells(numero, indicador).Value -
Worksheets("PropiedadesAgua").Cells(numero + 1, indicador).Value) /
(Worksheets("PropiedadesAgua").Cells(numero, ind).Value -
```

```
Worksheets("PropiedadesAgua").Cells(numero + 1, ind).Value)) +
Worksheets("PropiedadesAgua").Cells(numero, indicador).Value
 End If
 ReturnValue = variable
End Function
Public Function InterAmmonia(ByVal indT As Integer, ByVal T As Double, ByVal
indP As Integer, ByVal Pressure As Double, ByVal indicador As Integer, ByVal
numerodedatos As Long, ByRef variable As Double)
'Comienzo de la interpolación la variable indicada, T o P'
 If indT <> Empty And indP <> Empty Then
  MsgBox "invalid data, no se puede interpolar con T y P paralelalmente"
 End If
 i = 1
 If indT = 1 And indP = 0 Then
  valormin = Worksheets("PropiedadesAmmonia").Cells(3, 1).Value
  valormax = Worksheets("PropiedadesAmmonia").Cells(numerodedatos + 2, 1).Value
  valoraevaluar = T
  ind = 1
 End If
 If indP = 1 And indT = 0 Then
  valormin = Worksheets("PropiedadesAmmonia").Cells(3, 2).Value
  valormax = Worksheets("PropiedadesAmmonia").Cells(numerodedatos + 2, 2).Value
  valoraevaluar = Pressure
  ind = 2
 End If
 If valoraevaluar < valormin Then
  MsgBox "temperatura suministrada es menor que la reportada en tablas"
  numero = 0.1
  variable = Worksheets("PropiedadesAmmonia").Cells(3, 1).Value
 End If
 If (valoraevaluar > valormax) Then
  MsgBox "temperatura suministrada es mayor que la reportada en tablas"
  numero = 0.2
  If indicador <> 1 Then
   variable = Worksheets("PropiedadesAmmonia").Cells(numerodedatos + 2, 1).Value
  End If
  If indicador = 1 Then
   variable = Exp(-Ao * T + Bo)
  End If
  variable = Worksheets("PropiedadesAmmonia").Cells(numerodedatos + 2,
indicador).Value
 End If
 If valoraevaluar <= valormax And valoraevaluar >= valormin Then
 'ubicar la linea donde se encuentra el valor a evaluar'
  i = 1
  Do While i < (numerodedatos + 1)
   If valoraevaluar >= Worksheets("PropiedadesAmmonia").Cells(Int(i) + 2, ind).Value
Then
```

```
   numero = Int(i) + 2
  End If
  i = i + 1
 Loop
 variable = ((valoraevaluar - Worksheets("PropiedadesAmmonia").Cells(numero,
ind).Value) * (Worksheets("PropiedadesAmmonia").Cells(numero, indicador).Value -
Worksheets("PropiedadesAmmonia").Cells(numero + 1, indicador).Value) /
(Worksheets("PropiedadesAmmonia").Cells(numero, ind).Value -
Worksheets("PropiedadesAmmonia").Cells(numero + 1, ind).Value)) +
Worksheets("PropiedadesAmmonia").Cells(numero, indicador).Value
 End If
 ReturnValue = variable
End Function

Sub arreglosdelapagina(ByVal n As Integer)
'Vaciar las celdas'
 Range("g1:z200").Select
 Selection.ClearContents

 'Limpiar los colores de la corrida anterior'
 Range("A1:AZ200").Select
 Selection.Borders(xlDiagonalDown).LineStyle = xlNone
 Selection.Borders(xlDiagonalUp).LineStyle = xlNone
 Selection.Borders(xlEdgeLeft).LineStyle = xlNone
 Selection.Borders(xlEdgeTop).LineStyle = xlNone
 Selection.Borders(xlEdgeBottom).LineStyle = xlNone
 Selection.Borders(xlEdgeRight).LineStyle = xlNone
 Selection.Borders(xlInsideVertical).LineStyle = xlNone
 Selection.Borders(xlInsideHorizontal).LineStyle = xlNone
 Selection.Interior.ColorIndex = xlNone

 'Colocacion de los numeros de eventos'
 i = 1
 Do While i < (n + 1)
  Cells(Int(i) + 3, 1) = i
  i = i + 1
 Loop

 'rellenar de color morado la celda de los datos'
 i = 1
 Do While i < (n + 1)
  Cells(Int(i) + 3, 1).Select
  With Selection.Interior
     .ColorIndex = 39
     .Pattern = xlSolid
  End With
  Selection.Borders(xlDiagonalDown).LineStyle = xlNone
  Selection.Borders(xlDiagonalUp).LineStyle = xlNone
```

```
 With Selection.Borders(xlEdgeLeft)
      .LineStyle = xlContinuous
      .Weight = xlThin
      .ColorIndex = xlAutomatic
 End With
 With Selection.Borders(xlEdgeTop)
      .LineStyle = xlContinuous
      .Weight = xlThin
      .ColorIndex = xlAutomatic
 End With
 With Selection.Borders(xlEdgeBottom)
      .LineStyle = xlContinuous
      .Weight = xlThin
      .ColorIndex = xlAutomatic
 End With
 With Selection.Borders(xlEdgeRight)
      .LineStyle = xlContinuous
      .Weight = xlThin
      .ColorIndex = xlAutomatic
 End With
 i = i + 1
Loop

'rellenar de color amarillo la celda de los datos'
i = 1
j = 2
Do While j < (7)
 Do While i < (n + 1)
  Cells(Int(i) + 3, j).Select
  With Selection.Interior
     .ColorIndex = 6
     .Pattern = xlSolid
  End With
  'Range("D21").Select
  Selection.Borders(xlDiagonalDown).LineStyle = xlNone
  Selection.Borders(xlDiagonalUp).LineStyle = xlNone
  With Selection.Borders(xlEdgeLeft)
       .LineStyle = xlContinuous
       .Weight = xlThin
       .ColorIndex = xlAutomatic
  End With
  With Selection.Borders(xlEdgeTop)
        .LineStyle = xlContinuous
       .Weight = xlThin
       .ColorIndex = xlAutomatic
  End With
  With Selection.Borders(xlEdgeBottom)
       .LineStyle = xlContinuous
```

```
        .Weight = xlThin
        .ColorIndex = xlAutomatic
   End With
   With Selection.Borders(xlEdgeRight)
        .LineStyle = xlContinuous
        .Weight = xlThin
        .ColorIndex = xlAutomatic
   End With
   i = i + 1
  Loop
  j = j + 1
  i = 1
 Loop

 'Chequear que todos los valores sean numeros, para detertar futuros errores de calculo'
 i = 1
 Do While i < (n + 1)
  dato = Cells(i + 3, 2)
  If TypeName(dato) >= "Null" Then
   MsgBox "invalid data, fila "
   Exit Sub ' acer un break'
  End If
  If TypeName(dato) >= "Empty" Then
   MsgBox "invalid data, no se introdujeron el numero de datos esperados"
   Exit Sub "Function 'Function 'hacer un break'
  End If
  i = i + 1
 Loop

 'Chequear que no hayan datos en exceso, para detertar futuros errores de calculo'
 'esto implica que no puede haber nada escrito debajo de los "n" datos declarados'
 i = n + 1
 Do While i < (n + 1 + 5)
  dato = Cells(i + 3, 2)
  If TypeName(dato) <> "Empty" Then
   MsgBox "invalid data, se introdujeron mas datos de los esperados, favor chequee"
   Exit Sub ' 'Function ' Function 'hacer un break'
  End If
  i = i + 1
 Loop

 'Vaciar las celdas, para eliminar valores de corridas previas, aunque la'
 'subroutina reescribirá los datos es bueno limpiar antes de inicia la nueva corrida'
 Range("g3:AZ200").Select
 Selection.ClearContents

 'Colocacion de los numeros de eventos'
' i = 1
```

```
' Do While i < (n + 1)
'  Cells(Int(i) + 3, 6) = i
'  Cells(Int(i) + 3 + n + 3, 6) = i
'  Cells(Int(i) + 3 + n + 3 + n + 3, 6) = i
'  Cells(Int(i) + 3 + n + 3 + n + 3 + n + 3, 6) = i
'  i = i + 1
' Loop

End Sub

Sub constantes(ByVal m As Integer, ByVal n As Integer, ByRef Tmax As Double,
ByRef Tmin As Double, ByRef Pmax As Double, ByRef Pmin As Double, ByRef Cp
As Double, ByRef Cp_gas As Double, ByRef Ao As Double, ByRef Bo As Double,
ByRef visco As Double, ByRef visco_gas As Double, ByRef tensup As Double, ByRef
k As Double, ByRef R_gas As Double, ByRef numerodedatos As Integer, ByRef
den_medio As Double)

 den_medio = 1.2 '[Kg/m3] este valor corresponde al aire

 If (m = Empty) Then
  MsgBox "Usted seleccionó R134A como fluido"
  numerodedatos = 29
  Tmax = 374.3 '[K]
  Tmin = 240.15 '[K]
  Pmin = 73700 '[Pa]
  Pmax = 4064000 '[Pa]
  Cp = 1100 '[J/KgK] Reportado en mi transfer report
  Cp_gas = 850 '[J/KgK] Cv 30 degress, 0.065 KJ/molK and Cp/Cv=1.138889 and
M=120.93 g/mol
  Ao = 2716.08574
  Bo = 22.5038
  visco = 1 '[Kg/ms]
  visco_gas = 0.001 '[Kg/ms]
  tensup = 1 '[Pa/m]
  k = 1.13 'Cp/Cv [adim] Gas ideal
  R_universal = 8315 'J/kmolK
  PM = 102.03
  R_gas = R_universal / PM
 End If

 If (m = 1) Then
  MsgBox "Usted seleccionó Agua como fluido"
  numerodedatos = 55
  Tmax = 647.5 '[K]
  Tmin = 273.15 '[K]
  Pmin = 611 '[Pa]
  Pmax = 22120000 '[Pa]
  Cp = (4217 + 4218) / 2 '[J/KgK] a 1 atm 273K y 1 atm y 373 K
```

```
 Cp_gas = 2014 '[J/KgK] constante de Fluent materials
 Ao = 5405.65098
 Bo = 25.735245
 visco = 0.001787 '[Kg/ms] valor minimo reportado en Alexandrou (T=273.15)
 visco_gas = 0.00000802 '[Kg/ms] valor minimo reportado en Incropera (T=273.15)
 tensup = 0.0756 '[Pa/m] valor minimo reportado en Alexandrou (T=273.15)
 k = 1.4 'Cp/Cv [adim] Gas ideal
 R_universal = 8315 'J/kmolK
 PM = 18
 R_gas = R_universal / PM
End If

If (m = 2) Then
 MsgBox "Usted seleccionó Ammonia como fluido"
 numerodedatos = 51
 Tmax = 323.15 '[K]
 Tmin = 223.15 '[K]
 Pmin = 40860 '[Pa]
 Pmax = 2033320 '[Pa]
 Cp = (4520 + 5100) / 2 '[J/KgK] a sat -20C y sat 50C respectivamente
 Ao = 2827.944699
 Bo = 23.301629
 visco = 1 '[Kg/ms]
 visco_gas = 0.001 '[Kg/ms]
 tensup = 1 '[Pa/m]
 k = 1.4 'Cp/Cv [adim] Gas ideal
 R_gas = 1600
End If

If TypeName(m) >= "Null" Then
 MsgBox "invalid data, m debe ser un valor entero"
 Exit Sub ' Function ' Function 'hacer un break'
End If

If (n = Empty) Then
 MsgBox "invalid data, n no declarado, debe introducir un valor"
 Exit Sub ' Function ' Function 'hacer un break'
End If

If TypeName(n) >= "Null" Then
 MsgBox "invalid data, n debe ser un valor entero"
 Exit Sub ' Function ' Function 'hacer un break'
End If

End Sub
'MODELO II DE VELOCIDAD A LA SALIDA
Sub mod_vel_names(ByVal n As Integer)
```

```
 'Colocarle los nombre y las unidades a las varibles
 Cells(2, 7) = "MODELO DE VELOCIDAD I"
 Cells(1 * n + 1 * 2 + 3, 7) = "MODELO DE VELOCIDAD II"
 Cells(2 * n + 2 * 2 + 4, 7) = "MODELO DE VELOCIDAD III"
 Cells(3 * n + 3 * 2 + 5, 7) = "MODELO DE VELOCIDAD IV"
End Sub


'MODELO I DE VELOCIDAD A LA SALIDA / Liquid Discharge / Solomon (1985)
Wheatley (1987)

Public Sub mod_vel_Uno(ByVal i As Integer, ByVal Pinj As Long, ByVal Pamb As
Long, ByVal numerodedatos As Integer, ByVal n As Integer, ByRef variable As
Double, ByVal nombre As String, ByVal m As Integer)

 'Calidad a la salida, establecida como 0
 quality = 0
 Cells(i + 3, 7) = 0

 'Volumen específico del líquido'
 f = Inter(0, 0, 1, Pamb, 3, numerodedatos, variable, m)
 vesp_liq = variable
 Cells(i + 3, 8) = vesp_liq

 'Volumen específico del gas'
 vesp_gas = 0
 Cells(i + 3, 9) = 0

 'Volumen específico de la mezcla'
 vesp_mez = vesp_liq + quality * (vesp_gas - vesp_liq)
 Cells(i + 3, 10) = vesp_mez

 'Velocidad de líquido - Primer modelo'
 vel_liq = (2 * (Pinj - Pamb) * vesp_liq) ^ 0.5
 Cells(i + 3, 11) = vel_liq

 'Velocidad de gas - Primer modelo'
 vel_gas = 0
 Cells(i + 3, 12) = 0

 ' Velocidad de líquido - Primer modelo'
 vel_mez = vel_liq
 Cells(i + 3, 13) = (2 * (Pinj - Pamb) * vesp_liq) ^ 0.5

End Sub

'MODELO II DE VELOCIDAD A LA SALIDA / Descarga en equilibrio / Wheatley
(1987)
```

```
Sub mod_vel_Dos(ByVal i As Integer, ByVal Pinj As Double, ByVal Tinj As Double,
ByVal Pamb As Double, ByVal numerodedatos As Double, ByVal n As Integer, ByVal
Cp As Double, ByVal Ao As Double, ByVal Bo As Double, ByRef variable As Double,
ByVal m As Integer)

 despl = n + 6

 f = Inter(0, 0, 1, Pinj, 1, numerodedatos, variable, m)
 Tsat_Pinj = variable

 f = Inter(0, 0, 1, Pamb, 1, numerodedatos, variable, m)
 Tsat_Pamb = variable

 f = Inter(0, 0, 1, Pamb, 3, numerodedatos, variable, m)
 vesp_liq_Pamb = variable
 Cells(i + despl, 8) = vesp_liq_Pamb

 f = Inter(0, 0, 1, Pamb, 5, numerodedatos, variable, m)
 vesp_gas_Pamb = variable
 Cells(i + despl, 9) = vesp_gas_Pamb

 f = Inter(0, 0, 1, Pamb, 7, numerodedatos, variable, m)
 hfg_Pamb = variable

 'cálculo de la calidad
 Quality_Pamb = Log(Tsat_Pinj / Tsat_Pamb) * Cp * Tsat_Pamb / hfg_Pamb
 Cells(i + despl, 7) = Quality_Pamb

 'cálculo del volumen especifico de la mezcla
 vesp_mezcla_Pamb = vesp_liq_Pamb + Quality_Pamb * (vesp_gas_Pamb -
vesp_liq_Pamb)
 Cells(i + despl, 10) = vesp_mezcla_Pamb

 ' Velocidad de líquido - Segundo modelo'
 vel_mez = (2 * (((Pinj - Pamb) * vesp_liq_Pamb) + (Cp * (Tsat_Pinj - Tsat_Pamb)) -
(Cp * Tsat_Pamb * Log(Tsat_Pinj / Tsat_Pamb)))) ^ 0.5
 vel_liq = vel_mez
 vel_gas = vel_mez
 Cells(i + despl, 11) = vel_liq
 Cells(i + despl, 12) = vel_gas
 Cells(i + despl, 13) = vel_mez

End Sub

'MODELO II DE VELOCIDAD A LA SALIDA
'Sub mod_vel_Dos(ByVal i As Integer, ByVal Pinj As Double, ByVal Tinj As Double,
ByVal Pamb As Double, ByVal numerodedatos As Double, ByVal n As Integer, ByVal
```

```
Cp As Double, ByVal Ao As Double, ByVal Bo As Double, ByRef variable As Double,
ByVal m As Integer)

 'despl = n + 6

 'Colocarle los nombre y las unidades a las varibles
 'Cells(despl - 1, 6) = "MODELO DE VELOCIDAD II"

 'f = Inter(0, 0, 1, Pamb, 1, numerodedatos, variable, m)
 'Tsat_Pamb = variable

 'f = Inter(0, 0, 1, Pamb, 3, numerodedatos, variable, m)
 'vesp_liq_Pamb = variable
 'Cells(i + despl, 8) = vesp_liq_Pamb

 'f = Inter(0, 0, 1, Pamb, 5, numerodedatos, variable, m)
 'vesp_gas_Pamb = variable
 'Cells(i + despl, 9) = vesp_gas_Pamb

 'f = Inter(0, 0, 1, Pamb, 7, numerodedatos, variable, m)
 'hfg_Pamb = variable

 'cálculo de la calidad
 'If Tinj < Tsat_Pamb Then
 ' Cells(i + despl, 7) = 0
  'Else
  ' Quality_Pamb = Log(Tinj / Tsat_Pamb) * Cp * Tsat_Pamb / hfg_Pamb
 '  Cells(i + despl, 7) = Quality_Pamb
' End If
 'cálculo del volumen especifico de la mezcla
 'vesp_mezcla_Pamb = vesp_liq_Pamb + Quality_Pamb * (vesp_gas_Pamb -
vesp_liq_Pamb)
 'Cells(i + despl, 10) = vesp_mezcla_Pamb

 ' Velocidad de líquido - Segundo modelo'
' If Tinj < Tsat_Pamb Then
  'vel_mez = (2 * ((Pinj - Pamb) * vesp_liq_Pamb)) ^ 0.5
  'vel_liq = vel_mez
  'vel_gas = vel_mez
  'Cells(i + despl, 11) = vel_liq
  'Cells(i + despl, 12) = vel_gas
  'Cells(i + despl, 13) = vel_mez
  'Else
  ' vel_mez = (2 * (((Pinj - Pamb) * vesp_liq_Pamb) + (Cp * (Tinj - Tsat_Pamb)) - (Cp *
Tsat_Pamb * Log(Tinj / Tsat_Pamb)))) ^ 0.5
  ' vel_liq = vel_mez
  ' vel_gas = vel_mez
  ' Cells(i + despl, 11) = vel_liq
```

```
  ' Cells(i + despl, 12) = vel_gas
 '  Cells(i + despl, 13) = vel_mez
' End If
'End Sub


'MODELO III DE VELOCIDAD A LA SALIDA
Sub mod_vel_Tres(ByVal i As Integer, ByVal Pinj As Double, ByVal Tinj As Double,
ByVal Pamb As Double, ByVal Pmax As Double, ByVal Tmax As Double, ByVal
Pmin As Double, ByVal Tmin As Double, ByVal numerodedatos As Double, ByVal n
As Integer, ByVal Cp As Double, ByVal Ao As Double, ByVal Bo As Double, ByRef
variable As Double, ByVal m As Integer)

 'inicializar estos valores para poder entrar al ciclo
 valoractual = 1
 valorviejo = 1

 'ubicar la linea donde se encuentra el valor a evaluar'
 k = 1
 Do While k < (numerodedatos + 1)
  If m = 0 Then
   vesp_liq = Worksheets("PropiedadesR134a").Cells(k + 2, 3).Value
   P_calculo = Worksheets("PropiedadesR134a").Cells(k + 2, 2).Value
   T_calculo = Worksheets("PropiedadesR134a").Cells(k + 2, 1).Value
  End If
  If m = 1 Then
   vesp_liq = Worksheets("PropiedadesAgua").Cells(k + 2, 3).Value
   P_calculo = Worksheets("PropiedadesAgua").Cells(k + 2, 2).Value
   T_calculo = Worksheets("PropiedadesAgua").Cells(k + 2, 1).Value
  End If
  If m = 2 Then
   vesp_liq = Worksheets("PropiedadesAmmonia").Cells(k + 2, 3).Value
   P_calculo = Worksheets("PropiedadesAmmonia").Cells(k + 2, 2).Value
   T_calculo = Worksheets("PropiedadesAmmonia").Cells(k + 2, 1).Value
  End If
  parteAverifT = (vesp_liq * (Pinj - P_calculo)) + (Cp * (Tinj - T_calculo)) - (Cp *
T_calculo * Log(Tinj / T_calculo))
  parteBverifT = (Cp * T_calculo ^ 3) / ((P_calculo * Ao) ^ 2)
  parteCverifT = 1 + (((Ao / T_calculo) - 2) * Log(Tinj / T_calculo))
  parte1verifT = parteAverifT * parteBverifT * parteCverifT
  parte2verifT = -0.5 * (vesp_liq + ((Cp * T_calculo ^ 2) / (P_calculo * Ao)) * Log(Tinj
/ T_calculo)) ^ 2
  verifT = parte1verifT + parte2verifT
  valoractual = verifT
  If (valorviejo >= 0 And valoractual < 0) Or (valorviejo < 0 And valoractual >= 0) Then
   indicedefila = k
  End If
  k = k + 1
```

```
 valorviejo = valoractual
 Loop

 If m = 0 Then
  T_evaluar = (Worksheets("PropiedadesR134a").Cells(indicedefila + 2 - 1, 1).Value +
Worksheets("PropiedadesR134a").Cells(indicedefila + 2, 1).Value) / 2
 End If
 If m = 1 Then
  T_evaluar = (Worksheets("PropiedadesAgua").Cells(indicedefila + 2 - 1, 1).Value +
Worksheets("PropiedadesAgua").Cells(indicedefila + 2, 1).Value) / 2
 End If
 If m = 2 Then
  T_evaluar = (Worksheets("PropiedadesAmmonia").Cells(indicedefila + 2 - 1, 1).Value
+ Worksheets("PropiedadesAmmonia").Cells(indicedefila + 2, 1).Value) / 2

 End If

 If T_evaluar >= Tinj Then

  'Si se da esta condición entonces ninguna de las variables del modelo tienen sentido
físico,
  'es decir, no se puede generar la condicion de estrangulamiento en la salida de la tobera
  Cells(i + 2 * n + 2 * 3 + 3, 7) = 0
  Cells(i + 2 * n + 2 * 3 + 3, 8) = 0
  Cells(i + 2 * n + 2 * 3 + 3, 9) = 0
  Cells(i + 2 * n + 2 * 3 + 3, 10) = 0
  Cells(i + 2 * n + 2 * 3 + 3, 13) = 0
  Cells(i + 2 * n + 2 * 3 + 3, 11) = 0
  Cells(i + 2 * n + 2 * 3 + 3, 12) = 0

  Else
   'cálculo de la calidad de la mezcla
   f = Inter(1, T_evaluar, 0, 0, 7, numerodedatos, variable, m)
   hfg_evaluar = variable
   Quality_T_evaluar = Log(Tinj / T_evaluar) * Cp * T_evaluar / hfg_evaluar
   Cells(i + 2 * n + 2 * 3 + 3, 7) = Quality_T_evaluar

   'cálculo de la densidad de la mezcla
   f = Inter(1, T_evaluar, 0, 0, 3, numerodedatos, variable, m)
   vesp_liq_T_evaluar = variable
   Cells(i + 2 * n + 2 * 3 + 3, 8) = vesp_liq_T_evaluar

   'cálculo del volumen específico de la fase gaseosa
   f = Inter(1, T_evaluar, 0, 0, 5, numerodedatos, variable, m)
   vesp_gas_T_evaluar = variable
   Cells(i + 2 * n + 2 * 3 + 3, 9) = vesp_gas_T_evaluar

   'cálculo del volumen específico de la mezcla
```

```
   vesp_mezcla_T_evaluar = vesp_liq_T_evaluar + Quality_T_evaluar *
(vesp_gas_T_evaluar - vesp_liq_T_evaluar)
   Cells(i + 2 * n + 2 * 3 + 3, 10) = vesp_mezcla_T_evaluar

   'cálculo de la velocidad mezcla
   vel_mez = (2 * (((Pinj - Pamb) * vesp_liq_T_evaluar) + (Cp * (Tinj - T_evaluar)) -
(Cp * T_evaluar * Log(Tinj / T_evaluar)))) ^ 0.5
   Cells(i + 2 * n + 2 * 3 + 3, 13) = vel_mez

   'imposición de la condición velocidad del líquido igual a la de la mezcla por condicion
de no deslizamiento
   vel_liq = vel_mez
   Cells(i + 2 * n + 2 * 3 + 3, 11) = vel_liq

   'imposición de la condición velocidad del gas igual a la de la mezcla por condicion de
no deslizamiento
   vel_gas = vel_mez
   Cells(i + 2 * n + 2 * 3 + 3, 12) = vel_gas

 End If

End Sub

'MODELO IV DE VELOCIDAD A LA SALIDA, ver Solomon
Public Sub mod_vel_Cuatro(ByVal i As Integer, ByVal Pinj As Double, ByVal Tinj As
Double, ByVal Pamb As Double, ByVal Pmax As Double, ByVal Tmax As Double,
ByVal Pmin As Double, ByVal Tmin As Double, ByVal numerodedatos As Double,
ByVal n As Integer, ByVal Cp As Double, ByVal Cp_gas As Double, ByVal k As
Double, ByVal R_gas As Double, ByVal Ao As Double, ByVal Bo As Double, ByRef
variable As Double, ByVal m As Integer)

 'temperatura ambiente, tomada como la temperatura de saturación a la presión ambiente
 f = Inter(0, 0, 1, Pamb, 1, numerodedatos, variable, m)
 Tamb = variable

 'calculo de la presión crítica
 Pcrit = Pinj * (2 / (k + 1)) ^ (k / (k - 1))
 'verificar si la salida es critica o no
 If Pcrit <= Pamb Then
  P_sal = Pamb
  Else
   P_sal = Pcrit
 End If

 'temperauta a la salida, para cualquiera de los dos casos
 T_sal = Tinj * (P_sal / Pinj) ^ ((k - 1) / k)

  'densidad de gas varia con la salida
```

```
 vesp_gas = (R_gas * T_sal) / P_sal
 Cells(i + 3 * n + 3 * 3 + 3, 9) = vesp_gas

 'densidad de líquido se mantiene constante
 f = Inter(1, Tamb, 0, 0, 3, numerodedatos, variable, m)
 vesp_liq = variable
 Cells(i + 3 * n + 3 * 3 + 3, 8) = vesp_liq

 'cálculo de velocidad del líquido
 vel_liq = (2 * (Pinj - P_sal) * vesp_liq) ^ 0.5
 Cells(i + 3 * n + 3 * 3 + 3, 11) = vel_liq

 'cálculo de velocidad del gas
 vel_gas = (2 * Cp_gas * (Tinj - T_sal)) ^ 0.5
 Cells(i + 3 * n + 3 * 3 + 3, 12) = vel_gas

 'cálculo de la calidad
 quality = Cp * T_sal ^ 2 * Log(Tinj / T_sal) / (P_sal * Ao * ((R_gas * T_sal / P_sal) -
vesp_liq))
 Cells(i + 3 * n + 3 * 3 + 3, 7) = quality

 'densidad del flujo como mezcla
 vesp_mez = (vesp_liq + (vesp_gas - vesp_liq) * quality)
 Cells(i + 3 * n + 3 * 3 + 3, 10) = vesp_mez

 'velocidad del flujo como mezcla
 vel_mez = (vel_liq + (vel_gas - vel_liq) * quality)
 Cells(i + 3 * n + 3 * 3 + 3, 13) = vel_mez

 'cálculo del flujo másico
 mf = a_sal * (vel_liq + (vel_gas - vel_liq) * quality)
 'Cells(i + 3 * n + 3 * 3 + 3, 14) = calidad

End Sub

'MODELO V DE VELOCIDAD A LA SALIDA
Public Sub mod_vel_Cinco(ByVal i As Integer, ByVal Pinj As Double, ByVal Tinj As
Double, ByVal Pamb As Double, ByVal Pmax As Double, ByVal Tmax As Double,
ByVal Pmin As Double, ByVal Tmin As Double, ByVal numerodedatos As Double,
ByVal n As Integer, ByVal Cp As Double, ByVal k As Double, ByVal R_gas As
Double, ByVal Ao As Double, ByVal Bo As Double, ByRef variable As Double, ByVal
m As Integer)

 'temperatura ambiente, tomada como la temperatura de saturación a la presión ambiente
 f = Inter(0, 0, 1, Pamb, 1, numerodedatos, variable, m)
 Tamb = variable

 'calculo de la presión crítica
```

```
Pcrit = Pinj * (2 / (k + 1)) ^ (k / (k - 1))
'verificar si la salida es critica o no
If Pcrit <= Pamb Then
 P_sal = Pamb
 Else
  P_sal = Pcrit
End If

'temperauta a la salida, para cualquiera de los dos casos
T_sal = Tinj * (P_sal / Pinj) ^ ((k - 1) / k)

 'densidad de gas varia con la salida
vesp_gas = (R_gas * T_sal) / P_sal
Cells(i + 3 * n + 3 * 3 + 3, 9) = vesp_gas

'densidad de líquido se mantiene constante
f = Inter(1, Tamb, 0, 0, 3, numerodedatos, variable, m)
vesp_liq = variable
Cells(i + 3 * n + 3 * 3 + 3, 8) = vesp_liq

'cálculo de velocidad del líquido
vel_liq = (2 * (Pinj - P_sal) * vesp_liq) ^ 0.5
Cells(i + 3 * n + 3 * 3 + 3, 11) = vel_liq

'cálculo de velocidad del gas
vel_gas = (2 * Cp_gas * (Tinj - T_sal)) ^ 0.5
Cells(i + 3 * n + 3 * 3 + 3, 12) = vel_gas

'cálculo de la calidad
quality = Cp * T_sal ^ 2 * Log(Tinj / T_sal) / (P_sal * Ao * ((R_gas * T_sal / P_sal) -
vesp_liq))
Cells(i + 3 * n + 3 * 3 + 3, 7) = quality

'void fraction
void = (vel_liq * quality / vesp_liq) / (((vel_gas / vesp_gas) * (1 - quality)) + ((vel_liq /
vesp_liq) * quality))
Cells(i + 3 * n + 3 * 3 + 3, 10) = 0

'velocidad del flujo como mezcla
vel_mez = 0
Cells(i + 3 * n + 3 * 3 + 3, 13) = 0

'cálculo del flujo másico
mf = a_sal * ((void * vel_gas / vesp_gas) + ((1 - void) * (vel_liq / vesp_liq)))
'Cells(i + 3 * n + 3 * 3 + 3, 14) = calidad

'Cells(3 * n + 3 * 3 + 2, 6) = "MODELO DE VELOCIDAD VI"
```

```
 'densidad de gas varia con la salida

" Cells(i + 3 * n + 3 * 3 + 3, 9) = vesp_gas

 'densidad de líquido se mantiene constante
 "f = Inter(1, Tamb, 0, 0, 3, numerodedatos, variable, m) "
" vesp_liq = variable
" Cells(i + 3 * n + 3 * 3 + 3, 8) = vesp_liq

 'cálculo de velocidad del líquido
 "vel_liq = (2 * (Pinj - P_sal) * vesp_liq) ^ 0.5
 "Cells(i + 3 * n + 3 * 3 + 3, 11) = vel_liq

 'cálculo de velocidad del gas
' vel_gas = (2 * Cp * (Tinj - T_sal)) ^ 0.5
' Cells(i + 3 * n + 3 * 3 + 3, 12) = vel_gas

 'cálculo de la calidad
' quality = Cp * T_sal ^ 2 * Log(Tinj / T_sal) / (P_sal * Ao * ((R_gas * T_sal / P_sal) -
vesp_liq))
 'calidad = (Cp * Tinj - hliq_sal) / hfg_sal
' Cells(i + 3 * n + 3 * 3 + 3, 7) = quality

 'densidad del flujo como mezcla
' vesp_mez = (vesp_liq + (vesp_gas - vesp_liq) * quality)
' Cells(i + 3 * n + 3 * 3 + 3, 10) = vesp_mez

 'velocidad del flujo como mezcla
' vel_mez = (vel_liq + (vel_gas - vel_liq) * quality)
' Cells(i + 3 * n + 3 * 3 + 3, 13) = vel_mez

 'cálculo del flujo másico
 ' mf = a_sal * (vel_liq + (vel_gas - vel_liq) * quality)
 'Cells(i + 3 * n + 3 * 3 + 3, 14) = calidad

End Sub

Public Sub mod_dia_Uno(ByVal Tinj As Double, ByVal diametro As Double, ByVal
tensup As Double, ByVal vel_jet As Double, ByVal vesp_liq As Double, ByVal
linea_a_escribir As Double, ByVal den_medio As Double, ByVal j As Integer, ByVal
m As Integer)
 If vel_jet <> 0 And Tinj < 452.71 Then
  'Cálculo del número de Weber de la mezcla
  'importante se utiliza la densidad del gas que esta en el medio no la del fluido
  weber = den_medio * diametro * vel_jet ^ 2 / (2 * tensup)
  'este para verificar la aplicabilidad del metoido con los datos del paper
  'Cells(linea_a_escribir, 14) = weber
```

```
  'conversión a grados Farenheit
  Tinj_F = (9 * Tinj / 5) - 460

  'Cálculo del diámetro de la gotas según Brown & York
  d10_Brown_York = (1840 - 5.18 * (Tinj_F)) / weber
  Cells(linea_a_escribir, 15) = d10_Brown_York
 Else
  Cells(linea_a_escribir, 15) = 0
End If
End Sub

Public Sub mod_C(ByVal Tinj As Double, ByVal diametro As Double, ByVal tensup
As Double, ByVal vel_jet As Double, ByVal vesp_liq As Double, ByVal
linea_a_escribir As Double, ByVal den_medio As Double, ByVal j As Integer, ByVal
m As Integer)

 'Cálculo del número de Weber de la mezcla
 weber = den_medio * diametro * vel_jet ^ 2 / (2 * tensup)

 'Cálculo del diámetro de la gotas según Brown & York
 If weber < 12.5 Then
  C_Brown_York = 19.7 - 0.58 * weber
  Else
   C_Brown_York = 11.5 - 0.42 * weber
 End If
 'escribir el valor de C, Growth rate constant
 'Cells(linea_a_escribir, 1) = d10_Brown_York

End Sub

Public Sub mod_dia_Solomon(ByVal diametro As Double, ByVal vesp_liq As Double,
ByVal vesp_gas As Double, ByVal visco As Double, ByVal tensup As Double, ByVal
vel_liq As Double, ByVal vel_gas As Double, ByVal linea_a_escribir As Double,
ByVal j As Integer, ByVal m As Integer)

 'MODELO II - DIAMETRO
 If vesp_gas = 0 Then
  Cells(linea_a_escribir, 16) = 0
  Else
   d32_Solomon1 = 21.4 * (visco * (tensup * vesp_liq) ^ 0.5 / ((1 / vesp_gas) * vel_gas
^ 2)) ^ (2 / 3)
   'el resultado que da la equación is en metros, entonces lo multiplico por 1000000 para
llevarlo a micras
   Cells(linea_a_escribir, 16) = d32_Solomon1 * 1000000
 End If

 'MODELO III - DIAMETRO
```

```
 If vesp_gas = 0 Then  'para evitar las divisiones por cero, esto aplica para cuando el
modelo perimte solo liquido a la salida
  Cells(linea_a_escribir, 17) = 0
  Else
   d32_Solomon2 = 1.2 * diametro ^ 0.5 * (visco * (tensup * vesp_liq) ^ 0.5 / ((1 /
vesp_gas) * vel_liq ^ 2)) ^ (1 / 3)
   'el resultado que da la equación is en metros, entonces lo multiplico por 1000000 para
llevarlo a micras
   Cells(linea_a_escribir, 17) = d32_Solomon2 * 1000000
 End If

 'MODELO IV - DIAMETRO
 If vesp_gas = 0 Or vel_gas = 0 Then
  Cells(linea_a_escribir, 18) = 0
  Else
   aux1 = 0.073 * diametro ^ 0.4 * (vesp_gas / vesp_liq) ^ 0.1 * (tensup * vesp_gas /
(vel_gas ^ 2)) ^ 0.6
   aux2 = 0.0006 * (visco ^ 2 * diametro * vesp_gas / tensup) ^ 0.5
   aux3 = 1 + ((vesp_gas * vel_liq) / (vesp_liq * vel_gas))
   d32_Solomon3 = aux3 * (aux1 + aux2)
   'el resultado que da la equación is en metros, entonces lo multiplico por 1000000 para
llevarlo a micras
   Cells(linea_a_escribir, 18) = d32_Solomon3 * 1000000
  End If

 End Sub

Public Sub mod_dia_Wheathey(ByVal Tinj As Double, ByVal Pinj As Double, ByVal
Pamb As Double, ByVal diametro As Double, ByVal vesp_liq As Double, ByVal
vesp_gas As Double, ByVal vesp_mez As Double, ByVal visco As Double, ByVal
tensup As Double, ByVal vel_liq As Double, ByVal vel_gas As Double, ByVal
vel_mez As Double, ByVal numerodedatos As Integer, ByVal linea_a_escribir As
Double, ByVal j As Integer, ByVal m As Integer, ByVal vel_medio As Double)
 Dim variable As Double
 If vel_mez <> 0 Then
  'MODELO V - DIAMETRO
  ' introducir el calculo de las velocidades en el punto del flashing

  vel_flash = vel_mez
  vesp_liq_flash = vesp_liq
  vesp_air = vesp_medio

  weber = diametro * vel_flash ^ 2 / (tensup * vesp_liq)
  Re = vel_flash * diametro / (visco * vesp_liq)
  calculo1 = 1.89 * diametro * (1 + (3 * weber ^ 0.5) / Re) ^ 0.5
  calculo2 = 20 * tensup * vesp_air / (vel_flash ^ 2)
  If calculo1 >= calculo2 Then
   dmax_Wheathey = calculo1
```

```
   Else
    dmax_Wheathey = calculo2
  End If
  Cells(linea_a_escribir, 19) = dmax_Wheathey * 1000000
 Else
  Cells(linea_a_escribir, 19) = 0
 End If
End Sub

Public Sub mod_dia_Otros(ByVal Tinj As Double, ByVal Pinj As Double, ByVal Pamb
As Double, ByVal diametro As Double, ByVal vesp_liq As Double, ByVal vesp_gas
As Double, ByVal vesp_mez As Double, ByVal visco As Double, ByVal tensup As
Double, ByVal vel_liq As Double, ByVal vel_gas As Double, ByVal vel_mez As
Double, ByVal numerodedatos As Integer, ByVal linea_a_escribir As Double, ByVal j
As Integer, ByVal m As Integer, ByVal quality As Double)
 Dim variable As Double

If vel_mez <> 0 Then

 'MODELO VI - DIAMETRO
 If quality = 0 Then
  Cells(linea_a_escribir, 20) = 0
  Else
   d_Dunbar = 8.02 / (quality ^ 0.56 * ((Pinj - Pamb) / Pamb) ^ 0.46)
   Cells(linea_a_escribir, 20) = d_Dunbar
 End If

 'MODELO VII - DIAMETRO
 den_air = 1.2
' If vesp_gas = 0 Then
'  Cells(linea_a_escribir, 21) = 0
'  Else
   d_Deaves = 3.09 * ((visco) ^ 0.385) * ((tensup / vesp_liq) ^ 0.737) * ((den_air) ^
0.06) * ((Pinj - Pamb) ^ -0.54)

   Cells(linea_a_escribir, 21) = d_Deaves * 1000000
' End If

 'MODELO VIII - DIAMETRO
 f = Inter(0, 0, 1, Pamb, 1, numerodedatos, variable, m)
 Tsat_Pamb = variable
 f = Inter(0, 0, 1, Pinj, 1, numerodedatos, variable, m)
 Tsat_Pinj = variable
 deltaT_Gemci = (Tinj - Tsat_Pamb) / (Tsat_Pinj - Tsat_Pamb)
 K_Gemci = 2 * (Pamb - psat_Tamb) * vesp_mez / (vel_mez ^ 2)
 d_Gemci = 118.4 - 28.3 * (deltaT_Gemci - K_Gemci) 'ya esta en micras
 Cells(linea_a_escribir, 22) = d_Gemci
```

```
 'adapto las ecuaciones colocando la relacion de caudales como simplemente la relacion
de velocidades, ya que el area de salida es la misma
 'MODELO IX - DIAMETRO
 If vel_gas = 0 Or vel_gas = vel_liq Then
  Cells(linea_a_escribir, 23) = 0
  Else
   d32_Costas1 = ((0.585 / (vel_gas - vel_liq)) * (tensup * vesp_liq) ^ 0.5) + (0.001683
* ((visco * (vesp_liq ^ 0.5)) / (tensup ^ 0.5)) ^ 0.45) * (1000 * vel_liq / vel_gas) ^ 1.5
   Cells(linea_a_escribir, 23) = d32_Costas1 * 1000000
 End If

 'MODELO X - DIAMETRO
 If vel_gas = 0 Or vel_gas = vel_liq Then
  Cells(linea_a_escribir, 24) = 0
  Else
   d32_Costas2 = (0.0422 + 0.00577 * (1000 * vel_liq / vel_gas) ^ 1.932) / (vel_gas -
vel_liq) ^ 1.602
   Cells(linea_a_escribir, 24) = d32_Costas2 * 1000000
 End If

 Else
 'Para los casos no definidos de las ecuaciones se le asigna un valor nulo a las mismas
 Cells(linea_a_escribir, 20) = 0 'd_Dunbar
 Cells(linea_a_escribir, 21) = 0 'd_Deaves * 1000000
 Cells(linea_a_escribir, 22) = 0 'd_Gemci
 Cells(linea_a_escribir, 23) = 0 'd32_Costas1 * 1000000
 Cells(linea_a_escribir, 24) = 0 'd32_Costas2 * 1000000
 End If
End Sub
Public Sub mod_dia_Nagai(ByVal Tinj As Double, ByVal Pinj As Double, ByVal
Pamb As Double, ByVal diametro As Double, ByVal vesp_liq As Double, ByVal
vesp_gas As Double, ByVal vesp_mez As Double, ByVal visco As Double, ByVal
tensup As Double, ByVal vel_liq As Double, ByVal vel_gas As Double, ByVal
vel_mez As Double, ByVal numerodedatos As Integer, ByVal linea_a_escribir As
Double, ByVal j As Integer, ByVal m As Integer, ByVal quality As Double, ByVal
longitud As Double)
 Dim variable As Double

 'MODELO - DIAMETRO
 f = Inter(0, 0, 1, Pamb, 1, numerodedatos, variable, m)
 Tsat_Pamb = variable

 f = Inter(0, 0, 1, Pinj, 1, numerodedatos, variable, m)
 Tsat_Pinj = variable

 DeltaT_numerador = Tinj - Tsat_Pamb
 DeltaT_denominador = Tsat_Pinj - 373.15 'en la ecuación original es menos 100C
 deltaT_adimen = DeltaT_numerador / DeltaT_denominador
```

```
 'en principio la igualo a cero de manera que si se cumple alguna de las condiciones
descritas
 'para los modelo se cambia, en caso contrario queda el valor de cero
 Cells(linea_a_escribir, 25) = 0
 If vel_liq = 0 Or vesp_liq = 0 Then
  Reynolds = 0
  Else
   Reynolds = vel_liq * diametro / (visco * vesp_liq)
 End If

 aspect_ratio = longi / diametro

 If Reynolds > 10000 And 1 < deltaT_adimen > 0.55 And aspect_ratio < 7 Then
  d_Nagai = 36.8 * deltaT_adimen ^ -2.58 'd32
  Cells(linea_a_escribir, 25) = d_Nagai
 End If
 If Reynolds <= 10000 And 0 <= deltaT_adimen < 0.55 And aspect_ratio > 7.8 Then
  d_Nagai = 70.4 * (0.14 * (longi / diametro) - 1) ^ -0.22 * (diametro ^ 0.72) *
(deltaT_adimen ^ -0.38)
  Cells(linea_a_escribir, 25) = d_Nagai
 End If
 If Reynolds <= 10000 And 0.55 <= deltaT_adimen < 1 And aspect_ratio > 7.8 Then
  d_Nagai = 39.1 * (0.14 * (longi / diametro) - 1) ^ -0.22 * (diametro ^ 0.72) *
(deltaT_adimen ^ -0.38)
  Cells(linea_a_escribir, 25) = d_Nagai
 End If


End Sub

Public Sub mod_lon(ByVal Tinj As Double, ByVal Pinj As Double, ByVal Pamb As
Double, ByVal diametro As Double, ByVal vesp_liq As Double, ByVal vesp_gas As
Double, ByVal vesp_mez As Double, ByVal visco As Double, ByVal visco_gas As
Double, ByVal tensup As Double, ByVal vel_liq As Double, ByVal vel_gas As Double,
ByVal vel_mez As Double, ByVal numerodedatos As Integer, ByVal linea_a_escribir
As Double, ByVal m As Integer)
 Dim variable As Double

 'MODELO I - LONGITUD
 If vel_gas = 0 Or vel_gas = vel_liq Then
  Cells(linea_a_escribir, 27) = 0
  Else
  Ld_Unknow = 0.25 * vesp_liq * vel_liq * (visco * (vesp_gas * vel_gas ^ 2) / (tensup /
vesp_liq)) ^ -1
  Cells(linea_a_escribir, 27) = Ld_Unknow
 End If
```

```
'MODELO II listo
If vel_gas = 0 Or vel_gas = vel_liq Then
 Cells(linea_a_escribir, 28) = 0
 Else
 c1 = 1 ' es una constante a ajustar
 m_Lasheras = (vesp_gas * vel_gas ^ 2) / (vesp_liq * vel_liq ^ 2)
 Ld_Lasheras2 = 0.5 * (c1 * m_Lasheras ^ (2 / 3)) ^ (-1) * (tensup / (visco * vel_liq)) ^
(1 / 3) 'según revisión del Lasheras pag.281
 Cells(linea_a_escribir, 28) = Ld_Lasheras2 '*
End If

'MODELO III listo
If vel_gas = 0 Or vesp_gas = 0 Then
 Cells(linea_a_escribir, 29) = 0
 Else
 weber = (1 / vesp_gas) * diametro * vel_gas ^ 2 / tensup 'según revisión del Lasheras
pag.281
 Re = diametro * vel_liq / (visco * vesp_liq)
 c2 = 1
 a = 0.3 ' a esta entre 0.3 y 0.7
 b = 0.5
 Ld_Lasheras3 = c2 * weber ^ -a * Re ^ b
 Cells(linea_a_escribir, 29) = Ld_Lasheras3 '*
End If

'MODELO IV listo
If vel_gas = 0 Or vel_gas = vel_liq Then
 Cells(linea_a_escribir, 30) = 0
 Else
 m_Lasheras = (vesp_gas * vel_gas ^ 2) / (vesp_liq * vel_liq ^ 2)
 Ld_Rehab1 = 6 * (m_Lasheras ^ -0.5) * (Abs(1 - (vel_liq / vel_gas)) ^ -1)
 Cells(linea_a_escribir, 30) = Ld_Rehab1
End If

'MODELO V listo
If vel_gas = 0 Then
 Cells(linea_a_escribir, 31) = 0
 Else
 b = 0.001 ' según experimentos reportados pag 283
 b = -50 ' según experimentos reportados pag 283
 m_Lasheras = (vesp_gas * vel_gas ^ 2) / (vesp_liq * vel_liq ^ 2)
 Ld_Rehab2 = 6 * m_Lasheras ^ -0.5 * (1 - (b * tensup / (visco_gas * vel_gas))) ^ -0.5
 Cells(linea_a_escribir, 31) = Ld_Rehab2 '*
End If

'MODELO VI
If vel_gas = 0 Then
 Cells(linea_a_escribir, 32) = 0
```

```
  Else
  m_Lasheras = (vesp_gas * vel_gas ^ 2) / (vesp_liq * vel_liq ^ 2)
  C = 4 'es una variable a determinar
  Ld_Engelbert = C / m_Lasheras ^ 0.3
  Cells(linea_a_escribir, 32) = Ld_Engelbert '*
 End If

 'MODELO VII
 weber1 = vesp_liq * diametro * vel_liq ^ 2 / tensup 'de acuerdo al paper pag. 2418, solo
dice
                                                    'que se refiere al combustible y no al gas del ambiente
 weber2 = vesp_mez * diametro * vel_mez ^ 2 / tensup ' asi que decidi tomar el menor
valor entre el del liquido y
                                                    ' el del la mezcla, asi garantizo la longitud más
conservadora
 If weber1 <= weber2 Then
  weber = weber1
  Else
  weber = weber2
 End If
 Ld_Lee_Park = 8.51 * weber ^ 0.32
 Cells(linea_a_escribir, 33) = Ld_Lee_Park

 'MODELO VIII
 If vesp_gas = 0 Then
  Cells(linea_a_escribir, 34) = 0
  Else
  weber = vesp_gas * diametro * vel_gas ^ 2 / tensup 'según revisión del Lasheras
pag.281
  Re = diametro * vel_liq / (vesp_liq * visco)
  varT = (vesp_liq / vesp_gas) * (Re / weber) ^ 2
  ft = (3 ^ 0.5 / 6) * (1 - Exp(-10 * varT))
  Ld_Lin_Reitz = 4.04 * (vesp_gas / vesp_liq) / ft
  Cells(linea_a_escribir, 34) = Ld_Lin_Reitz
 End If

'MODELO IX
 T_exit = Tinj
 Pvapor_condiciones_amb = Pamb
 f = Inter(0, 0, 1, Pvapor_condiciones_amb, 1, numerodedatos, variable, m)
 Tsat_Pvapor_condiciones_amb = variable
 If Tsat_Pamb <> Tsat_Pamb Then
  Ld_Miyatake = 21.9 / (T_exit - Tsat_Pvapor_condiciones_amb) ^ (1 / 3)
  Cells(linea_a_escribir, 35) = Ld_Miyatake
  Else
  Cells(linea_a_escribir, 35) = 0
 End If
```

```
End Sub
Public Sub poner_nombres_unidades(ByVal j)

 'Colocarle los nombre y las unidades a las varibles
 Cells(j, 7) = "Quality [adim]"
 Cells(j, 8) = "Volumen especifico de liquido [m3/kg]"
 Cells(j, 9) = "Volumen especifico de gas [m3/kg]"
 Cells(j, 10) = "Volumen especifico de mezcla [m3/kg]"
 Cells(j, 11) = "Velocidad de líquido [m/s]"
 Cells(j, 12) = "Velocidad de gas [m/s]"
 Cells(j, 13) = "Velocidad de mezcla [m/s]"

 Cells(j, 15) = "d10_Brown_York"
 Cells(j, 16) = "d32_Solomon1"
 Cells(j, 17) = "d32_Solomon2"
 Cells(j, 18) = "d32_Solomon3"
 Cells(j, 19) = "dmax_Wheathey"
 Cells(j, 20) = "d_Dunbar"
 Cells(j, 21) = "d_Deaves"
 Cells(j, 22) = "d_Gemci"
 Cells(j, 23) = "d32_Costas1"
 Cells(j, 24) = "d32_Costas2"
 Cells(j, 25) = "dia_Nagai"

 'nombre para las longitudes de líquido
 Cells(j, 27) = "Ld_Unkonw"
 Cells(j, 28) = "Ld_Lasheras2"
 Cells(j, 29) = "Ld_Lasheras3"
 Cells(j, 30) = "Ld_Rehab1"
 Cells(j, 31) = "Ld_Rehab2"
 Cells(j, 32) = "Ld_Engelbert"
 Cells(j, 33) = "Ld_Lee_Park"
 Cells(j, 34) = "Ld_Lin_Reitz"
 Cells(j, 35) = "Ld_Miyatake"
End Sub
Public Sub mod_angle_Lasheras(ByVal Tinj As Double, ByVal Pinj As Double, ByVal
Pamb As Double, ByVal diametro As Double, ByVal vesp_liq As Double, ByVal
vesp_gas As Double, ByVal vesp_mez As Double, ByVal visco As Double, ByVal
visco_gas As Double, ByVal tensup As Double, ByVal vel_liq As Double, ByVal
vel_gas As Double, ByVal vel_mez As Double, ByVal numerodedatos As Integer,
ByVal linea_a_escribir As Double)
 Dim variable As Double

 'MODELO I - ANGLE
 If vel_gas = 0 Then
  angle_Lasheras = 0
  Cells(linea_a_escribir, 29) = angle_Lasheras
  Else
```

```
    m = (vesp_gas * vel_gas ^ 2) / (vesp_liq * vel_liq ^ 2)
    angle_liquid_shear = (Atn((m ^ 0.5) / 5)) * (180 / 3.14159265)
    angle_spray_liquid_shear = 45
    angle_Lasheras = 2 * (angle_spray_liquid_shear - (angle_liquid_shear / 2))
    Cells(linea_a_escribir, 29) = angle_Lasheras
  End If
End Sub
'Cuerpo principal del programa
'Public Sub mod_dia_Solomon(ByVal diametro As Double, ByVal vel_liq As Double,
ByVal vel_jet As Double, ByVal vesp_liq As Double)
Private Sub CommandButton1_Click()
 'Declaraciones'
 Dim variable As Double
 Dim Tmax As Double
 Dim Tmin As Double
 Dim Pmax As Double
 Dim Pmin As Double
 Dim Cp As Double
 Dim Cp_gas As Double
 Dim Ao As Double
 Dim Bo As Double
 Dim visco As Double
 Dim visco_gas As Double
 Dim tensup As Double
 Dim k As Double
 Dim R_gas As Double
 Dim nombre As String
 Dim numerodedatos As Integer
 Dim den_medio As Double

 'Asignacion de las distintas constantes deacuerdo a la selección del fluido
 m = Cells(1, 2)
 n = Cells(2, 2)
 Call constantes(m, n, Tmax, Tmin, Pmax, Pmin, Cp, Cp_gas, Ao, Bo, visco, visco_gas,
tensup, k, R_gas, numerodedatos, den_medio)

 'Verificar los posibles errores, borrar los datos de las corridas anteriores
 arreglosdelapagina (n)

 Call mod_vel_names(n)

 'Comienzo de los diferenets cálculos de velocidad
 i = 1
 Do While i < (n + 1)
  Pinj = Cells(i + 3, 3) 'Presión de injección
  Tinj = Cells(i + 3, 2) 'Temperatura de injección
  Pamb = Cells(i + 3, 4) 'Presión del ambiente
```

```
  'MODELO I DE VELOCIDAD A LA SALIDA / Liquid Discharge / Solomon (1985)
Wheatley (1987)
  Call mod_vel_Uno(i, Pinj, Pamb, numerodedatos, n, variable, nombre, m)

  'MODELO II DE VELOCIDAD A LA SALIDA / Descarga en equilibrio / Wheatley
(1987)
  Call mod_vel_Dos(i, Pinj, Tinj, Pamb, numerodedatos, n, Cp, Ao, Bo, variable, m)

  'MODELO III DE VELOCIDAD A LA SALIDA / Descarga en critica / Wheatley
(1987)
  Call mod_vel_Tres(i, Pinj, Tinj, Pamb, Pmax, Tmax, Pmin, Tmin, numerodedatos, n,
Cp, Ao, Bo, variable, m)

  'MODELO I DE VELOCIDAD A LA SALIDA /  / no  es Solomon (1985)
estrictamente
  Call mod_vel_Cuatro(i, Pinj, Tinj, Pamb, Pmax, Tmax, Pmin, Tmin, numerodedatos,
n, Cp, Cp_gas, k, R_gas, Ao, Bo, variable, m)
  i = i + 1
 Loop

 i = 1
 j = 0

 Do While j < (4)
  linea_a_evaluar = j * (n + 3) + 3
  Call poner_nombres_unidades(linea_a_evaluar)

  Do While i < (n + 1)
   'Datos iniciales de la simulación
   Tinj = Cells(i + 3, 2) 'Temperatura de injección
   Pinj = Cells(i + 3, 3) 'Presión de injección
   Pamb = Cells(i + 3, 4) 'Presión del ambiente
   diametro = Cells(i + 3, 5) 'diámetro de la tobera de salida del fluido
   longitud = Cells(i + 3, 6) 'longitud de la tobera

   'Producto del calculo de las velocidades
   vesp_liq = Cells(linea_a_evaluar + i, 8)
   'vesp_gas = 1
   vesp_gas = Cells(linea_a_evaluar + i, 9)
   vesp_mez = Cells(linea_a_evaluar + i, 10)
   vel_liq = Cells(linea_a_evaluar + i, 11)
   vel_gas = Cells(linea_a_evaluar + i, 12)
   'vel_gas = 50
   vel_mez = Cells(linea_a_evaluar + i, 13)
   quality = Cells(linea_a_evaluar + i, 7)
   linea_a_escribir = linea_a_evaluar + i
   Call mod_dia_Uno(Tinj, diametro, tensup, vel_mez, vesp_liq, linea_a_escribir,
den_medio, j, m)
```

```
   Call mod_dia_Solomon(diametro, vesp_liq, vesp_gas, visco, tensup, vel_liq, vel_gas,
linea_a_escribir, j, m)
   Call mod_dia_Wheathey(Tinj, Pinj, Pamb, diametro, vesp_liq, vesp_medio,
vesp_mez, visco, tensup, vel_liq, vel_gas, vel_mez, numerodedatos, linea_a_escribir, j,
m, den_medio)
   Call mod_dia_Otros(Tinj, Pinj, Pamb, diametro, vesp_liq, vesp_gas, vesp_mez, visco,
tensup, vel_liq, vel_gas, vel_mez, numerodedatos, linea_a_escribir, j, m, quality)
   Call mod_dia_Nagai(Tinj, Pinj, Pamb, diametro, vesp_liq, vesp_gas, vesp_mez, visco,
tensup, vel_liq, vel_gas, vel_mez, numerodedatos, linea_a_escribir, j, m, quality,
longitud)

   i = i + 1
  Loop
  j = j + 1
  i = 1
 Loop

 j = 0
 Do While j < (4)
  linea_a_evaluar = j * (n + 3) + 3
  Call poner_nombres_unidades(linea_a_evaluar)
 j = j + 1
 Loop

 i = 1
 j = 0
 Do While j < (4)
  linea_a_evaluar = j * (n + 3) + 3
  Do While i < (n + 1)
   'Datos iniciales de la simulación
   Tinj = Cells(i + 3, 2) 'Temperatura de injección
   Pinj = Cells(i + 3, 3) 'Presión de injección
   Pamb = Cells(i + 3, 4) 'Presión del ambiente
   diametro = Cells(i + 3, 5) 'diámetro de la tobera de salida del fluido
  'Producto del calculo de las velocidades
   vesp_liq = Cells(linea_a_evaluar + i, 8)
   vesp_gas = Cells(linea_a_evaluar + i, 9)
   vesp_mez = Cells(linea_a_evaluar + i, 10)
   vel_liq = Cells(linea_a_evaluar + i, 11)
   vel_gas = Cells(linea_a_evaluar + i, 12)
   vel_mez = Cells(linea_a_evaluar + i, 13)
   linea_a_escribir = linea_a_evaluar + i
   Call mod_lon(Tinj, Pinj, Pamb, diametro, vesp_liq, vesp_gas, vesp_mez, visco,
visco_gas, tensup, vel_liq, vel_gas, vel_mez, numerodedatos, linea_a_escribir, m)
   i = i + 1
  Loop
  j = j + 1
  i = 1
```

```
 Loop


 '''''''''''''''''''''''''''''''''''''''''''''''''''''''''''''''''''''
 'Cálculo de lso numeros adimensionales que creo puedan servir para establecer las
funciones
  i = 1
  j = 0
  Do While j < (4)
   linea_a_evaluar = j * (n + 3) + 3
   Do While i < (n + 1)
    'Datos iniciales de la simulación
    Tinj = Cells(i + 3, 2) 'Temperatura de injección
    Pinj = Cells(i + 3, 3) 'Presión de injección
    Pamb = Cells(i + 3, 4) 'Presión del ambiente
    diametro = Cells(i + 3, 5) 'Diámetro de la tobera de salida del fluido
    longitud = Cells(i + 3, 6) 'Longitud de la tobera

    f = Inter(0, 0, 1, Pinj, 1, numerodedatos, variable, m)
    Tsat_Pinj = variable

    'Valores numéricos producto del cálculo de las velocidades
    vesp_liq = Cells(linea_a_evaluar + i, 8)
    vesp_gas = Cells(linea_a_evaluar + i, 9)
    vesp_mez = Cells(linea_a_evaluar + i, 10)
    vel_liq = Cells(linea_a_evaluar + i, 11)
    vel_gas = Cells(linea_a_evaluar + i, 12)
    vel_mez = Cells(linea_a_evaluar + i, 13)
    linea_a_escribir = linea_a_evaluar + i
    If vesp_mez = 0 Then
     Cells(linea_a_evaluar + i, 45) = 0
     Cells(linea_a_evaluar + i, 46) = 0
     Cells(linea_a_evaluar + i, 47) = 0
     Cells(linea_a_evaluar + i, 48) = 0
     Cells(linea_a_evaluar + i, 49) = 0
     Cells(linea_a_evaluar + i, 50) = 0
     Cells(linea_a_evaluar + i, 51) = 0
     Cells(linea_a_evaluar + i, 52) = 0
     Cells(linea_a_evaluar + i, 53) = 0
     Cells(linea_a_evaluar + i, 54) = 0
    Else
     Cells(linea_a_evaluar + i, 45) = Pinj / (Cp * Tsat_Pinj * (1 / vesp_mez)) ' energía de
presión / energía térmica
     Cells(linea_a_evaluar + i, 46) = (Pinj - Pamb) / (Cp * Tsat_Pinj * (1 / vesp_mez)) '
energía de presión / energía térmica
     Cells(linea_a_evaluar + i, 47) = Cells(linea_a_evaluar + i, 46) * ((longitud /
diametro) ^ (3 / 5))
     Cells(linea_a_evaluar + i, 48) = (vel_mez ^ 2 / Tinj) / Cp
```

```
     Cells(linea_a_evaluar + i, 49) = Cells(linea_a_evaluar + i, 48) *
Cells(linea_a_evaluar + i, 45)
     Cells(linea_a_evaluar + i, 50) = Cells(linea_a_evaluar + i, 48) *
Cells(linea_a_evaluar + i, 46)
     Cells(linea_a_evaluar + i, 51) = Cells(linea_a_evaluar + i, 48) /
Cells(linea_a_evaluar + i, 45)
     Cells(linea_a_evaluar + i, 52) = Cells(linea_a_evaluar + i, 48) /
Cells(linea_a_evaluar + i, 46)
     Cells(linea_a_evaluar + i, 53) = (Cells(linea_a_evaluar + i, 48) /
Cells(linea_a_evaluar + i, 45)) ^ -1
     Cells(linea_a_evaluar + i, 54) = (Cells(linea_a_evaluar + i, 48) /
Cells(linea_a_evaluar + i, 46)) ^ -1


    End If
    i = i + 1
   Loop
   j = j + 1
   i = 1
  Loop
 ''''''''''''''''''''''''''''''''''''''''''''''''''''''''''''

  i = 1
  j = 0
  Do While j < (4)
   linea_a_evaluar = j * (n + 3) + 3
   Do While i < (n + 1)
    'Datos iniciales de la simulación
    Tinj = Cells(i + 3, 2) 'Temperatura de injección
    Pinj = Cells(i + 3, 3) 'Presión de injección
    Pamb = Cells(i + 3, 4) 'Presión del ambiente
    diametro = Cells(i + 3, 5) 'Diámetro de la tobera de salida del fluido
    longitud = Cells(i + 3, 6) 'Longitud de la tobera

    f = Inter(0, 0, 1, Pinj, 1, numerodedatos, variable, m)
    Tsat_Pinj = variable

    'Valores numéricos producto del cálculo de las velocidades
    vesp_liq = Cells(linea_a_evaluar + i, 8)
    vesp_gas = Cells(linea_a_evaluar + i, 9)
    vesp_mez = Cells(linea_a_evaluar + i, 10)
    vel_liq = Cells(linea_a_evaluar + i, 11)
    vel_gas = Cells(linea_a_evaluar + i, 12)
    vel_mez = Cells(linea_a_evaluar + i, 13)
    linea_a_escribir = linea_a_evaluar + i
    f = Inter(1, Tinj, 0, 0, 6, numerodedatos, variable, m)
    hf_Tinj = variable
    f = Inter(0, 0, 1, Pamb, 6, numerodedatos, variable, m)
    hf_Tamb = variable
```

```
   f = Inter(0, 0, 1, Pamb, 7, numerodedatos, variable, m)
   hfg_Tamb = variable
   Cells(linea_a_evaluar + i, 56) = (hf_Tinj - hf_Tamb) / hfg_Tamb
   i = i + 1
  Loop
  j = j + 1
  i = 1
 Loop


 i = 1
 j = 0
 Do While j < (4)
  linea_a_evaluar = j * (n + 3) + 3
  Do While i < (n + 1)
  'calculo de viscosidad y tension superficial para calcular We, Oh, Re y Ge
   f = Inter(1, Tinj, 0, 0, 27, numerodedatos, variable, m)
   visco_Tinj = variable
   Cells(linea_a_evaluar + i, 60) = visco_Tinj

   f = Inter(1, Tinj, 0, 0, 33, numerodedatos, variable, m)
   Tension_Tinj = variable
   Cells(linea_a_evaluar + i, 60) = Tension_Tinj
  Loop
  j = j + 1
  i = 1
 Loop

End Sub
```